Dissertation

submitted to the Combined Faculties for the Natural Sciences and Mathematics
of the Ruperto – Carola University of Heidelberg
for the degree of
Doctor of Natural Sciences

presented by
Diplom-Physiker Sebastian Diehl
born in Ludwigshafen, Germany

Oral Examination: 24. October 2006

The BCS – BEC Crossover
in
Ultracold Fermion Gases

Referees: Prof. Dr. Christof Wetterich
PD Dr. Jan M. Pawlowski

Der BCS – BEC Crossover in ultrakalten Fermiongasen

Zusammenfassung

Der kontinuierliche Crossover eines Bardeen-Cooper-Schrieffer (BCS)-artigen Suprafluids aus Fermionpaaren zu einem Bose-Einstein Kondensat (BEC) aus fest gebundenen bosonischen Molekülen kann auf die spontane Brechung der globalen $U(1)$-Eichsymmetrie zurückgeführt werden, die beiden Quanten-Kondensationsphänomenen zugrunde liegt. Dem Problem wurde in den letzten Jahren viel Aufmerksamkeit zuteil, da Feshbach-Resonanzen die experimentelle Realisierung der Crossover-Physik ermöglichen. Die starke Wechselwirkung nahe der Resonanz erfordert eine Analyse jenseits von Mean Field Theorie. Wir entwickeln einen systematischen Funktionalintegral-Zugang für die Beschreibung dieses Phänomens. Ausgehend von einem yukawaartigen Atom-Molekül-Modell erlaubt es eine Symmetriebetrachtung, sowohl die Zustandsgleichung zu konstruieren als auch die thermodynamischen Phasen einheitlich zu klassifizieren. Der Übergang in das suprafluide Regime wird durch die Entstehung einer masselosen Goldstonemode angezeigt, die mit der gebrochenen kontinuierlichen $U(1)$-Symmetrie assoziiert ist. Jenseits von Mean Field berücksichtigen wir selbstkonsistent Molekülfluktuationen durch die Lösung geeigneter Schwinger-Dyson Gleichungen. Das Phasendiagramm wird berechnet, und eine Vielzahl universeller Eigenschaften etabliert. Eine neue Form von Crossover – von einem exakt lösbaren Schmalresonanz-Limes hin zu breiten Resonanzen oder punktförmigen Wechselwirkungen – wird aufgezeigt. Unsere Resulate stimmen bei niedriger Temperatur gut mit Quanten Monte Carlo Simulationen sowie einem kürzlich durchgeführten Experiment überein. Unser Zugang wird im Rahmen von funktionalen Renormierungsgruppen-Gleichungen weiterentwickelt. Während die effektive bosonische Theorie im BEC-Regime die charakteristischen Eigenschaften einer Bogoliubov-Theorie bei tiefer Temperatur aufweist, ist der Phasenübergang zweiter Ordnung.

The BCS – BEC Crossover in Ultracold Fermion Gases

Abstract

The continuous crossover between a Bardeen-Cooper-Schrieffer (BCS)-type superfluid of fermion pairs and a Bose-Einstein condensate (BEC) of tightly bound bosonic molecules can be attributed to the spontaneous breaking of global $U(1)$ gauge symmetry which underlies both quantum condensation phenomena. Recently much attention has been paid to this problem, since Feshbach resonances allow for an experimental implementation of crossover physics in cold fermion gases. The strong interactions close to resonance call for an analysis beyond Mean Field Theory. We develop a systematic functional integral approach for the description of this phenomenon. Starting from a Yukawa-type atom-molecule model, a symmetry analysis allows to both construct the equation of state and to classify the thermodynamic phases in a unified way. The onset of superfluidity is signalled by the emergence of a massless Goldstone mode associated with the broken continuous $U(1)$ symmetry. Beyond Mean Field, we include fluctuations of the molecule field self-consistently via the solution of suitable Schwinger-Dyson equations. The phase diagram is computed, and a variety of universal features are established. A new form of crossover from an exactly solvable narrow resonance limit to broad resonances or pointlike interactions is found. At low temperature our results agree well with quantum Monte Carlo simulations and recent experiments. Our approach is further developed in the frame of functional renormalization group equations. While the effective bosonic theory in the BEC regime shows the characteristics of a Bogoliubov theory for small temperatures, the phase transition is of second order.

Contents

Chapter 1

Introduction

There are two cornerstones for the description of quantum condensation phenomena. The simplest scenario occurs in bosonic systems. At low enough temperature, bosons populate a single quantum state macroscopically: A Bose-Einstein condensate (BEC) forms [1; 2]. This collective quantum phenomenon can be macroscopically observed [3–5]. In principle, this condensation is a purely statistical effect and does not rely on interactions. The situation is different in fermionic systems. Here, Pauli's principle forbids the macroscopic population of a single quantum state. However, in case of weak attractive interactions a many-body fermion system exhibits the famous BCS instability at low temperature, discovered by Bardeen, Cooper and Schrieffer [6; 7]. In a very basic physical picture, two fermions form a "Cooper pair", which is a bosonic entity. These bosonic objects can successively condense.

Although the underlying pictures are thus quite different, both phenomena share a decisive feature in common: They can be described as the spontaneous breaking of the global symmetry of phase rotations, $U(1)$. Due to this similarity concerning the macroscopic properties of fermionic and bosonic systems, it is plausible that the two scenarios sketched above are connected by some smooth transition or crossover. The theoretical description of the crossover phenomenon was pioneered by Eagles, Leggett and Nozières *et al.* [8–10], and put into a functional integral formulation in [11]. The authors showed that, in a fermionic system whose interaction is uniquely characterized by the scattering length a, a crossover from BCS- to BEC-type physics takes place as a function of the *inverse* scattering length evolving from large negative (BCS regime) to large positive (BEC regime) values, passing a strongly interacting "crossover region". Again evoking a simple physical picture, the position-space delocalized Cooper pairs characteristic for the BCS regime undergo a localization process throughout the crossover, ending up as effectively pointlike bosonic particles or strongly bound molecules in the BEC regime.

At this point, ultracold fermion gases come into play [12–14]. The experimental

progress in trapping, cooling and manipulating such systems has been breathtaking throughout the last few years. The presence of Feshbach resonances in systems like ^{6}Li or ^{40}K is at the heart of recent developments. This phenomenon offers the unique possibility to tune the interaction strength between the atoms to arbitrary positive and negative values, thereby allowing for an experimental realization of the crossover [15–20]. This sparked a number of theoretical investigations, for which two major strategies can be identified.

In the spirit of the early approaches, Strinati *et al.* propose a purely fermionic or single-channel description of the crossover problem within the operator formalism [21–25]. A similar approximation scheme is advocated in [26].

Inspired by the observables of concrete physical systems, other approaches formulate the problem microscopically in terms of a Yukawa theory for fermionic atoms and bosonic molecules [27–38]. These two-channel models are, in part, motivated by a functional integral [28; 35; 36]. Approaches of this type feature more microscopic parameters, but are well suited for dealing with nonlocal interactions.

From a field theoretical perspective, ultracold quantum gases constitute a very attractive area of research. The microscopic physics is well under control and precisely known – this situation is very different from many high energy physics issues or condensed matter systems, where the microphysics is usually inaccessible to manipulations and/or only poorly known. For the many-body system, one can therefore hope to assess not only universal quantities as e.g. critical exponents, but also non-universal, i.e. system specific observables, examples being the critical temperature or the condensate fraction in the superfluid phase. In particular, the strong interactions in cold gases near a Feshbach resonance clearly motivate an analysis with advanced methods beyond mean field theory. Reversing the perspective, the wealth of experimental data can provide a benchmark for the predictivity and accuracy of modern field theoretical methods.

The aim of the investigation presented in this thesis is to provide a universal field theoretical description of the crossover problem. Microscopically, we start from the Yukawa-type model (3.1). The basic ingredient is the formulation of the full quantum mechanical problem in terms of a functional integral for the effective action. This enables us to fully exploit the power of symmetry considerations, allowing for both a systematic construction of the equation of state and the classification of the thermodynamic phases of the system. At the same time, it makes the crossover problem accessible to the wealth of techniques available in quantum field theory and statistical mechanics, as e.g. Schwinger-Dyson equations (chapt. 5) or functional renormalization group methods (chapt. 7). Among many other issues, our functional integral approach also reconciles the two strategies for modelling the problem discussed above, by showing in which limit they are equivalent.

In more detail, this thesis is organized as follows.

In chapt. 2, we discuss the relevant scales and interactions encountered in cold atom gases. Further, we sketch the basic features of Feshbach resonances, which constitute the microphysical basis for the experimental resolution of the crossover in cold fermion gases.

In chapt. 3 our microscopic model in terms of a Yukawa-type action for non-relativistic fermion (atom) and boson (composite molecule) fields is motivated. An efficient set of parameters for the description of the thermodynamics of the crossover problem is pointed out, which is related to a dimensionless "scaling form" of our model.

Chapt. 4 comprises the basic field theoretical construction for the analysis of the crossover. It is based on a functional integral representation of the effective action. By a successive elimination of fermion and boson modes, we evaluate the functional integral in a systematic one-loop approximation for both fermion and molecule fluctuations. This procedure already gives a full picture of the transition from BCS-to BEC-type physics. In this framework, we construct the equation of state from a symmetry consideration, and show how the important concept of dressed bosonic fields emerges naturally from our derivation. We also settle the connection to the thermodynamic construction of the equation of state, introducing the notion of an effective chemical potential. After some technical details concerning the ultraviolet renormalization of our theory, we pass to the classification of the thermodynamic phases in the effective action formalism. The superfluid regime is described in terms of spontaneous breaking of the global $U(1)$ symmetry.

In chapt. 5 we refine our approximation scheme by the use of suitable Schwinger-Dyson equations for the effective boson (or molecule) propagator. We give explicit formulae determining the observables in this approximation in the different thermodynamic phases. Applications are presented, and we find good agreement with Quantum Monte Carlo data at zero temperature, cf. fig. 5.5. We also discuss shortcomings of the Schwinger-Dyson approach which are most severe in the superfluid phase close to the critical temperature – in particular, the phase transition is of first order. We then pass to the discussion of a low density limit for the effective action in the Schwinger-Dyson approach. This allows to make contact to concrete atomic systems investigated experimentally, as ^{6}Li or ^{40}K. Furthermore, we successfully compare the predictions of our formalism to a recent experiment focusing on the "bare molecules", cf. fig. 5.11.

Chapt. 6 encompasses several aspects of "enhanced universality" which we have identified in the crossover problem. This notion refers to the irrelevance of different microscopic parameters in the sense of statistical mechanics. We first discuss enhanced universality qualitatively, taking our result for the phase diagram (fig. 6.1) as an example. We then make our statements more quantitative, considering the functional integral in certain limiting cases for the model parameters. Our analysis

covers narrow and broad resonances and a thorough discussion of BCS, BEC and resonance regime, and we investigate the validity of the approximations used. As a main result, we find a new form of crossover from narrow to broad resonances, physically interpreted as a crossover from weak nonlocal to strong pointlike interactions. For narrow resonances we provide an exact solution of the many-body problem, while we can establish the equivalence of our two-channel model with a purely fermionic approach in the broad resonance limit.

In chapt. 7 the first steps for the systematic analysis of the crossover problem in the frame of the functional renormalization group (FRG) are taken. First we analyze the two-body problem in detail. We can establish a substantial improvement for the ratio of molecular vs. fermionic scattering length compared to the Schwinger-Dyson approach. Concerning the many-body problem, we focus on the BEC regime. As a first success, we can establish the features of a Bogoliubov-type theory at low temperature, while the phase transition is of second order.

The last chapter contains a discussion of the results obtained in this thesis. It further points out the issues that should be attacked next, and gives a perspective where the formalism developed here could be applied in the future.

Large parts of this thesis are based on the references [39; 40].

Chapter 2

Interactions in Ultracold Gases

2.1 Scales and Interactions

In atomic physics, the true position space interaction potentials are, in general, complicated functions of the interparticle distance between the interacting atoms. However, at sufficiently low energies, the atoms behave like point particles with short-range interactions. In this section we will argue qualitatively why this is so, and introduce the most important length or momentum scales for interacting atoms at low temperature and density.

For neutral atoms, both the generic short-range and long-range behavior can be easily understood in terms of electromagnetic interactions: At small separations of the nuclei, the Born-Oppenheimer potential provided by the ground state energy of the electron clouds results in a short-range hard core repulsion. The length scale associated with this repulsion is the atomic radius r_A which is of the order of magnitude of several Bohr radii $a_B = 5.29177 \cdot 10^{-11}$m, e.g. for ^{6}Li $r_A \approx 3a_B$. This provides an ultraviolet cutoff $\Lambda = \pi/r_A$ in momentum space. At distances much larger than the extent of the electron cloud of each of the atoms, the interaction energy is dominated by van der Waals interactions which arise from the polarizability of the electron clouds – the electric dipole-dipole interactions cause a power-law behavior with the asymptotic form

$$V(r) \to -\frac{C_6}{r^6} \quad \text{for} \quad r \to \infty. \tag{2.1}$$

The shape of a typical position space interaction potential is depicted in fig. 2.1 (where we plot potentials characteristic for a Feshbach resonance). At the low energies available in an ultracold gas (see below), the interactions are dominated by the van der Waals tails of the potential. A characteristic length scale for the interaction

can be obtained from balancing kinetic and potential energy of the two particles [1],

$$\frac{1}{Mr^2} \approx \frac{C_6}{r^6}, \tag{2.2}$$

(M the atomic mass) resulting in the so-called van der Waals length or characteristic range

$$l_{vdW} = (MC_6)^{1/4}. \tag{2.3}$$

The van der Waals length for alkali atoms is roughly two orders of magnitude larger than the atomic radii (e.g. ^{6}Li : $62.5a_B$,^{40} K : $130a_B$). The van der Waals momentum is given by $k_{vdW} = 1/l_{vdW}$. It sets a natural scale for the interaction parameters which characterize the scattering of two particles.

The most important parameter describing low momentum scattering is the scattering length a. This quantity is extracted from the zero energy limit of the scattering amplitude in the center-of-mass system (cf. app. A for detailed definitions). At the low energies available in ultracold gases, scattering in higher angular momentum states is suppressed and the scattering is purely s-wave (angular momentum $l = 0$). If a momentum dependence of the s-wave scattering length needs to be included, this is parameterized to lowest order by the effective range (see appendix A for more precise definitions of these quantities). Importantly, the scattering length can be strongly enhanced compared to the natural scale l_{vdW}. This takes place when a bound state in the interaction potential is close to the scattering threshold and requires very particular circumstances, as realized e.g. near a Feshbach resonance.

Let us consider the typical length and momentum scales that appear in trapped dilute ultracold gases. They are set by the thermodynamic properties of the system, i.e. temperature (mean kinetic energy of a particle) and particle density. The latter are in the range of $10^{13}...10^{15}\mathrm{cm}^{-3}$, if we take the peak densities in a trap as a measure. This corresponds to typical particle interspacings $d = (3\pi^2 n)^{-1/3}$ between $(600...3000)a_B$. The corresponding momentum scale is the Fermi momentum [2] $k_F = 1/d$. A length scale characterizing the temperature is set by the thermal de Broglie wavelength $\lambda_{dB} = \sqrt{2\pi/(MT)}$, which is in the range of $(5...40)10^3 a_B$, i.e. roughly an order of magnitude larger than the interparticle spacing. "Ultracold" means $\lambda_{dB}/d \gg 1$ or $k_{dB}^2/k_F^2 = T/(4\pi\epsilon_F) \ll 1$, with $k_{dB} = 1/\lambda_{dB}$ the de Broglie wave number and $\epsilon_F = k_F^2/2M$ the Fermi energy. This is the regime where the statistics of the particles matter, and quantum effects play a crucial role. Finally, the trap is parameterized by the oscillator length l_{osc}, $(3...300)10^3 a_B$. The characteristic oscillator momentum is again defined as the reciprocal length scale $k_{osc} = 1/l_{osc}$.

[1] Our units are $\hbar = c = k_B = 1$.

[2] In bosonic systems, k_F is not related to the Fermi surface, but the definition $k_F = (3\pi^2 n)^{1/3}$ as a measure of typical inverse interparticle spacings is still sensible.

length	r_A/a_B	l_{vdW}/a_B	d/a_B	λ_{dB}/a_B	l_{osc}/a_B
	2..4	50..200	$(0.6..2.8)\cdot 10^3$	$(8.8..39)\cdot 10^3$	$(2.9..290)\cdot 10^3$
momentum	Λ/eV	k_{vdW}/eV	k_F/eV	k_{dB}/eV	k_{osc}/eV
	$(0.5..2)\cdot 10^3$	19..75	1.3 .. 6.1	0.1 .. 0.4	0.01 .. 1.3

Table 2.1: Typical length and momentum scales in ultracold atom systems. For a momentum k, the corresponding energy is given by $k^2/2M \ll k$. Energies and momenta should therefore not directly be compared for a nonrelativistic problem ($a_B = 5.29177\cdot 10^{-11}$m, 1eV$\hat{=}(3.7290\cdot 10^3 a_B)^{-1}$. 1eV corresponds to a density $n = 4.4\cdot 10^{12}\text{cm}^{-3}$.).

Obviously, these momentum scales are much below the typical scales for the interaction. In position space, this means that the atoms do not resolve the shape of the potential at much lower distances than the de Broglie wave length or the interparticle spacing. In turn, it is clear that the details of the short range interaction cannot play a role for the interaction in the ultracold gases. It is sufficient to characterize the interaction potential by a few numbers, and in many cases, the scattering length alone is enough. Furthermore, the precise shape of the potential at distances smaller than the characteristic range is irrelevant. Instead, the true interaction potential can be replaced by a model potential with the only constraint to reproduce the low energy observables as the scattering length and the effective range as measured in experiment. To see this, we consider a contact potential $V(\vec{r}) = \lambda_\Lambda \delta(\vec{r})$ characterized by a single number λ_Λ and compute the effective two-body interaction for fermionic particles by summing up all the particle-particle diagrams, regularizing the momentum space integrals with a sharp ultraviolet cutoff Λ,

$$a = \frac{M}{4\pi}\lambda_{eff} = \frac{M\lambda_\Lambda}{4\pi(1 + M\lambda_\Lambda\Lambda/(2\pi^2))}. \tag{2.4}$$

Clearly, the low energy scattering properties strongly depend on the choice of λ_Λ, and by tuning the microscopic contact interaction for a fixed cutoff Λ, arbitrary positive and negative values of the scattering length can be reached. On the other hand, a single parameter λ_Λ is sufficient to mimic the effects of a complicated interaction potential featuring the same scattering length a. This is the reason why the latter can be replaced by the very simple model potential. Much of the information on the way down to low momentum scales is lost. The fact that nature is organized in scales which do not "see" each other is called universality. In this work, we will also consider aspects of this phenomenon in chapt. 6.

A particularly interesting situation occurs when the scattering length a is tuned to values where it exceeds all other length scales in the problem. In this case, the length scale a drops out and the physics should become independent of a. For a thermodynamic situation at finite density and temperature, a large scattering length is already realized if the diluteness parameter $a/d = ak_F \gg 1$ with d the mean

interparticle spacing. This is another aspect of universality which we deal with in chapt. 6. In that sense, systems with large ak_F are not dilute, and ak_F cannot be used as an expansion parameter for any calculation as done for $ak_F \ll 1$ (e.g BCS and Bogoliubov theory, cf. the next chapter). For the two body problem, the condition for a large scattering length is $a/l_{vdW} \gg 1$. Such circumstances can indeed be created in systems exhibiting Feshbach resonances.

In this work, we consider systems whose basic constituents are fermions. Unlike for bosons and caused by Pauli's principle, two identical fermions cannot interact via s-wave collisions (their scattering cross section vanishes, cf. app. A). Hence the observed scattering length is related to scattering of distinguishable fermions, which can be discriminated by their spins.

We finally note that the mass M of the particles does not set a true scale for the problem. It corresponds to a much larger momentum than all other scales in the problem, comparing it e.g. to the ultraviolet cutoff we get $M \sim 10^6\Lambda$. This reflects the fact that we are dealing with a nonrelativistic problem. It sets the classical dispersion relation for the atoms, $E = k^2/2M$ – energy and momentum scale very differently in the nonrelativistic setup. We can account for this fact by rescaling energy and momentum differently. For a Fermi gas, we measure momenta in units of the Fermi momentum k_F and energies in units of the Fermi energy $\epsilon_F = k_F^2/(2M)$. This yields a dimensionless version of the problem where all numbers are $\mathcal{O}(1)$.

A review on effective field theories for nonrelativistic few-body systems is given in [41].

2.2 Feshbach Resonances

Feshbach resonances constitute the microphysical phenomenon which make the resolution of the crossover from BCS to BEC in cold fermion systems accessible to experiments. They allow to tune the effective interaction strength between the atoms to arbitrary values in a controlled way.

We consider the scattering of two alkali atoms whose internal states are characterized by the eigenvalues of the spin of the valence electron S and the nuclear spin I. The fermionic or bosonic nature is determined by the *total* spin of the atoms.

The occurrence of a Feshbach resonance is related to the spin of the valence electron. The picture described in the following therefore applies to both fermions and bosons. In a rough approximation, a single atom can viewed as an eigenstate of the spin operator $\mathbf{S}$ of the electron. Two atoms can either form a spin singlet or a triplet. The position space interaction potentials are very different for both

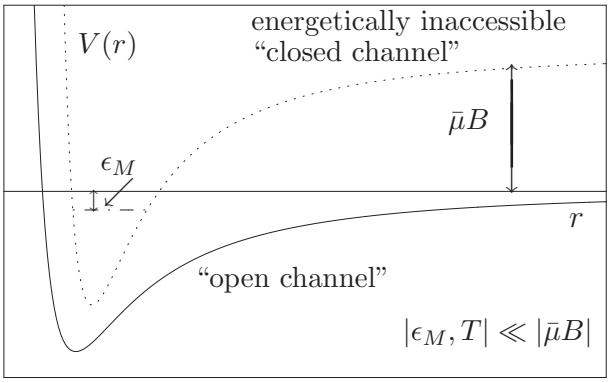

Figure 2.1: Interaction potentials for a Feshbach resonance. A resonance phenomenon is observed when the zero of energy in the open channel hits the energy level of a bound state in the closed channel. If the bound state level is below the zero of energy, a two-body bound state with binding energy ϵ_M forms.

two-body states. The singlet interaction potential is usually much deeper than the triplet potential due to Pauli's principle for the electron spins [3].

When the atoms are put in an external magnetic field, the zeroes of energy of the two internal states are shifted against each other due to Zeeman's effect by an amount $\bar{\mu}B$, where B is the magnetic field and $\bar{\mu}$ is related to the difference between the magnetic momenta of the triplet and singlet channel with $\mu_B = 5.788 \cdot 10^{-11}\,\mathrm{MeV/T} = 0.2963\,\mathrm{MeV}^{-1}$ the Bohr magneton, a rough estimate for the difference in magnetic moments is $\bar{\mu} \approx 2\mu_B$ – this just reflects the difference between the magnetic moments of singlet and triplet state. The energy difference between the two states is usually much larger than the typical energy scales in ultracold gases characterized e.g. by the temperature, $T \ll |\bar{\mu}B|$. The upper channel is therefore energetically inaccessible for atoms making up ultracold gases.

In real physical systems, singlet and triplet states are not orthogonal, but coupled to each other. The origin of this coupling is the hyperfine interaction $\propto \mathbf{S} \cdot \mathbf{I}$, which can cause spin flips in each of the atoms. This effectively mixes singlet and triplet states and might cause deviations from $\bar{\mu} = 2\mu_B$. Indeed, while for ^{6}Li the latter approximation is rather accurate [42], in ^{40}K one finds $\bar{\mu} = 1.57\mu_B$ [43]. We refer to the modified states for the two-body problem as the "open" and "closed" channel states. This situation is illustrated in fig. 2.1. The central ingredient for a Feshbach resonance is the existence of a bound state in the closed channel.

[3] An important exception is ^{6}Li, which we will consider in this work. Here the triplet potential is much deeper, having an anomalously large background scattering length adding to the Feshbach resonance.

To see this, we consider the atoms in the open channel at large interatomic separations. The resonance, as observed by the divergence of the scattering length [4], takes place when the zero of energy in the open channel hits a bound state level in the closed channel. Qualitatively, this can be understood from considering perturbation theory for the scattering amplitude, where the perturbation parameter is the coupling (squared transition matrix element) between the open and closed channel. The zero order contribution describes the non-resonant scattering in the open channel. The first order contribution vanishes, since the continuum states of the closed channel are energetically inaccessible as argued above. To second order, there is a contribution, exhibiting the characteristic resonance energy dependence $1/(E - E_0)$. The total scattering length takes the form

$$a(B) \;=\; a_{bg} + \frac{\kappa}{E - E_0} = a_{bg} + \frac{\kappa}{\bar{\mu}(B - B_0)} = a_{bg}\Big(1 + \frac{\Delta B}{B - B_0}\Big). \qquad (2.5)$$

Here a_{bg} represents the energy-independent non-resonant or "background" scattering in the open channel. κ is the (squared) transition matrix element between the scattering state in the open channel and the bound state in the closed channel. The dependence on the magnetic field relies on the assumption of a linear dependence of the energy on the magnetic field, with $\bar{\mu}$ the difference in magnetic moments for open channel and closed channel atom pairs (again, $\bar{\mu} \approx 2\mu_B$ if the mixing between singlet and triplet states is not very strong). This contribution is called the resonant scattering length. It is worth noting that the contributions to the total scattering length – which parameterize the coupling strength between the fermionic atoms – are physically clearly distinguished by the energy dependence of the second contribution. They describe different physical effects, which will motivate the model presented in the next section.

As mentioned above, the scattering length is associated to scattering at very low momenta. If the true interaction is pointlike, the scattering length indeed is sufficient to fully characterize scattering processes, and only the ratio $\Delta = \kappa/\bar{\mu}$ is a physical quantity. However, for non-local interactions (for nonrelativistic collisions, the simplest modification is through the effective range), a further scale is introduced in the problem and the information encoded in the scattering length alone is insufficient.

The last expression in (2.5) is the standard parameterization of a Feshbach resonance in terms of three parameters: background scattering length a_{bg}, width of

[4] In practice, the divergence of the scattering length is not observed, since at some point, the momentum dependence of the scattering amplitude cannot be neglected. The scales of these momenta are set by the de Broglie wavelength and the oscillator length. Indeed, the unitarity of the S-matrix does not allow for a diverging cross section. This has been observed in [44; 45]. The divergence of the scattering length can, however, be concluded on the BEC side of the resonance from the measurement of the binding energy vanishing as $\epsilon_M = -1/a^2$ in approaching the resonance [46].

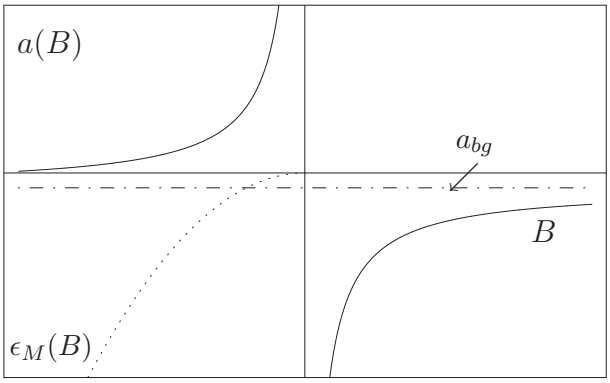

Figure 2.2: Schematic plot of the scattering length a and binding energy ϵ_M as a function of magnetic field B close to a Feshbach resonance. The observed scattering length is characterized by three parameters as described in the text.

the resonance ΔB and the resonance position B_0. Clearly, these parameters are not independent – the width of the resonance is characterized by the ratio $\kappa/\bar{\mu}$.

The key to create large scattering lengths is the fine-tuning of the interaction potentials close to a two-body bound state. As argued above, the divergence of the scattering length is a generic feature that can be observed for very simple contact or single-channel square well potentials. Here, the fine-tuning is provided by a variation of the strength of the potential, and the phenomenon is known as a shape resonance. It is, however, not easy to manipulate the shape of a given interaction potential in practice. The remarkable point about Feshbach resonances is to provide a means to manipulate the interaction strength by tuning an *external parameter*, i.e. the magnetic field B.

As mentioned in the introduction, it is the aim of this thesis to develop a quantum field theoretical description for the crossover problem. In the spirit of effective field theories, we do not ask for the microscopic mechanism responsible for the Feshbach resonance. Instead, we take a set of independent parameters which fully characterizes the two-body system as an input for our theory. Additionally, thermodynamic scales as temperature and particle density enter our formalism. All these parameters must be determined experimentally. The observables which we want to predict will then be expressed in terms of these variables. Most of these observables will be thermodynamic quantities (e.g. the condensate fraction or the critical temperature), but we can also focus on two-body observables as the effective molecule-molecule scattering length on the BEC side of the resonance, which is not an independent observable, but fully determined by the measured parameters indicated below.

For more extensive reviews on Feshbach resonances, cf. [36; 47; 48].

Chapter 3

Microscopic Model

With the physical picture from the last chapter in mind, we can write down the euclidean Yukawa-type bare microscopic action in position space [27–38]:

$$\begin{aligned} S[\bar{\psi},\bar{\phi}] \;=\; & \int d\tau \int d^3x \Big[\bar{\psi}^\dagger \big(\partial_\tau - \frac{\triangle}{2M} - \sigma\big)\bar{\psi} + \frac{\bar{\lambda}_{\psi,\Lambda}}{2}(\bar{\psi}^\dagger\bar{\psi})^2 \\ & + \bar{\phi}^* \big(\partial_\tau - \bar{A}_\phi^{(cl)}\triangle + \bar{\nu}_\Lambda - 2\sigma\big)\bar{\phi} - \frac{\bar{h}_{\phi,\Lambda}}{2}\Big(\bar{\phi}^*\bar{\psi}^T\epsilon\bar{\psi} - \bar{\phi}\bar{\psi}^\dagger\epsilon\bar{\psi}^*\Big)\Big]. \end{aligned} \tag{3.1}$$

Here, $\bar{\psi}$ and $\bar{\phi}$ can be viewed as classical fields – they will be quantized by the means of a functional integral in the next chapter. We refer to the fields with a bar on top as bare fields. In this work, we will also encounter "dressed" or "renormalized" fields which are related to the bare fields by a rescaling with a wave function renormalization factor. For those we omit the bar. In the following, we motivate this action in more detail. In particular, we explain the field and parameter content of this object. Further, we perform some preparations in the view of the thermodynamic situation which we analyze in the following chapters.

3.1 Field Content and Symmetries

Fermion Field

The fermion field $\bar{\psi}$ represents the stable atoms. It is a Grassmann valued non-relativistic 2-spinor $\bar{\psi} = (\bar{\psi}_1, \bar{\psi}_2)$ [1]. The dagger operation is implemented by $\bar{\psi}^\dagger = \bar{\psi}^{*T}$. The spin components $\bar{\psi}_1, \bar{\psi}_2$ represent eigenstates to the total spin operator $\mathbf{F} = \mathbf{S} + \mathbf{I}$. In experimental setups, one uses the two lowest hyperfine states

[1] The bar has nothing to do with a multiplication by the Dirac matrix γ^0 for relativisic 4-spinors.

$|1\rangle, |2\rangle$ (e.g. $|1\rangle = |F = 1/2, m_F = -1/2\rangle, |2\rangle = |F = 1/2, m_F = 1/2\rangle$ for ^{6}Li [2] and $|1\rangle = |F = 9/2, m_F = -9/2\rangle, |2\rangle = |F = 9/2, m_F = -7/2\rangle$ for ^{40}K).

Boson Field

A composite boson field $\bar{\phi}$ is coupled to the fermion fields in the Yukawa term in the second line. The resonant interaction between the fermions is modelled as an exchange of a boson. The corresponding tree-level process is depicted in fig. 3.1. The boson field, representing the closed channel molecules, is given a classical inverse propagator term according to simple symmetry considerations, see below.

Current σ

The current σ enters linearly in the microscopic action. It couples to both the operator $\bar{\psi}^\dagger\bar{\psi}$ and $2\phi^*\phi$. Its physical meaning depends on the situation we intend to analyze. For example, it plays the role of an effective chemical potential in the thermodynamic context. In the two-body system, which can also be described in the effective action formalism, it represents the binding energy of a molecule. It couples with double strength to the boson field due to their compositeness as mentioned above.

The theory has a global [3] $U(1)$ symmetry,

$$\bar{\psi} \to \exp(i\theta)\bar{\psi}, \qquad \bar{\phi} \to \exp(2i\theta)\bar{\phi}. \tag{3.2}$$

The corresponding conserved charge is the particle number. We will come back to this point in the next chapter. The double coupling strength of the bosons to the chemical potential is directly related to the double phase for $\bar{\phi}$ in (3.2) – the composite objects have atom number 2.

A second symmetry is global $SU(2)$, reflecting invariance of (3.1) under spin rotations. The ϕ field is invariant under this transformation, i.e. it represents a spin zero particle. Further, the kinetic terms for both the fermions and the bosons are Galilean invariant as appropriate for nonrelativistic particles.

The closed channel does not need to be included in our model by an extra fermion field, since its weight is suppressed by a factor $\exp -\bar{\psi}^\dagger_{cl}\bar{\mu}B\bar{\psi}_{cl}$ relative to the open

[2] Lithium (^{6}Li) is usually probed at high magnetic fields in the Paschen-Back regime ($B \gg 30$G) where the nuclear and the electronic spin decouple completely. Hence better quantum numbers are $|1\rangle = |S = 1/2, m_S = -1/2, I = 1, m_I = 1\rangle, |2\rangle = |S = 1/2, m_S = -1/2, I = 1, m_I = 0\rangle$. Here the triplet state is energetically below the singlet, unlike most other types of atoms.

[3] Do not expect a local gauge symmetry, though the true physical interactions are mediated by the electromagnetic field. Those interactions are "integrated out" from the outset, and replaced by the microscopic parameters of our model.

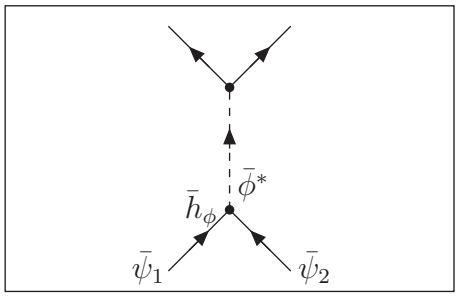

Figure 3.1: Tree exchange of a molecule.

channel atoms in the functional integral. The closed channel enters only implicitly in our formulation, giving rise to the resonant interaction between the open channel atoms.

The action (3.1) is local in position space. However, when two fermions $\bar{\psi}_1, \bar{\psi}_2$ in the hyperfine states $|1\rangle, |2\rangle$ interact to form a boson at $X_1 = (t_1, \vec{x}_1)$, this object can propagate to another position $X_2 = (t_2, \vec{x}_2)$ and decay into two fermions again. Hence this form of the interaction allows for effectively non-local processes. To be more precise, it is advantageous to consider the action (3.1) in momentum space – "momentum" here means frequency and spacelike momenta. Our conventions for momenta are

$$Q = (\omega, \vec{q}), \quad \int\limits_Q = \sum_{n=-\infty}^{\infty} T \int \frac{d^3q}{(2\pi)^3}. \tag{3.3}$$

The trace over frequency is a discrete sum over the Matsubara modes for finite temperature applications due to (anti-) periodic boundary conditions for fermion (boson) fields in timelike direction ($\omega_F = (2n+1)\pi T, \omega_\phi = 2n\pi T$ for fermions resp. bosons [4]). For the Fourier transforms we define

$$\bar{\psi}(X) = \int\limits_Q \exp(\mathrm{i}QX)\bar{\psi}(Q), \quad \bar{\psi}^\dagger(X) = \int\limits_Q \exp(-\mathrm{i}QX)\bar{\psi}^\dagger(Q), \tag{3.4}$$

and analogous for $\bar{\phi}(X), \bar{\phi}^*(X)$. We treat σ as a constant which is not Fourier trans-

[4] At zero temperature, the Matsubara sum is replaced by a continuous integration, $T \sum\limits_{n=-\infty}^{\infty} \to \int \frac{dq_0}{2\pi}$.

formed. Eq. (3.1) reads in momentum space

$$\begin{aligned} S &= \int_Q \bar{\psi}^\dagger(Q)\big(\mathrm{i}\omega_F + \frac{\vec{q}^2}{2M} - \sigma\big)\bar{\psi}(Q) + \bar{\phi}^*(Q)\big(\mathrm{i}\omega_\phi + \bar{A}_\phi^{(cl)}\vec{q}^2 + \bar{\nu}_\Lambda - 2\sigma\big)\bar{\phi}(Q) \\ &\quad -\frac{\bar{h}_{\phi,\Lambda}}{2}\int_{Q_1\ldots Q_3}\delta(Q_1-(Q_2+Q_3))\big[\bar{\phi}^*(Q_1)\bar{\psi}^T(Q_2)\epsilon\bar{\psi}(Q_3) - \bar{\phi}(Q_1)\bar{\psi}^\dagger(Q_2)\epsilon\bar{\psi}^*(Q_3)\big] \\ &\quad +\frac{\bar{\lambda}_{\psi,\Lambda}}{2}\int_{Q_1\ldots Q_4}\delta(Q_1-Q_2+Q_3-Q_4)(\bar{\psi}^\dagger(Q_1)\bar{\psi}(Q_2))(\bar{\psi}^\dagger(Q_3)\bar{\psi}(Q_4)). \end{aligned} \tag{3.5}$$

In order to investigate the momentum structure of the interaction, we can now integrate out the quadratic boson field by formally solving the field equation for $\bar{\phi}$, $\delta S/\delta\bar{\phi} = 0$, for nonvanishing $\bar{\psi}^T\epsilon\bar{\psi}$. This solution becomes then a functional of $\bar{\psi}$. Reinserting it into S yields the "tree contribution" to the four-fermion vertex, whose contribution to the action reads

$$S_{int,R} = \frac{1}{4}\int_{Q_1\ldots Q_4}\delta_{Q_1+Q_3,Q_2+Q_4}\big(\bar{\psi}^T(Q_1)\epsilon\bar{\psi}(Q_3)\big)\big(\bar{\psi}^\dagger(Q_2)\epsilon\bar{\psi}^*(Q_4)\big)\frac{\bar{h}^2_{\phi,\Lambda}}{\bar{P}_{\phi,cl}(Q_1+Q_3)} \tag{3.6}$$

($\delta_{K,P} = \delta(K-P)$) with the classical inverse boson propagator

$$\bar{P}_{\phi,cl}(Q) = \mathrm{i}\omega_\phi + \bar{A}_\phi^{(cl)}\vec{q}^2 + \bar{\nu}_\Lambda - 2\sigma. \tag{3.7}$$

This shows the equivalence of our Yukawa type theory (3.1) to a purely fermionic model with a particular frequency and momentum - dependence for the (resonant) four-fermion coupling $\bar{\lambda}_R(Q_1...Q_4)$. Importantly, we learn from eq. (3.6) that the propagation is strongest for *opposite* fermion momenta (for fixed mass term [5]), as it should be for a bound state. We will therefore often refer to the composite boson as a "molecule", though we are not always dealing with stable particles. This issue is treated in detail in chapts. 4 and 7.

We can rearrange the discrete index structure in (3.6) and collect the pieces of the effective four-fermion interaction together:

$$S_{int} = \frac{1}{2}\int_{Q_1\ldots Q_4}\delta_{Q_1+Q_3,Q_2+Q_4}\big(\bar{\psi}^\dagger(Q_1)\bar{\psi}(Q_2)\big)\big(\bar{\psi}^\dagger(Q_3)\bar{\psi}(Q_4)\big)\Big\{\bar{\lambda}_{\psi,\Lambda} - \frac{\bar{h}^2_{\phi,\Lambda}}{\bar{P}_{\phi,cl}(Q_1+Q_3)}\Big\}. \tag{3.8}$$

[5] In this expression we give the classical, not UV renormalized mass term. In a more thorough treatment, one should of course solve the field equation for ϕ of the effective action taking fluctuations into account, which always features a positive mass term. We will comment on this in chapts. 4 and 7.

In case of pointlike interactions (kinetic terms in (3.7) unimportant), the resonant and background interaction can be separated by measuring the interaction as a function of magnetic field, see below. This resolves the Feshbach resonance from the B-independent background scattering as parameterized in eq. (2.5).

3.2 Parameter Content and Choice of Variables

The "bare" quantities displayed in the microscopic action cannot directly be related to their corresponding parameters measured in the physical vacuum. This is due to vacuum fluctuations which are not included in (3.1). Relating the bare to the observable parameters is known as ultraviolet (UV) renormalization. We postpone this issue to the next chapter and chapt. 7 and point out the meaning of the observable, UV renormalized quantities here.
(i) The Yukawa or Feshbach coupling $\bar{h}_\phi$ measures the width of the Feshbach resonance. It represents the coupling of open and closed channels,

$$\bar{h}_\phi^2 = \kappa. \tag{3.9}$$

(ii) The detuning parameter $\bar{\nu}$ indicates the distance from the resonance. It is related to the magnetic field by

$$\bar{\nu} = \bar{\mu}(B - B_0). \tag{3.10}$$

The zero of $\bar{\nu}$ yields the position of the Feshbach resonance. This parameter makes the interaction (3.8) energy (magnetic field) dependent. Tuning B allows to sweep across the Feshbach resonance.
(iii) The pointlike four-fermion "background" interaction $\bar{\lambda}_{\psi,0}$. This term models the non-resonant scattering in the open channel and does not depend on external parameters as the magnetic field to a good approximation. It is therefore physically distinct from the resonant interaction, which corresponds to an explicit energy dependence (through the magnetic field) of an effective four-fermion interaction (cf. the next subsection). Its sign can be both negative (^{6}Li) and positive (^{40}K).
(iv) The classical gradient coefficient $\bar{A}_\phi^{(cl)}$ for the bosons. It is related to an effective range by

$$r_s = 2\bar{A}_\phi^{(cl)}/\bar{h}_\phi^2, \tag{3.11}$$

cf. app. A, eq. (A.8), and eq. (3.8). By a simple symmetry consideration one would conclude $\bar{A}_\phi^{(cl)} = 1/(4M)$ – the bosons then have double fermion mass. No UV renormalization is needed for $\bar{A}_\phi^{(cl)}$, such that we do not need to distinguish between $\bar{A}_\phi^{(cl)}$ and $\bar{A}_{\phi,\Lambda}^{(cl)}$.

The choice of 1 as coefficient of the frequency dependence in the classical boson propagator normalizes to a standard time evolution (in Minkowskian position space) of the closed channel molecules. This choice can also be viewed as measuring all the couplings in the boson propagator in units of the coefficient of $\mathrm{i}\omega$.

The space of model parameters for the crossover problem is hence spanned by $\{\bar{\nu}, \bar{h}_\phi^2, \bar{\lambda}_{\psi,0}, \bar{A}_\phi^{(cl)}\}$. However, another equivalent set of parameters, $\{a^{-1}, \bar{h}_\phi^2, \bar{\lambda}_{\psi,0}, \bar{A}_\phi^{(cl)}\}$, where a is an appropriately defined in-medium scattering length (see below), describes the system more efficiently and reveals the aspects of universality (chapt. 6) more clearly.

In the pointlike limit [6] the momentum dependence in eq. (3.8) can be neglected and the effective coupling is replaced by the "local interaction approximation"

$$\bar{\lambda}_\psi = -\frac{\bar{h}_\phi^2}{\bar{\nu} - 2\sigma} + \bar{\lambda}_{\psi,0}. \tag{3.12}$$

Using the relation between four-fermion coupling $\bar{\lambda}_\psi$ and a scattering length a for distinguishable fermions (cf. app. A, eq. (A.12)), we can define an effective in-medium *resonant* scattering length $a_R(\sigma)$ and a background scattering length a_{bg},

$$a_R(\sigma) = \frac{M\bar{\lambda}_R}{4\pi} = -\frac{M\bar{h}_\phi^2}{4\pi(\bar{\nu} - 2\sigma)}, \quad a_{bg} = \frac{M\bar{\lambda}_{\psi,0}}{4\pi}. \tag{3.13}$$

σ introduces a medium dependence on the resonant scattering length. The total in-medium scattering length reads

$$a(\sigma) = a_R(\sigma) + a_{bg}. \tag{3.14}$$

In the important case $a_{bg} = 0$ (which we will analyze most thoroughly in this work), we obviously have $a_R = a$.

The impact of the choice of variables $\{a^{-1}, \bar{h}_\phi^2, \bar{\lambda}_{\psi,0}, \bar{A}_\phi^{(cl)}\}$ instead of $\{\bar{\nu}, \bar{h}_\phi^2, \bar{\lambda}_{\psi,0}, \bar{A}_\phi^{(cl)}\}$ is twofold. First, it absorbs a good deal of the $\bar{h}_\phi$-dependence in the final results. In the language of critical phenomena, the scattering length a is a relevant parameter, whereas $\bar{h}_\phi$ is marginal. A more systematic discussion of the importance of the Feshbach coupling $\bar{h}_\phi$ is given in chapt. 6. Second, the choice of a relates our formulation based on a Yukawa model more closely to an interacting fermion system, where the effective scattering length is a crucial parameter as discussed above. However, a careful analysis of the vacuum properties of the crossover system shows that the physical fermionic scattering length is given by

[6] Later we will argue that the pointlike limit can be established by $\bar{h}_\phi \to \infty$, $\bar{\nu} \propto \bar{h}_\phi^2$. This settles the connection between broad Feshbach resonances and the pointlike limit, for which a purely fermionic description as discussed by Strinati *et al.* [21–25] is appropriate.

$a' = a(\sigma = 0)$ (and not the in-medium scattering length $a(\sigma)$), cf. sects. 5.5.2, 5.6.1. For the important case of broad resonances, this subtle distinction is quantitatively unimportant.

In sum there are five numbers that characterize the situation (two of them, $\bar{\mu}$ and B_0, appear in $\bar{\nu}$), though the full scattering length (2.5) was determined by three numbers only. However, as argued above, this quantity is the low frequency and momentum limit of the scattering amplitude only. Thus it contains no information on the frequency and momentum dependence of the interaction, parameterized by $\bar{A}_\phi$ and the normalization of the frequency coefficient. Our model allows for the description of the more general situation of non-local, i.e. frequency and momentum dependent couplings in the Feshbach channel. This will be important for "narrow" resonances (small Yukawa couplings, cf. sect. 6).

3.3 Scaling Form

Adding to the microphysical parameters, further scales are introduced by the thermodynamic variables temperature T and particle density n. Since we are mainly interested in analyzing the thermodynamics of the crossover system in this work, it is sensible to perform another manipulation of the action in order to better adapt to our needs. We recall from sect. 2.1 that the Fermi momentum sets a natural scale for momenta in a thermodynamic situation. We measure momenta in units of the Fermi momentum $k_F = (3\pi^2 n)^{1/3}$, and energies in units of the Fermi energy $\epsilon_F = k_F^2/2M$. This fixes the canonical scaling behavior of all couplings and fields.

Indeed we can bring the action (3.1) to a dimensionless form by rescaling coordinates and fields according to

$$\begin{aligned} \tilde{\vec{x}} &= k_F \vec{x}, \quad \tilde{\tau} = \epsilon_F \tau, \quad \tilde{T} = T/\epsilon_F, \ \tilde{q} = q/k_F, \\ \tilde{\psi} &= k_F^{-3/2} \bar{\psi}, \quad \tilde{\phi} = k_F^{-3/2} \bar{\phi}, \quad \tilde{\sigma} = \sigma/\epsilon_F. \end{aligned} \tag{3.15}$$

This yields the scaling form of the bare microscopic action

$$\begin{aligned} S[\tilde{\psi}, \tilde{\phi}] = \int d\tilde{\tau} d^3\tilde{x} \Big[& \tilde{\psi}^\dagger \big(\tilde{\partial}_\tau - \tilde{\triangle} - \tilde{\sigma} \big) \tilde{\psi} + \tilde{\phi}^* \big(\tilde{\partial}_\tau - \tilde{A}_\phi^{(cl)} \tilde{\triangle} + \tilde{\nu}_\Lambda - 2\tilde{\sigma} \big) \tilde{\phi} \\ & - \frac{\tilde{h}_{\phi,\Lambda}}{2} \Big(\tilde{\phi}^* \tilde{\psi}^T \epsilon \tilde{\psi} - \tilde{\phi} \tilde{\psi}^\dagger \epsilon \tilde{\psi}^* \Big) + \frac{\tilde{\lambda}_{\psi,\Lambda}}{2} (\tilde{\psi}^\dagger \tilde{\psi})^2 \Big]. \end{aligned} \tag{3.16}$$

Due to the different scaling of energy and momentum, the canonical scaling dimension of time is minus two and therefore the nonrelativistic Lagrangian has scaling dimension five and not four as for a relativistic quantum field theory.

According to eq. (3.16) all quantities derived from the partition function can be brought to a scaling form and can only depend on the dimensionless parameters (we display the UV renormalized quantities)

$$\tilde{\nu} = \bar{\nu}/\epsilon_F, \quad \tilde{h}_\phi = 2Mk_F^{-1/2}\bar{h}_\phi, \ \tilde{\lambda}_{\psi,0} = 2Mk_F\bar{\lambda}_{\psi,0}, \ \tilde{A}_\phi^{(cl)} = 2M\bar{A}_\phi^{(cl)}. \tag{3.17}$$

The dimensionless version of the in-medium scattering length (3.13) is

$$c = ak_F = -\frac{\tilde{h}_\phi^2}{8\pi(\tilde{\nu} - 2\tilde{\sigma})} + c_{bg} \tag{3.18}$$

with $c_{bg} = a_{bg}k_F = \tilde{\lambda}_{\psi,0}/(8\pi)$. We will refer to c as "concentration". Indeed, with the inverse Fermi momentum setting the scale for the average interparticle spacing d, the concentration c is a measure for the ratio between the in-medium scattering length a and the average distance, $c \sim a/d$. This defines "large" scattering lengths in the thermodynamic context. Note that through σ, this in-medium scattering length depends on the density. A more complete list of the relation between dimensionful and dimensionless parameters is given in app. B.

This scaling form shows a first important aspect of universality. All computations can be performed at a fiducial $k_F = 1\text{eV}$. Contact to a concrete physical situation is only made at the end by rescaling the results, using the value of $k_F = (3\pi^2 n)^{1/3}$ appropriate for the density n of a given experiment. For a homogeneous situation all dimensionless physical observables can be expressed in terms of the dimensionless variables c^{-1}, $\tilde{h}_\phi$, c_{bg} and $\tilde{T}$! The scale is then introduced by n.

To summarize this section and to get an impression of the physics connected to the various parameter ranges, we show a "cube of scales" with axes $\tilde{T}, c^{-1}, \tilde{h}_\phi^{-2}$ in fig. 3.2 (we omit a further axis for c_{bg}). We find the following regimes:

- The ultracold regime where the fermion system becomes degenerate, in this way allowing quantum effects to play a role at all, is determined by the condition $\tilde{T} < 1$ (or $\tilde{T}/(4\pi) \ll 1$ as stated in chapt. 2).

- For a small concentration $|c|$ the gas is dilute in the sense that scattering can be treated as a perturbation. For weak attractive interactions $c^{-1} < -1$ the system is in the "BCS regime". Weak repulsive interactions $c^{-1} > 1$ define the "BEC regime". In these ranges mean field theory is expected to work reasonably well and we provide quantitative arguments supporting this statement in chapt. 6.

- For strong interactions $|c^{-1}| < 1$, the in-medium scattering length exceeds the average distance between two atoms and fluctuation effects beyond mean field may play a crucial role. The crossover from BCS to BEC regime takes

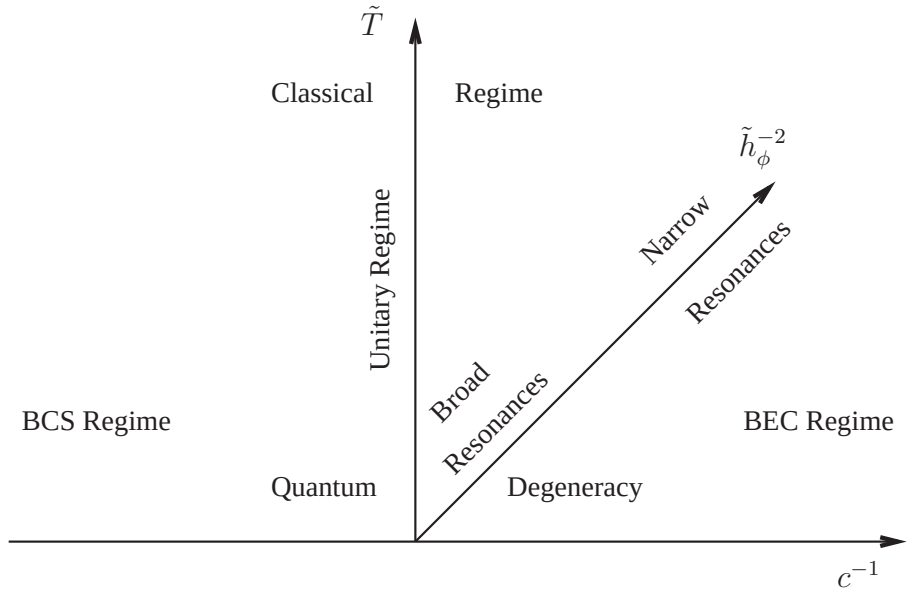

Figure 3.2: Cube of scales for the crossover problem.

place when evolving on this axis. c^{-1} is indeed the right variable – though the in-medium scattering length diverges at resonance, all thermodynamic observables behave continuously as we will see in the next chapters.

- The third axis discriminates between the broad ($\tilde{h}_\phi^2 \gg 1$) and the narrow resonance regime ($\tilde{h}_\phi^2 \ll 1$). In the narrow resonance limit we will establish an exact solution of the theory – controlled by the smallness of $\tilde{h}_\phi$ – where mean field theory becomes valid for arbitrary couplings or scattering lengths a. Such a solution is not possible for broad resonances – which are investigated in current experiments in ^{6}Li and ^{40}K.

The challenge is hence posed in the region around the origin of the cube of scales, where we deal indeed with a strongly interacting quantum field theory.

Chapter 4

Functional Integral for the Crossover Problem

4.1 Functional Integral and the Effective Action

4.1.1 Effective Action

We start from the functional integral representation of the partition function for the grand canonical ensemble $Z[J]$. For a brief review of the derivation of the functional integral representation from the Hamiltonian operator formalism, see e.g. [49]. We include a complex valued scalar bosonic field $\hat{\phi}, \hat{\phi}^*$ as well as a Grassmann valued fermionic two-spinor $\hat{\psi} = (\hat{\psi}_1, \hat{\psi}_2)^T$ as appropriate for the theory we intend to analyze. In this section, which provides some basic formalism, we do not distinguish between bare and dressed fields to be introduced in (4.2.2). Here, it is more important to clearly distinguish between fluctuating fields (with hat) which are quantized by the means of the functional integral, and "classical" fields of field expectation values (without hat, cf. eq. (4.8) for a definition). We further work in the Nambu-Gorkov formalism, i.e. we plug the fields together in a "superfield vector" [1],

$$\hat{\chi}(X) = \begin{pmatrix} \hat{\phi} \\ \hat{\phi}^* \\ \hat{\psi} \\ \hat{\psi}^* \end{pmatrix}(X), \qquad \hat{\chi}^T(X) = \left(\hat{\phi}, \hat{\phi}^*, \hat{\psi}^T, \hat{\psi}^\dagger\right)(X). \tag{4.1}$$

[1] We follow the conventions from [50], adjusting them to the nonrelativistic fermionic two-spinors. In the reference, real valued fields are included as well.

Here $\hat{\phi}, \hat{\phi}^*$ and $\hat{\psi}, \hat{\psi}^*$ are considered as independent field variables. Hence $\hat{\chi}, \hat{\chi}^T$ carry the same information [2]. The generalized (transposed) source term reads

$$J^T(X) = \big(j^*, j, \eta^\dagger, \eta^T\big)(X) \tag{4.2}$$

and similar for the column term. The bosonic entries j, j^* are complex valued, the fermionic sources η, η^* are Grassmann valued.

For later convenience, let us also introduce fermionic and bosonic Nambu fields,

$$\hat{\Psi}(X) = \begin{pmatrix} \hat{\psi} \\ \hat{\psi}^* \end{pmatrix}(X), \qquad \hat{\Phi}(X) = \begin{pmatrix} \hat{\phi} \\ \hat{\phi}^* \end{pmatrix}(X) \tag{4.3}$$

and corresponding sources J_ψ, J_ϕ which are Grassmann (complex) valued.

The partition function can now be written in a compact way,

$$Z[J] = \int \mathcal{D}\hat{\chi} \exp\big(-S[\hat{\chi}] + J^T\hat{\chi}\big). \tag{4.4}$$

Here we adopt a matrix notation for both discrete and continuous indices, i.e.

$$J^T\chi = \int_X J_i(X)\hat{\chi}_i(X). \tag{4.5}$$

The partition function formulates a quantum field theory in terms of an external source J: Successive derivatives with respect to the source term, evaluated at $J = 0$, generate an expansion of the partition function in terms of Green functions. It is often more practicable to organize the expansion in terms of *connected* Green functions, which is generated by considering the logarithm of the partition function,

$$W[J] = \log Z[J]. \tag{4.6}$$

This object, the Schwinger functional, still formulates the theory in terms of the source J,

$$W[J] = J^T\chi + \frac{1}{2}J^T W^{(2)} J + ... \tag{4.7}$$

The first two derivatives are of particular importance. The *classical field*, i.e. the vacuum field expectation value [3] or one-point function is defined as

$$\chi_i(X) := \langle\hat{\chi}_i(X)\rangle = \frac{\delta W[J]}{\delta J_i(X)}\Big|_{J=0}. \tag{4.8}$$

[2] Sticking to the convention for the Fourier transform (3.4), $\hat{\chi}(X) = \int_Q \exp(\mathrm{i}QX)\hat{\chi}(Q)$ we now find for the components $\hat{\chi}(Q) = (\hat{\phi}(Q), \hat{\phi}^*(-Q), \hat{\psi}(Q), \hat{\psi}^*(-Q))$ (column vector) and $\hat{\chi}^T(-Q) = (\hat{\phi}(-Q), \hat{\phi}^*(Q), \hat{\psi}^T(-Q), \hat{\psi}^\dagger(Q))$ (row vector). The minus sign in $\hat{\chi}^T(-Q)$ is introduced by hand to get the correct momentum structure of the bilinears.

[3] "Vacuum" refers to $J = 0$ here.

For fermions, due to Pauli's principle (on the level of fields: Grassmann valuedness), a fermion state can only be populated once such that a macroscopic occupation cannot occur,

$$\psi = \psi^* = 0. \tag{4.9}$$

The *connected two-point function* is given by

$$\begin{aligned} W^{(2)}_{ij}(X,Y) &= \frac{\overrightarrow{\delta}}{\delta J_i(X)} W[J] \frac{\overleftarrow{\delta}}{\delta J_j(Y)}\Big|_{J=0} \\ &= \langle \hat{\chi}^*_i(X)\hat{\chi}_j(Y)\rangle_c = \langle \hat{\chi}^*_i(X)\hat{\chi}_j(Y)\rangle - \chi^*_i(X)\chi(Y) \end{aligned} \tag{4.10}$$

with the two-point Green function

$$\langle \hat{\chi}^*_i(X)\hat{\chi}_j(Y)\rangle = \frac{1}{Z[0]} \frac{\overrightarrow{\delta}}{\delta J_i(X)} Z[J] \frac{\overleftarrow{\delta}}{\delta J_j(Y)}\Big|_{J=0}. \tag{4.11}$$

We can now construct the *effective action* via a Legendre transform with respect to the classical field (4.8),

$$\Gamma[\chi] = -W[J] + J^T\chi, \qquad J = J[\chi]. \tag{4.12}$$

Here $J[\chi]$ is to be understood as a solution of eq. (4.8). This corresponds to a change of the active variable $J \to \chi$, formulating the field theory in terms of the classical field χ. The vertex expansion

$$\begin{aligned} \Gamma[\chi] &= \sum_N \frac{1}{N!} \int\limits_{X_1 \ldots X_N} \Gamma^{(N)}_{i_1 \ldots i_N}(X_1 \ldots X_N)\chi_{i_1}(X_1)\cdot \ldots \cdot \chi_{i_N}(X_N) \\ &= \chi^T\Gamma^{(1)} + \frac{1}{2}\chi^T\Gamma^{(2)}\chi + \ldots \end{aligned} \tag{4.13}$$

generates the one-particle irreducible (1PI) Green functions (see, e.g., [51]).

From this definition of Γ we immediately derive the *field equations*

$$\begin{aligned} \frac{\delta\Gamma[\chi]}{\delta\chi_i(X)} &= -\int\limits_Y \frac{\delta J_j(Y)}{\delta\chi_i(X)} \frac{\delta W}{\delta J_j(Y)} + \int\limits_Y \frac{\delta J_j(Y)}{\delta\chi_i(X)}\chi_j(Y) + M_{ij}J_j(X) \\ &= M_{ij}J_j(X) = J_j(X)M_{ij} \end{aligned} \tag{4.14}$$

where we have introduced the "metric" in the space of discrete field indices (Nambu space) [4],

$$M = M^T = \mathrm{diag}(1,1,-1,-1). \tag{4.15}$$

[4]The signs in the fermion sector are necessary since we work with a left-derivative and $\delta(J^T_\psi\Psi)/\delta\Psi = -J^T_\psi$.

For vanishing sources $J = 0$, the effective action promotes the classical action principle to full quantum status,

$$\frac{\delta\Gamma[\chi]}{\delta\chi} = 0. \tag{4.16}$$

This motivates the names "classical field" and "effective action". Eq. (4.16) is the equation of motion for the field χ.

Using (4.4) and (4.12), we can write the effective action in a more elegant way

$$\begin{aligned} \exp -\Gamma[\chi] &= \int \mathcal{D}\hat{\chi} \exp -S[\hat{\chi}] + J^T(\hat{\chi} - \chi), \\ \frac{\delta\Gamma[\chi]}{\delta\chi} &= (MJ)^T. \end{aligned} \tag{4.17}$$

This is a functional integro-differential equation for the effective action, connecting the effective action and its derivative w.r.t. the classical field. On the level of the effective action, a vanishing source term gives an additional constraint on the effective action. Evaluating (4.17) with this constraint fixes the value of the field χ as the solution of the equation of motion (4.16).

Now we decompose the full field in a background or classical (not necessarily homogeneous) and a fluctuating part,

$$\hat{\chi}(X) = \chi(X) + \delta\hat{\chi}(X). \tag{4.18}$$

Eq. (4.8) shows that this implies

$$\langle \delta\hat{\chi}(X) \rangle = 0. \tag{4.19}$$

Further making use of the shift invariance of the functional measure,

$$\mathcal{D}\hat{\chi} = \mathcal{D}\delta\hat{\chi}, \tag{4.20}$$

we observe that the formulation (4.17) leads to the background field formalism in a natural way,

$$\exp -\Gamma[\chi] = \int \mathcal{D}\delta\hat{\chi} \exp -S[\delta\hat{\chi} + \chi] + J^T\delta\hat{\chi} \tag{4.21}$$

with $J[\chi]$ determined by the second eq. in (4.17). For later convenience, we note the important identity (omitting the continuous indices and integrations for simplicity)

$$\Gamma^{(2)}_{ij} W^{(2)}_{jk} = M_{jl} \frac{\delta J_l}{\delta\chi_i} \frac{\delta\chi_k}{\delta J_j} = M_{ik}, \tag{4.22}$$

stating that the second functional derivative of the effective action is the inverse propagator.

4.1.2 Symmetries

A continuous symmetry of the classical action yields a (classical) conserved charge – this is Noether's theorem. In the absence of anomalies, there is also a conserved charge for the full quantum theory. Here we briefly review the formalism for the construction of the conserved Noether charge from the effective action. We will need this formalism for the construction of the equation of state in the following section.

We consider a global symmetry transformation α acting on the field $\hat{\chi} \to \hat{\chi}^\alpha$. We further want to consider transformations whose linear piece in the transformation parameter α is at most linear in the field $\hat{\chi}$. A typical example is a global $U(1)$ symmetry, $\hat{\chi} \to e^{\mathrm{i}\alpha}\hat{\chi} \approx (1+\mathrm{i}\alpha)\hat{\chi}$. Invariance of the classical action is then expressed as

$$S[\hat{\chi}] \to S[\hat{\chi}^\alpha] = S[\hat{\chi}]. \tag{4.23}$$

This statement holds at least to linear order in the symmetry transformation α. We can formalize this by ($S = \int_X \mathcal{L}$)

$$\frac{\partial \mathcal{L}[\hat{\chi}^\alpha]}{\partial \alpha}\Big|_{\alpha=0} = 0. \tag{4.24}$$

The Schwinger functional can be expressed in terms of χ^α as

$$\exp W[J] = \int \mathcal{D}\hat{\chi}^\alpha \exp -S[\hat{\chi}^\alpha] + J^T\hat{\chi}^\alpha. \tag{4.25}$$

Assuming the invariance of the functional measure under α - transforms, the last equation takes the form

$$\exp W[J] = \int \mathcal{D}\hat{\chi} \exp -S[\hat{\chi}^\alpha] + J^T\hat{\chi}^\alpha. \tag{4.26}$$

This assumption holds if the transformation α is unitary [5]. α-invariance of the Schwinger functional can be expressed as

$$\frac{\delta W[J]}{\delta \alpha}\Big|_{\alpha=0} = 0 \quad \text{or} \quad J^T\frac{\delta \chi^\alpha}{\delta \alpha}\Big|_{\alpha=0} = \Big\langle \frac{\delta S[\hat{\chi}^\alpha]}{\delta \alpha}\Big|_{\alpha=0}\Big\rangle \tag{4.27}$$

where the expectation values are evaluated at arbitrary sources J. The symbol "δ" stands for the full variation or functional derivative, while "∂" denotes a partial derivative. Switching to the effective action by a Legendre transform relates the source J to the field derivative of the effective action:

$$\Big\langle \frac{\delta S[\hat{\chi}^\alpha]}{\delta \alpha}\Big|_{\alpha=0}\Big\rangle = \Big(\frac{\delta \Gamma}{\delta \chi^\alpha}\Big)^T\frac{\delta \chi^\alpha}{\delta \alpha}\Big|_{\alpha=0} = \frac{\delta \Gamma}{\delta \alpha}\Big|_{\alpha=0} \tag{4.28}$$

[5] There are cases where this assumption does not hold. One then deals with anomalies, which entail that the transformation α is not unitary.

where we use the chain rule for functional derivatives in the second step. Inserting the equation of motion (4.16), the last equation reads

$$\frac{\delta\Gamma}{\delta\alpha}\Big|_{\delta\Gamma/\delta\chi=0,\alpha=0} = 0. \tag{4.29}$$

We recover the standard formulation of Noether's theorem by specializing to a class of microscopic actions which depend only on the fields and their first derivatives, $S = S[\hat{\chi}, \partial_\mu\hat{\chi}]$. We carry out the functional derivative w.r.t. α explicitly,

$$0 = \frac{\delta S}{\delta\alpha}\Big|_{\alpha=0} = -\partial_\mu \frac{\partial\mathcal{L}}{\partial(\partial_\mu\alpha)}\Big|_{\partial_\mu\alpha=0} + \frac{\partial\mathcal{L}}{\partial\alpha}\Big|_{\alpha=0} = 0. \tag{4.30}$$

The first equality holds for the field equation, in analogy to eq. (4.28). The second term on the rhs vanishes for global symmetries (cf. eq. (4.24)), while the first one can be interpreted as the divergence of the classical Noether current,

$$j^\mu_{(cl)} = -\frac{\partial\mathcal{L}}{\partial(\partial_\mu\alpha)}\Big|_{\partial_\mu\alpha=0}, \tag{4.31}$$

For the Noether current of the full theory, we consequently get [6]

$$J^\mu = -\Big\langle \frac{\partial\mathcal{L}}{\partial(\partial_\mu\alpha)}\Big|_{\partial_\mu\alpha=0}\Big\rangle = -\frac{\partial\Gamma}{\partial(\partial_\mu\alpha)}\Big|_{\partial_\mu\alpha=0}. \tag{4.32}$$

These are closed explicit expressions for the Noether current. The conserved charge is related to the timelike component of the current, more precisely

$$Q = \int d^3x J^0 = -\int d^3x \frac{\partial\Gamma}{\partial\dot{\alpha}}\Big|_{\dot{\alpha}=0}. \tag{4.33}$$

This scheme can easily be generalized to microscopic actions depending on higher powers of derivatives – one simply has to figure out the generalization of eq. (4.30). E.g. for an action additionally depending on $\partial_\nu\partial_\mu\chi$ the additional term in (4.30) reads $\partial_\nu[\partial S/\partial(\partial_\nu\partial_\mu\alpha)]$.

For the global $U(1)$ symmetry relevant in the crossover problem, the conserved charge is the particle number, $Q = N$. We will use the above construction to compute the particle number for the crossover problem in the next section. The central ingredient for the concrete implementation is the representation of the effective action as a functional integral, which means to choose the particular basis of coherent states to represent the thermodynamic trace.

[6] In principle, one gets the rhs of (4.32) plus a quantity c^μ with $\partial_\mu c^\mu = 0$. For massive theories, inducing an exponential decay of c^μ for large distances, one can ignore this contribution.

4.2 Unified Description for the Crossover Problem

We present the derivation of our unified effective action description for the crossover problem. Special emphasis is put on the appropriate equation of state and the classification of the phases of the system via the field equation for the boson field expectation value.

We further introduce the notion of dressed (bosonic) fields, in distinction to the bare fields. As exposed in chapt. 3, the latter are defined as those fields which appear in the classical action and are subsequently quantized by the functional integral (or by an alternative quantization procedure, as e.g. by canonical commutation relations). The dressed (bosonic) fields are the right degrees of freedom to characterize the thermodynamic situation as we argue below. In order to clearly distinguish these objects, we denote the bare fields with a bar on top and omit this for the dressed fields.

4.2.1 Assembling the Functional Integral: Bogoliubov-type Theory

We start with the effective action written down in terms of the fermionic and bosonic Nambu fields (4.3),

$$\Gamma[\bar{\Psi},\bar{\Phi}] = -\log\int \mathcal{D}\delta\hat{\bar{\Psi}}\mathcal{D}\delta\hat{\bar{\Phi}}\exp -S[\hat{\bar{\Psi}},\hat{\bar{\Phi}}] + J_\phi^T\delta\hat{\bar{\Phi}} + J_\psi^T\delta\hat{\bar{\Psi}}. \tag{4.34}$$

Throughout this chapter, we consider the situation of negligible background interactions and set

$$\bar{\lambda}_\psi = 0. \tag{4.35}$$

In this case, the action (3.1) is quadratic in the fermions, such we can integrate them out in one step [7]. Inserting the physical fermion field expectation value $\bar{\Psi}=0$, this yields a purely bosonic theory,

$$\Gamma[\bar{\Psi}=0,\bar{\Phi}] = -\log\int \mathcal{D}\delta\hat{\bar{\Phi}}\exp -\bar{S}[\delta\hat{\bar{\Phi}}+\bar{\Phi}] + J_\phi^T\delta\hat{\bar{\Phi}} \tag{4.36}$$

with an intermediate action $\bar{S}$ depending on the fluctuating field $\hat{\phi}=\phi+\delta\hat{\phi}$, and given by the exact expression

$$\bar{S}[\hat{\bar{\Phi}}] = S_\phi^{(cl)}[\hat{\bar{\Phi}}] - \frac{1}{2}\log\det S^{(\psi\psi)}[\hat{\bar{\Phi}}] = S_\phi^{(cl)}[\hat{\bar{\Phi}}] - \frac{1}{2}\mathrm{Tr}\log S^{(\psi\psi)}[\hat{\bar{\Phi}}]. \tag{4.37}$$

[7] Additionally, the equation of motion for the fermions be satisfied, i.e. $J_\psi = 0$.

The second field variation with respect to the fermion fields appearing in the intermediate action $\bar{S}$ is given by

$$\begin{aligned} S^{(\psi\psi)}(Q,K;\hat{\bar{\Phi}}) &= \frac{\overrightarrow{\delta}}{\delta\hat{\bar{\Psi}}^T(-Q)} S \frac{\overleftarrow{\delta}}{\delta\hat{\bar{\Psi}}(K)} \\ &= \begin{pmatrix} -\epsilon_{\alpha\beta}\bar{h}_\phi\bar{\phi}^* & -\bar{P}_F(-Q)\delta_{\alpha\beta} \\ \bar{P}_F(Q)\delta_{\alpha\beta} & \epsilon_{\alpha\beta}\bar{h}_\phi\bar{\phi} \end{pmatrix} \delta(Q-K) \\ &\quad + \begin{pmatrix} -\epsilon_{\alpha\beta}\bar{h}_\phi\delta\hat{\bar{\phi}}^*(-(Q-K)) & 0 \\ 0 & \epsilon_{\alpha\beta}\bar{h}_\phi\delta\hat{\bar{\phi}}(Q-K) \end{pmatrix} \end{aligned} \tag{4.38}$$

with the frequency and momentum dependent part of the classical fermion propagator

$$\bar{P}_F(Q) = \mathrm{i}\,\omega_F + \frac{q^2}{2M} - \sigma. \tag{4.39}$$

In (4.38) we have decomposed into a "propagator part" $\bar{\mathcal{P}}_F$ and a "fluctuating field" contribution $\bar{\mathcal{F}}$. $\bar{\mathcal{P}}_F$ is diagonal in momentum space and depends on the background field $\bar{\Phi}$ which we treat as momentum independent (homogeneous in position space). $\bar{\mathcal{F}}$ depends on the fluctuating, momentum dependent fields $\delta\hat{\bar{\phi}}(Q-K), \delta\hat{\bar{\phi}}^*(K-Q)$.

The determinant over the discrete indices of the propagator part of this matrix reads

$$\begin{aligned} \det_{4\times4}(\bar{\mathcal{P}}_F) &= \left(\bar{P}_F(Q)\bar{P}_F(-Q) + \bar{h}_\phi^2\bar{\phi}^*\bar{\phi}\right)^2 = \left(\omega_F^2 + (q^2/2M-\sigma)^2 + \bar{h}_\phi^2\bar{\phi}^*\bar{\phi}\right)^2 \\ &=: \left(\bar{P}_F^{|2|}(Q)\right)^2. \end{aligned} \tag{4.40}$$

We can now make progress by expanding the intermediate action in powers of the fluctuation $\delta\hat{\phi}$,

$$S_\phi^{(cl)}[\hat{\bar{\Phi}}] = S_\phi^{(cl)}[\bar{\Phi}] + \left(\frac{\delta S}{\delta\hat{\bar{\Phi}}}\right)^T \delta\hat{\bar{\Phi}} + S_\phi^{(cl)}[\delta\hat{\bar{\Phi}}], \tag{4.41}$$

$$\begin{aligned} -\frac{1}{2}\mathrm{Tr}\log\left(\bar{\mathcal{P}}_F + \bar{\mathcal{F}}\right) &= -\frac{1}{2}\mathrm{Tr}\log\bar{\mathcal{P}}_F - \frac{1}{2}\mathrm{Tr}\bar{\mathcal{P}}_F^{-1}\bar{\mathcal{F}} + \frac{1}{4}\mathrm{Tr}(\bar{\mathcal{P}}_F^{-1}\bar{\mathcal{F}})^2 \\ &\quad -\frac{1}{6}\mathrm{Tr}(\bar{\mathcal{P}}_F^{-1}\bar{\mathcal{F}})^3 + \frac{1}{8}\mathrm{Tr}(\bar{\mathcal{P}}_F^{-1}\bar{\mathcal{F}})^4 \mp \ldots \end{aligned}$$

As it turns out, even for the qualitative description of the crossover problem it is crucial to keep the momentum dependence of the fermion loops. We find for the zero order contribution

$$S_\phi^{(cl)}[\bar{\Phi}] - \frac{1}{2}\mathrm{Tr}\log\bar{\mathcal{P}}_F[\bar{\Phi}] = S_\phi^{(cl)}[\bar{\Phi}] - V\int\limits_Q \log\bar{P}_F^{|2|}(Q). \tag{4.42}$$

This is an explicit formula for the Gaussian integral for the fermions in a bosonic background $\bar{\Phi}$. For the symmetry consideration we will perform in the next section, it is preferable to have the explicit functional integral representation,

$$-\frac{1}{2}\mathrm{Tr}\log\bar{\mathcal{P}}_F[\bar{\Phi}] = -\log\int\mathcal{D}\hat{\bar{\Psi}}\exp-\frac{1}{2}\int\limits_Q\hat{\bar{\Psi}}^T(-Q)\bar{\mathcal{P}}_F(Q)\hat{\bar{\Psi}}(Q). \tag{4.43}$$

Truncating the expansion after this term yields the fermionic mean field effective action. It is already enough to describe the BCS mechanism and we will come back to this issue in chapt. 6. This part factorizes from the functional integral (4.36), which consequently can be written as

$$\begin{aligned}\Gamma[\bar{\Psi}=0,\bar{\Phi}] \;=\; & S_\phi^{(cl)}[\bar{\Phi}] - \frac{1}{2}\mathrm{Tr}\log\bar{\mathcal{P}}_F[\bar{\Phi}] \\ & -\log\int\mathcal{D}\delta\hat{\bar{\Phi}}\exp\big(-\big\{\Big(\frac{\delta S}{\delta\hat{\bar{\Phi}}}\Big)^T\delta\hat{\bar{\Phi}} + S_\phi^{(cl)}[\delta\hat{\bar{\Phi}}] \\ & \qquad -\frac{1}{2}\mathrm{Tr}\bar{\mathcal{P}}_F^{-1}\bar{\mathcal{F}} + \frac{1}{4}\mathrm{Tr}(\bar{\mathcal{P}}_F^{-1}\bar{\mathcal{F}})^2 - \frac{1}{6}\mathrm{Tr}(\bar{\mathcal{P}}_F^{-1}\bar{\mathcal{F}})^3 \\ & \qquad +\frac{1}{8}\mathrm{Tr}(\bar{\mathcal{P}}_F^{-1}\bar{\mathcal{F}})^4 \mp ...\big\} + J_\phi^T\delta\hat{\bar{\Phi}}\big).\end{aligned} \tag{4.44}$$

In the remainder of this section, let us evaluate the functional integral (4.44) in a Bogoliubov approximation. This provides a motivation for the truncation of the bosonic inverse propagator, and gives an ideal starting point for the construction of the equation of state for the crossover problem.

In Bogoliubov theory, interactions are not completely neglected, but treated in a mean field sense. For example, an interaction $(\hat{\phi}^*\hat{\phi})^2$ is expanded around the expectation value ϕ^*, ϕ, and truncated at second order in the expansion parameter, the fluctuating field $\delta\hat{\phi}^*, \delta\hat{\phi}$. This is precisely what we obtain in the Tr log expansion in the background field formalism: We recover the Bogoliubov approximation for the effective action (4.44) by neglecting terms $O((\bar{\mathcal{P}}_F^{-1}\bar{\mathcal{F}})^3)$. In this case the functional integral is again Gaussian and can be performed analytically.

To make further progress, we note that the terms linear in $\delta\hat{\bar{\Phi}}$ in (4.44) precisely fulfill the equation of motion in a quadratic truncation of the exponent, and thus cancel with the source term $J_\phi^T\delta\hat{\bar{\Phi}}$. In the next step, we rewrite the remaining trace in a more explicit way by rearranging the field indices according to the Nambu formalism:

$$\begin{aligned}\frac{1}{4}\mathrm{Tr}(\bar{\mathcal{P}}_F^{-1}\bar{\mathcal{F}})^2 &= \frac{V^2}{2}\int\limits_K\delta\hat{\bar{\Phi}}^T(-K)\bar{\mathcal{P}}_\phi(K)\delta\hat{\bar{\Phi}}(K) \\ &= \frac{V^2}{2}\int\limits_K\big(\delta\hat{\bar{\phi}}(-K),\delta\hat{\bar{\phi}}^*(K)\big)\begin{pmatrix}\bar{\lambda}_\phi(K)\bar{\phi}^*\bar{\phi}^* & \bar{P}_\phi(K)\\ \bar{P}_\phi(-K) & \bar{\lambda}_\phi(K)\bar{\phi}\bar{\phi}\end{pmatrix}\begin{pmatrix}\delta\hat{\bar{\phi}}(K)\\ \delta\hat{\bar{\phi}}^*(-K)\end{pmatrix}.\end{aligned} \tag{4.45}$$

The effective inverse propagator for the bosons has the explicit entries ($\bar{\rho} = \bar{\phi}^* \bar{\phi}$)

$$\begin{aligned}
\bar{P}_\phi(K) &= \bar{P}^*_\phi(-K) = \bar{P}^{(cl)}_\phi(K) - \bar{h}^2_\phi \int\limits_Q \frac{\bar{P}_F(-Q-K)\bar{P}_F(Q)}{\bar{P}^{|2|}_F(Q)\bar{P}^{|2|}_F(Q+K)} \\
&= \bar{P}^{(cl)}_\phi(K) - \bar{h}^2_\phi \int\limits_Q \frac{1}{\bar{P}_F(-Q)\bar{P}_F(Q+K)} + \rho \cdot \bar{h}^4_\phi \int\limits_Q \frac{1}{\bar{P}^{|2|}_F(Q)\bar{P}^{|2|}_F(Q+K)}, \\
\bar{\lambda}_\phi(K) &= \bar{\lambda}_\phi(-K) = \bar{h}^4_\phi \int\limits_Q \frac{1}{\bar{P}^{|2|}_F(Q)\bar{P}^{|2|}_F(Q+K)}
\end{aligned} \tag{4.46}$$

and we note the appearance of $\bar{\lambda}_\phi(K)$ in the first expression. (Explicit expressions for these fermionic diagrams after Matsubara summation are provided in the next chapter where we specify the approximation scheme beyond renormalization with fermion diagrams only, which we use for our numerical results.) These matrix elements feature a complex momentum dependence. In order to make progress, we perform a "derivative expansion", i.e.

$$\begin{aligned}
\bar{P}_\phi(K) &= \bar{M}^2_\phi + \mathrm{i} Z_\phi \omega + \bar{Y}_\phi \omega^2 + \bar{A}_\phi \vec{k}^2 + ..., \\
\bar{\lambda}_\phi(K) &= \bar{\lambda}_\phi(0) + \bar{L}^\omega_\phi \omega^2 + \bar{L}^k_\phi \vec{k}^2
\end{aligned} \tag{4.47}$$

where the coefficients are defined as the derivatives w.r.t. the respective variables evaluated at zero momentum and frequency, e.g.

$$\bar{M}^2_\phi = \bar{P}_\phi(0), \quad Z_\phi = \mathrm{Im} \frac{\partial \bar{P}_\phi(K)}{\partial \omega}\Big|_{\omega=\vec{k}=0}, \quad \bar{A}_\phi = \frac{\partial \bar{P}_\phi(K)}{\partial \vec{k}^2}\Big|_{\omega=\vec{k}=0}, \quad \bar{\lambda}_\phi = \bar{\lambda}_\phi(0). \tag{4.48}$$

The effective coupling $\bar{\lambda}_\phi$ starts *quadratically* in the frequency since it is an even function of K (cf. (4.46)). We might further decompose the mass term in a direct and a condensate part which is nonzero only in the case of spontaneous symmetry breaking (cf. sect. 4.2.4),

$$\begin{aligned}
\bar{M}^2_\phi &= \bar{m}^2_\phi + \bar{\lambda}_\phi \bar{\rho}, \\
\bar{m}^2_\phi &= \bar{\nu}_\Lambda - \bar{h}^2_\phi \int\limits_Q \frac{1}{\bar{P}^{|2|}_F(Q)}.
\end{aligned} \tag{4.49}$$

Keeping only the leading terms in frequency and momentum for the off-diagonal entries, and only frequency and momentum independent terms for the anomalous (diagonal) terms, we get

$$\bar{\mathcal{P}}_\phi(K) = \begin{pmatrix} \bar{\lambda}_\phi \bar{\phi}^* \bar{\phi}^* & Z_\phi \mathrm{i}\omega + \bar{A}_\phi \vec{k}^2 + \bar{m}^2_\phi + \bar{\lambda}_\phi \bar{\rho} \\ -Z_\phi \mathrm{i}\omega + \bar{A}_\phi \vec{k}^2 + \bar{m}^2_\phi + \bar{\lambda}_\phi \bar{\rho} & \bar{\lambda}_\phi \bar{\phi} \bar{\phi} \end{pmatrix}. \tag{4.50}$$

This expansion is accurate to $\mathcal{O}(\partial_\tau)$ since $\bar{\lambda}_\phi(K)$ is even, cf. eq. (4.46). Indeed, this matrix precisely has the structure of the inverse propagator in a Bogoliubov approximation for a complex nonrelativistic boson with ϕ^4 interactions! It is crucial to note that the frequency and momentum dependence of the fermion loops (4.46) dictate the frequency and momentum dependence of the effective inverse boson propagator - this is the origin of the crossover from a BCS to a BEC-type state described by an effective bosonic theory with the above inverse propagator, and we discuss this issue in detail in chapt. 6. However, the coefficients are not fundamental microscopic quantities: On top of the classical part stemming from the classical inverse boson propagator, they feature a piece obtained from integrating out the fundamental fermionic constituents of the underlying theory. At this point we note that the renormalization procedure in our Bogoliubov approximation only involves fermionic diagrams. In the next chapter, we will go beyond this scheme, where also effective bosonic fluctuations will be included. They modify the effective boson propagator.

We can rescale the bosonic fields $\hat{\bar{\Phi}}$ in (4.45) as

$$\hat{\bar{\Phi}} \to \hat{\Phi} = Z_\phi^{1/2} k_F^{-3/2} \hat{\bar{\Phi}}, \quad \bar{\rho} \to \rho = Z_\phi k_F^{-3} \bar{\rho}. \tag{4.51}$$

The fields $\hat{\Phi}$ (without a bar) are the "dressed" fields [36; 39; 52] – those are the right effective degrees of freedom for the description of the thermodynamics of the crossover system. Additionally, we have rescaled with k_F in order to arrive at the dimensionless formulation appropriate for the thermodynamic system, cf. chapt. 3. Requiring invariance of the effective boson propagator (4.45), the rescaling transform (4.51) generates the "dressed" dimensionless inverse propagator

$$\mathcal{P}_\phi(K) = \frac{\bar{\mathcal{P}}_\phi(K)}{Z_\phi \epsilon_F} = \begin{pmatrix} \lambda_\phi \phi^* \phi^* & \mathrm{i}\tilde{\omega} + A_\phi \tilde{k}^2 + m_\phi^2 + \lambda_\phi \rho \\ -\mathrm{i}\tilde{\omega} + A_\phi \tilde{k}^2 + m_\phi^2 + \lambda_\phi \rho & \lambda_\phi \phi \phi \end{pmatrix}. \tag{4.52}$$

The rescalings of the matrix entries are listed in app. B. For later convenience, we introduce the momentum and frequency dependent part of the effective inverse boson propagator similar to the fermions,

$$\begin{aligned} P_\phi(\tilde{K}) &= P_\phi(\tilde{K})/(Z_\phi \epsilon_F) = \mathrm{i}\tilde{\omega} + A_\phi \tilde{k}^2 + m_\phi^2, \\ P_\phi^{|2|}(\tilde{K}) &= P_\phi(\tilde{K}) P_\phi(-\tilde{K}) + \lambda_\phi \rho (P_\phi(\tilde{K}) + P_\phi(-\tilde{K})). \end{aligned} \tag{4.53}$$

The dressed bosons have a standard time evolution, as signalled by the coefficient 1 for the frequency term. The impact of dressed bosonic fields is further clarified in the next section.

We can now evaluate the functional integral (4.44) in the combined Bogoliubov and derivative expansion. This yields a one-loop bosonic contribution to the effective

action

$$\Gamma_1^{(B)} = \frac{V}{2}\mathrm{Tr}\log\mathcal{P}_\phi = \frac{V}{2}\int\limits_{\tilde{Q}}\log\left(P_\phi^{|2|}(\tilde{Q}) + \lambda_\phi\rho(P_\phi(\tilde{Q}) + P_\phi(-\tilde{Q}))\right). \tag{4.54}$$

Throughout this work we will deal with homogeneous situations. (Though the effective action formalism is well suited for extensions to weak inhomogeneities as encountered in a trap, cf. [40].) It therefore makes sense to work with the effective potential $\bar{U}$ instead of the effective action Γ,

$$\bar{U} = \frac{\Gamma}{V}. \tag{4.55}$$

Further we can perform the Matsubara sums in eqs. (4.42) and (4.54) using eqs. (D.34) and (D.41), and omitting an infinite constant which is irrelevant for the thermodynamics since it does not involve any physical scale. Let us put the results together here. We write, working with the dimensionless effective potential $\tilde{u} = k_F^{-3}\epsilon_F^{-1}\bar{U}$,

$$\tilde{u}_\Lambda = \tilde{u}_\Lambda^{MFT} + \tilde{u}_{1,\Lambda}^{(B)} = \tilde{u}_\Lambda^{(cl)} + \tilde{u}_{1,\Lambda}^{(F)} + \tilde{u}_{1,\Lambda}^{(B)}, \tag{4.56}$$

where the summands on the right abbreviate the classical, one-loop fermionic, and one-loop bosonic part of the effective potential. The classical plus fermionic contribution represent the mean field approximation. The index Λ indicates that the integrals are formally divergent and have to be regularized, e.g. by an upper limit Λ for the momentum space integrals. Our renormalization prescription is presented in sect. 4.2.3. The contributions read explicitly

$$\begin{aligned}
\tilde{u}_\Lambda^{(cl)} &= \tilde{\phi}^*(\tilde{\nu}_\Lambda - 2\tilde{\sigma})\tilde{\phi}, \\
\tilde{u}_{1,\Lambda}^{(F)} &= -2\tilde{T}\int\frac{d^3\tilde{q}}{(2\pi)^3}\log\cosh\gamma_\phi, \\
\tilde{u}_{1,\Lambda}^{(B)} &= \tilde{T}\int\frac{d^3\tilde{q}}{(2\pi)^3}\log\sinh\alpha_\phi.
\end{aligned} \tag{4.57}$$

with the dimensionless, Z_ϕ - rescaling invariant functions

$$\begin{aligned}
\gamma_\phi &= \frac{1}{2\tilde{T}}\left[(\tilde{q}-\tilde{\sigma})^2 + h_\phi^2\rho\right]^{1/2}, \\
\alpha_\phi &= \frac{1}{2\tilde{T}}\left[(A_\phi\tilde{q}^2 + m_\phi^2)^2 + 2\lambda_\phi\rho(A_\phi\tilde{q}^2 + m_\phi^2)\right]^{1/2}.
\end{aligned} \tag{4.58}$$

These and some further useful functions are discussed in app. D.4.3.

4.2.2 Equation of State: Bare and Dressed Fields

Derivation from a symmetry consideration

Let us derive the equation of state for the crossover problem by applying the formalism presented in sect. 4.1.2 to the effective action (4.34). We will proceed in two steps: First, we give an exact, but impracticable expression for the particle density, and then derive an expression which is adapted to the approximation scheme discussed above. This will introduce the concept of dressed bosonic fields in a natural way.

The infinitesimal $U(1)$ transform is given by

$$\begin{aligned} \psi &\rightarrow \psi^\alpha = (1+\mathrm{i}\alpha)\psi, \quad \psi^\dagger \rightarrow \psi^{\dagger\alpha} = (1-\mathrm{i}\alpha)\psi^\dagger, \\ \phi &\rightarrow \phi^\alpha = (1+2\mathrm{i}\alpha)\phi, \quad \phi^* \rightarrow \phi^{*\alpha} = (1-2\mathrm{i}\alpha)\phi^*. \end{aligned} \tag{4.59}$$

The double phase for the bosons is required by invariance of the Yukawa terms in the classical action (3.16). The zero component of the classical Noether current obtained via (4.31) reads

$$j^0 = \hat{\bar{\psi}}^\dagger(X)\hat{\bar{\psi}}(X) + 2\hat{\bar{\phi}}^*(X)\hat{\bar{\phi}}(X) \tag{4.60}$$

such that the conserved charge [8] is given by ($\langle\hat{\bar{\phi}}^*\hat{\bar{\phi}}\rangle = \langle\hat{\bar{\phi}}^*\hat{\bar{\phi}}\rangle_c + \bar{\phi}^*\bar{\phi}$)

$$N = \int d^3x \Big(\langle\hat{\bar{\psi}}^\dagger(X)\hat{\bar{\psi}}(X)\rangle_c + 2\langle\hat{\bar{\phi}}^*(X)\hat{\bar{\phi}}(X)\rangle_c + 2\bar{\phi}^*(X)\bar{\phi}(X)\Big), \tag{4.61}$$

or, in a homogeneous situation

$$\begin{aligned} n &= \frac{N}{V_3} = \langle\hat{\bar{\psi}}^\dagger\hat{\bar{\psi}}\rangle_c + 2\langle\hat{\bar{\phi}}^*\hat{\bar{\phi}}\rangle_c + 2\bar{\phi}^*\bar{\phi} \\ &= \bar{n}_F + 2\bar{n}_M + \bar{n}_C. \end{aligned} \tag{4.62}$$

These equations are exact. They express the equation of state in terms of the bare fields. We stress that the use of "bare" in this context is of course not related to the absence of fluctuations. $\bar{n}_F$ is the full bare fermion density, $\bar{n}_M$ the full bare boson density, and $\bar{n}_C$ the contribution from the full bare condensate.

In the presence of interactions it is hard to evaluate the full bare correlation functions in the above form explicitly – it premises the solution of the full quantum field theory. Therefore, a more practicable form for the equation of state is desirable.

[8] All the connected density contributions in this section are formally divergent and thus need UV renormalization. In order not to overload the notation, we choose here the abbreviations used later for the UV renormalized objects.

In the following, we present a derivation of such a formulation of the equation of state based on the effective action in the form (4.44), which gives the notion of dressed fields a more formal footing.

Again we reduce the problem of the construction of the equation of state to the computation of the zero component of the Noether current (4.31,4.32). We work with the Bogoliubov plus derivative expansion for the functional integral (4.44) specified in the last section. In this case, the intermediate action in (4.44) is indeed of the type $\bar{S}[\hat{\bar{\Phi}}, \partial_\mu \hat{\bar{\Phi}}]$ such that eqs. (4.32,4.33) are directly applicable.

The $U(1)$ transform acts both on the classical and the fluctuating fields. The classical part of the effective action yields the following contribution to the Noether current,

$$j^0_{cl} = 2\bar{\phi}^* \bar{\phi}, \tag{4.63}$$

i.e. it involves the expectation value of the bare field. There is no fermionic contribution since $\bar{\Psi} = 0$. The fluctuation part reads

$$j^0_{fluct} = \langle \delta\hat{\bar{\psi}}^\dagger(X) \delta\hat{\bar{\psi}}(X) \rangle^{MFT} + 2Z_\phi \langle \delta\hat{\bar{\phi}}^*(X) \delta\hat{\bar{\phi}}(X) \rangle. \tag{4.64}$$

Using $\langle \delta\hat{\bar{\phi}}^* \delta\hat{\bar{\phi}} \rangle = \langle \hat{\bar{\phi}}^* \hat{\bar{\phi}} \rangle_c$, eqs. (4.63, 4.64) finally yield an approximation to the equation of state,

$$N = \int d^3x \Big(\langle \hat{\bar{\psi}}^\dagger(X) \hat{\bar{\psi}}(X) \rangle_c^{MFT} + 2Z_\phi \langle \hat{\bar{\phi}}^*(X) \hat{\bar{\phi}}(X) \rangle_c + 2\bar{\phi}^*(X) \bar{\phi}(X) + ... \Big), \tag{4.65}$$

or, in the homogeneous case,

$$\begin{aligned} n &= \langle \hat{\bar{\psi}}^\dagger \hat{\bar{\psi}} \rangle_c^{MFT} + 2Z_\phi \langle \hat{\bar{\phi}}^* \hat{\bar{\phi}} \rangle_c + 2\bar{\phi}^* \bar{\phi} \\ &= n_F^{MFT} + 2n_M + \bar{n}_C. \end{aligned} \tag{4.66}$$

Here we introduce the density contributions

$$n_F^{MFT} = \langle \hat{\bar{\psi}}^\dagger \hat{\bar{\psi}} \rangle_c^{MFT}, \quad n_M = Z_\phi \langle \hat{\bar{\phi}}^* \hat{\bar{\phi}} \rangle_c = \langle \hat{\phi}^* \hat{\phi} \rangle_c \tag{4.67}$$

and we see that the approximation of the equation of state features the full bare condensate density $\bar{n}_C$. Our equation of state involves the full bare connected boson correlator $\bar{n}_M = \langle \hat{\bar{\phi}}^* \hat{\bar{\phi}} \rangle_c$ – the precise form of both $\bar{n}_C$ and $\bar{n}_M$ will depend on the concrete evaluation of the remaining functional integral for the boson field (4.44) and is improved beyond the Bogoliubov approximation in the next chapter.

Further our approximation implies the mean field fermion density n_F^{MFT}, where the standard free Fermi distribution function is modified by the presence of a condensate or gap in the case of spontaneous symmetry breaking. This contribution

also appears in BCS theory. Interestingly, the modification of the fermion density through the one-point function $\bar{\phi}$ is already present in the mean field or Gaussian part of the equation of state – this is a rooted in the use of the background field formalism. Had we organized our expansion with the fermion propagator appropriate for the normal gas phase and no background field, obtaining this result would require an infinite summation. At zero temperature, where boson correlations play a subleading role, a qualitative picture of the crossover can therefore already be obtained in mean field theory. On the other hand, it completely fails above T_c, in the absence of a condensate. Indeed, the expected bosonic nature of the thermodynamic system in the BEC regime is then fully contained in the effective bosonic two-point function.

In the view of a physical interpretation in terms of dressed bosonic fields, we decompose the fermion contribution into a piece from unbound fermions described by the standard Fermi distribution and an appropriately defined "condensate part",

$$\begin{aligned} n_F^{MFT}(\bar{\rho}) &= n_F' + 2\Delta Z_\phi' \bar{\rho}, \\ n_F' &= n_F^{MFT}(0), \quad \Delta Z_\phi' = \frac{1}{2}\frac{n_F^{MFT}(\bar{\rho}) - n_F^{MFT}(0)}{\bar{\rho}}. \end{aligned} \tag{4.68}$$

n_F' can be interpreted as the density contribution from unbound fermions. We refer to it as "dressed fermions". The dressed condensate then involves both the bare condensate and the fluctuation induced part,

$$n_C' = (1 + \Delta Z_\phi')\bar{\rho}. \tag{4.69}$$

$\Delta Z_\phi'$ yields an alternative , but very similar definition of the fluctuation part of the wave function renormalization (4.48). We can compare (4.68) with the definition via a derivative expansion (4.47,4.48) by rewriting

$$Z_\phi = \mathrm{Im}\frac{\partial \bar{P}_\phi(Q)}{\partial \omega}\Big|_{\omega=\vec{q}=0} = 1 + \Delta Z_\phi \tag{4.70}$$

with

$$\begin{aligned} \Delta Z_\phi &= \mathrm{Im}\frac{\partial \Delta\bar{P}_\phi(Q)}{\partial \omega}\Big|_{\omega=\vec{q}=0} = -\frac{1}{2}\frac{\partial \Delta\bar{P}_\phi(Q)}{\partial \sigma}\Big|_{\omega=\vec{q}=0} = -\frac{1}{2}\frac{\partial \bar{m}_\phi^2}{\partial \sigma} \\ &= -\frac{1}{2}\frac{\partial^2 U^{MFT}(\bar{\rho})}{\partial\sigma\partial\bar{\rho}} = \frac{1}{2}\frac{\partial n_F^{MFT}(\bar{\rho})}{\partial\bar{\rho}}. \end{aligned} \tag{4.71}$$

The second equality holds since $\Delta\bar{P}_\phi$ depends solely on the combination

$$\mathrm{i}\omega - 2\sigma. \tag{4.72}$$

In the next equality, we use the decomposition (4.46) and the evenness of $\bar{\lambda}_\phi(K)$ in K. For small $\bar{\rho}$, or if the the piece linear in $\bar{\rho}$ dominates the mean field potential,

both definitions (4.68) and (4.71) coincide. The latter situation actually occurs in the BEC regime, the first in the BCS regime, cf. chapt. 6. For our results, we prefer working with Z_ϕ instead of Z'_ϕ, and therefore define the dressed condensate and dressed fermion density as

$$n_C = 2Z_\phi \bar{\rho}, \qquad n_F = n - n_C - 2n_M. \tag{4.73}$$

Expressed in these quantities, the approximate equation of state reads

$$n = n_F + 2n_M + n_C, \tag{4.74}$$

where n_M and n_C are expressed in terms of dressed boson fields (4.51). The dressed molecule density and condensate fraction are now multiplicatively related to their bare counterparts,

$$\begin{aligned} n_M &= Z_\phi \langle \hat{\bar{\phi}}^* \hat{\bar{\phi}} \rangle_c = Z_\phi \bar{n}_M, \\ n_C &= = 2Z_\phi \langle \hat{\bar{\phi}}^* \rangle \langle \hat{\bar{\phi}} \rangle = Z_\phi \bar{n}_C. \end{aligned} \tag{4.75}$$

We can also express the equation of state (4.74) in a dimensionless version, obtained by dividing by the total particle number $n = k_F^3/(3\pi^2)$,

$$\begin{aligned} 1 &= \Omega_F + \Omega_M + \Omega_C, \\ \Omega_F &= n_F/n, \quad \Omega_M = 2n_M/n, \quad \Omega_C = n_C/n. \end{aligned} \tag{4.76}$$

This discussion reveals a certain degree of arbitrariness in the definitions of dressed molecule density and dressed condensate fraction. We oppose the alternative definitions of the wave function renormalization, Z'_ϕ (4.68) and Z_ϕ (4.71) which enter the condensate fraction Ω'_C, Ω_C in fig. 4.1. As expected the deviation is strongest in the crossover region. (All the plots in this chapter are obtained in the frame of Schwinger-Dyson equations discussed in the next chapter.) The concept of dressed fields is, however, physically sensible if the system is probed macroscopically, at scales much larger than the typical interparticle spacing k_F^{-1}. At these scales, one should indeed observe the effective bosonic low energy degrees of freedom described by the dressed, bosonic fields ϕ^*, ϕ which are invariant under a rescaling with the wave unction renormalization Z_ϕ (see below). Such observations are implemented in measurements of the condensate fraction in [15; 16]. Further, in the deep BEC regime we can prove that the dressed fields are indeed the appropriate degrees of freedom corresponding to dynamically generated bound states as discussed in chapts. 5 and 6.

On the other hand, a number of observables – e.g. the critical temperature – is of course not affected by the precise definition of dressed and bare quantities, but only depends on the sum of the density contributions. Even without the physically appealing interpretation in terms of dressed and bare fields, our approximation (4.66)

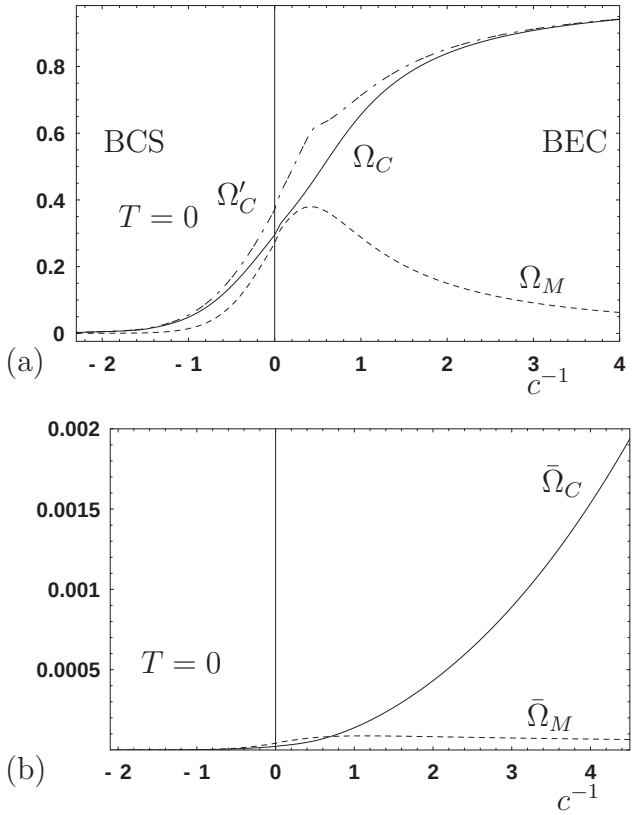

Figure 4.1: (a) Contributions to the total particle density in the large $\tilde{h}_\phi$ limit at $T = 0$: The fraction of dressed molecules Ω_M (dashed line) is largest in the crossover regime. The condensate fraction Ω_C (solid line) grows to one in the BEC regime. The solid line corresponds to $\Omega_C = Z_\phi \bar{\Omega}_C$ whereas the dashed-dotted line uses Z'_ϕ instead of Z_ϕ. (b) Fractions of the bare or closed channel molecules. In contrast to the dressed molecules, they are $\mathcal{O}(\tilde{h}_\phi^{-2})$. The dominant contribution arises from the condensed bare molecules $\bar{\Omega}_C$ (solid line). The contribution from noncondensed bare molecules $\bar{\Omega}_M$ at $T = 0$ remains small.

based on a systematic derivative expansion yields an unambiguous starting point for the determination of these quantities.

We can get further insight into the status of eq. (4.66) by decomposing the wave function renormalization Z_ϕ into the classical part (already present at the microscopic level) and a piece induced by the fermion fluctuations as done in eq. (4.70). We can then rewrite eq. (4.66) as

$$n = (n_F^{MFT} + 2\Delta Z_\phi \bar{n}_M) + 2\bar{n}_M + \bar{n}_C \tag{4.77}$$

and we see that the density of "fluctuation induced molecules" $2\Delta Z_\phi \bar{n}_M$ can be

viewed as a correction to the full fermion two point function,

$$\bar{n}_F = n_F^{MFT} + 2\Delta Z_\phi \bar{n}_M. \tag{4.78}$$

The presence of fundamental molecules is not necessary for the BCS – BEC crossover. In this case the equation of state obtained by the symmetry consideration simply reads

$$n = \bar{n}_F, \tag{4.79}$$

and the effective boson correlations are generated purely dynamically by the fermion fluctuations. We will discuss this limit in chapt. 6.

In the general case, we can now also formulate the equation of state in appropriately defined "bare" density fractions as

$$\begin{aligned} 1 &= \bar{\Omega}_F + \bar{\Omega}_M + \bar{\Omega}_C, \\ \bar{\Omega}_F &= \bar{n}_F/n, \quad \bar{\Omega}_M = 2\bar{n}_M/n, \quad \bar{\Omega}_C = \bar{n}_C/n. \end{aligned} \tag{4.80}$$

The use of "bare" for the fermions might be slightly misleading since $\bar{n}_F$ includes fluctuations beyond mean field even. It is used here since this quantity is closest to the exact equation of state (4.62).

The procedure described above allows for a practically implementable approximation for the equation of state. It can be systematically improved in the sense of a derivative expansion. The "zero order" contribution consists in the mean field Fermi density. To first order in the derivative expansion we get the dressed molecules. From our derivation it is clear that the emergence of dressed molecules is associated to the importance of the frequency and momentum dependence of the interactions induced by fermion fluctuations.

Improvements can be made in two directions: First, one can go to higher orders in the derivative expansion for the effective boson fluctuation matrix $\bar{\mathcal{P}}_\phi$ by considering higher frequency powers in the inverse propagator. Second, higher orders in the correlation functions can be taken into account, by considering the frequency dependence of the higher order terms in $\bar{\mathcal{F}}$. However, power counting arguments suggest that these expansions yield less and less important contributions to the particle density – only the wave function renormalization Z_ϕ is a marginal operator in the sense of naive power counting for the classical action, $\dim(Z_\phi) = 0$. The next contribution in the derivative expansion has dimension -2 ($\dim(\omega) = 2$), the first nontrivial contribution from higher correlations even has dimension -3.

We finally note that the fermion fields are not affected by a rescaling transformation with a nontrivial wave function renormalization Z_ψ, i.e. $Z_\psi = 1$. This is of course rooted in the fact that they are integrated out in the present approximation scheme. In the frame of the functional renormalization group, the mode elimination for fermions and bosons is performed simultaneously. In this case, also a nontrivial wave function renormalization can emerge, driven by mixed boson-fermion loops.

Connection to Thermodynamics: Effective Chemical Potential

The derivation of the equation of state via a symmetry consideration bares close similarity to the thermodynamic construction from the grand canonical ensemble where the particle number density is obtained from

$$n = \frac{1}{V}\frac{\partial W}{\partial \sigma} = -\frac{\partial U}{\partial \sigma}, \tag{4.81}$$

where the last equality holds because the current σ is a spectator of the Legendre transform only. The symmetry consideration, however, reveals the status of our equation of state as a derivative expansion more clearly and underlines the importance of a dynamically generated term linear in the frequency as the basic mechanism driving the BCS - BEC crossover. For example, the derivative w.r.t. σ acts on all matrix entries in (4.45, 4.46) in the same way, not being sensitive to the actual frequency dependence of these entries. On the other hand, we can *define* an "effective chemical potential" σ by (4.81) for both fermionic and bosonic contributions to the effective potential, requiring that it acts such that the correct equation of state (4.66) is reproduced. This is implemented by the conditions

$$\frac{\partial \bar{P}_F}{\partial \sigma} = -1, \quad \frac{\partial U_1^{(B)}}{\partial \sigma} = \frac{\partial \bar{m}_\phi^2(\sigma)}{\partial \sigma}\frac{\partial U_1^{(B)}}{\partial \bar{m}_\phi^2}, \quad \frac{\partial \bar{m}_\phi^2(\sigma)}{\partial \sigma} = -2Z_\phi \tag{4.82}$$

The first condition is satisfied automatically (cf. eq. (4.39)) in our approximation based on an expansion in the inverse fermion propagator. The conditions for the boson potential are nontrivial. They state that the σ - derivative must act exclusively on the m_ϕ^2 - piece of the effective boson propagator (4.50) in order to match the result from the symmetry derivation. It follows from an inspection of eq. (4.71). This is actually anticipated by our ansatz for the bare microscopic action (3.1) from simple symmetry considerations.

Having established the connection of the conserved charge with the thermodynamic construction of taking the derivative w.r.t. the effective chemical potential once, the latter has the crucial advantage of not relying on the explicit functional integral representation of the thermodynamic trace. Instead, one can perform the functional integrations, and simply take the σ derivative of the remaining momentum space integrals.

Rescaling Transformations: Gap Parameter and Condensate Fraction

We have introduced dressed boson fields by the rescaling transformation

$$\mathcal{Z} : \tilde{\phi} \to \phi = Z_\phi^{1/2}\tilde{\phi}. \tag{4.83}$$

Requiring invariance of the effective action under the rescaling transform $\mathcal{Z}$ induces transformations of the couplings. A one-parameter transformation leaving the effective action invariant is also called a renormalization group transformation, therefore the rescaled couplings and fields are also termed "renormalized". The rescaled couplings and fields are invariant under a further $\mathcal{Z}$ transform – in other words, $\mathcal{Z}$ is involutory, $\mathcal{Z}^2 = \mathcal{Z}$. A complete list for the rescaling of the couplings is given in app. B. Here we discuss some particular objects only.

We observe that the fermionic determinant (4.40) only depends on the combination

$$\tilde{r} := \tilde{h}_\phi^2 \tilde{\phi}^* \tilde{\phi} = h_\phi^2 \phi^* \phi = h_\phi^2 \rho. \tag{4.84}$$

This combination plays the role of the (squared) dimensionless gap parameter $\tilde{\Delta} = \Delta/\epsilon_F = \sqrt{\tilde{r}}$. The second equality reveals that the squared gap is an invariant under the rescaling transformation $\mathcal{Z}$, cf. eqs. (B.5,B.6).

On the other hand, the equation of state in the form (4.74) involves the dressed or renormalized boson density and condensate. We focus on the latter quantity,

$$\rho = \phi^* \phi = Z_\phi \tilde{\phi}^* \tilde{\phi}. \tag{4.85}$$

The appearance of a condensate in the equation of state is characteristic for the BEC mechanism. Gap and dressed condensate are, however, related by (4.84). The dressed condensate also is invariant under a rescaling transformation due to the fact that $\mathcal{Z}$ is an involution (note $\mathcal{Z}[Z_\phi] = 1$).

Within our Yukawa formalism, we can also compute the *bare* condensate fraction as

$$k_F^{-3} \bar{\rho} = \frac{\rho}{Z_\phi} = \frac{\tilde{r}}{h_\phi^2 Z_\phi} = \frac{\tilde{r}}{\tilde{h}_\phi^2}. \tag{4.86}$$

This quantity is obviously not rescaling invariant, but scales $\propto Z_\phi^{-1}$ or $\propto \tilde{h}_\phi^{-2}$. For objects of this type, Z_ϕ or $\tilde{h}_\phi$ are obviously crucial quantities. This is reflected in fig. 4.1 where we compare the fraction of dressed (a) and bare (b) molecules. While the dressed quantities are quite insensitive w.r.t. the value of $\tilde{h}_\phi$ (for a more thorough discussion of this issue, cf. chapt. 6, sects. 6.2,6.3), the bare quantities scales directly with $\tilde{h}_\phi^{-2}$. For the large values of $\tilde{h}_\phi$ appropriate for the Feshbach resonances investigated in current experiments, the bare density fractions are small.

We finally note that the concentration c is another invariant under the $\mathcal{Z}$ - transformation.

4.2.3 UV Renormalization

In this section we present our scheme to deal with the ultraviolet divergencies present in this nonrelativistic quantum field theory. The bare microscopic action (3.1) depends explicitly on the bare microscopic parameters, but an additional parameter is introduced implicitly by the ultraviolet cutoff Λ in order to regularize the momentum space integrals. (Besides this, the results depend on the thermodynamic variables T and n. However, these low energy scales do not affect the UV renormalization.)

In the approximation scheme presented above, where the fermions are integrated out in one step, it turns out that it is sufficient to perform the ultraviolet renormalization in two instances. The first one concerns the connected correlation functions $\langle\hat{\psi}^\dagger\hat{\psi}\rangle_c$ and $\langle\hat{\phi}^*\hat{\phi}\rangle_c$. Carefully relating these field expectation values to their counterparts in the operator formalism shows that the divergences $\propto\Lambda^3$ are due to a zero point shift of the density [40] [9]. The second divergence for $\Lambda\to\infty$ is associated to the bare detuning $\bar{\nu}_\Lambda$.

When switching on the pointlike four-fermion interaction, we encounter the necessity for an UV renormalization in two further instances: First, $\bar{\lambda}_{\psi,\Lambda}$ needs to be renormalized, and second, such a coupling induces renormalization of the Yukawa coupling $\bar{h}_{\phi,\Lambda}$, which also exhibits a divergence for $\Lambda\to\infty$ and consequently needs UV renormalization. These issues are discussed in sects. 5.6.1 and 7.3, while we restrict to the renormalization of the two-point functions and the bare detuning here. $\bar{h}_{\phi,\Lambda}$ plays the role of a free parameter.

Two-point function

We can illustrate the problems with the two-point function by considering the fermion fluctuation contribution to the effective potential $\bar{U}_1^{(F)}$. Taking the σ - derivative yields, for $\phi=0$ [10],

$$\bar{n}_\Lambda=-\frac{\partial\bar{U}_{1,\Lambda}^{(F)}}{\partial\sigma}=-\int\frac{d^3q}{(2\pi)^3}\tanh\gamma\propto\Lambda^3,\quad\gamma=\frac{\tilde{q}^2-\tilde{\sigma}}{2\tilde{T}}. \tag{4.87}$$

We can clarify the relation between the "naive" particle density $\bar{n}_\Lambda$ obtained in this way and the physical particle density. For this purpose we consider a single fermionic degree of freedom first. The expectation value $\langle\psi^\dagger\psi\rangle$ can be related to the

[9] In our setting the contributions of the fermionic fluctuations are cancelled by the bosonic (molecule) fluctuations and no renormalization is necessary in this respect. This, however, should be seen as a funny coincidence.

[10] Similar to T and k_F, the condensate affects the infrared sector of our theory, such that a nonvanishing condensate cannot alter the UV renormalization procedure.

expectation values of products of the usual annihilation and creation operators $a, a^\dagger$, which obey the anticommutation relation $a^\dagger a + aa^\dagger = 1$,

$$\begin{aligned} \langle \psi^\dagger \psi \rangle &= \frac{1}{2}\langle \psi^\dagger \psi - \psi\psi^\dagger \rangle = \frac{1}{2}\langle a^\dagger a - aa^\dagger \rangle \\ &= \langle a^\dagger a \rangle - 1/2 = n - 1/2. \end{aligned} \tag{4.88}$$

Here the second equality holds since this combination of operators is invariant with respect to permutations of the ordering. Applying this idea to our nonrelativistic atoms, the relation between the true fermion density n and the naive fermion density $\bar{n}_\Lambda$ becomes

$$\begin{aligned} \bar{n}_\Lambda(\vec{x}) &= \langle \psi^\dagger(\vec{x})\psi(\vec{x}) \rangle \\ &= \frac{1}{2}\langle \int_y \sum_{i,j} \left[\psi_i^\dagger(\vec{x})\psi_j(\vec{y}) - \psi_j(\vec{y})\psi_i^\dagger(\vec{x}) \right] \delta_{ij}\delta(\vec{x}-\vec{y}) \rangle \\ &= \frac{1}{2}\langle \int_y \sum_{i,j} \left[a_i^\dagger(\vec{x})a_j(\vec{y}) - a_j(\vec{y})a_i^\dagger(\vec{x}) \right] \delta_{ij}\delta(\vec{x}-\vec{y}) \rangle \\ &= \frac{1}{2}\langle \int_y \sum_{i,j} \left[2a_i^\dagger(\vec{x})a_j(\vec{y}) - \delta_{ij}\delta(\vec{x}-\vec{y}) \right] \delta_{ij}\delta(\vec{x}-\vec{y}) \rangle \\ &= \langle a^\dagger(\vec{x})a(\vec{x}) \rangle - \delta(0) = n(\vec{x}) - \int \frac{d^3q}{(2\pi)^3} \\ &= n(\vec{x}) - \hat{n}. \end{aligned} \tag{4.89}$$

The volume factor in momentum space, $\delta(0)$, diverges in the limit of infinite momentum cutoff. The physical particle density $n(\vec{x})$ and the naive particle density $\bar{n}_\Lambda(\vec{x}) = \langle \psi^\dagger(\vec{x})\psi(\vec{x}) \rangle$ are therefore related by an additive shift that depends on the momentum cutoff.

The physical fermionic particle density now reads

$$n_F = -\int \frac{d^3q}{(2\pi)^3} \{\tanh\gamma - 1\} = 2\int \frac{d^3q}{(2\pi)^3} \frac{1}{\mathrm{e}^{2\gamma}+1} \tag{4.90}$$

which features the standard Fermi distribution.

We can now modify the fermionic contribution of the effective potential such that the physical particle number is generated by the σ - derivative (here we work in the dimensionful version),

$$\bar{U}_1^{(F)} = -2T \int \frac{d^3q}{(2\pi)^3} \log\left(e^{\gamma_\phi - \gamma} + e^{-\gamma_\phi - \gamma} \right) \tag{4.91}$$

where we have dropped another irrelevant infinite constant.

The very same considerations can be applied to the bosonic effective potential and the corresponding particle number. The modified Bogoliubov effective potential reads

$$\bar{U}_1^{(B)} = T \int \frac{d^3q}{(2\pi)^3} \log\left(e^{\alpha_\phi - \alpha} - e^{-\alpha_\phi - \alpha}\right). \tag{4.92}$$

Detuning

The second divergence for $\Lambda \to \infty$ is associated to the bare detuning $\bar{\nu}_\Lambda$. Let us first consider the mean field potential $\bar{U}^{MFT} = (\bar{\nu}_\Lambda + 2\sigma)\bar{\rho} + \bar{U}_1^{(F)}(\sigma, \bar{\rho})$. We can project on the bosonic mass term $\bar{m}_\phi^2$ (in MFT and in the symmetric phase) by

$$\bar{m}_\phi^2 = \frac{\partial \bar{U}^{MFT}}{\partial \bar{\rho}}\Big|_{\bar{\rho}=0} = (\bar{\nu}_\Lambda + 2\sigma) - \frac{\bar{h}_\phi^2}{4T} \int \frac{d^3q}{(2\pi)^3} \gamma^{-1} \tanh \gamma. \tag{4.93}$$

The integral exhibits an UV divergence $\propto \Lambda$. The divergent term also involves the Yukawa coupling $\bar{h}_\phi$. However, in the case of vanishing background scattering, it is not renormalized and constitutes a free parameter of the theory. In this case, the UV divergence can be absorbed by a renormalization of the detuning,

$$\bar{\nu} = \bar{\nu}_\Lambda - \frac{\bar{h}_\phi^2 M \Lambda}{2\pi^2}. \tag{4.94}$$

This prescription corresponds to a renormalization of the effective (resonant) atom interaction strength $\bar{\lambda}_R$, which is directly related to the (resonant) scattering length. We will describe this connection in detail in the next chapter, where we will also relate our model parameters to physical observables.

Expressing the effective potential $\bar{U}^{MFT}$ in terms of $\bar{\nu}$ the momentum integral becomes ultraviolet finite and reads

$$\begin{aligned} \bar{U}^{MFT} &= (\bar{\nu} - 2\sigma)\bar{\rho} + \bar{U}_1^{(F)}, \\ \bar{U}_1^{(F)} &= -2T \int \frac{d^3q}{(2\pi)^3} \Big[\ln\left(\mathrm{e}^{\gamma_\phi - \gamma} + \mathrm{e}^{-\gamma_\phi - \gamma}\right) - \frac{\bar{h}_\phi^2 \bar{\rho} M}{2Tq^2} \Big]. \end{aligned} \tag{4.95}$$

The remaining cutoff dependence is $\mathcal{O}(\Lambda^{-1})$, the precise value of Λ therefore being unimportant.

In sum, expressed in terms of $\bar{\nu}$ and $\bar{h}_\phi$ the effective potential becomes very insensitive to the microscopic physics, i.e. the value of the cutoff Λ. Without much loss of accuracy we can take the limit $\Lambda \to \infty$ for the computation of $\bar{U}^{MFT}$.

We note that the bosonic potential exhibits the same problem with a linear UV divergence for its ρ - derivative. As usual this is rooted in an insufficient treatment of

the high momentum modes. In our formalism, we can even trace this back to an explicit artifact of our approximation scheme, more precisely the derivative expansion. If we had kept the full momentum dependence in eqs. (4.45,4.46), then the corresponding integrals would be smoothly cut off by the momentum dependence of the effective propagator obtained from integrating out the underlying fermionic modes. Actually, this is a nice explicit example of how effective field theories work, and how the appearance of ultraviolet divergencies can be understood. We will present a (rather crude) remedy to this UV problem for the bosonic effective potential in the next chapter, and refine this point in chapt. 7.

4.2.4 Classification of Thermodynamic Phases

We can use the effective action formalism to classify the phases of the system. In a homogeneous situation, we can consider the effective potential (not necessarily bound to the approximation specified above) which can only depend on the invariant $\rho = \phi^*\phi$. The field equation reads

$$\frac{\partial \tilde{u}}{\partial \phi^*} = \frac{\partial \tilde{u}}{\partial \rho}(\rho) \cdot \phi = m_\phi^2(\rho) \cdot \phi = 0. \tag{4.96}$$

We have defined a bosonic mass term as the derivative of the full effective potential. This generalizes the definition (4.49), where the mass term is defined as the derivative of the mean field effective potential. This simple equation can be used to classify the phases of the system (ρ_0 denotes the solution of the field equation (4.96)):

$$\begin{aligned} \text{Symmetric phase :} \quad & \rho_0 = 0, \quad m_\phi^2 > 0, \\ \text{Symmetry broken phase :} \quad & \rho_0 > 0, \quad m_\phi^2 = 0, \\ \text{Phase transition :} \quad & \rho_0 = 0, \quad m_\phi^2 = 0. \end{aligned} \tag{4.97}$$

In the symmetric phase (SYM), we deal with a normal gas: there is no condensate, $\rho_0 = 0$, and the bosonic mass does not vanish. The precise determination of the boson mass is obviously a central requirement for any approximation scheme. It can be done in a self-consistent manner in the frame of Schwinger-Dyson equations which will be presented in the next section. The symmetry broken phase (SSB) is characterized by a nonvanishing field expectation value. For the field equation (4.96) to be satisfied, this requires the vanishing of the mass term m_ϕ^2. The massless mode reflects Goldstone's theorem and is responsible for superfluidity, the diverging inverse mass being associated with the spatial correlation length $\xi = \sqrt{A_\phi/m_\phi^2}$. The roles of m_ϕ^2 and ρ_0 are exchanged compared to the symmetric phase – now ρ_0 should be determined self-consistently. The complex scalar boson corresponds to two degrees of freedom ($O(2)$ model). In an appropriate basis in field space, one of them can be

associated with the massless Goldstone mode (angular mode), while the other one is massive (radial mode). It is this Goldstone mass which is represented by m_ϕ^2, but our approximation scheme also accounts for the radial mode. The phase transition is characterized by the simultaneous vanishing of the mass term and the condensate. The additional constraint allows to solve (4.96) for the critical temperature.

Let us discuss Goldstone's theorem for our nonrelativistic effective bosonic model in more detail. The symmetries and the momentum dependence of eq. (4.50) show that we deal with a nonrelativistic $O(2)$ (or $U(1)$) model. There is a subtlety associated with the characteristic frequency dependence for the nonrelativistic setup which contrasts the generic behavior of relativistic $O(N)$ models. We change the basis in field space in order to make Goldstone's theorem manifest, starting from eq. (4.45) in the derivative expansion (4.50). Again, in the following we are constrained to the derivative expansion which determines the form of the frequency dependence of the inverse propagator, but the couplings and ρ can be determined in approximation schemes beyond the Bogoliubov approximation. This is implemented by choosing the basis of real fields $\hat{\phi}_1, \hat{\phi}_2$.

$$\begin{aligned} \hat{\phi}(Q) &= (\hat{\phi}_1(Q) + \mathrm{i}\hat{\phi}_2(-Q))/\sqrt{2}, \quad \hat{\phi}^*(Q) = (\hat{\phi}_1(-Q) - \mathrm{i}\hat{\phi}_2(Q))/\sqrt{2}, \\ \rho &= (\phi_1^2 + \phi_2^2)/2 \end{aligned} \tag{4.98}$$

which decomposes into a radial part ($\hat{\phi}_1$) and a "phase" part: without loss of generality the vacuum expectation value can be chosen real such that $\phi_2 = 0$, see below. The generalized field vector now reads

$$\hat{\Phi}_r(Q) = \begin{pmatrix} \hat{\phi}_1(Q) \\ \hat{\phi}_2(-Q) \end{pmatrix}, \qquad \hat{\Phi}_r^T(-Q) = \big(\hat{\phi}_1(-Q), \hat{\phi}_2(Q)\big). \tag{4.99}$$

The index "r" stands for real. The unitary transformation matrix between the bases reads

$$U = \frac{1}{\sqrt{2}} \begin{pmatrix} 1 & \mathrm{i} \\ 1 & -\mathrm{i} \end{pmatrix}, \tag{4.100}$$

acts as

$$U\hat{\Phi}_r(Q) = \hat{\Phi}(Q), \qquad \hat{\Phi}^T(-Q) = \hat{\Phi}_r^T(-Q)U^T \tag{4.101}$$

and we note $U^T = (U^\dagger)^* = (U^{-1})^*$. SYM and SSB phases are now characterized by the field expectation values at the minimum of the potential

$$\begin{aligned} \text{SYM}: &\qquad \phi_{1,0} = \phi_{2,0} = 0, \\ \text{SSB}: &\qquad \phi_{1,0} = \sqrt{2\rho_0}, \quad \phi_{2,0} = 0. \end{aligned} \tag{4.102}$$

In SSB, $\phi_{1,0}$ points in the radial direction of the potential, $\phi_{2,0}$ in the degenerate angular direction. At the minimum of the potential, the inverse propagator hence reads

$$\begin{pmatrix} A_\phi \tilde{q}^2 + m_\phi^2 + 2\lambda_\phi \rho_0 & -\tilde{\omega} \\ \tilde{\omega} & A_\phi \tilde{q}^2 + m_\phi^2 \end{pmatrix}. \tag{4.103}$$

The $\delta\hat{\phi}_2, \delta\hat{\phi}_2$ entry reflects the massless Goldstone mode in SSB ($m_\phi^2 = 0$), while $\delta\hat{\phi}_1, \delta\hat{\phi}_1$ is massive in the presence of the condensate. In SYM $\rho_0 = 0$ and the inverse propagator is degenerate. Importantly, the off-diagonal matrix entries feature the frequency dependence of the propagator and couple the $\delta\hat{\phi}_1, \delta\hat{\phi}_2$ modes, such that the determinant *does not factorize*. This is different in relativistic $O(N)$ models where the dependence on frequency and momentum is of the form $\tilde{\omega}^2 + \tilde{q}^2$ and consequently appears on the diagonal entries only.

For given matrix entries A_ϕ, λ_ϕ, and ρ_0, we can compute the dispersion relation for the bosons as

$$\begin{aligned} \det \mathcal{P}_\phi &\stackrel{!}{=} 0, \\ \tilde{\omega} &= \sqrt{A_\phi \tilde{q}^2 (A_\phi \tilde{q}^2 + 2\lambda_\phi \rho_0)}, \end{aligned} \tag{4.104}$$

and we can read off the dispersion for low momenta ($\tilde{q} \to 0$) characteristic for nonrelativistic bosons in the presence of spontaneous symmetry breaking,

$$\tilde{\omega} \approx \sqrt{2A_\phi \lambda_\phi \rho_0}\ \tilde{q}. \tag{4.105}$$

The existence of this "phonon mode" is often referred to as Goldstone's theorem in condensed matter literature – indeed it is a direct consequence of the massless mode.

The classification (4.97) for the phases of the system reveals the universality of the condensation phenomenon itself: One and the same criterion can be used throughout the whole crossover. Indeed the "macroscopic" characteristic of superfluidity, the spontaneous breaking of the global $U(1)$ symmetry, is the same for all values of the coupling. This is the reason why we merely deal with a crossover instead of a sharp phase transition when tuning the inverse scattering length from large negative (BCS regime) to large positive (BEC regime) values. Interestingly, this crossover terminates in a sharp second order phase transition if density and temperature are lowered down to zero at fixed scattering length – physically, this situation describes the vacuum limit. (However, since there is no condensation in vacuum, an order parameter different from ρ_0 must be chosen. This is discussed in sect. 5.5.)

Chapter 5

Schwinger-Dyson Analysis

Before embarking the derivation, let us briefly motivate the need for the use of Schwinger-Dyson equations (SDEs) by considering the mass term in the Bogoliubov approximation. The functional integration of the fermion field generates a (Goldstone) mass term (4.49), which we now denote with a further index signalling that here only fermion fluctuations are included,

$$\bar{m}_\phi^{(F)\,2} \;=\; \bar{\nu}_\Lambda - \bar{h}_\phi^2 \int\limits_Q \frac{1}{\bar{P}_F^{|2|}(Q)}. \tag{5.1}$$

On the other hand, the mass term can also be computed from the field equation for the effective action resp. effective potential (4.96), which in the Bogoliubov approximation reads

$$\bar{m}_\phi^2 \;=\; \bar{m}_\phi^{(F)\,2} + \frac{\partial U_1^{(B)}}{\partial \bar{\rho}}. \tag{5.2}$$

The mass term is obviously modified by the effective boson fluctuations – it is not determined self-consistently in the frame of Bogoliubov theory. This shortcoming can be remedied by the use of SDEs.

If the effective boson fluctuations are small ($\partial U_1^{(B)}/\partial\bar{\rho} \ll \bar{m}_\phi^{(F)\,2}$), then the Bogoliubov approximation works well since the self-consistency problem is weak. This is the case for small temperatures as we will see below. On the other hand, close to the phase transition where the theory is approximately massless, the boson fluctuations should not be ignored.

5.1 Schwinger-Dyson Equations: General Formulation

Schwinger-Dyson equations (SDEs) [53; 54] are a simple consequence of the shift invariance of the functional integral. From this point of view, they are a symmetry of the functional integral itself. Since they give an explicit representation of the derivative of the effective action with respect to the classical field, they are often referred to as the "quantum equations for motion". We will first give the general form of the SDEs following the formalism provided in [55], and then apply it to the crossover problem.

The shift invariance of the functional integral for a bosonic theory in the Nambu representation which we have analyzed on the Bogoliubov level in the last chapter reads

$$\begin{aligned} 0 &= \frac{1}{Z[J]} \int \mathcal{D}(\delta\hat{\Phi}) \, \frac{\delta}{\delta\hat{\Phi}} \exp -S[\hat{\Phi}] + J^T \delta\hat{\Phi} \\ &= \frac{1}{Z[J]} \int \mathcal{D}(\delta\hat{\Phi}) \Big(-\frac{\delta S}{\delta\hat{\Phi}} + J \Big)^T \exp -S[\hat{\Phi}] + J^T \delta\hat{\Phi}. \end{aligned} \tag{5.3}$$

Switching to the effective action, i.e. requiring $J = \delta\Gamma/\delta\Phi$, the above equation turns into

$$\frac{\delta\Gamma}{\delta\Phi} = \Big\langle \frac{\delta S}{\delta\hat{\Phi}} \Big\rangle \Big|_{J=\delta\Gamma/\delta\Phi}. \tag{5.4}$$

This is the SDE for the effective action. The field Φ is the classical field defined as an expectation value $\Phi = \langle\hat{\Phi}\rangle$, cf. eq. (4.8). It does not *a priori* satisfy the equation of motion. The classical action for our problem is the intermediate action $\bar{S}$ (4.37) obtained by integrating out the fermions. We can write down the classical action in a vertex expansion about the classical field, $\hat{\Phi} = \Phi + \delta\hat{\Phi}$, analogous to (4.13). In order to make the notation more concise, we choose a representation with multiindices where both discrete (Nambu) and continuous (spacetime or momentum space) indices are collected in a single index, denoted with a Greek letter. Summation over double indices is understood:

$$\begin{aligned} S[\hat{\Phi}] &= S + \sum_{N=1}^{N_{max}} \frac{1}{N!} S^{(N)}_{\alpha_1 \ldots \alpha_N} \delta\hat{\Phi}_{\alpha_1} \cdot \ldots \cdot \delta\hat{\Phi}_{\alpha_N}, \\ \frac{\delta S}{\delta\hat{\Phi}_\beta} &= \frac{\delta S}{\delta(\delta\hat{\Phi}_\beta)} = \sum_{N=1}^{N_{max}} \frac{1}{(N-1)!} S^{(N)}_{\alpha_1 \ldots \alpha_{N-1}\beta} \delta\hat{\Phi}_{\alpha_1} \cdot \ldots \cdot \delta\hat{\Phi}_{\alpha_{N-1}}. \end{aligned} \tag{5.5}$$

S and $S^{(N)}$ still depend on the classical field Φ. Plugging the vertex expansion into eq. (5.4) relates the field derivative of the effective action to 1PI Green functions up

to order N_{max}. For the intermediate action $\bar{S}$ (4.37), $N_{max} = \infty$. We can turn the SDE into a manifestly closed equation, i.e. an equation which is expressed solely in terms of the effective action and its functional derivatives. For this purpose, we note the identity

$$\begin{aligned}\langle\delta\hat{\Phi}_{\alpha_1}\dots\delta\hat{\Phi}_{\alpha_i}\dots\delta\hat{\Phi}_{\alpha_{N-1}}\rangle\big|_{J[\Phi]} &= \frac{\delta}{\delta J_{\alpha_i}}\langle\delta\hat{\Phi}_{\alpha_1}\dots 1\dots\delta\hat{\Phi}_{\alpha_{N-1}}\rangle\big|_{J[\Phi]} \qquad (5.6)\\ = \frac{\delta\Phi_{\kappa_i}}{\delta J_{\alpha_i}}\frac{\delta}{\delta\Phi_{\kappa_i}}\langle\delta\hat{\Phi}_{\alpha_1}\dots 1\dots\delta\hat{\Phi}_{\alpha_{N-1}}\rangle\big|_{J[\Phi]} &= \big(\Gamma^{(2)\,-1}\big)_{\alpha_i\kappa_i}\frac{\delta}{\delta\Phi_{\kappa_i}}\langle\delta\hat{\Phi}_{\alpha_1}\dots 1\dots\delta\hat{\Phi}_{\alpha_{N-1}}\rangle\big|_{J[\Phi]}\end{aligned}$$

where we have used the chain rule for functional derivatives and (4.22) [1]. For notational convenience, we introduce the full propagator,

$$G_{\alpha\beta} = W^{(2)}_{\alpha\beta} = \big(\Gamma^{(2)\,-1}\big)_{\alpha\beta}. \qquad (5.7)$$

Iterating eq. (5.6), we can write, for $N \geq 4$,

$$\Big[\prod_{i=3}^{N-1} G_{\alpha_i\kappa_i}\frac{\delta}{\delta\Phi_{\kappa_i}}\Big]\langle\delta\hat{\Phi}_{\alpha_1}\delta\hat{\Phi}_{\alpha_2}\rangle = \Big[\prod_{i=3}^{N-1} G_{\alpha_i\kappa_i}\frac{\delta}{\delta\Phi_{\kappa_i}}\Big]G_{\alpha_1\alpha_2} \qquad (5.8)$$

again making use of (4.22). For $N = 4$ the derivative operator in the squared brackets is just the unit matrix. Hence the SDE reads

$$\begin{aligned}\frac{\delta\Gamma}{\delta\Phi_\beta} &= S^{(1)}_\beta + S^{(2)}_{\alpha_1\beta}\langle\delta\hat{\Phi}_{\alpha_1}\rangle + \frac{1}{2!}S^{(3)}_{\alpha_1\alpha_2\beta}G_{\alpha_1\alpha_2} \qquad (5.9)\\ &\quad + \sum_{N=4}^{\infty}\frac{1}{(N-1)!}S^{(N)}_{\alpha_1\dots\alpha_{N-1}\beta}\Big[\prod_{i=3}^{N-1} G_{\alpha_i\kappa_i}\frac{\delta}{\delta\Phi_{\kappa_i}}\Big]G_{\alpha_1\alpha_2}.\end{aligned}$$

The second term in the first line vanishes due to the definition of the fluctuation (4.18,4.19) [2]. Of course, also the full propagator depends on the classical field, $G = G[\Phi]$.

This is an exact functional differential equation for the effective action. Unfortunately, it cannot be solved in a closed form for most interacting theories. However, it is well suited for truncations and we will specify our procedure in the next section. Further, it interesting to note that the SDE features the *classical* vertices from the classical action S quantized by the functional integral. In our case, the classical vertices (i) stem from the classical inverse boson propagator and (ii) are generated by the fermion fluctuations.

[1] Since we are dealing with bosonic fields here, we do not need to care about the order of the functional derivatives.

[2] Had we expanded about another field configuration, this term would be present.

5.2 Application to the Crossover Problem

5.2.1 Truncation

With the Bogoliubov results from the last chapter in mind, we can specify a reasonable truncation scheme for the SDE (5.9) for our practical computations:

- We only consider terms up to fourth order in the field for the intermediate action. This is an effective ϕ^4 theory with non-local (frequency and momentum dependent) effective classical vertices. With this approximation, we can go beyond the Gaussian Bogoliubov theory of the last chapter and, in particular, solve the self-consistency problem for mass and coupling terms exposed above. This approximation implies $S^{(N)} = 0$ for $N \geq 5$.
- For these classical vertices, we perform the derivative expansion (4.50). In particular, we only consider the leading frequency and momentum dependencies for the effective inverse propagator term, i.e. for the "ϕ^2 - vertices". The ϕ^3, ϕ^4 vertices are treated in a zero momentum approximation.
- We work in a one-loop approximation, i.e. we omit the two-loop graph in fig. 5.1. This approximation (loop expansion) might be questionable close to the second order phase transition, where one generically deals with strong fluctuation effects.
- We also impose the ϕ^4 truncation plus derivative expansion for the full theory. This scheme exploits that the effective action shares the symmetries of the "classical" (or intermediate) action.

The truncation advocated here results in an effective action for the boson field

$$\begin{aligned} \Gamma[\phi^*, \phi] &= k_F^3 \epsilon_F V \int_{\tilde{Q}} \left(\tilde{\phi}^*(Z_\phi \mathrm{i}\tilde{\omega} + \tilde{A}_\phi \vec{\tilde{q}}^{\,2})\tilde{\phi} + \tilde{u}[\tilde{\rho}] \right), \qquad (5.10) \\ \tilde{u} &= \tilde{m}_\phi^2(\tilde{\rho} - \tilde{\rho}_0) + \frac{\tilde{\lambda}_\phi}{2}(\tilde{\rho} - \tilde{\rho}_0)^2 = \begin{cases} \tilde{m}_\phi^2 \tilde{\rho} + \frac{1}{2}\tilde{\lambda}_\phi \tilde{\rho}^2 + ... & \text{SYM} \\ \frac{\tilde{\lambda}_\phi}{2}(\tilde{\rho} - \tilde{\rho}_0)^2 + ... & \text{SSB} \end{cases} . \end{aligned}$$

Here we work in the representation in terms of complex scalar fields ϕ^*, ϕ. In the second line, we have written down the effective potential in SYM and SSB phase after inserting the conditions (4.97). This expresses that our expansion is about the minimum of the effective potential. It is maybe worth stressing that the classical fields (expectation values) ϕ^*, ϕ are just another, equivalent representation to $\Phi = (\phi, \phi^*)$ in the SDE (5.9), while $\tilde{\rho}_0$ has the status of a parameter similar to $\tilde{m}_\phi$. However,

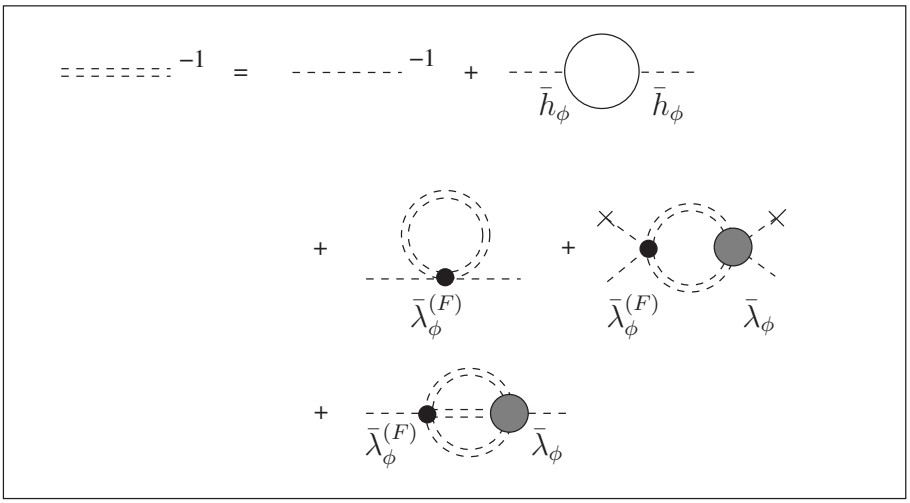

Figure 5.1: Schwinger-Dyson equation for the inverse molecule propagator (double dashed line). The first two terms on the rhs denote the "mean field inverse propagator" after integrating out the fermionic fluctuations with a dashed line for the classical inverse molecule propagator and a solid line for the fermion propagator. The terms in the second line account for the one-loop molecule fluctuations. Here $\bar{\lambda}_\phi^{(F)}$ is the molecule self-interaction induced by the fermion fluctuations. The two-loop term is neglected in our calculations. We omit combinatoric factors here.

the construction is such that at the minimum of the potential, or equivalently at the solution of the field equation for Γ, we have $\rho = \rho_0$.

The truncation obviously implies that the four-boson coupling is characterized by a single number, i.e. the discrete index structure is very simple,

$$\frac{1}{2}\lambda_\phi \rho^2 = \frac{1}{8}\lambda_\phi \delta_{\alpha\beta}\delta_{\gamma\delta}\Phi_\alpha\Phi_\beta\Phi_\gamma\Phi_\delta \tag{5.11}$$

when expressed the basis of bosonic Nambu fields (4.3) appropriate for the above derivation of the SDE. This of course leads to a simple index structure of $S^{(3)}, S^{(4)}$ and $\Gamma^{(3)}, \Gamma^{(4)}$ as well.

5.2.2 Schwinger-Dyson Equation for the Boson Propagator

Eq. (5.9) now reads [3]

$$\begin{aligned}\frac{\delta\Gamma}{\delta\Phi_\beta} &= S^{(1)}_\beta + \frac{1}{2!}S^{(3)}_{\alpha_1\alpha_2\beta}G_{\alpha_1\alpha_2} \\ &\quad -\frac{1}{3!}S^{(4)}_{\alpha_1\alpha_2\alpha_3\beta}G_{\kappa_3\alpha_3}G_{\alpha_1\delta_1}\Gamma^{(3)}_{\delta_1\delta_2\kappa_3}G_{\delta_2\alpha_2}.\end{aligned} \tag{5.12}$$

Here we have kept the two-loop term in the second line in order to show the structure of the full SDE for the effective ϕ^4 theory. In our approximation scheme, we will ignore it. At this stage of the approximation the above equation involves the full one-loop boson propagator $G_{\alpha\beta}$, which in general differs from the effective boson propagator modified by fermion fluctuations only. We can now compute the full one-loop propagator in a parametric sense, and we choose the ϕ_1, ϕ_2 basis for this purpose since this separates radial and Goldstone mode in a clear way. Here we need to consider arbitrary classical field configurations and find from eq. (5.10)

$$\begin{aligned}&\frac{\Gamma^{(2)}[\tilde\phi_1,\tilde\phi_2]}{\epsilon_F V} \\ &= \begin{pmatrix} \tilde A_\phi\tilde q^2 + \tilde m_\phi^2 + \tilde\lambda_\phi(\frac{3}{2}\tilde\phi_1^2 + \frac{1}{2}\tilde\phi_2^2 - \tilde\rho_0) & -Z_\phi\tilde\omega - 2\tilde\lambda_\phi\tilde\phi_1\tilde\phi_2 \\ Z_\phi\tilde\omega - 2\tilde\lambda_\phi\tilde\phi_1\tilde\phi_2 & \tilde A_\phi\tilde q^2 + \tilde m_\phi^2 + \tilde\lambda_\phi(\frac{1}{2}\tilde\phi_1^2 + \frac{3}{2}\tilde\phi_2^2 - \tilde\rho_0) \end{pmatrix}.\end{aligned} \tag{5.13}$$

Here we work in dimensionless, but not renormalized units since we also want to determine Z_ϕ explicitly. Inserting the conditions at the minimum of the potential ($\phi_1 = \sqrt{2\rho_0}, \phi_2 = 0$) this equation reduces to (4.103).

We can asses all the parameters of the truncation (5.10) by applying a further field derivative to eq. (5.12). This actually gives the desired self-consistency condition on the *full* effective boson propagator G:

$$G^{-1}_{\gamma\beta} = S^{(2)}_{\gamma\beta} + \frac{1}{2}S^{(4)}_{\beta\gamma\alpha_1\alpha_2}G_{\alpha_1\alpha_2} - \frac{1}{2}S^{(3)}_{\beta\alpha_1\alpha_2}G_{\alpha_1\delta_1}\Gamma^{(3)}_{\gamma\delta_1\delta_2}G_{\delta_2\alpha_2}. \tag{5.14}$$

The one-loop contribution features a single full inner bosonic line and is therefore frequency and momentum independent.

We can now assess the above couplings by appropriate projection prescriptions applied to (5.12). Further, we can exploit the conditions (4.97) which characterize SYM and SSB phases. For example, inspection of (5.13) reveals that the mass

[3] The differentiation rule for matrix inverses is

$$\frac{\partial}{\partial x}A^{-1} = -A^{-1}\frac{\partial}{\partial x}A\ A^{-1}.$$

.

term m_ϕ^2 can be obtained from the ϕ_2, ϕ_2 entry at zero external frequency and momentum $\tilde{\omega} = \tilde{q} = 0$ and at the minimum of the potential $\phi_{1,0} = \sqrt{2\rho_0}, \phi_{2,0} = 0$. The momentum and kinetic terms involve appropriate derivatives w.r.t frequency and momentum analogous to (4.48). The four-boson coupling is e.g. obtained from applying

$$\frac{1}{\epsilon_F V}\frac{\partial^2\Gamma^{(2)}_{11}}{\partial\tilde{\phi}_2\partial\tilde{\phi}_2}\Big|_{\tilde{\omega}=\vec{\tilde{q}}=0,\tilde{\phi}_{1,0}=\sqrt{2\tilde{\rho}_0},\tilde{\phi}_{2,0}=0} = \frac{\partial^4\tilde{u}}{\partial\tilde{\phi}_1\partial\tilde{\phi}_2\partial\tilde{\phi}_1\partial\tilde{\phi}_2}\Big|_{\tilde{\phi}_1=\sqrt{2\tilde{\rho}_0},\tilde{\phi}_2=0} = \frac{\partial^2\tilde{u}}{\partial\tilde{\rho}^2}\Big|_{\rho=\tilde{\rho}_0}. \tag{5.15}$$

Here $\tilde{u}$ is the Schwinger-Dyson improved effective potential, in contrast to the Bogoliubov potential from the last chapter. Indeed the above prescription corresponds to a projection on the four-boson vertex at zero external frequency and momentum.

In the symmetric phase, the structure of the SDE (5.14) is particularly simple, since $S^{(3)} \propto \rho_0 = 0$ in this case. In SSB the importance of this term is subdominant as we have checked numerically, and we neglect it for the computation of the frequency and momentum dependent pieces in the inverse boson propagator. Since the loop contribution in the first and line of (5.14) are frequency and momentum independent, the wave function renormalization and gradient coefficient are the same as in Bogoliubov theory.

In the one-loop approximation, the SDE (5.12) can actually be integrated w.r.t. to the field Φ [56]. This yields an effective action (or effective potential) which has precisely the form of (4.57). However, the coefficients entering the bosonic part are different from the Bogoliubov approximation – the modification stems from the inclusion of effective boson fluctuations and is called the "one-loop improvement" of the bosonic vertices. With this insight, we can demonstrate that the approximate equation of state remains valid, provided we replace the couplings modified by fermion fluctuations by the "full" couplings extracted from the solution of (5.14). This procedure has, however, some problems associated to the derivative expansion which are discussed below.

In the following we give the explicit gap equations obtained by applying the above projection prescriptions and carrying out the discrete and continuous index contractions in (5.14) in the different phases of the system. We discuss some structural aspects of their solution analytically, and present results of their numerical solution in some applications. The equations given below also form the basis for the results presented in the next chapter.

In addition to the SDEs we additionally have to satisfy the equation of state for the particle density. Conceptually, this equation determines the effective chemical potential $\tilde{\sigma}$ which is an *a priori* free parameter in eqs. (5.14). The physical value of the effective chemical potential throughout the crossover is displayed in fig. 5.2 at

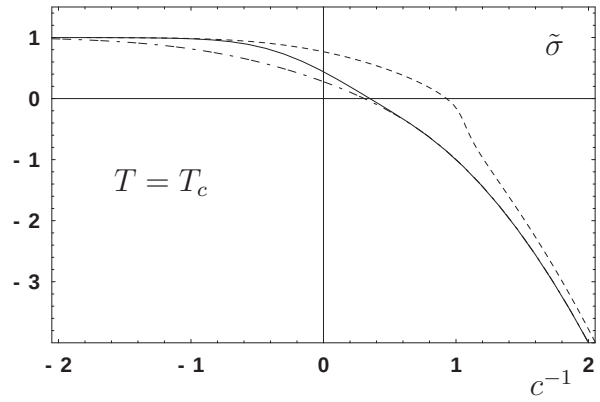

Figure 5.2: Crossover at the critical temperature in the broad resonance limit: Effective dimensionless chemical potential $\tilde{\sigma}$ at the critical temperature as a function of the inverse concentration c^{-1}. We compare the results for two versions of the gap equation as discussed in the text (solid and dashed line). Additionally, the result for the narrow resonance limit is indicated (dashed-dotted).

the critical temperature and in 5.5 (a) at $T = 0$. In the BCS regime it approaches $\tilde{\sigma} = 1$ as expected for a weakly interacting Fermi gas at low temperature, while it behaves $\tilde{\sigma} \propto -c^{-2} \to -\infty$ in the deep BEC regime (cf. also sect. 6.4).

5.3 Exploring the Phase Diagram

For the results presented in this section, we work in the limit of broad resonances $\tilde{h}_\phi \to \infty$. This limit physically corresponds to pointlike interactions as discussed in detail in chapt. 6.

5.3.1 Symmetric Phase

The gap equation for m_ϕ^2 takes the form

$$\begin{aligned} m_\phi^2 &= m_\phi^{(F)\,2} + m_\phi^{(B)\,2}, && (5.16)\\ m_\phi^{(F)\,2} &= \frac{\tilde{\nu} - 2\tilde{\sigma}}{Z_\phi} + \frac{\partial \tilde{u}_1^{(F)}}{\partial \rho} \\ &= \frac{\tilde{\nu} - 2\tilde{\sigma}}{Z_\phi} - \frac{h_\phi^2}{4\tilde{T}} \int \frac{d^3\tilde{q}}{(2\pi)^3} \Big[\frac{1}{\gamma} \tanh\gamma - \frac{2\tilde{T}}{\tilde{q}^2} \Big], \\ m_\phi^{(B)\,2} &= \int \frac{d^3\tilde{q}}{(2\pi)^3} \lambda_\phi^{(F)} \coth\alpha. && (5.17) \end{aligned}$$

with γ defined in eq. (D.45) and

$$\alpha = \frac{A_\phi \tilde{q}^2 + m_\phi^2}{2\tilde{T}}. \tag{5.18}$$

We see how m_ϕ^2 "feeds back" in the above equation since it appears both on the lhs and rhs. $m_\phi^{(F)\,2}$ is precisely eq. (4.49) after the UV renormalization has been carried out – this is the "classical" vertex in (5.14). In order to distinguish fermion from boson fluctuation contributions, we append the indices "F" and "B" here. Here $\lambda_\phi^{(F)}$ is the effective vertex induced by the fermion fluctuations. It is specified below in eq. (5.22). Inspection of $m_\phi^{(B)\,2}$ in eq. (5.16) reveals that the boson loop is plagued with a linear UV divergence – this is similar to the fermion loop. We can trace it back to the derivative expansion. In principle, (5.14) features a term

$$\begin{aligned} m_\phi^{(B)\,2} &= 2\sum_n \tilde{T} \int \frac{d^3\tilde{q}}{(2\pi)^3} \lambda_\phi^{(F)}(\tilde{q}, \tilde{\omega}_n) P_\phi^{-1}(\tilde{q}, \tilde{\omega}_n) \\ &\approx \int \frac{d^3\tilde{q}}{(2\pi)^3} \lambda_\phi^{(F)}(\tilde{q}) \coth\alpha \end{aligned} \tag{5.19}$$

where the approximate equality holds if we neglect the $\tilde{\omega}_n$ - dependence, i.e. we replace $\lambda_\phi^{(F)}(\tilde{q}, \tilde{\omega}_n) \to \lambda_\phi^{(F)}(\tilde{q}) \equiv \lambda_\phi^{(F)}(\tilde{q}, \tilde{\omega}_n = 0)$. In this case we can perform the Matsubara sum. We have not yet computed the momentum dependence of $\lambda_\phi^{(F)}(\tilde{q})$ but a simple qualitative consideration of the relevant diagram shows that for large $\tilde{q}^2$ one has a fast decay $\lambda_\phi^{(F)}(\tilde{q}) \propto \tilde{q}^{-4}$. This makes the momentum integral (5.19) ultraviolet finite. It will be dominated by small values of $\tilde{q}^2$. For our purpose we consider a crude approximation where we replace $\lambda_\phi^{(F)}(\tilde{q}) \to \lambda_\phi^{(F)} \equiv \lambda_\phi^{(F)}(\tilde{q} = 0)$. Of course, we have now to restrict the momentum integration to low momenta. This can be done efficiently by subtracting the leading UV divergence similar to the computation of n_M, i.e. replacing $\coth x$ by $\coth x - 1$. This yields

$$m_\phi^{(B)\,2} = 2\lambda_\phi^{(F)} \int \frac{d^3\tilde{q}}{(2\pi)^3} \Big(\exp 2\alpha - 1 \Big)^{-1}. \tag{5.20}$$

We recognize on the rhs of eq. (5.20) the expression for the number density of dressed molecules n_M and obtain the gap equation

$$m_\phi^2 = m_\phi^{(F)\,2} + \frac{\lambda_\phi^{(F)} \Omega_M}{3\pi^2} \tag{5.21}$$

where we recall that $\Omega_M = n_M/n$ depends on m_ϕ^2. Our gap equation has a simple interpretation: The bosonic contribution to m_ϕ^2 vanishes in the limit where only very few dressed molecules play a role ($\Omega_M \to 0$, BCS side) or for vanishing coupling $\lambda_\phi^{(F)} \propto c$ in the BEC regime. Hence boson fluctuations are strongest in the crossover

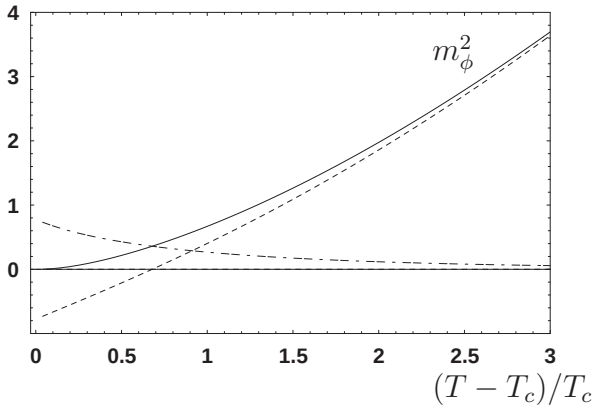

Figure 5.3: Temperature dependence of the bosonic mass term m_ϕ^2 for $c^{-1} = 0, \tilde{h}_\phi \to \infty$. The vanishing of the mass term m_ϕ^2 is approached continuously (solid line). We also plot the separate contributions from "mean field" (classical plus fermions, dashed) and boson fluctuations (dashed-dotted). For $T > T_c$ the latter become unimportant away from the phase transition.

regime. The importance of boson fluctuations contributing to the mass term in this region of the phase diagram is assessed in fig. 5.3. As expected, the bosonic fluctuations are strongest close to T_c where the massless bosonic mode develops.

We are aware that our treatment of the suppression of the high momentum contributions is somewhat crude. It accounts, however, for the relevant physics of the many body system [4] and a more reliable treatment in the frame of SDEs would require a quite involved computation of $\lambda_\phi^{(F)}(\tilde{q}, \tilde{\omega})$. This complication is an inherent problem of gap equations which often require the knowledge of effective couplings over a large momentum range. As an alternative method one may employ functional renormalization [57; 58], where only the knowledge of couplings in a narrow momentum interval is required at every renormalization step. The UV renormalization is successfully implemented in this framework in chapt. 7.

The molecule fluctuations give a positive contribution to m_ϕ^2, opposite to the fermionic fluctuations. This has a simple interpretation. The fermion fluctuations induce a self-interaction between the molecules $\sim \lambda_\phi^{(F)}$. In turn, the fluctuations of the molecules behave similarly to interacting fundamental bosons and modify the two point function for the molecules. We emphasize that an additional microscopic molecule interaction could now easily be incorporated by adding to the mean field value for $\lambda_\phi^{(F)}$ a "classical part" $\lambda_\phi^{(cl)}$. In this case the renormalization of $\bar{\nu}_\Lambda$ discussed in sect. 4.2.3 would be modified. For a constant $\lambda_\phi^{(cl)}$ the UV - divergent part would

[4] In the physical vacuum (discussed below) it fails, since it eliminates the effects of bosonic vacuum fluctuations contributing to the renormalization of the effective bosonic scattering length. This is cured in chapt. 7 in the frame of functional renormalization group equations.

contribute to $m_\phi^2(T=0,n=0)$ and a nonvanishing Δ_ν would modify the relation (4.94). Incorporating Δ_ν into $\bar{\nu}_\Lambda$ one would again end up with a contribution of the form (5.20), now with $\lambda_\phi^{(F)}$ replaced by $\lambda_\phi^{(cl)}+\lambda_\phi^{(F)}$. Our approximation (5.20) deals the interactions of dressed molecules similar to fundamental interacting bosons.

The four-boson coupling λ_ϕ is determined by the SDE

$$\lambda_\phi \;=\; \lambda_\phi^{(F)}+\lambda_\phi^{(B)}=\lambda_\phi^{(F)}+\lambda_\phi\cdot I_\lambda.$$

with

$$\lambda_\phi^{(F)}=\frac{\partial^2\tilde{u}_1^{(F)}}{\partial\rho^2}=\frac{h_\phi^4}{32\tilde{T}^3}\int\frac{d^3\tilde{q}}{(2\pi)^3}\gamma^{-3}\big[\tanh\gamma-\gamma\cosh^{-2}\gamma\big], \tag{5.22}$$

$$\lambda_\phi^{(B)}=-\frac{3\lambda_\phi^{(F)}\lambda_\phi}{2\tilde{T}}\int\frac{d^3\tilde{q}}{(2\pi)^3}\alpha^{-1}\big[(\exp 2\alpha-1)^{-1}+2\alpha\sinh^{-2}\alpha\big].$$

In the symmetric phase, eq. (5.22) decouples from the gap equation for the mass (5.16), and the solution reads

$$\lambda_\phi=\frac{\lambda_\phi^{(F)}}{1-I_\lambda}. \tag{5.23}$$

For $m_\phi^2\to 0$ the last term in eq. (5.22) becomes infrared divergent. Divergences of this type of quantum corrections to quartic couplings are familiar from quantum field theory and statistical physics of critical phenomena. Indeed, the point $m_\phi^2=0$ corresponds to the critical line (or hypersurface) for the phase transition to superfluidity - for negative m_ϕ^2 the symmetric phase becomes unstable. The remedy to this infrared problem has been well understood from the solution of functional renormalization group (FRG) equations: the strong fluctuation effects drive λ_ϕ to zero at the critical line [59–61]. We will come back to this issue in chapt. 7 in the frame of FRG equations.

Our gap equations recover this important feature in a direct way. As m_ϕ^2 approaches zero the negative last term in eq. (5.22) becomes more and more important as compared to λ_ϕ on the left hand side. The solution to eq. (5.22) implies

$$\lim_{m_\phi\to 0}\lambda_\phi(m_\phi)\to 0. \tag{5.24}$$

For small values of m_ϕ^2 in the vicinity of the phase transition we can expand the integral in eq. (5.22) as

$$I_\lambda=-15\tilde{T}\lambda_\phi^{(F)}\int\frac{d^3\tilde{q}}{(2\pi)^3}\big(A_\phi\tilde{q}^2+m_\phi^2\big)^{-2}. \tag{5.25}$$

One infers the characteristic scaling $\lambda_\phi \propto m_\phi$ according to

$$\lambda_\phi = \frac{8\pi}{15\tilde{T}} A_\phi^{3/2} m_\phi. \tag{5.26}$$

As argued above, the kinetic coefficients are only renormalized by fermion diagrams in our approximation. They read, in the dimensionless version,

$$\begin{aligned} Z_\phi &= \frac{\tilde{h}_\phi^2}{16\tilde{T}^2} \int \frac{d^3\tilde{q}}{(2\pi)^3} \gamma^{-2} \big[\tanh\gamma - \gamma \cosh^{-2}\gamma \big], \\ \tilde{A}_\phi &= \frac{1}{2} + \frac{\tilde{h}_\phi^2}{48\tilde{T}^3} \int \frac{d^3\tilde{q}}{(2\pi)^3}\ \tilde{q}^2 \gamma^{-3} \big[\tanh\gamma - \gamma \cosh^{-2}\gamma \big]. \end{aligned} \tag{5.27}$$

The explicit appearance of the wave function renormalization Z_ϕ can be eliminated by applying the rescaling transform $\mathcal{Z}$ (4.83) to the couplings of the theory, cf. eqs. (B.5,B.6). To make our approximation scheme complete, we need to specify the equation of state,

$$1 = \Omega_F^{MFT} + \Omega_M \tag{5.28}$$

which uses the dressed density fractions. Here

$$\Omega_F^{MFT} = 6\pi^2 \int \frac{d^3\tilde{q}}{(2\pi)^3} \big(\mathrm{e}^{2\gamma} + 1\big)^{-1}, \tag{5.29}$$

$$\Omega_M = 6\pi^2 \int \frac{d^3\tilde{q}}{(2\pi)^3} \Big(\mathrm{e}^{2\alpha} - 1\Big)^{-1} = \frac{3\Gamma(3/2)}{2} \Big(\frac{\tilde{T}}{A_\phi}\Big)^{3/2} \mathrm{Li}_{3/2}\big(e^{-m_\phi^2/\tilde{T}}\big). \tag{5.30}$$

5.3.2 Superfluid Phase

The location of the minimum ρ_0 is determined by the condition

$$\hat{m}_\phi^{(F)\,2} + \hat{m}_\phi^{(B)\,2} = 0, \quad \hat{m}_\phi^{(B)\,2} = \frac{\partial \tilde{u}_1^{(B)}}{\partial \rho}\Big|_{\rho=\rho_0}. \tag{5.31}$$

This defines the gap equation for ρ_0, which is the equivalent of eq. (5.21) for the superfluid phase. The computation of the bosonic contribution $\hat{m}_\phi^{(B)\,2}$ encounters the same problems as for $m_\phi^{(B)\,2}$ in the symmetric phase. Again we replace $\lambda_\phi^{(F)}(q)$ by a constant $\lambda_\phi^{(F)}$ evaluated for $q = 0$ and subtract the leading UV divergence of the momentum integral the gap equation for ρ_0

$$m_\phi^{(F)\,2} \ + \ 2\lambda_\phi^{(F)} \int \frac{d^3\tilde{q}}{(2\pi)^3} \frac{\alpha + \kappa/2}{\alpha_\phi} \big(\exp 2\alpha_\phi - 1\big)^{-1} = 0 \tag{5.32}$$

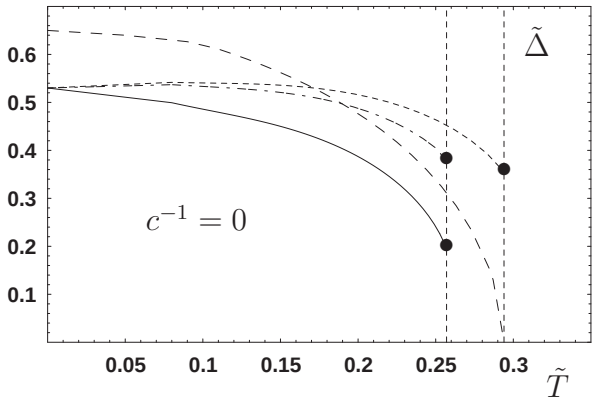

Figure 5.4: Temperature dependence of the gap $\tilde{\Delta} = \sqrt{\tilde{r}}$ at the resonance. The role of molecule fluctuations and the uncertainties in their treatment for $T \to T_c$ are demonstrated by four choices of λ_ϕ in the gap and density equation. The critical temperatures are indicated by vertical dashed lines, with values $\tilde{T}_c = 0.255, 0.292$.

with $\alpha, \kappa, \alpha_\phi$ specified in app. D.4.3, eq.(D.45).

The quantity α_ϕ contains a mass term $2\lambda_\phi \rho_0$ which involves the "full" vertex $\lambda_\phi = \lambda_\phi^{(F)} + \lambda_\phi^{(B)}$ – the equation for mass and coupling term do not decouple in the broken phase. The SDE for λ_ϕ reads

$$\lambda_\phi = \lambda_\phi^{(F)} - \frac{3\lambda_\phi^{(F)}\lambda_\phi}{2\tilde{T}} \int \frac{d^3\tilde{q}}{(2\pi)^3} \alpha_\phi^{-3} \big[\big(\alpha - \kappa\big)^2 \big(\exp 2\alpha_\phi - 1 \big)^{-1} + 2\big(\alpha + \kappa/2\big)^2 \alpha_\phi \sinh^{-2} \alpha_\phi \big]. \tag{5.33}$$

For zero momentum $\tilde{q} \to 0$ we find that λ_ϕ vanishes in the superfluid phase. The Goldstone boson fluctuations renormalize λ_ϕ to zero, as found in [59–61]. This is, however, only part of the story since the gap equation involves a momentum dependent vertex $\lambda_\phi(\tilde{q})$. In order to demonstrate the uncertainty arising from our lack of knowledge of $\lambda_\phi(\tilde{q})$ we present in fig. 5.4 our results for different choices of λ_ϕ in the gap eq. (5.32).

Furthermore, the contribution from the fluctuations of the radial mode in eqs. (5.22) and (5.33) are not treated very accurately. The $\phi_1^2\phi_2^2$ vertex contains in principle a contribution $\propto \nu_\phi \rho_0$ (ν_ϕ the coefficient of the contribution $\propto (\rho - \rho_0)^3$) which shifts $\lambda_\phi^{(F)} \to \lambda_\phi^{(F)} + 2\nu_\phi^{(F)}\rho_0$ and is neglected here.

Finally, we are now in the position to discuss the relevance of the second term in the second line in fig. 5.1. It is only present in the superfluid phase, manifesting itself $\propto \lambda \rho_0^{1/2}$. This term contributes to the Schwinger-Dyson equation for m_ϕ^2, but vanishes for $\lambda_\phi = 0$. Nevertheless, for a momentum dependent λ_ϕ one has to take it into account, as well as similar corrections to the Schwinger-Dyson equation for λ_ϕ.

In detail, we show in fig. 5.4 four approximation scenarios: (i) the "standard" BCS gap equation (long dashed) neglects the molecule fluctuations, i.e. $\lambda_\phi = \lambda_\phi^{(F)} = 0$ in both the gap and the density equation. This yields a second order transition but disagrees with QMC results for $T \to 0$. (ii) Bogoliubov density (short dashed) with $\lambda_\phi^{(F)}$ in the density equation, while the molecule fluctuations in the gap equation are neglected. This improves the behavior for $T \to 0$, but induces a fake first order phase transition for $T \to T_c$. (iii) Neglection of molecule fluctuations in the effective coupling λ_ϕ (dashed-dotted), i.e. we use $\lambda_\phi = \lambda_\phi^{(F)}$ in the density and gap equation. (iv) Our best estimate (solid line) includes also corrections from molecule fluctuations for λ_ϕ. As described in this section we use λ_ϕ in the propagator of the diagram in the gap equation, whereas the coefficient multiplying the diagram is given by $\lambda_\phi^{(F)}$. The first order nature is weaker than in (iii), but still present.

For the results in the Schwinger-Dyson analysis, we use $\lambda_\phi^{(F)}$ in the density equation. This is inspired by the fact that the vanishing of the boson coupling only takes place in the very deep infrared, i.e. for momentum modes which are not relevant for the bosonic particle density – the importance of these low momentum modes is limited since they are weighted by a momentum space volume factor $\propto d(\log q)q^3$ [5]. We encounter here a central challenge posed by the crossover problem: We have to work at fixed particle density, which is an intrinsically *nonlocal* observable – it is the momentum space trace of the full propagator. In principle, this needs knowledge of the full momentum dependence of all couplings entering the trace in the relevant range (for high momenta, the trace is cut off exponentially by the Bose distribution). If the momentum dependence is strong, the derivative expansion is not expected to be quantitatively precise. Especially for the molecule fluctuations, a more accurate treatment seems mandatory before the behavior near T_c in the superfluid phase can be definitely settled. A resolution of this issue is possible in the frame of FRG equations as discussed in chapt. 7.

At low temperature the shortcomings of our approximation scheme are by far less severe than close to T_c – the approximation schemes (ii) – (iv) coincide at $T = 0$. In fig. 5.5 we plot the effective chemical potential and the gap parameter at zero temperature, obtained within the scheme (iv). The inclusion of the molecule density n_M is important for quantitative accuracy even for $T = 0$ – this effect is generically absent in a mean field treatment which neglects the bosonic two-point function from the outset. Additionally we plot in fig. 5.5 (b) the crossover for the gap $\tilde{\Delta}$ as a function of c^{-1}. The agreement with quantum Monte Carlo simulations [62] is substantially improved as compared to mean field theory.

For completeness, we give the formulae for the dimensionless kinetic coefficients

[5] This consideration holds as long as the bosons are not completely massless. In the massless case ate the phase transition, the suppression is $\propto d(\log q)q$ only.

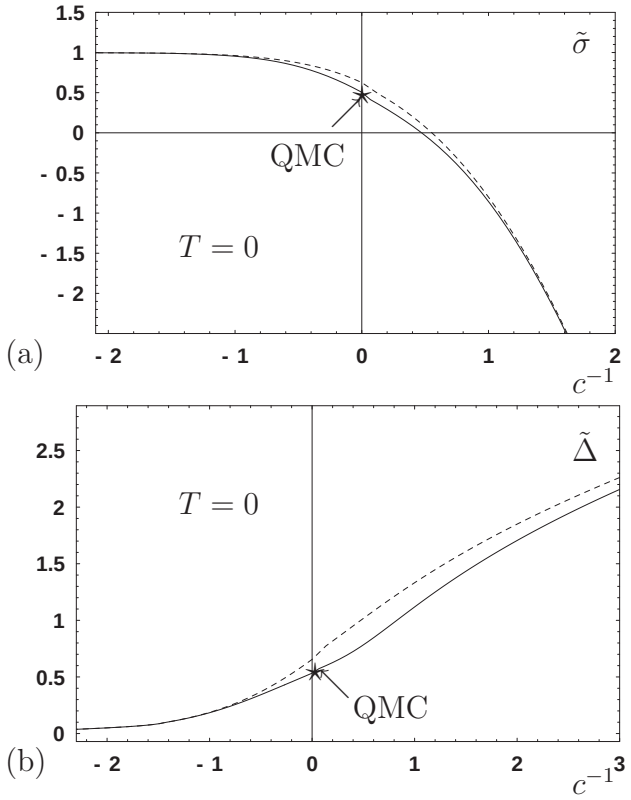

Figure 5.5: Solutions of the coupled gap and density equations at $T = 0$, (a) effective chemical potential, (b) gap parameter $\tilde{\Delta} = \sqrt{\tilde{r}}$. We also show (dashed)the mean field result (obtained by setting the bosonic contribution $n_M = 0$ in the density equation). Our result can be compared to QMC calculations [62] performed at $c^{-1} = 0$ which find $\tilde{\sigma} = 0.44, \tilde{\Delta} = 0.54$. Our solution yields $\tilde{\sigma} = 0.50, \tilde{\Delta} = 0.53$, and improves as compared to the MFT result $\tilde{\sigma} = 0.63, \tilde{\Delta} = 0.65$.

in SSB,

$$Z_\phi = 1 + \frac{h_\phi^2}{16\tilde{T}^2} \int \frac{d^3\tilde{q}}{(2\pi)^3} \gamma\gamma_\phi^{-3} \big[\tanh\gamma_\phi - \gamma_\phi \cosh^{-2}\gamma_\phi \big], \tag{5.34}$$

$$A_\phi = \frac{1}{2} + \frac{h_\phi^2 A_\psi^2}{288\tilde{T}^3} \int \frac{d^3\tilde{q}}{(2\pi)^3}\, \tilde{q}^2\gamma_\phi^{-7} \big[3(5\gamma^4 - 5\gamma^2\gamma_\phi^2 + 2\gamma_\phi^4)[\tanh\gamma_\phi - \gamma_\phi \cosh^{-2}\gamma_\phi] + 2\gamma^2\gamma_\phi(\gamma^2 - \gamma_\phi^2)[\gamma_\phi \cosh^{-4}\gamma_\phi - 6\tanh\gamma_\phi - 2\gamma_\phi \tanh^2\gamma_\phi] \big]. \tag{5.35}$$

For our practical computations in SSB, we work in the form (4.66) for the equation of state,

$$\Omega_F^{MFT} + \Omega_M + \bar{\Omega}_C = 1 \tag{5.36}$$

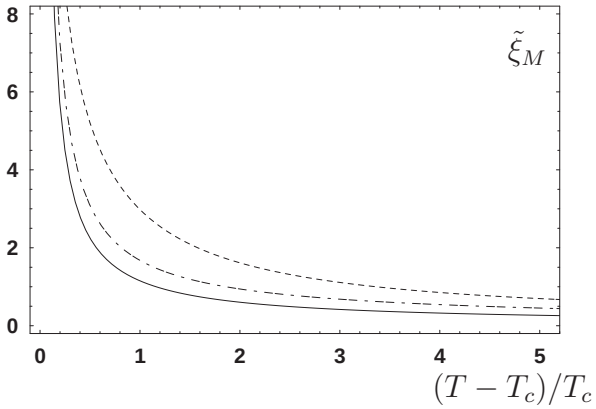

Figure 5.6: Molecular correlation length $\tilde{\xi}_M$ as a function of the reduced temperature $(T-T_c)/T_c$. We consider three regimes: crossover ($c^{-1}=0$, solid), BCS ($c^{-1}=-1.5$, dashed), BEC ($c^{-1}=1.5$, dashed-dotted) and the broad resonance limit $\tilde{h}_\phi \to \infty$.

where the individual terms are given by

$$\begin{aligned}
\Omega_F^{MFT} &= \frac{3\pi^2 n_F^{MFT}}{k_F^3} = -3\pi^2 \int \frac{d^3\tilde{q}}{(2\pi)^3}\Big(\frac{\gamma}{\gamma_\phi}\tanh\gamma_\phi - 1\Big), \qquad (5.37)\\
\Omega_M &= \frac{6\pi^2 n_M}{k_F^3} = 3\pi^2 \int \frac{d^3\tilde{q}}{(2\pi)^3}\Big(\frac{\alpha+\kappa}{\alpha_\phi}\coth\alpha_\phi - 1\Big),\\
\bar{\Omega}_C &= \frac{6\pi^2\tilde{r}}{\tilde{h}_\phi^2}.
\end{aligned}$$

5.3.3 Phase Transition

For $T=T_c$ the gap equations (5.21,5.22) and (5.32,5.33) match since $\rho_0=0$, $\alpha_\phi=\alpha$, $\kappa=0$. Also the expression for the molecule density becomes particularly simple

$$n_M = k_F^3 \frac{\Gamma(3/2)\zeta(3/2)}{4\pi^2}\Big(\frac{\tilde{T}}{A_\phi}\Big)^{3/2}. \qquad (5.38)$$

5.4 Correlation Length and Scattering Length for Molecules

In this section we provide further applications of our formalism.

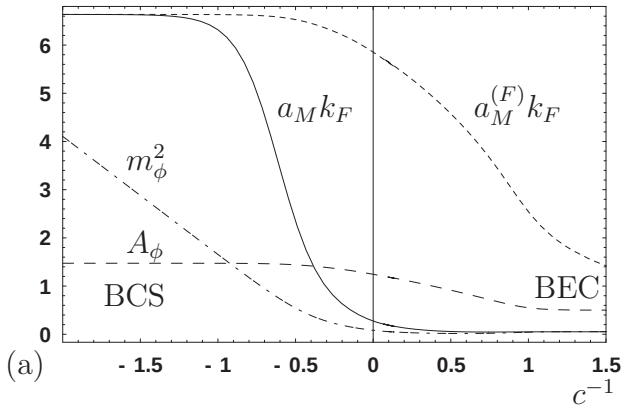

Figure 5.7: Effective potential in the crossover region, $\tilde{T} = 0.33, \tilde{h}_\phi \to \infty$. The solid line expresses the quartic coupling λ_ϕ in terms of the renormalized molecule scattering length obtained with $a_M k_F = \lambda_\phi/(4\pi)$. The short dashed line neglects the molecule fluctuations and shows $a_M^{(F)} k_F = \lambda_\phi^{(F)}/(4\pi)$. Large renormalization effects are observed in the crossover regime. In the BEC limit, the bosons are only weakly interacting. In addition, we plot the renormalized mass term for the molecule field m_ϕ^2 (dashed-dotted) and the renormalized gradient coefficient A_ϕ (long dashed).

In the symmetric phase the static effective molecule propagator reads (for zero Matsubara frequency)

$$\bar{G}_\phi(q) = \bar{P}_\phi^{-1}(\omega = 0, \vec{q}) = \frac{1}{\bar{A}_\phi \vec{q}^{\,2} + \bar{m}_\phi^2}. \tag{5.39}$$

We approximate here $\bar{A}_\phi$ as a constant. The Fourier transform of $\bar{G}_\phi$ decays for large distances r exponentially

$$\bar{G}_\phi(r) \sim \exp(-\xi_M r) \tag{5.40}$$

with spatial correlation length

$$\xi_M = \sqrt{\frac{\bar{A}_\phi}{\bar{m}_\phi^2}}. \tag{5.41}$$

(More precisely, ξ_M^{-2} corresponds to the location of the pole of the propagator for negative q^2 and therefore $\bar{A}_\phi$ should be evaluated at the location of the pole instead of $q^2 = 0$ as approximated here.) At the critical temperature T_c the correlation length ξ diverges since $\bar{m}_\phi = 0$.

In the superfluid phase the propagators for the radial and Goldstone modes differ. The correlation length for the Goldstone fluctuations (ϕ_2) is infinite according

to eq. (5.31). In the "radial direction" (ϕ_1) the effective mass term for the fluctuations around the minimum reads $2\bar{\lambda}_\phi\bar{\rho}_0$. It vanishes (at zero momentum) since our approximation based on Schwinger-Dyson equations [40] yields $\bar{\lambda}_\phi = 0$ for the deep infrared value of the molecule coupling. Hence we obtain in our approximation a diverging correlation length for the radial mode. Nevertheless, the pole is actually not located at $q^2 = 0$ - using a momentum dependent $\bar{\lambda}_\phi(q^2)$ in $\bar{m}_\phi^2$ or taking this effect into account in the form of $\bar{A}_\phi(q^2)$ would be a better approximation. Here we do not discuss further the effects that render the radial correlation length finite for $T < T_c$.

The dimensionless molecular correlation length in the symmetric phase

$$\tilde{\xi}_M = \xi_M k_F = A_\phi^{1/2}/m_\phi \tag{5.42}$$

is expressed in terms of the dimensionless renormalized quantities A_ϕ and m_ϕ^2

$$\tilde{\xi}_M^{-2} \;=\; A_\phi^{-1}\Big\{\nu - 2\frac{\tilde{\sigma}}{Z_\phi} + \Delta m_\phi^{(F)\,2} + \frac{\lambda_\phi^{(F)}}{3\pi^2}\Omega_M\Big\}. \tag{5.43}$$

The renormalized boson mass, displayed in curly brackets in eq. (5.43), was plotted in fig. 5.3.

The condition $\tilde{\xi}_M^{-2} = 0$ defines the critical temperature where the molecule correlation length diverges. Fig. 5.6 displays $\tilde{\xi}_M$ in the BEC, crossover and BCS regime. We observe that the molecular correlation length remains larger than the average distance between atoms or molecules $\sim k_F^{-1}$ even rather far away from the critical temperature. This feature is quite independent of the BEC, BCS and crossover regime. It indicates the importance of collective phenomena.

For $\tilde{\xi}_M \gg 1$ the correlation length exceeds by far the average distance between two atoms. We do not expect the loop expansion to remain accurate in this limit. This is the typical range for the universal critical behavior near a second order phase transition which is known to be poorly described by MFT or a loop expansion. A proper renormalization group framework is needed for $\tilde{\xi}_M \gg 1$. In contrast, for $\tilde{\xi}_M \ll 1$ the molecules are essentially uncorrelated.

Let us define an effective "many-body" molecule scattering length $a_M k_F$ for the dressed molecules in analogy to the two-body case extensively discussed in sect. 7.3, eq. (7.60)

$$a_M k_F = \frac{\lambda_\phi}{8\pi A_\phi}, \quad a_M^{(F)} k_F = \frac{\lambda_\phi^{(F)}}{8\pi A_\phi}. \tag{5.44}$$

A second possible criterion for the validity of the loop expansion is the smallness of the molecular self interaction λ_ϕ. Typically, a one loop expression becomes questionable for $a_M k_F \gg 1$.

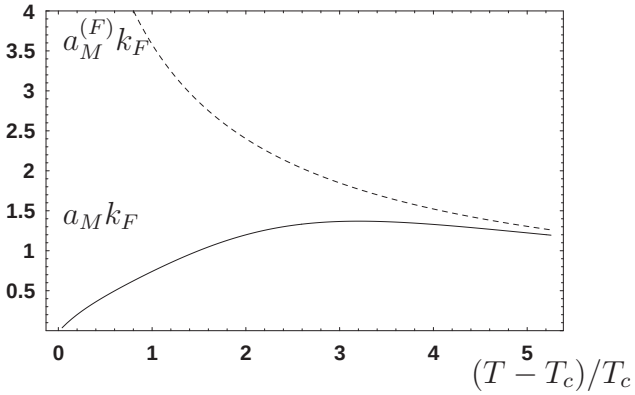

Figure 5.8: "Many-body" scattering length for molecules $a_M k_F$ as a function of the reduced temperature $(T - T_c)/T_c$ in the crossover regime ($c^{-1} = 0, \tilde{h}_\phi \to \infty, \tilde{T}_c = 0.255$). Boson fluctuations renormalize the bosonic many-body scattering length down to zero in the vicinity of the critical temperature. This may be compared to the increase of the fermion fluctuation induced part $a_M^{(F)} k_F$.

We plot $a_M k_F$ and $a_M^{(F)} k_F$ in fig. 5.7 as a function of c^{-1} and in fig. 5.8 as a function of temperature. Both plots are for the broad resonance limit. While $a_M^{(F)} k_F$ grows large near T_c the "full" molecule scattering length $a_M k_F$ goes to zero. The reader should be warned, however, that for $T \to T_c$ the momentum dependence of $\lambda_\phi(q)$ becomes crucial - for $T = T_c$ one has $\lambda_\phi(q) \propto \sqrt{q^2}$ such that λ_ϕ vanishes only for $q = 0$. At T_c the interaction between the dressed molecules cannot be approximated by a pointlike interaction.

As a last application of our formalism we compute the speed of sound as extracted from the low energy dispersion relation $\omega = v_m |q|$, cf. eq. (4.105). In the dimensionless formulation $\tilde{v}_s = 2M v_s / k_F$ it takes the form

$$\tilde{v}_s = \sqrt{2 \lambda_\phi \rho_0 A_\phi}. \tag{5.45}$$

For the broad resonance limit the result is plotted at $T = 0$ throughout the crossover in fig. 5.9. Here we also use $\lambda_\phi = \lambda_\phi^{(F)}$.

5.5 Two-body Limit

So far we have developed a rather complete formalism for the phase diagram for ultracold fermionic atoms in terms of the parameters c and $\tilde{h}_\phi$. In order to make contact with experiment we should relate these parameters to observable quantities. In particular, we will see how the concentration c is related to the magnetic field. As

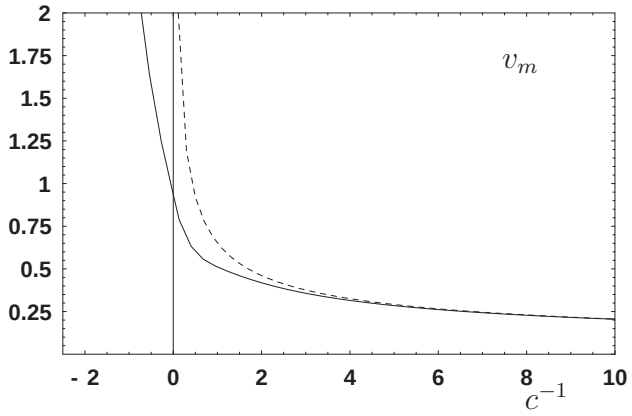

Figure 5.9: Dimensionless speed of sound $\tilde{v}_s$ for the molecules at $T = 0$. In the extreme BEC regime it approaches $\tilde{v}_s \to 2\sqrt{c/(3\pi)}$. This limit (plotted dashed) is obtained by neglecting the contribution from the boson density in the equation of state.

discussed in the introduction, one of the great goals for ultracold atom gases is the realization of systems with well controlled microscopic parameters. This is a central advantage as compared to solids or liquids for which usually the precise microscopic physics is only poorly known. In order to achieve this goal the "microphysical parameters" should be fixed by the properties of the individual atoms and molecules, e.g. by scattering in the vacuum or by the determination of binding energies. The microscopic parameters are then a matter of atomic or molecular physics and do not involve collective effects of many atoms or molecules.

Our functional integral approach relates the microscopic parameters to "macroscopic observables". It can be used for arbitrary values of the density and temperature. In particular, it can be employed for the computation of properties of excitations in the vacuum at zero density and temperature. Within one formalism we can therefore not only compute the properties of many-body systems, but also the scattering behavior of individual atoms or molecules in the vacuum. This enables us to relate our bare microscopic parameters (appearing in the bare microscopic action (3.1)) to observables in atomic or molecular physics. What is needed for this purpose is a computation of binding energies and scattering cross sections in an appropriately performed limit $T \to 0$, $n \to 0$. This will be done in the present section. First we concentrate on the situation $\bar{\lambda}_\psi = 0$ or $a_{bg} = 0, c = a_R(\tilde{\sigma})k_F$, i.e. we only deal with resonant scattering. In sect. 5.6.1, we generalize our results to arbitrary $\bar{\lambda}_\psi$.

5.5.1 Atom and Molecule Phase

We are interested in the limit where the density goes to zero while $\tilde{T} = T/\epsilon_F$ is kept fixed at some value $\tilde{T} > \tilde{T}_c$. Of course, then also T goes to zero, but we do not have to bother with condensation phenomena or critical phenomena (for $\tilde{T}$ sufficiently larger than $\tilde{T}_c$). In the limit $n \to 0, k_F \to 0$ also the concentration c vanishes. Actually, we have to consider two limits $|c| \to 0$ separately, one for positive and the other for negative c. For positive c the low density limit corresponds to a gas of molecules, while for negative c one obtains a gas of fermionic atoms. If the scattering length is much smaller than the average distance between two atoms or molecules, the properties of the dilute gas are directly related to the physics of individual atoms or molecules.

First we focus on the "fermion gas limit" or "atom phase". It is realized for positive $\bar{\nu}$ or negative resonant in-medium scattering length a_R (or negative c). In this case the molecular binding energy is positive such that the excitation of "molecule resonances" requires energy. Since for fixed $\tilde{T}$ and $k_F \to 0$ the temperature becomes very low, $T = \tilde{T}\epsilon_F$, the excited states become strongly suppressed and can be neglected. In this limit one finds $\tilde{\sigma} \to 1$ and therefore $\sigma \to \epsilon_F \to 0$ and $a_R \to -\bar{h}_\phi^2/(4\pi\bar{\nu})$. At fixed $\bar{\nu}$ and $\bar{h}_\phi$ the concentration vanishes $c = a_R k_F \to 0$. Therefore the interaction effects are small. In particular, $\tilde{T}_c$ vanishes in the limit $c \to 0_+$, cf. fig. 6.1.

The discussion of the "molecule phase" obtained for a negative molecular binding energy or $\bar{\nu} < 0$ in the low density and temperature limit is more involved. Now the number density of the fermionic atoms is suppressed since for zero momentum their energy is higher as compared to the molecules. We will show that this "molecule phase" is characterized by a nonzero negative value of σ.

Let us consider the quadratic term for $\bar{\phi}$ in the effective potential or the term linear in $\bar{\rho} = \bar{\phi}^*\bar{\phi}$,

$$\bar{m}_\phi^2 = \frac{\partial U}{\partial \bar{\rho}}(0) = \bar{\nu} - 2\sigma + \frac{\partial U_1^{(F)}}{\partial \bar{\rho}}(0) + \frac{\partial U_1^{(B)}}{\partial \bar{\rho}}(0). \tag{5.46}$$

According to eq. (5.29) or [6]

$$n_M = \int \frac{d^3q}{(2\pi)^3}\Big[\exp\Big(\frac{\bar{A}_\phi(q)q^2 + \bar{m}_\phi^2}{Z_\phi T}\Big) - 1\Big]^{-1} \tag{5.47}$$

the "mass term" $\bar{m}_\phi^2$ dominates the behavior for $T \to 0$ unless it vanishes. Our limit corresponds to $n_M \propto k_F^3 \to 0$, $T \propto \tilde{T}k_F^2 \to 0$ or $n_M \propto T^{3/2} \to 0$. This requires that

[6] Eq. (5.47) becomes exact if the frequency dependence of the correction to $\bar{A}_\phi$ can be neglected (cf. the appendix in [40]) and $\bar{m}_\phi^2 + \bar{A}_\phi(q^2)q^2$ is used to parameterize the exact inverse propagator at zero frequency.

$\bar{m}_\phi^2$ must vanish $\propto k_F^2$. In consequence, the chemical potential σ reaches a nonzero negative value

$$\lim_{k_F\to 0}\sigma = \sigma_A = \frac{1}{2}\Big(\bar{\nu} + \frac{\partial \bar{U}_1^{(F)}}{\partial\bar{\rho}}(0) + \frac{\partial \bar{U}_1^{(B)}}{\partial\bar{\rho}}(0)\Big). \tag{5.48}$$

Here $\frac{\partial \bar{U}_1^{(F)}}{\partial\bar{\rho}}(\bar{\rho}=0)$ and $\frac{\partial \bar{U}_1^{(B)}}{\partial\bar{\rho}}(\bar{\rho}=0)$ have to be evaluated for $\sigma=\sigma_A$. We will see below that $(\partial U_1/\partial\bar{\rho})(\bar{\rho}=0)$ does not vanish for $\sigma_A<0$, $n\to 0$, $T\to 0$ due to the fermionic contribution. We arrive at the important conclusion that for $\bar{\nu}<0$ the vacuum or zero density limit does not correspond to a vanishing effective chemical potential but rather to negative $\sigma_A<0$.

In the molecule phase the nonzero $\sigma_A<0$ adapts the additive constant in the energy such that the molecular energy level is a zero. In consequence, $-\sigma_A$ appears as a positive energy (gap or mass term) in the propagator of the fermionic atoms. As it should be this suppresses the relative number of fermionic atoms in the limit $T\to 0$ and we end with a dilute gas of molecules. The two low density limits (with $\bar{\nu}\neq 0$) therefore both correspond to the limit of vanishing concentration $|c|\to 0$. Positive and negative c correspond to pure gases of molecules or fermionic atoms, respectively.

In sum, the conditions projecting on the physical vacuum read

$$k_F\to 0 \quad \text{for} \quad \tilde{T}>\tilde{T}_c \quad \text{and such that} \quad n\propto k_F^3\to 0. \tag{5.49}$$

These prescriptions result in the following constraints,

$$\begin{aligned} \text{BCS } (a^{-1}<0) \;&:\quad \sigma_A=0, \quad \bar{m}_\phi^2>0, \\ \text{BEC } (a^{-1}>0) \;&:\quad \sigma_A<0, \quad \bar{m}_\phi^2=0, \\ \text{Resonance } (a^{-1}=0) \;&:\quad \sigma_A=0, \quad \bar{m}_\phi^2=0. \end{aligned} \tag{5.50}$$

The constraints $\sigma_A=0$ in the BCS phase and $\bar{m}_\phi^2=0$ on the BEC side are exact properties which have to be met in any approximation scheme. The precise values of $\bar{m}_\phi^2, \sigma_A$ in the respective regimes can, instead, depend on the approximation which we choose. Note the close analogy to the constraints (4.97) which characterized the thermodynamic phases of the system. In the language of thermodynamics, eqs. (5.50) describe the "phase transition" between the atom - and the molecule phase. We will comment on this issue below.

5.5.2 Fermionic Scattering Length and Molecular Binding Energy

In this section we discuss the scattering of atoms in vacuum, and extract the physical fermionic scattering length as well as the molecular binding energy from an

appropriate on-shell limit of the scattering amplitude. For this purpose we first have to reconstruct the scattering amplitude from our partially bosonized setting. The discussion will clarify the relation between the in-medium resonant scattering length $a_R(\sigma)$ (3.13) and the physical resonant scattering length on both sides of the resonance.

Once the effective action Γ is computed it contains directly the information on the one-particle irreducible Green functions including corrections from fluctuations. Therefore the scattering amplitudes can be extracted without much further calculation. Contact to the observable parameters can directly be established in the vacuum limit of our approach.

The amplitude for the elastic scattering of two atoms corresponds to the effective four-fermion amplitude. In presence of a field for the molecules we have two contributions: from the tree exchange of molecules and from the one-particle irreducible four-fermion vertex. We focus on the resonant part here and again set $\bar{\lambda}_\psi = 0$. The tree exchange contribution can be obtained formally by solving the field equation for ϕ for nonvanishing $\psi\epsilon\psi$. This solution becomes then a functional of ψ. Reinserting this solution into Γ yields the "tree contributions" to the four-fermion amplitude, as already discussed in sect. 3.1.

The general expression for the resonant part of the scattering amplitude reads

$$\bar{\lambda}_{\psi,R}(\omega,\vec{q}) \;=\; -\frac{\bar{h}_\phi^2}{\bar{P}_\phi(\mathrm{i}\omega,-2\sigma_A,\vec{q})}. \tag{5.51}$$

All quantities are evaluated at the physical value for the chemical potential, σ_A. Here $\bar{P}_\phi(\omega,-2\sigma_A,\vec{q})$ is the full (fluctuations included) bare (not rescaled with Z_ϕ) inverse boson propagator with σ_A determined by the vacuum conditions (5.50). The boson propagator computed in our formalism corresponds to an euclidean version and must be analytically continued to Minkowski space in order to describe propagating particles [39], justifying the factor "i" in the inverse propagator. Further $\bar{h}_\phi^2$ denotes the full Yukawa coupling. It is affected by fluctuation corrections only in the presence of a pointlike four-fermion coupling (cf. eq. (C.25)). In our present scheme it is a free parameter, but we will consider renormalization effects in sect. 5.6.1 in the frame of Schwinger-Dyson equations and in sect. 7.3 with the functional RG.

In the present scheme we approximate the full boson propagator by the classical plus one-loop term. The frequency and momentum dependent one-loop correction to the boson propagator can be read off from (C.23) in app. C. In the vacuum limit, the integrals can be performed analytically for arbitrary external (Minkowski-

) frequency and momentum. We write

$$\begin{aligned}
\bar{P}_\phi(\mathrm{i}\omega,-2\sigma,\vec{q}) &= \bar{P}_\phi^{(cl)}(\mathrm{i}\omega,-2\sigma,\vec{q})+\Delta\bar{P}_\phi(\mathrm{i}\omega,-2\sigma,\vec{q}), \qquad (5.52)\\
\bar{P}_\phi^{(cl)}(\mathrm{i}\omega,-2\sigma,\vec{q}) &= -\omega-2\sigma+\frac{\vec{q}^{\,2}}{4M},\\
\Delta\bar{P}_\phi(\mathrm{i}\omega,-2\sigma,\vec{q}) &= \frac{\bar{h}_\phi^2 M^{3/2}}{4\pi}\sqrt{-\omega-2\sigma+\frac{\vec{q}^{\,2}}{4M}}.
\end{aligned}$$

$\vec{q}=\vec{q}_1+\vec{q}_2$ and $\omega=\vec{q}_1{}^2/(2M)+\vec{q}_2{}^2/(2M)$ are the total momentum and total kinetic energy of the molecule. In the following another decomposition of $\bar{P}_\phi$ in a zero momentum part and a piece containing the momentum dependence is more useful,

$$\begin{aligned}
\bar{P}_\phi(\mathrm{i}\omega,-2\sigma,\vec{q}) &= \bar{m}_\phi^2+\delta\bar{P}_\phi(\mathrm{i}\omega,-2\sigma,\vec{q}), \qquad (5.53)\\
\bar{m}_\phi^2 &= \bar{P}_\phi(0,-2\sigma,\vec{0})=\bar{\nu}-2\sigma+\Delta\bar{P}_\phi(0,-2\sigma,\vec{0}),\\
\delta\bar{P}_\phi(\mathrm{i}\omega,-2\sigma,\vec{q}) &= -\omega+\frac{\vec{q}^{\,2}}{4M}+\Delta\bar{P}_\phi(\mathrm{i}\omega,-2\sigma,\vec{q})-\Delta\bar{P}_\phi(0,-2\sigma,\vec{0})
\end{aligned}$$

such that

$$\begin{aligned}
\delta\bar{P}_\phi(0,-2\sigma,\vec{0}) &= 0,\\
\delta\bar{P}_\phi(-2\mathrm{i}\sigma,-2\sigma,\vec{0}) &= \bar{\nu}-\bar{m}_\phi^2 \qquad (5.54)
\end{aligned}$$

for *arbitrary* σ. Expressing the boson mass in terms of $\bar{\nu}$ instead of $\bar{\nu}_\Lambda$ takes care of the UV renormalization, and the mass reads explicitly

$$\bar{m}_\phi^2 = \bar{\nu}-2\sigma+\frac{\bar{h}_\phi^2 M^{3/2}}{4\pi}\sqrt{-2\sigma} \qquad (5.55)$$

with magnetic field dependent detuning $\bar{\nu}=\bar{\mu}(B-B_0)$. Here we have absorbed the linear term -2σ from the classical molecule energy in the definition of the mass term.

This scattering amplitude has to be evaluated under an appropriate on-shell condition for frequency ω and total momentum $\vec{q}$ to yield the physical resonant scattering length for a given physical vacuum condition ($\sigma=\sigma_A$). In the center of mass frame, we have $\vec{q}=0$. For the further discussion we have to distinguish atom and molecule phase.

Atom Phase $a^{-1}<0$

Here we have $\sigma_A=0$ and $\bar{m}_\phi^2>0$. The first constraint implies the vanishing of the loop correction to the mass term (5.55). If we want to extract the physical resonant

scattering length a'_R, we further have to consider the zero kinetic energy limit $\omega \to 0$ – since $\sigma_A = 0$, a fermion at rest is already at the scattering threshold. Hence we end up with

$$\begin{aligned} \bar{m}_\phi^2 &= \bar{\nu}, \quad \delta\bar{P}_\phi(0,0,\vec{0}) = 0, \\ a'_R &= \frac{M\bar{\lambda}_{\psi,R}(0,\vec{0})}{4\pi} = -\frac{M\bar{h}_\phi^2}{4\pi\bar{\nu}} = a_R(\sigma_A = 0). \end{aligned} \tag{5.56}$$

where we use the relation between four-fermion vertex and scattering amplitude for non-identical fermions, eq. (A.12). The physical scattering length extracted in this way coincides with our definition of a_R (3.14) derived from the *classical* action for vanishing chemical potential – the absence of renormalization effects reflects our choice of UV renormalization conditions ($\sigma = 0, T = 0$).

As a remark on the side, we note that our formalism can also account for realistic atom-atom scattering at non-zero energy and momentum. We find resonant scattering with a Breit-Wigner form [39].

Molecule Phase $a^{-1} > 0$

Now we have $\sigma_A < 0$ and $\bar{m}_\phi^2 = 0$. The situation is more complex: σ_A has to be computed as a function of the microscopic parameters $\bar{\nu}$ and $\bar{h}_\phi$.

Before doing the calculation, we provide a physical interpretation of the "chemical potential in vacuum", σ_A, as half the molecular binding energy in vacuum, ϵ_M,

$$\epsilon_M = 2\sigma_A. \tag{5.57}$$

We may find this relation by comparing the densities of molecules and fermionic atoms in the low density limit. For small enough density and temperature the interactions become unimportant and the ratio n_F/n_M should only depend on the binding energy in vacuum. Indeed, in our limit $\tilde{\sigma}$ is negative and diverges

$$\lim_{k_F \to 0} \tilde{\sigma} \to \frac{2M\sigma_A}{k_F^2}. \tag{5.58}$$

This simplifies the momentum integrals in the loops considerably. For large negative $\tilde{\sigma}$ one finds $A_\phi = \tilde{A}_\phi/Z_\phi = 1/2$. One therefore has $\bar{A}_\phi/Z_\phi = 1/4M$ and n_M corresponds to a gas of dressed molecules with mass $2M$. On the other hand, the small fraction of fermionic atoms obeys

$$n_{F,0} = 2\int \frac{d^3q}{(2\pi)^3} \big[\exp\big\{ \frac{1}{T}\big(\frac{q^2}{2M} - \sigma_A\big)\big\} + 1\big]^{-1}. \tag{5.59}$$

In the low density limit the interactions become negligible and $n_{F,0}$ should reduce to the density of the free gas of atoms with mass M. However, even for zero momentum the energy of a single atom does not vanish - it is rather given by half the binding energy that is necessary for the dissociation of a molecule. This corresponds precisely to eq. (5.59), provided we identify $\epsilon_M = 2\sigma_A$. We conclude that the binding energy is not simply given by $\bar{\nu}$ (which is defined for $\sigma = 0$ and in the absence of molecule fluctuations) but rather obeys

$$\begin{aligned} \epsilon_M &= \bar{\nu} + \frac{\partial \bar{U}_1}{\partial \bar{\rho}}\big(\bar{\rho} = 0, \sigma = \sigma_A, T = 0\big) = \bar{\nu} + \Delta \bar{P}_\phi(0, -2\sigma_A, \vec{0}) \\ &= \bar{\nu} + \frac{\bar{h}_\phi^2 M^{3/2}}{4\pi}\sqrt{-2\sigma_A}. \end{aligned} \tag{5.60}$$

A measurement of the binding energy of molecules in vacuum, ϵ_M, can relate $\bar{\nu}$ to observation.

For $\sigma < 0$ the non-analytic behavior $\propto \sqrt{-\sigma}$ has an interesting consequence for the threshold behavior near $\epsilon_M = 0$. The equation determining σ_A in the molecule phase (i.e. $\bar{m}_\phi^2(\sigma_A) = 0$) reads

$$\bar{\nu} + \frac{\bar{h}_\phi^2}{4\pi} M^{3/2}(-2\sigma_A)^{1/2} - 2\sigma_A = 0. \tag{5.61}$$

Independently of the value of σ_A and $\bar{h}_\phi$ eq. (5.61) can be transformed into

$$\epsilon_M = 2\sigma_A = -\frac{16\pi^2(\bar{\nu} - 2\sigma_A)^2}{\bar{h}_\phi^4 M^3} = -\frac{1}{M a_R^2(\sigma_A)}. \tag{5.62}$$

where we use the definition (3.13) in the last step. Hence we recover the well known universal result for the scattering length $a_R(\sigma_A)$ [35; 36]. This result is independent of the value of the Feshbach coupling. One concludes $\epsilon_M(\bar{\nu} \to 0) \to 0$. This is, however, only a universal relation between the appropriately defined resonant in-medium scattering length $a_R(\sigma)$ and the binding energy – the rhs of (5.62) still involves σ_A. If one is interested in the relation of $\bar{\nu}(B) = \bar{\mu}(B - B_0)$ and the binding energy (i.e. the magnetic field dependence of the binding energy), one must solve (5.62) for $\bar{\nu}$. We find two distinct regimes. Close to the threshold ($\sigma_A \to 0$), the last term in eq. (5.61) becomes subdominant and the fluctuation term dominates, implying a quadratic behavior

$$\epsilon_M \approx -\frac{1}{M a_R(\sigma = 0)^2} = -\frac{16\pi^2 \bar{\nu}^2}{\bar{h}_\phi^2 M^3} \propto (B - B_0)^2. \tag{5.63}$$

In contrast, far away from threshold the fluctuation term is negligible and the binding energy equals the "classical binding energy",

$$\epsilon_M \approx \bar{\nu} \propto (B - B_0). \tag{5.64}$$

For broad resonances, the linear regime will only be approached far away from the resonance when $\sqrt{-\sigma_A} \gg (2M)^{3/2}\bar{h}_\phi^2/(16\pi)$ – the fluctuation dominated regime extends over a broad domain of magnetic fields. The deviation from the quadratic behavior can be viewed as a scaling violation induced by the finite size of $\bar{h}_\phi$ – in other words by the classical energy dependence of the four-fermion interaction as will become clear in the next chapter. The quadratic dependence of the binding energy on the magnetic field close to the resonance and the linear behavior far off resonance are in agreement with experiments. This is an important check for both our calculation and the modelling.

Coming back to the computation of the physical scattering length on the BEC side, we first observe that each of the scattering fermions must carry a kinetic energy $\omega_{1,2} = -\sigma_A$ in order to reach the scattering threshold, such that $\omega = -2\sigma_A$. Hence we have to work with the second line in eq. (5.54),

$$\begin{aligned} \bar{m}_\phi^2 &= 0, \quad \delta\bar{P}_\phi(-2\mathrm{i}\sigma_A, -2\sigma_A, \vec{0}) = \bar{\nu}, \\ a_R' &= \frac{M\bar{\lambda}_R(-2\sigma_A, \vec{0})}{4\pi} = -\frac{M\bar{h}_\phi^2}{4\pi\bar{\nu}} = a_R(\sigma = 0). \end{aligned} \tag{5.65}$$

The roles of $\bar{m}_\phi^2$ and $\Delta\bar{P}_\phi$ are reversed compared to (5.56).

Eqs. (5.56) and (5.65) state that both on the atom and on the molecule side of the resonance the physical resonant scattering length is given by

$$a_R' = -\frac{M\bar{h}_\phi^2}{4\pi\bar{\nu}} = a_R(\sigma = 0). \tag{5.66}$$

While this relation is obvious for the atom side $\sigma_A = 0$, it is maybe unexpected on the BEC side for the nontrivial vacuum $\sigma_A < 0$. However, in this case the physical scattering length is not a vacuum property any more – the fermions need to be excited to the scattering threshold by a finite kinetic energy $\omega = -2\sigma_A$. Since the boson propagator (5.52) depends on the combination $\omega - 2\sigma_A$ only, this precisely compensates for the binding energy $\epsilon_M = -2\sigma_A$, and only the magnetic field dependent classical part $\bar{\nu}(B)$ remains.

On the other hand, $a_R(\sigma_A)$ is the relevant combination for the description of vacuum properties of the system. It is the right quantity to reveal universal aspects most clearly. For example, had we chosen $(a_R(\sigma = 0)k_F)^{-1}$ instead of the full concentration parameter $c^{-1} = (a_R(\sigma)k_F)^{-1}$ in fig. 6.1, broad and narrow resonance limit could not be compared in a single plot. This is the reason for our choice of the concentration c^{-1} as the universal interaction variable.

If we want to make contact to experimental observation (e.g. resolve a magnetic field dependence, cf. the next section) we have to solve the universal concentration parameter for $\bar{\nu}(B)$. This is discussed below in the last paragraph of the next section.

In the broad resonance limit, and not too far off the resonance, the concentration and the dimensionless physical fermionic scattering length are almost indistinguishable.

As argued in [39], the inverse boson propagator in eq. (5.51), together with the explicit result (5.52), can be used to determine the molecular dispersion relation on the BEC side $\sigma_A < 0$ without an expansion in frequency and momentum. Indeed we can read off

$$\omega = \frac{q^2}{4M} \tag{5.67}$$

corresponding to the dispersion relation of pointlike bosonic particles of mass $2M$. This is another sign for the formation of a true molecular bound state. As to the classical part in the boson propagator, the dispersion relation has been introduced "by hand" in our ansatz for the classical action. The fluctuation part, however, carries this information as a consequence of the frequency and momentum dependence of the fermion loop.

Quantum Phase Transition at $a^{-1} = 0$

We finally comment on the resonance limit $a^{-1} \to 0$ in vacuum. The value of ϵ_M could, in principle, differ between the two limits $n \to 0$ with negative or positive ϵ_M, due to the different ground state values of σ. It is interesting to address in more detail the question of continuity as the magnetic field switches between the two situations. In fact, we may view this qualitative change as a "quantum phase transition" in vacuum as a function of B. The corresponding "order parameter" is the value of σ. For $B > B_0$ the "atom phase" is characterized by $\sigma = 0$ and the mass term $\bar{m}_\phi^2 = \partial U/\partial\bar{\rho}(\bar{\rho} = 0, \sigma = 0)$ is positive (positive "binding energy"). The "molecule phase" for $B < B_0$ shows a nonvanishing order parameter $\sigma = \sigma_A$. Now the mass term vanishes, $\bar{m}_\phi^2 = 0$, whereas the atoms experience a type of gap $|\sigma_A|$. The binding energy is negative, $\epsilon_M < 0$. We find a continuous ("second order") transition where $-\sigma_A$ approaches zero as B approaches B_0. In this case one has $\epsilon_M(B_0) = 0$ and $\bar{m}_\phi^2(B_0) = 0$ for B approaching B_0 either from above or below. (As a logical alternative, a discontinuous first order transition would correspond to a discontinuous jump of σ at B_0. Then also ϵ_M may jump and not be equal to zero at B_0.) As common for second order phase transitions we find a non-analytic behavior at the transition point $B = B_0$.

5.5.3 Relation to Experimental Parameters

So far we have described the universal crossover physics in terms of two parameters c and $\tilde{h}_\phi$. For comparison with experiment these parameters have to be related to

the microphysical properties of a given atomic system and to the external magnetic field B. More precisely, the three parameters in the bare microscopic action (3.1), $\bar{\nu}_\Lambda, \bar{h}_{\phi,\Lambda}$ and $\bar{\lambda}_{\psi,\Lambda}$ have to be known as functions of B and the effective UV cutoff Λ. The dependence on Λ can be eliminated by trading the cutoff dependent parameters for appropriately renormalized quantities. In this section we treat again a situation where the background scattering is neglected. In this case the Yukawa coupling is not affected by direct renormalization effects and we can set $\bar{h}_{\phi,\Lambda} = \bar{h}_{\phi,0}$ where $\bar{h}_{\phi,0}$ is measured in vacuum. Neglecting the background scattering is good close to the resonance and we can extract our parameters $\bar{\nu}$ and $\bar{h}_{\phi,0}$ there. The mass term $\bar{\nu}_\Lambda$ instead needs to be replaced by its renormalized, magnetic field dependent counterpart $\bar{\nu}(B)$ connected to the atomic physics of individual atoms, i.e. evaluated for vanishing density and temperature. Furthermore, $\bar{\nu}$ can be replaced by the physical resonant scattering length which thereby becomes B dependent,

$$a'_R = a_R(\sigma = 0; B) = -\frac{\bar{h}^2_{\phi,0} M}{4\pi\bar{\nu}(B)}. \tag{5.68}$$

The situation is more complex in the presence of a residual pointlike four-fermion interaction which can be related to the background scattering length. This issue is addressed in the next section and in chapt. 7.

Concentration

We may use the measurements of $\epsilon_M(B)$ in order to gain information about our parameters. Consider ^{6}Li in a setting where the "open channel" consists of two atoms in the lowest energy states with nuclear spin $m_I = 1$ and $m_I = 0$, respectively. (These two lowest hyperfine states correspond to our two component fermion ψ.) The binding energy near threshold has been measured [46] for four different values of B and fits well in this range with

$$\epsilon_M \;=\; -\beta(B - B_0)^2, \tag{5.69}$$

where, for ^{6}Li,

$$\begin{aligned} \beta^{(\mathrm{Li})} &= (7.22 \cdot 10^{13}\mathrm{G}^2/\mathrm{eV})^{-1} = (27.6\mathrm{keV}^3)^{-1}, \\ B_0^{(\mathrm{Li})} &= 834.1\mathrm{G} = 16.29\,\mathrm{eV}^2. \end{aligned} \tag{5.70}$$

The corresponding values for ^{40}K are [15]

$$\begin{aligned} \beta^{(\mathrm{K})} &= (4.97 \cdot 10^{9}\mathrm{G}^2/\mathrm{eV})^{-1} = (1.89 \cdot 10^{-3}\mathrm{keV}^3)^{-1}, \\ B_0^{(\mathrm{K})} &= 202.10\mathrm{G} = 3.95\,\mathrm{eV}^2. \end{aligned} \tag{5.71}$$

From eq. (5.62) it is clear that β could also be extracted from scattering experiments as described in the appendix of [39]. However, spectroscopic measurements probing

the binding energy have proven to be most precise. Close to the resonance we can therefore relate the concentration parameter $c = a_R(\sigma_A)k_F$ with the magnetic field [7] by

$$c^{-1}(B) = -\Big(\frac{\beta M}{k_F^2}\Big)^{1/2}(B - B_0) = -\tau_B(B - B_0). \tag{5.72}$$

The relation (5.72) remains actually also valid for the "atom gas", $B > B_0$. In this case one has $\sigma = 0$ and

$$\bar{\nu} = \bar{\mu}(B - B_0) = -\frac{\bar{h}_{\phi,0}^2 M}{4\pi a_R(\sigma = 0)} \tag{5.73}$$

implies

$$k_F c^{-1}(B) = \frac{4\pi\bar{\mu}}{\bar{h}_{\phi,0}^4 M}(B_0 - B). \tag{5.74}$$

It is experimentally verified that the relation $a^{-1} = \sqrt{\beta M}(B_0 - B)$ holds with the same value of β (5.70) as extracted from ϵ_M and we can confirm this by a "computation from microphysics", cf. eqs. (5.56,5.65). This establishes the relation

$$\beta = \frac{16\pi^2\bar{\mu}^2}{\bar{h}_{\phi,0}^4 M^3} \tag{5.75}$$

such that eqs. (5.72) and (5.74) coincide.

The definition of β (5.75) does not involve the scale k_F, while τ_B as fixed by eq. (5.72) does. In principle, there is no need to associate k_F with the physical particle density – in this case the fiducial choice $k_F = 1\text{eV}$ just sets the units. In a thermodynamic situation, $k_F = (3\pi^2 n)^{1/3}$ and τ_B is the appropriate dimensionless quantity for our computations.

The relation (5.72) permits direct experimental control of our concentration parameter for $T = 0$ and $n = 0$. For ^{6}Li and ^{40}K one finds in the (here arbitrary) unit $k_F = 1\text{eV}$

$$\begin{aligned} \tau_B^{\text{Li}} &= 0.0088\text{G}^{-1} = (113.1\text{G})^{-1} = 0.45\text{eV}^{-2}, \\ \tau_B^{\text{K}} &= 2.745\text{G}^{-1} = (0.36\text{G})^{-1} = 140.55\text{eV}^{-2}. \end{aligned} \tag{5.76}$$

This will be easily extended to $T \neq 0$ and arbitrary n below. The microscopic relation that is independent of T and n involves β according to

$$\frac{4\pi\bar{\nu}}{M\bar{h}_{\phi,0}^2} = (\beta M)^{1/2}(B - B_0) = \tau_B k_F(B - B_0). \tag{5.77}$$

[7] More precisely, $c(B)$ stands for $c(B, k_F, \sigma_A)$.

We emphasize that the determination of τ_B in eq. (5.72) does not require knowledge of $\bar{h}_\phi$ since we can use directly the experimental determination of β from eq. (5.69).

We note that our parameter β relates to the parameter Δ in the standard parameterization (2.5) for Feshbach resonances as

$$\Delta = -a_{bg}^{-1}(\beta M)^{-1/2}. \tag{5.78}$$

However, from an inspection of (2.5) it is clear that the characteristic quantity for resonant scattering is β, making sense in the absence of background scattering also. The values for Δ are

$$\Delta^{\mathrm{Li}} = 300\mathrm{G}, \quad \Delta^{\mathrm{K}} = -7.8\mathrm{G}. \tag{5.79}$$

Yukawa Coupling

Let us denote the effective Yukawa coupling in vacuum in the atom phase by $\bar{h}_{\phi,0}$ or $\tilde{h}_{\phi,0}$ for the dimensionless counterpart. From eq. (5.75) and the experimental determination of β in the atom phase we can extract the ratio

$$\frac{\bar{h}_{\phi,0}^2}{\bar{\mu}} = \frac{4\pi}{(M^3\beta)^{1/2}} = 2.516 \cdot 10^{-7}\mathrm{eV}^{-2}\mathrm{G} = 4.915 \cdot 10^{-9}. \tag{5.80}$$

(Here the numerical value is given for ^{6}Li.) For the broad Feshbach resonance in the ^{6}Li system the molecule state belongs to a singlet of the electron spin, resulting in $\mu_M \approx 0$. The microscopic value of $\bar{\mu} = \partial\bar{\nu}/\partial B$ obtains its essential contribution from the magnetic moment of the atoms in the open channel, which is well approximated [42] by the Bohr magneton $\mu_B = 5.788 \cdot 10^{-11}\mathrm{MeV/T} = 0.2963\mathrm{MeV}^{-1}$. For ^{40}K we take $\bar{\mu} = 1.57\mu_B$ [43]. With

$$\bar{\mu}^{(\mathrm{Li})} = 2\mu_B, \quad \bar{\mu}^{(\mathrm{K})} = 1.57\mu_B, \tag{5.81}$$

and $k_F = 1\mathrm{eV}$ this yields high values

$$\begin{aligned} \tilde{h}_{\phi,0}^{\mathrm{Li}} &= 610, \quad (\tilde{h}_{\phi,0}^{\mathrm{Li}})^2 = 3.72 \cdot 10^5, \\ \tilde{h}_{\phi,0}^{\mathrm{K}} &= 79, \quad (\tilde{h}_{\phi,0}^{\mathrm{K}})^2 = 6.1 \cdot 10^3. \end{aligned} \tag{5.82}$$

Using the broad resonance criterion $\tilde{h}_\phi^2 > 100$, we see that indeed ^{6}Li and ^{40}K belong to this class, cf. fig. 6.2.

Though we will only need it in the next section, we display the values of the background coupling $c_{bg} = a_{bg}k_F = \tilde{\lambda}_{\psi,0}/(8\pi)$ for $k_F = 1\mathrm{eV}$,

$$c_{bg}^{\mathrm{Li}} = -0.380, \quad c_{bg}^{\mathrm{K}} = +0.0466. \tag{5.83}$$

Finally we discuss an alternative possibility to determine the Yukawa coupling. The determination of $\epsilon_M = 2\sigma_A$ amounts to the condition

$$\frac{\bar{m}_\phi^2(\sigma_A)}{\bar{h}_\phi^2} = \frac{\bar{\nu} - 2\sigma_A}{\bar{h}_\phi^2} + \frac{\partial \bar{U}_1}{\partial r}(r = 0, \sigma_A) = 0. \tag{5.84}$$

The bosonic fluctuation contribution vanishes for $T \to 0$ and $\partial \bar{U}_1^{(F)}/\partial r$ only depends on σ, but not on $\bar{h}_\phi$ or $\bar{\mu}$. This is the reason why the behavior for $B \to B_0$ can be used to determine c and the ratio (5.80), but not $\tilde{h}_\phi$ separately. In principle, independent experimental information on $\tilde{h}_{\phi,0}$ can be gained from measurements of the binding energy outside the resonance. Indeed, for $\epsilon_M < 0$ the general relation between ϵ_M and $\bar{\nu}$ reads

$$\begin{aligned} \epsilon_M &= \bar{\nu} - \bar{\gamma}(1 - \sqrt{1 - 2\bar{\nu}/\bar{\gamma}}), \\ \bar{\gamma} &= \frac{\bar{h}_{\phi,0}^4 M^3}{32\pi^2}. \end{aligned} \tag{5.85}$$

Measurement of $\epsilon_M(B)$ over a wide enough range allows for the extraction of both $\bar{h}_{\phi,0}^2$ and $\bar{\nu}$ independently [8]. Far away from the resonance one has $|\bar{\gamma}/\bar{\nu}| \ll 1$ such that $\epsilon_M = \bar{\nu}$. From this range we extract the B - dependence of $\bar{\nu}$, $\partial\epsilon_M/\partial B = \partial\bar{\nu}/\partial B = \bar{\mu}$. On the other hand, close to the resonance the opposite limit $|\bar{\gamma}/\bar{\nu}| \gg 1$ applies. Then $\epsilon_M = -\bar{\nu}^2/(2\bar{\gamma})$ involves the concentration c, and, using $\bar{\nu} = \bar{\mu}(B - B_0)$, one can extract $\bar{h}_{\phi,0}$ from $\bar{\gamma} = -\bar{\nu}^2/(2\epsilon_M)$. A further alternative for the extraction of $\bar{\nu}(B)$ and $\bar{h}_{\phi,0}(B)$ is provided from a detailed investigation of the atom scattering near the resonance, as discussed in the appendix of [39].

General Relation between c^{-1} and B

Above we have related the physical scattering length $a_R(\sigma = 0)$ in the atom vacuum with the detuning magnetic field $B - B_0$. This can be used directly for establishing the relation between the concentration c and $B - B_0$ for nonzero T and n (or k_F), using the definition (3.13) and the relation between dimensionful and dimensionless parameters (B.1),

$$c^{-1} = k_F^{-1}\Big(a_R^{-1}(\sigma = 0) + \frac{8\pi\sigma}{\bar{h}_\phi^2 M}\Big). \tag{5.86}$$

One finds

$$\frac{1}{c} - \frac{16\pi\tilde{\sigma}}{\tilde{h}_\phi^2} = -\tau_B(B - B_0) = -\tilde{b}. \tag{5.87}$$

[8] This consideration holds for $a_{bg} = 0$.

Employing the relation

$$\tilde{b} = \frac{8\pi\tilde{\nu}}{\tilde{h}_\phi^2} \tag{5.88}$$

we may also write eq. (5.86) in the form

$$\tilde{\nu} = 2\tilde{\sigma} - \frac{\tilde{h}_\phi^2}{8\pi c} = \frac{2M\bar{\mu}(B - B_0)}{k_F^2}. \tag{5.89}$$

For practical calculations we use the relation (5.89) between $\tilde{\nu}$ and $B - B_0$.

In the broad resonance limit for large values of $\tilde{h}_\phi^2$ of the same order of magnitude as the vacuum values (5.82) the terms $\sim \tilde{h}_\phi^{-2}$ in eq. (5.87) can be neglected if $|\tilde{\sigma}|$ is not too large. This yields the simple expression

$$c^{-1} = -\tilde{b}. \tag{5.90}$$

We recall, however, that this formula should not be used far in the BEC regime where $\tilde{\sigma}$ takes large negative values which diverge in the vacuum limit. For moderate or small values of $\tilde{h}_\phi$ the term $\propto \tilde{\sigma}$ in eq. (5.87) should always be included.

5.6 Dressed and Bare Molecules: Comparison to Experiments

5.6.1 Renormalization of Feshbach and Background Coupling

So far we have considered situations where the background coupling $\bar{\lambda}_\psi$ was neglected. For the Feshbach resonance which is most actively experimentally investigated – ^{6}Li at $B_0 = 834.1$G – the background coupling is, however, substantial and cannot be neglected. The associated scattering length has been determined to be $a_{bg} = -0.38\text{eV}^{-1}$. A systematic treatment of the background coupling does not allow for an integration of the fermionic fluctuations at the Gaussian level. However, the experiment described below is carried out at very low dimensionless temperature, where we have established that bosonic fluctuations are subdominant except for the bosonic two-point function. This is, however, already captured in a Gaussian treatment of the boson fluctuations. Hence, our strategy here is based on a simple one-loop treatment of the boson fluctuations (implying that the couplings in the boson propagator are only renormalized by fermion fluctuations), while we now treat the renormalization of the Feshbach coupling $\bar{h}_\phi$ and the background interaction $\bar{\lambda}_\psi$

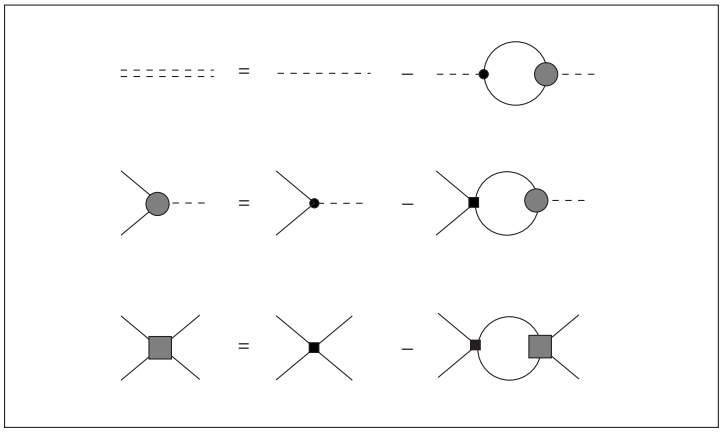

Figure 5.10: Graphical representation of the one-loop Schwinger-Dyson equations (5.91) for the Yukawa theory with additional background interaction. Additional effective boson fluctuations are neglected in this approximation. Small circles (squares) signal bare Yukawa (background) couplings, large shaded symbols represent the full vertices.

by suitable Schwinger-Dyson equations. A similar strategy has been followed in [52].

In principle, the SDE's can be evaluated at arbitrary (analytically continued) frequency iω and momentum $\vec{q}$. This is necessary if we are not only interested in vacuum properties, but also in excitations. The most important object in this respect is the physical fermionic scattering length on the BEC side, where the vacuum is nontrivial, the ground state being a bound molecule. We have seen that the fermionic fluctuation integrals depend on the combination $e = -\omega - 2\sigma$ only, hence we introduce this object as the energy variable. Further, we work in the center of mass frame with total momentum $\vec{q} = 0$. Under these circumstances, the couplings $\bar{\lambda}_\psi, \bar{h}_\phi$ now depend on e, i.e. on ω and σ [9].

Before UV renormalization, the set of SDEs reads

$$\begin{aligned} \bar{P}_\phi &= \bar{\nu}_\Lambda + e - \bar{h}_{\phi,\Lambda}\bar{h}_\phi \bar{J}_\Lambda, \\ \bar{h}_\phi &= \bar{h}_{\phi,\Lambda} - \bar{\lambda}_{\psi,\Lambda}\bar{h}_\phi \bar{J}_\Lambda, \\ \bar{\lambda}_\psi &= \bar{\lambda}_{\psi,\Lambda} - \bar{\lambda}_{\psi,\Lambda}\bar{\lambda}_\psi \bar{J}_\Lambda \end{aligned} \tag{5.91}$$

with

$$\bar{J}_\Lambda(e,T,r) = \frac{1}{4T}\int \frac{d^3q}{(2\pi^3)}\frac{\tanh\gamma_\phi}{\gamma_\phi}. \tag{5.92}$$

[9] Note that for analytically continued external frequency, the couplings can still be factored out of the frequency integrals (or Matsubara sums).

This integral is well known from the evaluation strategy implemented above – the equation for the mass term $\bar{m}_\phi^2$ reduces to the result (4.49,4.93) if one replaces the full Yukawa coupling in (5.91) by the bare one. From the discussion in sect. 4.2.3 we know that the integral is linearly UV divergent. In chapt. 4 we have performed a "perturbative" UV renormalization where the physical detuning was fixed by an observable. This was concretized in the last section, where we have specified the actual low energy observables in particular atomic systems. Now we generalize this procedure by eliminating the Λ - dependent couplings by their observable counterparts. This amounts to a "nonperturbative" UV renormalization procedure. As argued above, we assume that the couplings are measured in the physical vacuum in the atom phase of the system, i.e. for $\omega = \sigma = T = 0$ (cf. eq. (5.50)). The couplings which we introduce in this way thus have the status of full "renormalized" couplings on the atom side – no renormalization effects can alter their values on the BCS side in the two-body limit. On the other hand, we have seen that the vacuum has a different structure on the BEC side, such that one can expect renormalization effects in this regime even in the two-body limit!

For the practical implementation of the UV renormalization procedure we consider the ground state ($\omega = 0, e = -2\sigma$). Let us decompose $\bar{J}_\Lambda$ in the UV divergent part and a physical part encoding the dependence on T, σ and r which vanishes in the atom vacuum and is very insensitive to Λ (such that we can formally work with $\Lambda = \infty$),

$$\bar{J}_\Lambda(-2\sigma, T, r) = \bar{J}(-2\sigma, T, r) + k_\Lambda, \quad k_\Lambda = \frac{M\Lambda}{2\pi^2}, \quad \bar{J}(0,0,0) = 0. \tag{5.93}$$

Now we have to eliminate $\bar{\lambda}_{\psi,\Lambda}, \bar{h}_{\phi,\Lambda}, \bar{\nu}_\Lambda$ and Λ in favor of the vacuum observables $\bar{\lambda}_{\psi,0}, \bar{h}_{\phi,0}, \bar{\nu}$. As argued above, the conditions determining the observables can be extracted from the full equations (5.91) in the limit $\omega = \sigma = T = r = 0$,

$$\begin{aligned} \bar{m}_{\phi,0}^2 &= \bar{\nu}_\Lambda - \bar{h}_{\phi,\Lambda}\bar{h}_{\phi,0}\bar{k}_\Lambda, \\ \bar{h}_{\phi,0} &= \bar{h}_{\phi,\Lambda} - \bar{\lambda}_{\psi,\Lambda}\bar{h}_{\phi,0}\bar{k}_\Lambda, \\ \bar{\lambda}_{\psi,0} &= \bar{\lambda}_{\psi,\Lambda} - \bar{\lambda}_{\psi,\Lambda}\bar{\lambda}_{\psi,0}\bar{k}_\Lambda. \end{aligned} \tag{5.94}$$

For $\omega = 0$ the bosonic propagator in (5.91) reduces to the mass term. We observe a hierarchy in eqs. (5.91,5.94): The third equation decouples from the first two, and the second from the first for given solution of the last one. Hence we follow a consecutive strategy: First we solve the last equation in (5.94) for $\bar{\lambda}_{\psi,0}$ and use this result to express the last equation in (5.91) in terms of $\bar{\lambda}_{\psi,0}$ and $\bar{J}$ only. This provides the UV renormalization of the background coupling. These equations, together with the condition in the second line of (5.94), allow for the UV renormalization of the second line in (5.91). The same procedure is then applied to the first equation. The couplings $\bar{\lambda}_{\psi,0}, \bar{h}_{\phi,0}$ are assumed to be independent of the magnetic field B. The mass

term instead parameterizes the crossover and we decompose, according to eq. (5.73),

$$\bar{\nu}_\Lambda = \bar{\nu}(B) + \delta\bar{\nu}_\Lambda, \quad \bar{\nu}(B) = \bar{\mu}(B - B_0) \tag{5.95}$$

which fixes the resonance at $\bar{\nu}(B_0)$. The result of our nonperturbative renormalization procedure is very simple and reads

$$\begin{aligned} \bar{m}_\phi^2 &= \bar{\nu}(B) - 2\sigma - \frac{\bar{h}_{\phi,0}^2 \bar{J}}{1 + \bar{\lambda}_{\psi,0}\bar{J}}, \\ \bar{h}_\phi &= \frac{\bar{h}_{\phi,0}}{1 + \bar{\lambda}_{\psi,0}\bar{J}}, \\ \bar{\lambda}_\psi &= \frac{\bar{\lambda}_{\psi,0}}{1 + \bar{\lambda}_{\psi,0}\bar{J}}. \end{aligned} \tag{5.96}$$

In addition to the UV renormalization, this set of equations gives explicit expressions for the full couplings $\bar{m}_\phi^2, \bar{h}_\phi, \bar{\lambda}_\psi$ as a function of the vacuum observables, i.e. it solves (5.91) as a function of the vacuum observables.

With these preparations in mind, we are now in the position to generalize the discussion of the physical fermionic scattering length. Now $\bar{h}_\phi$ and $\bar{\lambda}_\psi$ contain a dependence on frequency ω and binding energy ϵ_M. The general expression for the scattering amplitude reads, in the center of mass frame

$$\begin{aligned} \bar{\lambda}(\omega, \vec{0}) &= \bar{\lambda}_R(\omega, \vec{0}) + \bar{\lambda}_\psi(\omega, \vec{0}) \\ &= -\frac{\bar{h}_\phi^2(\omega, \vec{0})}{\bar{P}_\phi(\omega, -2\sigma_A, \vec{0})} + \bar{\lambda}_\psi(\omega, \vec{0}). \end{aligned} \tag{5.97}$$

We must use the full, renormalized couplings in the two-body limit here.

On the BCS side, our construction implies that there are no renormalization effects modifying the couplings $\bar{m}_{\phi,0}^2, \bar{h}_{\phi,0}, \bar{\lambda}_{\psi,0}$ since $\bar{J}(0,0,0) = 0$. The full physical scattering length thus reads

$$a' = \frac{M\bar{\lambda}_R(0,\vec{0})}{4\pi} + \frac{M\bar{\lambda}_\psi(0,\vec{0})}{4\pi} = \frac{M\bar{h}_{\phi,0}^2}{4\pi\bar{\nu}(B)} + \frac{M\bar{\lambda}_{\psi,0}}{4\pi} = a_R(\sigma = 0) + a_{bg} = a(\sigma = 0). \tag{5.98}$$

Note that there is no problem with the Fierz ambiguity – we have uniquely fixed the parameters by observation at low energies.

On the BEC side, the situation is more complex since $\sigma_A < 0$. Defining

$$\bar{J}_0 = \bar{J}(e = -2\sigma_A, 0, 0) = -\frac{M}{4\pi}(-2M\sigma_A)^{1/2} = \Delta\bar{P}_\phi(0, -2\sigma_A, \vec{0}), \tag{5.99}$$

we can give the set of equations determining the vacuum. The equation for the mass now reads

$$0 = \bar{m}_\phi^2 = \bar{\nu} - 2\sigma_A - \frac{\bar{h}_{\phi,0}^2 \bar{J}_0}{1 + \bar{\lambda}_{\psi,0}\bar{J}_0}. \tag{5.100}$$

The full couplings in the BEC vacuum are given by

$$\bar{h}_\phi(\omega = 0, \sigma_A) = \frac{\bar{h}_{\phi,0}}{1 + \bar{\lambda}_{\psi,0}\bar{J}_0}, \tag{5.101}$$

$$\bar{\lambda}_\psi(\omega = 0, \sigma_A) = \frac{\bar{\lambda}_{\psi,0}}{1 + \bar{\lambda}_{\psi,0}\bar{J}_0}. \tag{5.102}$$

If we want to extract the physical fermionic scattering length, we have to evaluate the integrals as $\omega = -2\sigma_A$ or $e = 0$ to put the fermions on shell. Hence, the renormalization effects are compensated by the finite excitation energy, and we end up with the full physical fermionic scattering length

$$a' = a'_R + a_{bg} = a(\sigma = 0) \tag{5.103}$$

as on the BCS side.

We can have a look at the behavior of the gap parameter $\tilde{r}$ if we take a background scattering into account. In our approximation, the gap is given by the solution of

$$0 = \bar{\nu}(B) - 2\sigma - \frac{\bar{h}_{\phi,0}^2 \bar{J}}{1 + \bar{\lambda}_{\psi,0}\bar{J}}. \tag{5.104}$$

Using dimensionless variables, this can be transformed into

$$\tilde{J}(-2\tilde{\sigma}, \tilde{T}, \tilde{r}) = -\frac{1}{8\pi c} \tag{5.105}$$

where $c = a_R k_F + c_{bg}$ is the *full* concentration, including the in-medium effect from $\tilde{\sigma}$. Hence, the solution $\tilde{r}$ of this equations transforms as $\tilde{r}(a_R k_F) \to \tilde{r}(c)$ if $a_R k_F \to c$. There is *no* separate dependence on $a_R k_F$ and c_{bg}, $\tilde{r}$ only depends on the renormalization group invariant full concentration c. Obviously, the concentration is the right quantity as far as the universal vacuum properties of the crossover are concerned. It is thus the natural generalization of the dimensionless resonant concentration parameter of sect. 5.5.2.

5.6.2 Bare Molecules

We are now in the position to compare the findings of our formalism to experiments. The fraction of closed channel molecules is given by $\bar{\Omega}_B = \bar{\Omega}_M + \bar{\Omega}_C$. It has been

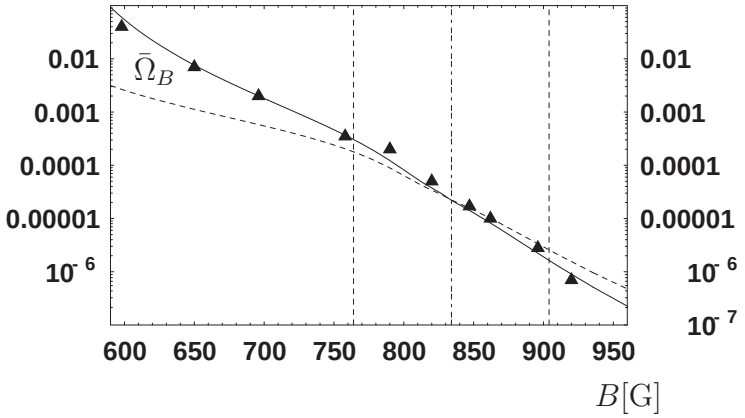

Figure 5.11: Fraction of closed channel molecules $\bar{\Omega}_B = \bar{\Omega}_C + \bar{\Omega}_M$, compared to experimental values [63], for $T = 0$ and $k_F = 0.493\text{eV} \hat{=} 250\text{nK}$. On the BEC side, we find that our results are quite insensitive to the precise choice of k_F. The strongly interacting region $c^{-1} < 1$ is indicated by vertical lines, where the center line denotes the position of the resonance. The dashed line omits the renormalization effects discussed in the text.

measured by a laser probe that induces a transition to an excited molecular level - the quantity Z in [63] equals $\bar{\Omega}_B$. Indeed, the laser probe couples directly to the total number of "bare molecules" $\langle\hat{\phi}^*\hat{\phi}\rangle$. Importantly, we will shortly see that this quantity involves the Yukawa $\tilde{h}_\phi$ coupling explicitly. In fig. 5.11 we compare our results with the measured value for Li, using $T = 0$, $k_F = 0.493\text{eV} \hat{=} 250\text{nK}$. The solid line uses $c = k_F(a_R(B) + a_{bg})$ (5.103) for the whole range of B. The agreement with the measured value is very convincing. We emphasize that the inclusion of the renormalization (5.91) for the Yukawa coupling is crucial. Omitting this effect (dashed line) for $B < B_0$ in fig. 5.11 results in a clear discrepancy from the observations sufficiently far away from the resonance.

At this place we may give a few more details of our computation of $\bar{\Omega}_B$,

$$\bar{\Omega}_B = \bar{\Omega}_M + \bar{\Omega}_C = 3\pi^2\big(\frac{k_F^{-3} n_M}{Z_\phi} + 2\frac{\tilde{r}}{\tilde{h}^2_{\phi,0}}\big) = \frac{3\pi^2}{\tilde{h}^2_{\phi,0}}\big(k_F^{-3} h_\phi^2 n_M + 2\tilde{r}\big). \tag{5.106}$$

We use the Yukawa coupling as defined in (5.91) in the place where it appears explicitly. The renormalized Yukawa coupling h_ϕ is very insensitive to $\tilde{h}_{\phi,0}$ for broad resonances. All other quantities are taken from the solution of the equations determining the crossover problem in the superfluid phase in the approximation advocated here, eqs. (5.36,5.37,5.91). The formula for $\bar{\Omega}_C$,

$$\bar{\Omega}_C = \frac{6\pi^2}{k_F^3}|\bar{\phi}_0|^2 = 6\pi^2(1 - a_{bg}/a)^2\frac{\tilde{r}_0}{\tilde{h}^2_{\phi,0}} \tag{5.107}$$

relates the closed channel condensate fraction to the superfluid order parameter $\tilde{r}_0$. In that sense Partrigde *et al.* indirectly measure the superfluid order parameter! From $\bar{\Omega}_C$ we can infer $\bar{\Omega}_B = \bar{\Omega}_C(1 + \bar{\Omega}_M/\bar{\Omega}_C)$ by extracting the ratio $\bar{\Omega}_M/\bar{\Omega}_C$ from fig. 4.1. In the BEC limit $\bar{\Omega}_M/\bar{\Omega}_C$ becomes negligible, while at resonance ($c^{-1} = 0$) we find $\bar{\Omega}_M/\bar{\Omega}_C = 1.89$.

Let us briefly comment on the density dependence of our result. This is particularly simple in our dimensionless formulation. Since $\tilde{r}_0$ is taken from the solution of the crossover problem it does not depend on k_F if c is kept fixed. However, in order to find the right dimensionless value $\tilde{h}_\phi = 2M\bar{h}_\phi/k_F^{1/2}$, k_F must be inserted. For fixed c this yields $\bar{\Omega}_C \propto k_F$. The ratio $\bar{\Omega}_M/\bar{\Omega}_C$ depends also on c. The dependence of $\bar{\Omega}_B$ on c introduces an additional density dependence of $\bar{\Omega}_B$ if the scattering length a is kept fixed. (Only for fixed ak_F one always has $\bar{\Omega}_B \propto k_F$ in the broad resonance limit.)

In the scaling limit $c^{-1} = 0$ the value $\tilde{r}_0$ and the ratio $\bar{\Omega}_M/\bar{\Omega}_C$ are independent of k_F if we assume the broad resonance limit $\tilde{h}_\phi \to \infty$. In this limit we thus can confirm the simple scaling law at resonance advocated by Ho [64], $\bar{\Omega}_B \propto k_F$. A similar result has been obtained by Levin *et al.* [65], though neglecting the contribution $\bar{\Omega}_M$ which is of the same order of magnitude at the resonance, cf. fig. 4.1 (b).

In the BEC limit $\bar{\Omega}_M/\bar{\Omega}_C$ becomes negligible. Furthermore, since $\tilde{r}_0 \propto c^{-1} \propto k_F^{-1}$, one finds that $\bar{\Omega}_B$ becomes independent of k_F. Note that this result is only valid for k_F which respect the BEC regime condition, $c^{-1} = (ak_F)^{-1} > 1$ or $k_F < a^{-1}$.

In the deep BCS regime $|c|^{-1} = |ak_F|^{-1} \gg 1$, we also find numerically that $\bar{\Omega}_M/\bar{\Omega}_C \ll 1$. Using the standard BCS result relating the superfluid order parameter at $T = 0$ and c^{-1}, our scaling form yields $\bar{\Omega}_B \propto k_F \exp(-\pi/(ak_F))$. Again, in order to stay in the desired regime, k_F must be restricted to values $k_F \ll |a|^{-1}$. In sum, we find the following scaling behaviors with k_F

$$\bar{\Omega}_B \propto \begin{cases} \text{const.} & \text{BEC} \\ k_F & \text{Resonance} \\ k_F \mathrm{e}^{-\pi/(ak_F)} & \text{BCS} \end{cases} . \tag{5.108}$$

Note that the naive power counting $\bar{n}_B \propto k_F^3$ (or $\bar{\Omega}_B = \text{const.}$) is only valid in the deep BEC regime. Substantial deviations from this scaling are found when evolving away from this region.

5.6.3 Dressed Molecules

The condensate fraction measured in [15; 16] qualitatively refers to the condensation of "dressed molecules" or di-atom states. At the present stage, however, the precise relation between the measured observables and the condensate fraction Ω_C has not

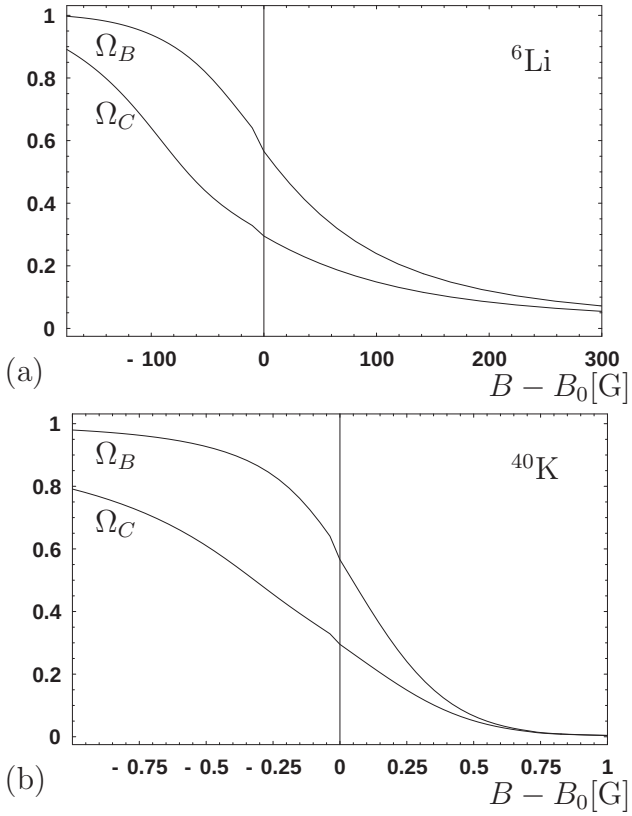

Figure 5.12: Condensate fraction Ω_C and total fraction of dressed molecules $\Omega_B = \Omega_M + \Omega_C$ at $T = 0$, for ^{6}Li (a) and ^{40}K (b). Due to the nonlinear relation of c^{-1} and $B - B_0$ which is particularly strong for ^{6}Li due to the large background scattering value, the curves are twisted compared to the $\Omega(c^{-1})$ plots. We adjust k_F to the values found in [15] ($k_F = 1.50\text{eV} \hat{=} (2500 a_B)^{-1}$) and [16] ($k_F = 1.39\text{eV} \hat{=} (2700 a_B)^{-1}$).

yet been established with sufficient quantitative accuracy. As argued in sect. 4.2.2, Ω_C (4.76) is given by the expectation value of the renormalized field

$$\Omega_C \;=\; 6\pi^2 Z_\phi \tilde{\rho} = 6\pi^2 \rho. \tag{5.109}$$

In fig. 5.12 we plot our result for the condensate fraction of dressed molecules at zero temperature as a function of magnetic field, for both the ^{6}Li (fig. 5.12 (a)) and the ^{40}K system (fig. 5.12 (b)). Unlike the condensate fraction of bare molecules, the contribution from the dressed condensate is an $\mathcal{O}(1)$ quantity.

We find qualitative agreement with the observations [15; 16] whereas for a quantitative comparison one would need a more accurate relation between the measured observables and the condensate fraction Ω_C as defined in our setting. First, the scales of the magnetic field B for which Ω_C decreases from rather large values to small values match the scales found in the experiments. This is another confirmation of our universal relation between B, the particle density (or k_F) and the quantities $c^{-1}, \tilde{h}_\phi$. We find that in the BEC limit, the condensate fraction approaches 1 very slowly. The observed condensate depletion is the effect of the interaction between the dressed molecules, as expected for a weakly interacting Bogoliubov gas.

An interesting quantity is the value of the condensate fraction at the location of the resonance, $B = B_0$. For $T = 0$ we find a universal value $\Omega_C^0 = \Omega_C(T = c^{-1} = 0) = 0.30$, which therefore should apply both [10] for ^{6}Li and ^{40}K. In order to judge the reliability of this universal result we may consider the relation

$$\Omega_C = \frac{6\pi^2 \tilde{r}_0}{h_\phi^2} \tag{5.110}$$

which involves the renormalized Yukawa coupling $h_\phi^2 = \tilde{h}_\phi^2 / Z_\phi$. In the broad resonance limit and for $T = 0$ the value $\tilde{r}_0^0 = \tilde{r}_0(T = c^{-1} = 0) = 0.28$ is universal. The size of Ω_C^0 is therefore determined by h_ϕ^2, $\Omega_C^0 = 16.85 h_\phi^{-2}$. In the same limit we find

$$h_\phi^{-2} = \frac{1}{8\pi^2} \int_0^\infty d\tilde{q} \frac{\tilde{q}^2(\tilde{q}^2 - \tilde{\sigma})}{[(\tilde{q}^2 - \tilde{\sigma})^2 + \tilde{r}_0]^{3/2}} \tag{5.111}$$

where $\tilde{\sigma}^0 = \tilde{\sigma}(T = c^{-1} = 0) = 0.50$. This yields $h_\phi^{-2} = 0.018$, $\Omega_C^0 = 0.30$ as seen in fig. 5.12. Away from the resonance both $\tilde{r}_0$ and $\tilde{\sigma}$ depend on c. In the BEC limit the scale set by the gap drops out and the value of the renormalized coupling is governed by the scaling behavior

$$h_\phi^{-2} = \frac{c}{32\pi} \quad \text{or} \quad h_\phi^2 = 32\pi c^{-1}. \tag{5.112}$$

[10] If one would identify the "condensate fraction" quoted in refs. [15; 16] with our definition of Ω_C one obtains at the resonance $\Omega_C(\tilde{T} = 0.08, c^{-1} = 0) = 0.13$ for ^{40}K [15] and $\Omega_C(\tilde{T} = 0.05, c^{-1} = 0) = 0.7$ for ^{6}Li [16].

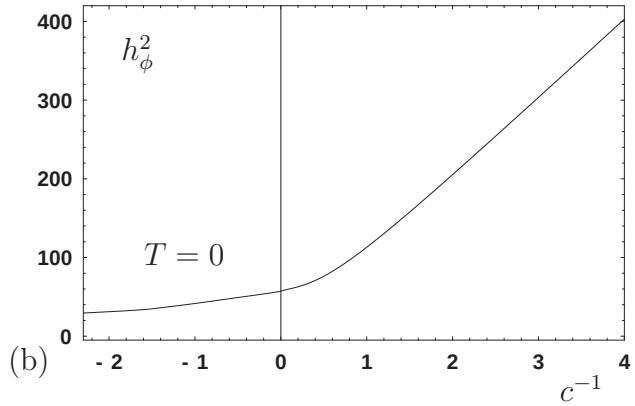

Figure 5.13: Renormalized Yukawa coupling h_ϕ^2 as a function of c^{-1} at zero temperature in the broad resonance limit.

In fig. 5.13 we show h_ϕ^2 as a function of c^{-1} for $\tilde{T} = 0$. The linear scaling in the BEC regime is obvious from this plot.

To judge the robustness of this statement we can consider the generalization of eq. (5.111) when relaxing the broad resonance condition, i.e. $\tilde{h}_{\phi,0}$ now is finite. For this purpose we have to generalize the expression for the wave function renormalization Z_ϕ, $h_\phi^{-2} = Z_\phi/\tilde{h}_{\phi,0}^2$. Instead of simply computing it from the fermion loop, we now extract it from the frequency and momentum dependent Schwinger-Dyson equation for the bosonic propagator (graphically represented in the first line of fig. 5.91), and projecting on the piece linear in the frequency by an appropriate derivative. At $T = 0$, the calculation yields

$$h_\phi^{-2} = \tilde{L} + \frac{(1 + \tilde{\lambda}_{\psi,0}\tilde{J})^2}{\tilde{h}_{\phi,0}^2} \tag{5.113}$$

where $\tilde{L}$ is the integral in eq. (5.111). We can now discuss how deviations from complete universality emerge for h_ϕ, being an example of a dressed quantity. Deviations are of order $\tilde{h}_{\phi,0}^{-2}$: Interestingly, corrections induced by the background scattering appear only in connection with an incomplete broad resonance limit – for $\tilde{h}_{\phi,0}^{-2} \to \infty$, they are absent! We note that this statement is not bound to zero temperature – the integrals $\tilde{L}, \tilde{J}$ may in general depend on $\tilde{T}$ and $\tilde{\sigma}$.

In the strict broad resonance limit the value of the renormalized Yukawa coupling only depends on c^{-1} and $\tilde{T}$. This universal value $h_\phi^2(c^{-1}, \tilde{T})$ is reminiscent of the existence of a partial infrared fixed point as some suitable infrared cutoff scale is lowered. The value of h_ϕ at the fixed point typically depends on c^{-1} and $\tilde{T}$, but otherwise the memory on the initial conditions of the flow (e.g. $\bar{h}_{\phi,\Lambda}$) is lost. Eq. (5.113) suggests that the fixed point associated to $\tilde{h}_\phi \to \infty$ also causes a loss of

memory concerning other couplings – for example the effects of a background coupling on the dressed quantities vanish in this limit. If this picture is true, the precise location of the fixed point may change as the approximation method is improved, for example by taking the molecule fluctuations into account for the computation of Z_ϕ. Nevertheless, if both the ^{6}Li and the ^{40}K system are within the range of attraction of the fixed point, the value of Ω_C for $T = c^{-1} = 0$ must be the same! Inversely, if the observations should establish different values of Ω_C^0 this would imply that either no such fixed point exists or that one of the systems is not yet close enough to the fixed point. Only in this case the system could keep additional memory of the microscopic Yukawa coupling (e.g. $\bar{h}_{\phi,0}$) or the background scattering length a_{bg} such that Ω_C^0 could depend on these parameters. Our findings so far, however, strongly suggest the universal behavior predicting for broad resonances a universal curve $\Omega_C(c^{-1})$ for $T = 0$.

Chapter 6

Universality

6.1 Universality and Enhanced Universality: Qualitative Discussion

Universality refers to the "loss of memory" concerning details of the microscopic physics of a system. A prominent example, which is often identified with the notion of universality, is the universal long-range behavior of thermodynamic systems close to a second order phase transition. The long distance physics is then governed by a few numbers, called critical exponents, which are in turn determined by the basic symmetries of the underlying theory, but independent of the precise values of the couplings in the microscopic theory. This allows to group theories from very different branches of physics into universality classes – for example, the $U(1)$ or $O(2)$ symmetry of our bosonic degrees of freedom suggest that the universal long range behavior should be the same as for the XY model in condensed matter physics (in three dimensions).

In this work we use the idea of universality in a wider sense. Actually, we have already encountered two examples of this phenomenon: First, the UV renormalization procedure (in its most general form presented in sects. 5.6.1 and 7.3), provides an effective low energy formulation which is very insensitive to the physics at the UV scale Λ. This reflects the fact that nature is organized in scales, as argued in chapt. 2. Second, the scaling form of the classical theory (3.16), which directly generalizes to the full effective action, allows for density independent statements, if we express our observables in dimensionless units (cf. e.g. the phase diagram fig. 6.1). As a practical advantage, one can perform all computations with a fiducially chosen $k_F = 1\text{eV}$. The scale set by the density only enters in the end, when we compare our results to a particular experimental situation for an observed $k_F = (3\pi^2 n)^{1/3}$. We can then rescale the axes of fig. 6.1 to arrive at absolute values for our observables.

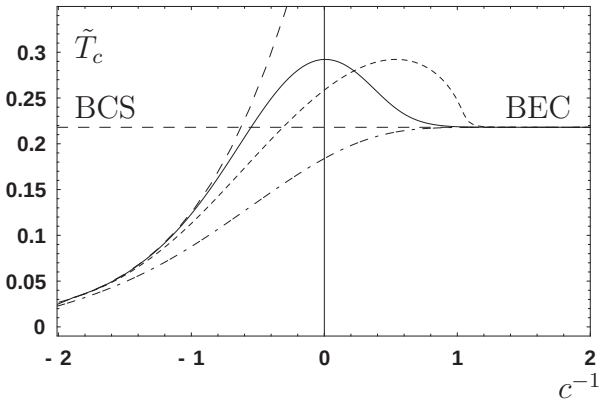

Figure 6.1: Crossover phase diagram. The dependence of the critical temperature $\tilde{T}_c = T_c/\epsilon_F$ on the inverse concentration $c^{-1} = (ak_F)^{-1}$ is shown for the broad resonance limit $\tilde{h}_\phi \to \infty$ (solid and short-dashed line) and for the narrow resonance limit $\tilde{h}_\phi \to 0$ (dashed-dotted line). We also indicate the standard BEC (dashed horizontal line) and BCS (dashed rising line) limits which do not depend on the choice of the Yukawa coupling. For the broad resonance limit we plot two different approximations which are specified in the last chapter.

These universal features concern our formulation of the crossover problem as a whole. Further aspects of universality can be found when considering specific parameter regimes in the cube of scales 3.2. We refer to them as "enhanced universality". This phenomenon occurs in situations where one of the two parameters $c, \tilde{h}_\phi$ becomes irrelevant (or fixed). This concerns the limits of narrow and broad Feshbach resonances ("narrow resonance limit", $\tilde{h}_\phi \to 0$ and "broad resonance limit", $\tilde{h}_\phi \to \infty$), the BCS and BEC regimes, $c \to 0$, and the scaling limit, $c \to \infty$. For a given $\tilde{T}$ the crossover for narrow and broad Feshbach resonances can be described by a single parameter c^{-1}. Results for the BCS, BEC and scaling limit can only depend on $\tilde{h}_\phi$ and become parameter free for narrow or broad resonances.

We can qualitatively discuss the limits of enhanced universality taking the phase diagram in fig. 6.1 as an example. The values of c^{-1} and $\tilde{h}_\phi$ determine the phase diagram completely, i.e. the critical temperature depends only on these two parameters, $T_c = T_c(c^{-1}, \tilde{h}_\phi)$. We display the dimensionless critical temperature $\tilde{T}_c$ as a function of c^{-1} and compare the limits $\tilde{h}_\phi \to 0$ (dashed) and $\tilde{h}_\phi \to \infty$ (two approximations, solid and short dashed, cf. the preceding chapter). For intermediate values of $\tilde{h}_\phi$, a monotonic change between the two limits is found, cf. also fig. 6.2. Though the impact of the marginal parameter $\tilde{h}_\phi$ is moderate, the precise value of $\tilde{h}_\phi$ influences the details of the crossover and will be important for precision estimates for concrete physical systems, in particular when narrower resonances than those presently investigated in ^{6}Li or ^{40}K will be explored.

Fig. 6.1 clearly reveals an $\tilde{h}_\phi$ - independent approach to the limiting BCS and BEC regimes: for $|c^{-1}| \to \infty$, $\tilde{h}_\phi$ becomes an irrelevant parameter and the system can be described in terms of the concentration only. For comparison, we have also plotted the extrapolated standard BCS (dashed, rising line) and BEC (dashed, horizontal line) results.

The narrow resonance limit corresponds to an exact solution of the many-body problem. It requires $\tilde{h}_\phi \to 0$ and additionally a vanishing four-fermion background interaction, but is free of further approximations. The broad resonance limit, instead, corresponds to a strongly interacting field theory, whose approximate solution still involves quantitative uncertainties, in particular close to the critical temperature (cf. the preceding chapter). This is reflected by the two critical lines obtained in different approximations in the broad resonance limit. The difference between the solid line and the short dashed line reflect the uncertainty in the treatment of the molecule fluctuations. For the solid line our result at the resonance $\tilde{T}_c = 0.292$ is in agreement with the theoretical value obtained in [66; 67] and compatible with the measurements reported in [67] $\tilde{T}_c = 0.31 \pm 0.04$. Including the molecule fluctuations in the gap equation (short dashed line) yields $\tilde{T}_c(c^{-1} = 0) = 0.255$. The maximum of $\tilde{T}_c(c^{-1})$ has a similar value for both approximations. Recent Quantum Monte Carlo simulations suggest an even smaller value of the critical temperature in the broad resonance limit and on resonance, $\tilde{T}_c = 0.152(7)$ [68].

We find a new form of crossover from the narrow to broad resonance limit in dependence on the Yukawa or Feshbach coupling $\tilde{h}_\phi$. This is shown in fig. 6.2, where we plot $\tilde{T}_c$ (fig. 6.2 (a)) as a function of $\tilde{h}_\phi$ for $c^{-1} = 0$. (The curves for other values of large $|c|$ are similar.) One clearly sees a smooth interpolation between the regimes. Within the broad resonance regime the precise value of $\tilde{h}_\phi$ is not relevant for $\tilde{T}_c$ or, more generally, for all quantities not involving explicitly the microscopic constituents ("bare fields"). Renormalization effects for $\tilde{h}_\phi$ even as large as a factor of ten do not matter. In contrast, in the "crossover regime" of intermediate $\tilde{h}_\phi \approx 10$ the physical results depend on the value of $\tilde{h}_\phi$. Now renormalization effects must be taken into account carefully for a reliable computation. Furthermore, we have seen in sect. 4.2.2, and more explicitly in 5.6.1, that observations related to "bare observables" like the fraction of closed channel atoms (or microscopic molecules) can depend strongly on $\tilde{h}_\phi$ even in the broad resonance regime. We also show in fig. 6.2 (b) the gradient coefficient A_ϕ for $T = T_c$, $c^{-1} = 0$.

Let us now discuss in more detail the status of the different limits of enhanced universality.

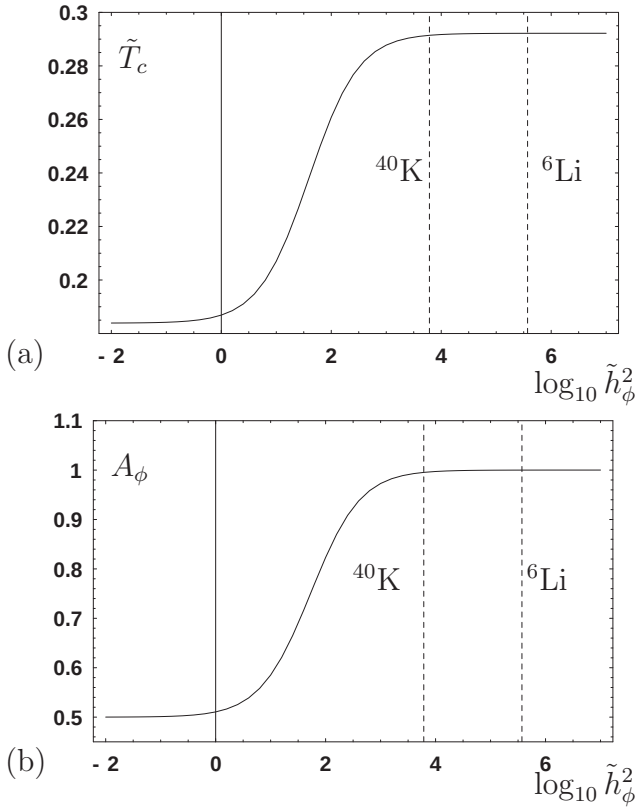

Figure 6.2: Enhanced universality for large and small $\tilde{h}_\phi$. For $c^{-1} = 0$ we plot the dependence on $\tilde{h}_\phi$ of (a) the dimensionless critical temperature $\tilde{T}_c$ and (b) the gradient coefficient A_ϕ for $T = T_c$. For small $\tilde{h}_\phi < 1$, a stable universal narrow resonance limit is approached. For large $\tilde{h}_\phi$ we find a very pronounced insensitivity of $\tilde{T}_c$ and A_ϕ to the precise value of $\tilde{h}_\phi$ – note that we plot on a logarithmic scale. The "crossover" regime interpolates smoothly between the universal limits. The dashed lines correspond to the actual value of $\tilde{h}_\phi^2$ for ^{6}Li and ^{40}K, cf. sect. 5.5. Indeed they belong to the class of broad resonances.

6.2 Exact Narrow Resonance Limit

A nontrivial exact limit exists for which $\tilde{h}_\phi \to 0$ and $\tilde{\lambda}_\psi \to 0$ while c and $\tilde{T}$ are kept fixed. It applies to the symmetric phase including the location of the critical line. This exact limit remains valid for arbitrary concentration c, even if the scattering length a is arbitrarily large. The molecules and fermionic atoms decouple in the limit $\tilde{h}_\phi \to 0$ such that the Gaussian (one-loop) approximation becomes exact. Nevertheless, our limit can describe the full BCS-BEC crossover as visible from fig. 6.1. In practice, the applicability of this limit corresponds to a narrow resonance, much narrower than the ones currently investigated for lithium or potassium. Alter-

natively, we can interpret this limit as describing a situation with a large effective range.

We learn from eq. (3.13) that our limit corresponds to $\bar{\nu} - 2\sigma \propto \bar{h}_\phi^2 \to 0$. Due to the simultaneous vanishing of $\bar{\nu} - 2\sigma$ and $\bar{h}_\phi$ our limit is not the trivial limit of a mixture of a noninteracting atom gas plus a noninteracting molecule gas. Nevertheless, we will see that in the narrow resonance limit an appropriate mean field theory becomes exact and can describe the high temperature phase including the approach to the critical temperature of the phase transition. (This mean field theory differs from standard BCS mean field theory results, cf. fig. 6.1.) The existence of this limit guarantees that mean field theory remains valid as long as $\tilde{h}_\phi$ remains small, say $\tilde{h}_\phi < 1$. This is confirmed in fig. 6.2.

In order to establish the exact results for this limit we first perform in eq. (4.34) the functional integral for the fermions ψ, which for $\bar{\lambda}_\psi = 0$ can be done exactly – this strategy has also been implemented in chapt. 4. As shown there, the Gaussian integral yields an intermediate action $\bar{S}[\hat{\Phi}]$ depending only on $\hat{\Phi}$, with

$$\Gamma[\Phi] = -\log \int \mathcal{D}\hat{\Phi}\ e^{-\bar{S}[\hat{\Phi}]+J^T\delta\hat{\Phi}}. \tag{6.1}$$

Let us discuss the properties of $\bar{S}[\hat{\Phi}]$ in the limit $\tilde{h}_\phi \to 0$. This is most easily done by considering (4.44). The effective potential $\tilde{u}$ in (4.44) corresponds to the mean field potential and we note that $\tilde{u} = -\tilde{r}/(8\pi c(\tilde{\sigma})) + \tilde{u}_1^{(F)}(\tilde{r}, \tilde{\sigma})$ depends on the gap parameter $\tilde{r} = \tilde{h}_\phi^2 \tilde{\phi}^* \tilde{\phi}$ but not explicitly on $\tilde{h}_\phi$ (for the explicit mean field formula cf. eq. (4.95)) The loop correction to the inverse boson propagator $\bar{\mathcal{P}}_\phi(Q)$ in the remaining functional integral for $\hat{\Phi}$ vanishes for $\tilde{h}_\phi \to 0$ due to the overall factor $\tilde{h}_\phi^2$. In consequence, the inverse bosonic propagator for $\hat{\phi}$ is precisely given by the classical part $P_\phi^{(cl)} = 2\pi i n T + \bar{A}_\phi^{(cl)} q^2 + \bar{\nu} - 2\sigma$. This is the inverse propagator for free bosons with an effective mass associated to $\bar{A}_\phi^{(cl)}$ – a simple symmetry consideration as done in chapt. 3 suggests $\bar{A}_\phi^{(cl)} = 1/(4M)$. In the more general case, $\bar{A}_\phi^{(cl)}$ should be associated to an effective range $r_s = 2\bar{A}_\phi^{(cl)}/\bar{h}_\phi^2$, cf. chapt. 3. All terms in $\bar{S}[\hat{\Phi}]$ with more than two powers of $\hat{\Phi}$ also involve powers of $\tilde{h}_\phi$ and therefore vanish in our limit. In consequence, the functional integral for $\hat{\Phi}$ becomes Gaussian in the limit $\tilde{h}_\phi = 0$ and we can solve (6.1) exactly. In our limit it should be evaluated for $\sigma = \bar{\nu}/2$. The number density of microscopic molecules $\bar{n}_M$ then corresponds to the density of free nonrelativistic bosons of effective mass $2M$ (or $1/(2\bar{A}_\phi^{(cl)})$ in the general case) with vanishing bosonic "chemical potential", as given by the canonical partition function.

In the narrow resonance limit the mean field approximation for the effective potential becomes exact. This yields exact estimates for the critical temperature and all quantities of the symmetric phase for $T \geq T_c$. In contrast, the low temperature

phase has only a partially meaningful limit for $\tilde{h}_\phi \to 0$. For nonzero $\tilde{r}$ the bare condensate fraction $\bar{\Omega}_C = 6\pi^2\tilde{r}/\tilde{h}_\phi^2$ (cf. sect. 4.2.2) diverges. The constraint $\bar{\Omega}_C \leq 1$ then implies that $\tilde{r}$ has to vanish $\propto \tilde{h}_\phi^2$.

In summary, the limit $\tilde{h}_\phi \to 0$ corresponds to a universal phase diagram in the narrow resonance limit, as given by the lowest curve in fig. 6.1. For small $\tilde{h}_\phi$ this universal curve is smoothly approached (fig. 6.2). All corrections to the "narrow resonance universality" are proportional to the dimensionless quantity $\tilde{h}_\phi^2$. Obviously, for $\tilde{h}_\phi \to 0$ all exact results depend only on the parameters c and $\tilde{T}$, whereby every point in the $(c, \tilde{T})$-plane may be realized by different combinations of a (or $\bar{\nu}$), n (or σ) and T.

At this point a comment on the interpretation of the narrow resonance limit is in order. The choice of the classical values for the coefficients in the boson propagator on the microscopic level corresponds to an intrinsically nonlocal situation. The actual values used in the figures are found by simple physical considerations, i.e. $\bar{A}_\phi^{(cl)} = 1/4M$ as the gradient coefficient for bosons of mass $2M$ and chemical potential -2σ for particle number two. This should, at least, give the right order of magnitude for the effective range. The association $r_s = 2\bar{A}_\phi^{(cl)}/\bar{h}_\phi^2$ (3.11) reveals that for $\bar{h}_\phi \to 0$ at *fixed* gradient coefficient $\bar{A}_\phi^{(cl)}$ and rescaled field $\hat{\varphi} = \bar{h}_\phi\hat{\phi}$, we deal with a diverging effective range, while the concentration remains also fixed by construction. The diverging effective range provides a (momentum dependent) large mass term weighted as [1]

$$\sim \exp - \int \frac{r_s}{2}\, \hat{\varphi}^* \vec{q}^{\,2} \hat{\varphi}, \qquad r_s \to \infty, \tag{6.2}$$

making the remaining functional integral Gaussian. The functional integral formulation hence shows the mechanism controlling the approximation in the narrow resonance limit in a very clear way, at the same time demonstrating that the narrow resonance limit can be physically interpreted as a situation with large effective range. This consideration holds irrespective to the actual value of c^{-1} and is in particular applicable close to the resonance – this has actually been used in [69] which advocates a controlled approximation scheme at the resonance for large effective ranges. It is worth noting that our narrow resonance limit is not scale free. The precise choice of $\bar{A}_\phi^{(cl)}$ influences the results of our calculations; in this work we always use $\bar{A}_\phi^{(cl)} = 1/(4M)$ for definiteness. For realistic narrow Feshbach resonances additional physical features, such as a nonvanishing $\bar{\lambda}_\psi$, may become important as well. This situation is different from the broad resonance limit, which is indeed scale-free at resonance and therefore lacks an obvious ordering principle.

[1] Of course, also the frequency term diverges $\propto \bar{h}_\phi^{-2}$. What is actually kept fixed is the ratio of the classical gradient coefficient and the classical wave function renormalization, $\bar{A}_\phi^{(cl)}/Z_\phi^{(cl)}$; here we have normalized $Z_\phi^{(cl)} = 1$ for the bare boson fields as appropriate for "fundamental" particles.

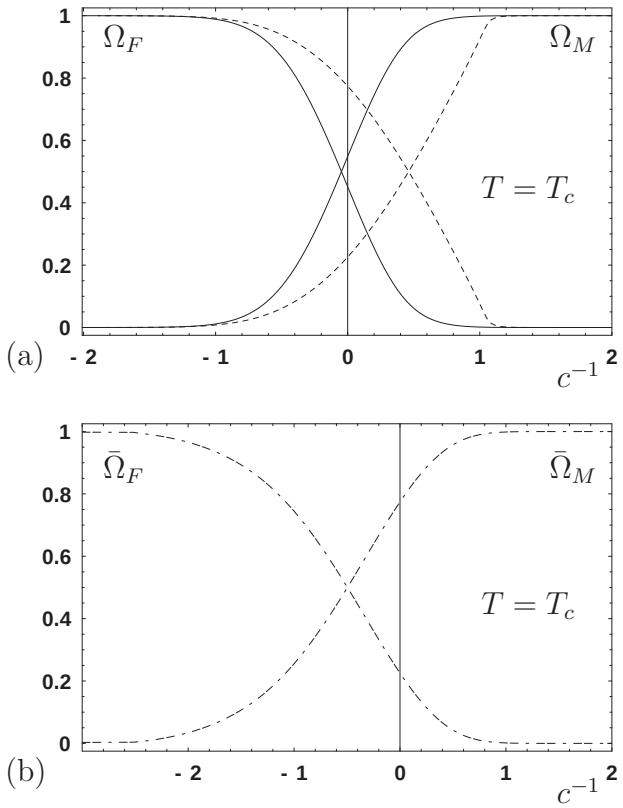

Figure 6.3: Crossover at the critical temperature: Contributions to the total particle number, showing the crossover from fermion to boson dominated physics. (a) Fractions of "dressed" densities in the large $\tilde{h}_\phi$ limit. We compare the results for two versions of the gap equation as in fig. 6.1. (b) Fractions of "bare" densities in the exact narrow resonance limit $\tilde{h}_\phi \to 0$. Though the pictures are similar, the physical interpretation of the two plots differs as described in the text.

In fig. 6.3 we compare the results for the density fractions defined in eqs. (4.76, 4.80) as a function of c^{-1} in broad and narrow resonance limits. The broad resonance case (fig. 6.3 (a)) is discussed below. Fig. 6.3 (b) shows the bare density fractions $\bar{\Omega}_F$ and $\bar{\Omega}_M$ as a function of the inverse concentration c^{-1} for $T = T_c$. For small $\tilde{h}_\phi \lesssim 1$ the BEC-BCS crossover is indeed the crossover from small to large $\bar{\Omega}_F$, since fluctuation effects modifying the classical boson propagator are suppressed as argued above. The density fractions are insensitive to the fluctuation modifications, but depend on the classical values entering the boson propagator.

6.3 Broad Resonance Limit

The broad resonance limit obtains for $\tilde{h}_\phi \to \infty$ while keeping c fixed. We will see that it corresponds to a model for fermionic atoms with local interaction and without explicit molecule degrees of freedom. For $\tilde{h}_\phi \to \infty$ all quantities depend only on c and $\tilde{T}$. The broad resonance limit therefore shows a particularly high degree of universality. For fixed c and finite $\tilde{\sigma}$ the limit $\tilde{h}_\phi \to \infty$ is accompanied by $\tilde{\nu} \to \infty$ according to eq. (3.13)

$$c = -\frac{\tilde{h}_\phi^2}{8\pi\tilde{\nu}}. \tag{6.3}$$

This relation is independent of $\tilde{\sigma}$. For finite $\tilde{\sigma}$ the resonant in-medium scattering length $a_R(\sigma)$ coincides with the reduced resonant scattering length $a_R(\sigma = 0)$. In the simultaneous limit $|\tilde{\nu}| \to \infty$, $\tilde{h}_\phi \to \infty$, the "classical" terms $\tilde{A}_\phi^{(cl)} \vec{\nabla}\hat{\phi}^* \vec{\nabla}\hat{\phi}$ and $\hat{\phi}^* \partial_\tau \hat{\phi}$ become subdominant and can be neglected. In the fermionic language (3.8) our model therefore reduces to a purely local four-fermion interaction. Our partially bosonized description has to match the purely fermionic description with a pointlike interaction term.

As the scale set by $\tilde{h}_\phi$ drops out in this limit, we can express the crossover in terms of a single parameter, the inverse dimensionless scattering length c^{-1}. In the superfluid phase we can use for the order parameter the squared dimensionless fermionic mass gap $\tilde{r} = h_\phi^2 \rho$. These are precisely the generic parameters used in a purely fermionic description. They characterize the system uniquely in the strict limit $\tilde{h}_\phi \to \infty$, but also remain very efficient for $\tilde{h}_\phi \gg 1$. Corrections will be $\mathcal{O}(\tilde{h}_\phi^{-2})$ or less.

The systems currently investigated experimentally are ^{6}Li and ^{40}K. Both range in the broad resonance regime, as can be seen from fig. 6.2 and discussed in sect. 5.5. This clearly motivates the theoretical investigation of this regime.

In contrast to the narrow resonance limit the broad resonance limit cannot be solved exactly. It still corresponds to an interacting fermion model, as discussed in detail by Strinati *et al.* [21–25]. Nevertheless, it allows us to make a detailed matching with a purely fermionic description and to compare all physical results directly by computing the concentration c in both approaches. Furthermore, the broad resonance limit can be used as a starting point for a systematic investigation of corrections beyond a local four-fermion interaction.

Our present calculations in the broad resonance limit still involve quantitative uncertainties related to our approximation scheme. The shortcomings are most severe in the crossover regime due to the absence of an obvious ordering principle. This differs from the exactly solvable narrow resonance limit. On the other hand,

due to the "loss of memory" concerning the details of the microscopic interaction vertex (3.8), this limit has a higher degree of robustness as compared to the narrow resonance limit, where the details of the microscopic interactions must be known.

Finally, we would like to point out that a further "crossover problem", i.e. the crossover from small to large $\tilde{h}_\phi$, emerges from the above discussion as anticipated in the introduction to this chapter. We leave this exciting field, physically describing the crossover from nonlocal to pointlike interactions, for future work. Our interpretation of the narrow and broad resonance limits is confirmed in the numerical study [70] comparing different types of interaction potentials.

For the large values of $\tilde{h}_\phi$ encountered in the broad Feshbach resonances in ^{6}Li and ^{40}K the contributions from the closed channel molecules $\bar{\Omega}_M, \bar{\Omega}_C$ become very small (cf. fig. 4.1 (b)). The dressed molecules differ substantially from the bare molecules (large Z_ϕ) and the "macroscopic" crossover physics is better described in terms of dressed molecules (4.76). We display in fig. 6.3 (a) the fraction of dressed unbound atoms Ω_F and dressed molecules Ω_M (cf. eq. (4.76)) for large values of $\tilde{h}_\phi$ and $T = T_c$. The fractions are not sensitive to the precise value of $\tilde{h}_\phi$ in the broad resonance limit $\tilde{h}_\phi \to \infty$, similar to the behavior found for small $\tilde{h}_\phi$.

This discussion reconciles the evaluation in a purely fermionic setup (single-channel model) with the evaluation of the crossover problem starting from a Yukawa type model (two-channel model). A comparison of purely fermionic vs. Yukawa-type approach based on the computation of several observables in both models has recently been performed [71]. Working with the microscopic parameters appropriate for ^{40}K, almost no difference is found between the two approaches. This is consistent with our investigation, classifying ^{40}K in the broad resonance regime where the two approaches become indeed equivalent.

6.4 BCS and BEC Regimes

The BCS and BEC regimes correspond to the limits $c \to 0_-$ and $c \to 0_+$. In the limit of small $|c|$, the marginal parameter $\tilde{h}_\phi$ turns irrelevant. Formally, this can be seen form the microscopic four-fermion vertex (3.8): In these limits, the absolute value of $|\tilde{\nu} - 2\tilde{\sigma}|$ becomes large compared to the momentum dependent terms. Indeed, the temperature and momentum dependent terms in the denominator of eq. (3.8) are typically of the order $\epsilon_F = k_F^2/(2M)$ whereas $|\bar{\nu} - 2\sigma| \sim \epsilon_F \tilde{h}_\phi^2/|c|$. For $|c| \to 0$ the interaction becomes therefore effectively pointlike for any given nonzero value of $\tilde{h}_\phi^2$. In consequence, the results can only depend on $\bar{\lambda}_\psi$ or c, but not on $\tilde{h}_\phi$ separately.

Though an intuitively expected result, this kind of universality is interesting from a conceptual point of view. It is associated to a loss of memory concerning

field degrees of freedom: On the BCS side, the molecules could have been omitted, and the BCS picture of a weakly interacting Fermi gas exhibiting the formation of Cooper pairs becomes valid. On the BEC side, we end up with an effective theory for the "dressed" molecules. They behave exactly like weakly interacting pointlike fundamental bosons (see below), whereas atom degrees of freedom are completely negligible for the macroscopic features.

The reason for this behavior can be seen directly from the functional integral (4.34) and the microscopic action (3.1). We can introduce the variables c^{-1} and $\hat{\varphi} = \bar{h}_\phi \hat{\bar{\phi}}$ [2] ($\varphi^*\varphi = r$), which is an exhaustive set to describe these limits. With these preparations, let us sketch the basic picture for the limiting cases: For $c^{-1} \to -\infty$ (BCS limit), the classical contribution to $\partial\tilde{u}/\partial\tilde{r}$ acts as a large positive mass term $\propto -c^{-1}$ for the bosons, and the correlation functions associated to $\hat{\varphi}$ are heavily suppressed. On the other hand, for $c^{-1} \to +\infty$ (BEC limit), the solution of the crossover problem implies for the effective chemical potential $\tilde{\sigma} \to -\infty$, and $-\tilde{\sigma}$ constitutes a mass term for the fermions, similarly suppressing their propagation. Though the interaction between fermions and bosons remains strong through $\hat{\varphi}\psi^\dagger\epsilon\psi^*$, the overall role of one of the two different degrees of freedom becomes unimportant in the two respective limits. In the next two sections, we discuss the BCS and BEC regimes in more detail. In particular, we will comment on the mechanisms which provide for an ordering principle in these regime. This discussion can possibly give some guidance for future extensions of the present work.

6.4.1 BCS

As argued above, $c^{-1} \to -\infty$ provides a mass term for the bosons. More precisely, boson fluctuations are suppressed as long as the "classical" mass term c^{-1} in the remaining bosonic functional integral (4.44) is much larger than the contribution from fermion fluctuations $\partial\tilde{u}/\partial\tilde{r}$. In this case, the fermionic mean field theory becomes well controlled and we can safely neglect bosonic correlations encoded in (4.44). As an immediate consequence, the equation of state reduces to the mean field result.

As a caveat to keep in mind, we note that the criterion for the phase transition in BCS theory is the vanishing of the effective mass term,

$$-\frac{1}{8\pi c} + \frac{\partial\tilde{u}_1}{\partial\tilde{r}} = 0. \tag{6.4}$$

Hence close to the phase transition, the bosonic fluctuations cannot be neglected as expected. A similar problem is encountered in the superfluid phase in presence of a massless Goldstone mode, which is actually responsible for the phenomenon of

[2] Note the close analogy to the rescaling transform $\mathcal{Z}$ (4.83).

superfluidity. Our Schwinger-Dyson approach generates a term $\propto \lambda_\phi^{(F)} n_M$ (cf. eq. (5.21)) - since n_M is small in the BCS regime, we find no significant deviation from the BCS results.

As an orientation for future work, we note that deviations from the BCS result can be expected from the inclusion of the $\psi^\dagger\psi$ interaction channel on top of the $\psi\psi$ channel, which we have investigated with our partial bosonization strategy implemented in chapts. 4 and 5. Indeed, a careful inclusion of fluctuations in this channel lowers the dimensionless critical temperature of BCS theory by a factor of ≈ 2.2 as shown by Gorkov and Melik-Barkhudarov [72] (for a review see e.g. [47]),

$$\tilde{T}_c^{BCS} = \varpi e^{\frac{\pi}{2}\, c^{-1}} \;\rightarrow\; \tilde{T}_c^{G} = (4e)^{-1/3} \tilde{T}_c^{BCS}. \tag{6.5}$$

(Here the prefactor $\varpi = 8\gamma/(\pi e^2) \approx 0.61$.) This result, known as Gorkov's correction, does not seem to be in reach with the evaluation strategy presented in chapts. 4 and 5 – we find precisely $\tilde{T}_c^{BCS}$ in the BCS regime, cf. fig. 6.1. On the other hand, it constitutes an interesting challenge for the analysis in the frame of the functional renormalization group in a more extended truncation.

So far we have argued with the large value of c^{-1} providing an ordering principle in the BCS regime. However, it is possible to argue in a different way, based on a consideration of the chemical potential. Inspection of figs. 5.2, 5.5 reveals that in the BCS regime, the chemical potential $\tilde{\sigma}$ is very close to the value characteristic for the free Fermi gas, $\tilde{\sigma} = \sigma/\epsilon_F = 1$; at low $\tilde{T}$, the Fermi surface therefore is very sharp, $\tilde{\sigma}/\tilde{T} = \sigma/T \gg 1$. This, in turn, makes it plausible why the dressed molecules do not play a role in the BCS regime: Available momenta are strongly confined to the Fermi surface, and therefore all interactions can be taken effectively momentum independent. The density of dressed molecules counts the available frequency and momentum modes and therefore is a measure of the non-locality induced by the interaction. Hence the equation of state is strongly dominated by the fermionic mean field density. In our approximation this is reflected by the kinetic coefficients for the bosons growing large in the BCS regime – this leads to a suppression of bosonic modes. The kinetic coefficients are plotted in fig. 6.4. In sum, the sharpness of the Fermi surface gives an complementary justification for the validity of BCS mean field theory, which is not directly based on the smallness of the coupling c. This statement can be made more rigorous in a renormalization group framework, where a power counting different from our naive scaling analysis (3.15) is established [73]. As it turns out, in this power counting scheme the four-fermion interaction at zero external momentum is a marginal operator. A "derivative expansion" of the fully momentum dependent interaction which separates momenta tangential and perpendicular to the Fermi surface generates marginal operators for the tangential components and irrelevant operators for the perpendicular components. It is worth noting that Gorkov's result is obtained by a careful treatment of these momentum

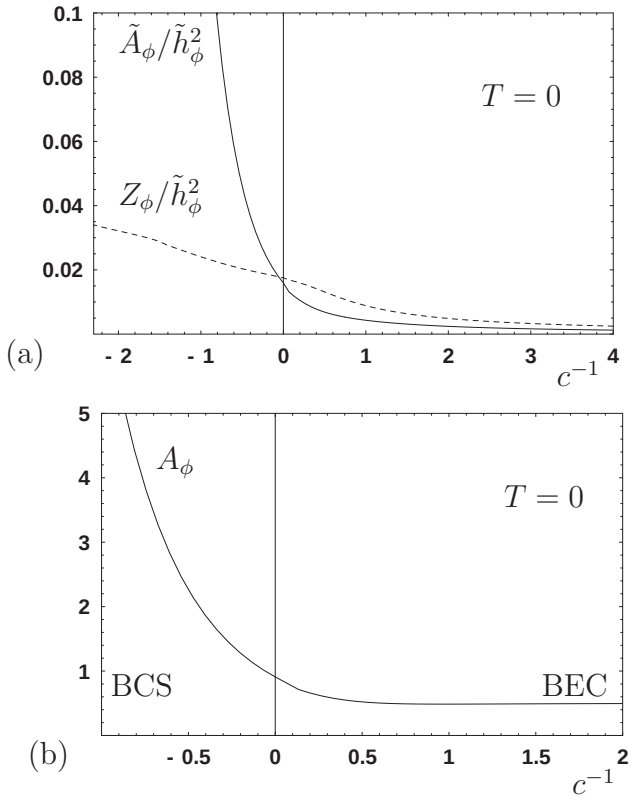

Figure 6.4: (a) Dimensionless gradient coefficient $\tilde{A}_\phi = 2M\bar{A}_\phi$ and wave function renormalization Z_ϕ. We divide by $\tilde{h}_\phi^2$ in order to get numbers $\mathcal{O}(1)$ and use $\tilde{h}_\phi^2 = 3.72 \cdot 10^5$ as appropriate for ^{6}Li. (b) Dimensionless renormalized gradient coefficient $A_\phi = \tilde{A}_\phi/Z_\phi$ for $T = 0$, as a function of the inverse concentration. In the BCS limit, A_ϕ grows large, suppressing the propagation of dressed bosons. In the BEC limit, A_ϕ takes the classical value $1/2$ for elementary bosons of mass $2M$.

dependent interactions; in particular it involves an averaging over the tangential momentum components.

6.4.2 BEC

In the BEC regime the coupling becomes small as well, $c^{-1} \to -\infty$ and we expect a simple mean field description to become valid. Indeed we can identify an ordering principle also in this limit. From figs. 5.2, 5.5 we infer that the effective chemical potential $\tilde{\sigma} \to -\infty$. More precisely, the two-body result (5.62) suggests a scaling behavior $\tilde{\sigma} \propto -c^{-2}$ and we will see that this formula is also extends to the thermodynamic situation.

Based on this observation, we consider the functional integral (4.44) again in the limit $\tilde{\sigma} \to -\infty$ and concentrate on the quadratic piece (4.45) first. More precisely we consider a situation where we can ignore terms

$$\mathcal{O}\Big(\frac{\tilde{T}}{-\tilde{\sigma}}\Big), \quad \mathcal{O}\Big(\frac{\tilde{r}}{-\tilde{\sigma}}\Big) \tag{6.6}$$

or higher in $(-\tilde{\sigma})^{-1/2}$. In this limit we can evaluate the fermionic momentum space integrals (4.46, 4.49) analytically. We separate the momentum dependent from the zero momentum part and find for the mass term (in dimensionless units, the UV renormalization has been taken into account, cf. eqs. (4.93,4.94) [3])

$$\tilde{m}_\phi^2 \;=\; \tilde{\nu} - 2\tilde{\sigma} + \frac{\tilde{h}_\phi^2\sqrt{-\tilde{\sigma}}}{8\pi}. \tag{6.7}$$

The momentum dependent part reads

$$\begin{aligned} \tilde{P}_\phi(\tilde{K}) - \tilde{m}_\phi^2 &= \mathrm{i}\tilde{\omega} + \tilde{q}^2/2 + \frac{\tilde{h}_\phi^2}{8\pi\sqrt{2}}\big(\sqrt{\mathrm{i}\tilde{\omega} + \tilde{q}^2/2 - 2\tilde{\sigma}} - \sqrt{-2\tilde{\sigma}}\big) \\ &= \mathrm{i}\tilde{\omega} + \tilde{q}^2/2 + \frac{\tilde{h}_\phi^2}{32\pi\sqrt{-\tilde{\sigma}}}\big(\mathrm{i}\tilde{\omega} + \tilde{q}^2/2\big) + ... \\ &= Z_\phi\big(\mathrm{i}\tilde{\omega} + A_\phi\tilde{q}^2\big) + ... \end{aligned} \tag{6.8}$$

with

$$Z_\phi = 1 + \frac{\tilde{h}_\phi^2}{32\pi\sqrt{-\tilde{\sigma}}}, \quad A_\phi = \frac{\tilde{A}_\phi}{Z_\phi} = \frac{1}{2} \tag{6.9}$$

for our choice $A_\phi^{(cl)} = 1/2$. In the second step in (6.8) we have additionally assumed that the negative chemical potential is much larger than all relevant frequencies and momenta (for a thermodynamic situation, these are restricted by the thermal distribution functions which are strongly suppressed for high momenta). The diagonal entries in eq. (4.45) read

$$\tilde{\lambda}_\phi(K) \;=\; \frac{\tilde{h}_\phi^4}{128\pi\sqrt{-\tilde{\sigma}^3}} + \mathcal{O}(\tilde{q}^2/\sqrt{-\sigma}^5) = \Delta Z_\phi^2\frac{8\pi}{\sqrt{-\tilde{\sigma}}} + ... \tag{6.10}$$

The frequency and momentum dependence of $\tilde{\lambda}_\phi(K)$ is suppressed by an additional power of $(-\tilde{\sigma})^{-1}$ compared to the momentum independent part such that we can neglect it here.

[3] We assume that still $\sqrt{-\sigma} \ll \Lambda$.

The integrals evaluated in the BEC limit (6.6) depend on a *single* dimensionful parameter σ only [4]. As an important consequence, we observe that the naive scaling with k_F, ϵ_F expected from power counting holds, very similar to (3.15). In this sense, the effective "microscopic" couplings (induced by the fermion fluctuations) become independent of the thermodynamic scales like density (k_F) and temperature – they can be treated on the same grounds as the classical couplings in a quantum theory for fundamental bosons!

Eq. (6.8) shows that our derivative expansion becomes exact in the limit $\tilde{\sigma} \to -\infty$. The appearance of Z_ϕ in the above formula demonstrates that the concept of dressed fields is very efficient in this limit.

Further, in the BEC limit interactions are suppressed. For example, the ϕ^4 coupling of the remaining bosonic integral is $\mathcal{O}(\sqrt{-\tilde{\sigma}} \sim c)$ and thus becomes unimportant. Hence the Bogoliubov approximation becomes well controlled in the sense of an expansion in c. However, there is (at least) one quantity which necessitates resummation of larger classes of diagrams – even in the vacuum limit where the scales set by temperature and density drop out! The ratio of molecular and fermionic scattering length is found to obey $a_M/a = 2$ in the Bogoliubov approximation advocated above (this result was first obtained by Haussmann in [74]), while a solution of the Schrödinger equation for the four-body problem [75] suggests a universal scaling coefficient $a_M/a = 0.6$. Of course here one focuses on a relative quantity measured in units of a, such that the smallness of a itself is useless. We will come back to this issue in the next chapter, where we also define the bosonic scattering length, eq. (7.60).

The Schwinger-Dyson equation for the mass reduces to the standard BCS gap equation in this regime: The bosonic term is suppressed $\sim \tilde{\lambda}_\phi^{(F)} \tilde{\Omega}_M = \mathcal{O}((-\tilde{\sigma})^{-1})$, which has to be compared to the fermionic contribution $\mathcal{O}(\sqrt{-\tilde{\sigma}})$. Here the unimportance of the molecule fluctuations is due to the small value of the coupling, unlike the BCS regime where the boson density is small. In the approximation (6.6), the BCS equation then reduces to

$$c^{-1} = \sqrt{-\tilde{\sigma}} \quad \text{or} \quad 2\sigma = \epsilon_M = -1/(Ma^2) \tag{6.11}$$

where we have divided out k_F in the second equality. I.e. the gap equation reduces to the density independent two-body result (5.62), in line with the above scaling arguments.

The equation of state (5.36,5.37) also simplifies considerably,

$$1 = 3\pi^2\Big(\frac{\tilde{r}}{16\pi\sqrt{-\tilde{\sigma}}} + 2n_M\Big) = 3\pi^2\Big(2\frac{Z_\phi \tilde{r}}{\tilde{h}_\phi^2} + 2n_M\Big) = \Omega_C + \Omega_M. \tag{6.12}$$

[4] This is different in the general case, where the fermionic integrals are additionally functions of the gap and temperature

In the first line of eq. (6.12) the first term is the explicit result for Ω_F^{MFT}. In the next step we use the explicit result for Z_ϕ (6.9) and we recover the definition of Ω_C which can be read off from the second line of (4.75) and (4.76). In this approximation scheme the mean field fermion density hence implies the condensate fraction in the BEC regime. Interestingly, this will be quite different in the FRG treatment presented in the next chapter. Eq. (6.12) precisely has the form of the equation of state for Bose-Einstein condensation – obviously the system has lost all its memory of the fermionic constituents if one considers thermodynamic observables as the particle density. The density contribution Ω_M is of Bogoliubov type. Indeed we can compare our expression for the particle density in SSB with the standard Bogoliubov form,

$$n_M = \frac{1}{2}\int \frac{d^3q}{(2\pi)^3}\Big(|v_q|^2 + \frac{|u_q|^2+|v_{-q}|^2}{\exp 2\alpha_\phi - 1}\Big) \tag{6.13}$$

when identifying the Bogoliubov transformation coefficients and our expressions (listed in app. D.4.3, eq. (D.45))

$$|v_q|^2 = \frac{1}{2}\big(\frac{\alpha+\kappa}{\alpha_\phi}-1\big), \quad |u_q|^2+|v_{-q}|^2 = \frac{\alpha+\kappa}{\alpha_\phi}. \tag{6.14}$$

Let us now perform the broad resonance limit $\tilde{h}_\phi \to \infty$ on top of the BEC limit to see the relation to standard Bogoliubov theory most clearly. In this case, the classical pieces for the kinetic terms become unimportant such that $\Delta Z_\phi = Z_\phi$ and the inverse propagator matrix reads, in dimensionful renormalized units in SSB

$$\frac{\bar{\mathcal{P}}_\phi(K)}{Z_\phi} = \begin{pmatrix} \frac{4\pi a}{M}\bar{\phi}^*\bar{\phi}^* & \mathrm{i}\omega + \frac{\vec{k}^{\,2}}{4M} + \frac{4\pi a}{M}\bar{\rho} \\ -\mathrm{i}\omega + \frac{\vec{k}^{\,2}}{4M} + \frac{4\pi a}{M}\bar{\rho} & \frac{4\pi a}{M}\bar{\phi}\bar{\phi} \end{pmatrix}. \tag{6.15}$$

The dimensionful renormalized bosonic coupling $\bar{\lambda}_\phi/Z_\phi^2 = 4\pi a/M$ can be related to the scattering length for identical composite bosons of mass $2M$ yielding $a_M = 2a$, cf. eq. (7.60) in sect. 7.3. Hence this is precisely the inverse propagator matrix for fundamental bosons of mass $2M$, interacting through an effective scattering length $2a$.

In SYM the diagonal entries vanish and the mass term $\bar{m}_\phi^2$ appears in the off diagonal parts. It then plays the role of an effective chemical potential and has the derivative

$$\frac{\partial \bar{m}_\phi^2}{\partial \sigma} = -2Z_\phi, \tag{6.16}$$

as expected for the chemical potential of composite particles, and as advocated in (4.82).

We emphasize that we can perform first the limit $\tilde{h}_\phi \to \infty$ where we recover a purely fermionic model with pointlike interaction and no explicit molecule degrees of freedom. Subsequently we may consider large c^{-1} where the approximations leading to eq. (6.13) become valid. This shows that the Bogoliubov formula for weakly interacting "fundamental" bosons can be recovered from a purely fermionic model! In our approach, this result emerges in the simultaneous limit $c^{-1} \to \infty$ (BEC regime), $\tilde{h}_\phi \to \infty$ (broad resonance regime). Our Z_ϕ - renormalization procedure generates precisely the macrophysics we would have obtained when starting microscopically with a purely bosonic action. The bosons emerge dynamically. We do not require the assumption of microscopic bosons. A similar result has been established by Strinati *et al.* [21–25] who work in a purely fermionic setting, or, in our language, in the broad resonance limit $\tilde{h}_\phi \to \infty$ from the outset. On the other hand, we are not limited to the broad resonance case, and we can compute corrections to it. For example, for large $\tilde{h}_\phi$ the contributions from the bare molecules are suppressed $\sim \tilde{h}_\phi^{-2}$.

From a conceptual point of view, the BEC regime is very interesting: the large negative value of the chemical potential leads to a decoupling of the basic fermionic constituents and the effective molecular degrees of freedom. This is an example of scale separation which finally underlies effective field theories in any branch of physics. Here we can study this phenomenon explicitly. The double chemical potential -2σ in this region should be interpreted as the binding energy for the dynamically generated molecules. In an energetic picture, propagation of the fermions is suppressed by a gap $-\sigma$ compared to the zero of energy determined by the molecules on the BEC side, cf. eq. (5.50). This, in turn, suppresses all fermionic correlation functions. In a position space picture, the molecules are strongly localized entities, whose internal structure is not resolved at low temperature. They can therefore be considered as fundamental particles, for which correlation functions can be extracted from the remaining bosonic functional integral.

We finally note that a large negative chemical potential acts as a mass term for both the fermions and the bosons, if we consider σ as a free parameter and do not fix the particle density *a priori*. In other words, it acts as an infrared regulator. This, together with the observation that the σ - derivative of the effective action as constructed in sect. 4.2.2 generates precisely the structure of the exact renormalization group equation derived in [57] (for a larger class of infrared regulators), motivates the choice of σ as the cutoff function for the functional renormalization group analysis presented in the next chapter.

6.5 Unitary Limit

A further interesting form of universality was pointed out by Ho [64] in the limit $c^{-1} \to 0$ [5]. It is argued that if the scattering length drops out, then the only remaining scales are the density (or k_F) and the temperature T, and the thermodynamics of the system should be governed by simple scaling laws.

In this form the argument is not complete since it assumes in addition a strictly pointlike interaction. Deviations from the pointlike structure, as reflected in the Feshbach coupling $\bar{h}_\phi$, introduce new scales and therefore new dimensionless parameters as $\tilde{h}_\phi$. This is clearly seen by the $\tilde{h}_\phi$ dependence of the quantities $\tilde{T}_c$ and A_ϕ (effective gradient coefficient for the dressed bosons) in fig. 6.2, which indeed refers to the resonance $c^{-1} = 0$. For example, a given $\bar{h}_\phi$ corresponds to a particular density $k_F^{(cr)}$ for the crossover from a broad to a narrow resonance. (We may define $k_F^{(cr)}$ by the condition $\tilde{h}_\phi(\bar{h}_\phi, k_F^{(cr)}) = 10$.) In this sense the unitary limit does not exhibit complete universality since it depends on an additional parameter.

Nevertheless, for a broad resonance the actual value of $\tilde{h}_\phi$ is irrelevant for the dressed quantities (as long as we are in a range of k_F sufficiently away from $k_F^{(cr)}$). Thus Ho's argument becomes valid in the double limit [6] $c^{-1} \to 0, \tilde{h}_\phi \to \infty$: For dressed quantities all dimensionless numbers and ratios can be predicted completely independently of the microphysical details of the system!

Our results for a broad Feshbach resonance extend this argument also away from the location of the resonance. Universality holds not only for one particular value of B at the Feshbach resonance. For arbitrary B in the whole crossover region a single parameter c^{-1} describes all relevant macroscopic properties of the dressed quantities. The concrete microphysics of a system is only needed to relate c to B, i.e. it is only reflected in one function $c(B)$ which varies from one system to another.

The unitary limit (also called resonance or scaling limit) for broad resonances at moderate and low temperatures is the most challenging region of the crossover phase diagram, and our approximations are plagued with the most severe uncertainties in this regime. This can be understood qualitatively by the absence of an obvious ordering principle – both in the BEC and BCS regime we can establish such a principle based on the large value of $|c^{-1}|$ which suppresses either fermion or boson correlations. This is most prominent in the discrepancy of our estimate for the critical temperature at unitarity (fig. 6.1), and the QMC result $\tilde{T}_c = 0.152(7)$ [68]. We might speculate that this is due to a medium effect similar to Gorkov's correction reducing the BCS critical temperature by a factor 2.2, see above. This conjecture

[5] A similar argument was proposed even earlier in the context of bosonic systems in [76].

[6] In our approach this also holds for the narrow resonance limit $c^{-1} \to 0, \tilde{h}_\phi \to 0, \bar{\lambda}_\psi \to 0$. However, in practice $\bar{\lambda}_\psi$ or similar terms will not vanish and induce scaling violations.

is based on the simple observation that at low temperatures at the resonance, one still deals with a substantial Fermi surface, cf. figs. 5.2, 5.5 (Quantum Monte Carlo simulations confirm this size of the chemical potential, cf. [62] at $T = 0$ and [68] at $T = T_c$.), such that the Gorkov correction, which is known to be important for quantitative accuracy even in the BCS regime, could be important in this regime also. Interestingly, the pronounced Fermi surface at low temperature could provide an approximate ordering principle at the resonance which does not rely on the large size of the inverse coupling c^{-1}. We believe that the above effect can be captured by a proper rebosonization treatment [50] in the frame of functional renormalization group equations.

Chapter 7

Renormalization Group Analysis

In this chapter we present the results obtained so far in the frame of Functional Renormalization Group (FRG) equations.

In the two-body limit, we can substantially improve our result for the ratio a_M/a for bosonic and fermionic scattering length (cf. sect. 6.4.2) and provide an UV renormalization procedure which is equivalent to the one presented in the frame of Schwinger-Dyson equations in sect. 5.6.1. We stress that there is a basic difference in our problem and many high energy applications of the FRG. In high energy physics, especially QCD, one deals with a situation where the high energy limit is well controlled (asymptotic freedom) and experimentally accessible in collider experiments. Starting from a well-known classical action at a high momentum scale, one can then follow the RG evolution to low momentum scales. In ultracold gas physics instead, the low temperatures and densities do not allow for a resolution of the high energy sector of the theory as argued in chapt. 2. Instead, low energy properties are extracted from two-particle scattering in the physical vacuum, i.e. at zero temperature and density. Our UV renormalization prescription encompasses precisely this issue.

For the many-body problem, our focus is on the BEC regime. Here, we deal with a well-controlled situation which is therefore well suited for the development of the most important conceptual advances. The results presented here still have a preliminary character and have to be consolidated in ongoing work, but are quite promising. We recover an effective Bogoliubov theory as in the Schwinger-Dyson analysis, which however quantitatively differs from our earlier results. We now obtain very good agreement with QMC calculations performed at $T = 0$ in the BEC regime [77]. As a further important improvement of the Schwinger-Dyson approach, at higher temperature we now obtain a second order phase transition, instead of a first order as typical in Bogoliubov-type approximation schemes. As an important conceptual result, our approach reconciles the generic infrared freedom of bosonic

$O(N)$ models in the spontaneously symmetry broken phase [60] with Bogoliubov theory, which implies that remnants of interactions on higher momentum scales manifest themselves via a condensate depletion at zero temperature.

In the next step, the whole phase diagram should be mapped out. A quantitatively accurate completion of this task might also need an extension of the truncation presently used.

The FRG which we use [57] is conceptually very close to the block-spin idea of Kadanoff [78], which was later further developed and put into practical use in the context of statistical mechanics by Wilson [79] and Wegner [80].

In order to sketch the basic idea, we consider the functional integral for a classical action S_Λ depending on the scalar field φ and parameterized by a set of couplings g^i_Λ, which are defined at some high momentum scale Λ. We then divide the functional integration in an integration over high momentum modes ($\Lambda > q \geq \Lambda'$) collected in the field $\varphi_>$, and over low momentum modes $q < \Lambda'$, encoded in $\varphi_<$:

$$\begin{aligned} \int \mathcal{D}\varphi \exp -S_\Lambda[\varphi] &= \int \mathcal{D}\varphi_< \mathcal{D}\varphi_> \exp -S_\Lambda[\varphi_<, \varphi_>] \\ &= \int \mathcal{D}\varphi_< \exp -S^W_{\Lambda'}[\varphi_<] \end{aligned} \tag{7.1}$$

where the fields $\varphi_{>/<}$ vanish in the complementary domain of momenta. $S^W_{\Lambda'}$ is the "Wilsonian effective action" [1] includes the effects of fluctuations which have been integrated out

$$\exp -S^W_{\Lambda'}[\varphi_<] = \int \mathcal{D}\varphi_> \exp -S_\Lambda[\varphi_<, \varphi_>]. \tag{7.2}$$

The impact of this formalism is twofold: First, it explains how fluctuations cause the couplings of a theory to change with scale, $g^i_\Lambda \to g^i_{\Lambda'}$. This gives rise to a "coarse graining" picture of the renormalization program: Lowering the cutoff Λ' at fixed Λ, the functional integration averages over more and more extended domains in position space. The interpolation between the "microphysics" defined at a scale Λ and the "macrophysics" approached for $\Lambda' \ll \Lambda$ is mirrored in a change of the couplings with scale, and done in a smooth and beautifully intuitive way. Second, it sheds light on the status of effective theories defined at the scale Λ, which can always be interpreted as resulting from an averaging process operative on even higher momentum scales.

Of course, eqs. (7.1,7.2) do not yield a practical prescription of how to perform the mode elimination. For this purpose, the functional integral is projected on the couplings $g^i_{\Lambda'}$. The process of the successive inclusion of fluctuations is highly nonlinear – therefore a sequence of infinitesimal renormalization group steps is necessary.

[1] Conceptually, it is closer to the generating functional of the connected Green functions W than to the 1PI effective action Γ.

This gives rise to a coupled set of first order differential renormalization group equations for the couplings $g^i_{\Lambda'}$, where the response of the couplings w.r.t. the change of scale Λ' is studied. The rhs of these equations are the famous β-functions.

We use a functional renormalization group equation for the effective (average) action Γ_k [57]. It is based on the concept of the effective action Γ as introduced in chapt. 4, i.e. the generating functional of the 1PI Green functions. The difference between Γ and Γ_k originates from an artificially introduced k-dependent mass term which acts as an infrared regulator – only modes $q \gtrsim k$ are included in Γ_k. The FRG then studies the reaction of Γ_k w.r.t. the change of the scale k. One then deals with an *exact* partial functional differential equation for Γ_k, where exact refers to the fact that the solution of the FRG for $k \to 0$ is the full quantum effective action, $\Gamma_{k\to 0} = \Gamma$. The FRG thus is a fully nonperturbative concept, and may be viewed as a formulation of a quantum theory complementary to the functional integral. It has a simple interpretation in terms of coarse graining: Starting the flow at high momentum scale k or small length, fluctuations are completely suppressed. Evolving to smaller values of k, fluctuations (thermal and quantum) are smoothly included – in position space, this corresponds to an averaging over larger and larger domains. Finally, for $k \to 0$ one reaches a macroscopic probe size, and all fluctuations are taken into account. The derivation of this equation is presented in the next section. Of course, a closed solution for nontrivial applications is in general not possible – it would constitute an exact solution of a quantum theory. However, the choice of a sensible truncation makes this concept a very powerful computational tool. For a review including practical guidance cf. [58].

The problem of pairing in nonrelativistic many-fermion systems at zero temperature has been investigated in the frame of the FRG by Krippa *et al.* [81–83].

7.1 Effective Average Action and Flow Equation

In this section we derive the FRG equation for the effective average action, working in the Nambu-Gorkov formalism introduced in chapt. 4. The starting point is again the generating functional for the connected Green functions (4.6). We modify the classical action in this functional by a scale (k) dependent cutoff or regulator term,

$$S[\hat{\chi}] \to S_k[\hat{\chi}] = S[\hat{\chi}] + \Delta S_k[\hat{\chi}], \tag{7.3}$$

where the cutoff term is quadratic in the fields and reads in momentum space

$$\Delta S_k[\hat{\chi}] = \frac{1}{2} \int\limits_Q \hat{\chi}^T(Q) R_k(Q) \hat{\chi}(Q). \tag{7.4}$$

The cutoff function R_k can be chosen momentum (Q) dependent in general. It should not be confused with the UV cutoff Λ. For fixed Q we require

$$\begin{aligned} R_k(Q) &\geq 0, \quad R_k(Q) = 0 \Leftrightarrow k = 0, \\ \lim_{k\to 0} R_k(Q) &\to 0, \quad \lim_{k\to\infty} R_k(Q) \to \infty. \end{aligned} \tag{7.5}$$

Here Q is a typical physical momentum for a given problem. The limit condition in the second constraint in line two can as well be replaced by $k \to \Lambda$, since for an UV cutoff Λ one has $\Lambda/\sqrt{Q^2} \gg 1$ – the cutoff scale is far beyond all available momenta. We will supplement this discussion by further remarks after having derived the FRG equation.

The regulator term introduces an artificial scale dependence on the generating functional,

$$W_k[J] = \log \int \mathcal{D}\hat{\chi} \exp -S_k[\hat{\chi}] + J^T\hat{\chi} \tag{7.6}$$

– seen from another perspective, we now consider a theory with classical action S_k instead of S. The first constraint in eq. (7.5) implies that in the limit of completely removed cutoff $k \to 0$, we recover the original generating functional

$$\lim_{k\to 0} W_k \to W \tag{7.7}$$

encoding the full information of the quantum field theory.

We can now define the effective average action Γ_k by a modified Legendre transform,

$$\Gamma_k[\chi] = \hat{\Gamma}_k[\chi] - \Delta S_k[\chi] \tag{7.8}$$

which involves the standard Legendre transform of W_k,

$$\hat{\Gamma}_k[\chi] = -W_k + J_k^T\chi. \tag{7.9}$$

Here$\hat{\Gamma}_k$ is the k-dependent effective action corresponding to W_k. The use of the modification of the standard Legendre transform will become clear below. The field equation for the effective average action reads

$$\frac{\delta\Gamma_k[\chi]}{\delta\chi^T} + R_k\chi = MJ_k. \tag{7.10}$$

Eqs. (7.3,7.6,7.8) and (7.10) allow for a functional integral representation of the effective average action,

$$\begin{aligned} \Gamma_k &= -\log \int \mathcal{D}\delta\hat{\chi} \exp -S_k[\hat{\chi}] + J_k^T(\hat{\chi} - \chi) + \Delta S_k[\chi] \\ &= -\log \int \mathcal{D}\delta\hat{\chi} \exp -S[\chi + \delta\hat{\chi}] + \frac{\delta\Gamma_k}{\delta\chi^T}\delta\hat{\chi} + \Delta S_k[\delta\hat{\chi}]. \end{aligned} \tag{7.11}$$

Note the appearance of the fluctuation $\delta\hat{\chi} = \hat{\chi} - \chi$ in the first line – the full field $\hat{\chi}$ comes from the functional integral representation of W_k (7.6), while the expectation value stems from the Legendre transform (7.8). In the second step we have used (7.10) and the identity

$$\Delta S_k[\hat{\chi}] = \Delta S_k[\chi] + \int_Q \left(\chi^T R_k(Q)\delta\hat{\chi} + \delta\hat{\chi}^T R_k(Q)\chi\right) + \Delta S_k[\delta\hat{\chi}]. \tag{7.12}$$

The cutoff function R_k enters (7.11) only through a piece depending on the fluctuation $\delta\hat{\chi}$ – this would be different for the k-dependent effective action $\hat{\Gamma}_k$.

We discuss the limiting cases for the effective average action defined through (7.11). In the limit $k \to 0$ the cutoff is removed by the first constraint in (7.5), such that we end up with the full effective action, defined by the microscopic action S and fully including all fluctuations similar to (7.7),

$$\lim_{k\to 0} \Gamma_k = \Gamma. \tag{7.13}$$

Obviously, the k-dependent effective action $\hat{\Gamma}_k$ has the same property, $\lim_{k\to 0} \hat{\Gamma}_k = \Gamma$.

In the limit $k \to \infty$, fluctuations are suppressed – indeed $\exp -\Delta S_k[\delta\hat{\chi}]$ acts as a δ-functional $\sim \delta[\delta\hat{\chi}]$. Neglecting fluctuations at all [2] we find

$$\lim_{k\to\Lambda} \Gamma_k = S. \tag{7.14}$$

The definition (7.8) ensures that the classical action is approached. The standard Legendre transform of W_k, instead, approaches $\lim_{k\to 0} \hat{\Gamma}_k \to S + \Delta S_k$. Hence, if the classical action S is known, Γ_k is the appropriate quantity setting an initial condition for the flow. The flow equation to be derived next then directly interpolates between the classical and the full quantum effective action Γ.

In next to leading (quadratic) order in the fluctuation $\delta\hat{\chi}$, we can evaluate the Gaussian integral and recover the structure of one-loop perturbation theory in the form (the "supertrace" is defined in app. C, eq. (C.21))

$$\lim_{k \text{ large}} \Gamma_k \approx S + \frac{1}{2}\mathrm{STr}\left(S^{(2)} + R_k\right). \tag{7.15}$$

From this perspective, a large cutoff provides an ordering principle (small fluctuations) guaranteeing the validity of perturbation theory. However, this result does not have too much physical impact since the *a priori* unphysical cutoff function appears in (7.15). In the case of perturbatively relevant couplings (like the mass term in our problem), the corresponding perturbation term will be present even for $R_k \to \infty$.

[2] This might not be justified in the presence of perturbatively relevant couplings as discussed below.

Now we derive the flow equation for the effective average action Γ_k. First we study the reaction of $\hat{\Gamma}_k$ to a change of the artificial cutoff scale – this yields the flow equation for $\hat{\Gamma}_k$:

$$\begin{aligned}\partial_k \hat{\Gamma}_k &= -e^{\hat{\Gamma}_k}\partial_k e^{-\hat{\Gamma}_k} = e^{\hat{\Gamma}_k}\int \mathcal{D}\hat{\chi}\ \partial_k S_k[\hat{\chi}]\ \exp -S_k[\hat{\chi}] + J_k^T\delta\hat{\chi} \\ &= \frac{1}{2}\int_Q \partial_k R_k\Big(\langle\hat{\chi}^T\hat{\chi}\rangle_{c,k} + \chi^T\chi\Big). \end{aligned} \tag{7.16}$$

In the second line we have used that the classical source terms from $\hat{\Gamma}_k$ and the functional integral in the first line cancel such that the correctly normalized two-point function appears. We have written down the decomposition in connected and disconnected part for this object in the second line. Now, since $\hat{\Gamma}_k$ is nothing but the usual Legendre transform of W_k, we can use the identity for their second functional derivatives eq. (4.22),

$$\langle\hat{\chi}^T\hat{\chi}\rangle_{c,k} = W_k^{(2)} = \big(\hat{\Gamma}_k^{(2)}\big)^{-1} = \big(\Gamma_k^{(2)} + R_k\big)^{-1}. \tag{7.17}$$

Using the definition (7.8), we thus find for the flow of the effective average action

$$\partial_k\Gamma_k = \frac{1}{2}\int_Q \partial_k R_k\Big(\Gamma_k^{(2)} + R_k\Big)^{-1}. \tag{7.18}$$

This is a *closed* functional differential equation – it only involves Γ_k and its second functional derivative. By construction, its solution for $k \to 0$ yields the full quantum effective action Γ and therefore is an *exact* flow equation. It has a simple one-loop structure, where the cutoff derivative is represented by the insertion of a dot.

Finally we discuss the role of the cutoff function in more detail. In the IR regime $|Q| \ll k$, the cutoff function acts as a mass term regulating possible IR divergences, since it is positive for $k > 0$ (cf. eq. (7.5)). This implies that only modes with $|Q| \gtrsim k$ can contribute to the flow. The FRG therefore is an appropriate tool for the investigation of situations which are plagued with IR divergences, as we have encountered them in the frame of Schwinger-Dyson equations.

In the UV regime, R_k can be chosen to act as a regulator, too. For this purpose, one requires in addition to the constraints (7.5)

$$\lim_{|Q|\to\infty} \partial_k R_k(Q) \to 0 \quad \text{sufficiently fast} \tag{7.19}$$

for fixed k. The appearance of $\partial_k R_k$ in eq. (7.18) then ensures the UV finiteness of the flow equation. Together with an "initial condition" $\Gamma_{k=\Lambda} = S$, this defines a regularization scheme ("ERGE scheme").

Eq. (7.19) leads to a local flow in momentum space. Since R_k acts as a mass term in the IR and $\partial_k R_k$ cuts off in the UV, the contribution to the flow at a scale k comes from a narrow window in momentum space only. Further identifying the scale k with the physical momentum scale Q, one can argue that the flow resolves a good part of the momentum dependence of the couplings.

In this work we use a cutoff which does not depend on the momentum Q and consequently does not respect (7.19). It has the conceptual advantage of a physical flow as discussed below. On the other hand, it is not optimized for the resolution of the momentum dependence of the couplings, and alternative cutoff functions respecting (7.19) should be studied in the future.

7.2 Flow Equations for the Crossover Problem

7.2.1 Truncation

In the spirit of the effective average action, we allow for a scale dependence of the coefficients of the microscopic action (3.5). This leads to the following ansatz for the effective average action on a scale k,

$$\begin{aligned}\Gamma_k \;=\; & \int\limits_{\tilde{X}} \Big[Z_\psi \tilde{\psi}^\dagger \big(\tilde{\partial}_\tau - A_\psi \tilde{\triangle} - \tilde{\sigma}\big)\tilde{\psi} + Z_\phi \tilde{\phi}^* \big(\tilde{\partial}_\tau - A_\phi \tilde{\triangle}\big)\tilde{\phi} + u(\tilde{\phi}^*\tilde{\phi}) \\ & \qquad - \frac{\tilde{h}_\phi}{2}\Big(\tilde{\phi}^* \tilde{\psi}^T \epsilon \tilde{\psi} - \tilde{\phi}\tilde{\psi}^\dagger \epsilon \tilde{\psi}^*\Big) + \frac{\tilde{\lambda}_\psi}{2}(\tilde{\psi}^\dagger\tilde{\psi})^2\Big] \\ = \; & \int\limits_{\tilde{X}} \Big[\psi^\dagger \big(\tilde{\partial}_\tau - A_\psi \tilde{\triangle} - \tilde{\sigma}\big)\psi + \phi^* \big(\tilde{\partial}_\tau - A_\phi \tilde{\triangle}\big)\phi + u(\phi^*\phi) \\ & \qquad - \frac{h_\phi}{2}\Big(\phi^* \psi^T \epsilon \psi - \phi\psi^\dagger \epsilon \psi^*\Big) + \frac{\lambda_\psi}{2}(\psi^\dagger\psi)^2\Big]. \end{aligned} \tag{7.20}$$

Here we work in the dimensionless version where all couplings are expressed in terms of suitable combinations of the Fermi momentum k_F and the Fermi energy $\epsilon_F = k_F^2/(2M)$. After the second equality, we have additionally switched to the renormalized version of the couplings. The relations between dimensionful, dimensionless, and dimensionless renormalized quantities are summarized in app. B. All couplings are now k-dependent quantities; the renormalized fields acquire a scale dependence through the premultiplication with the square root of the respective wave function renormalization factors.

As we have done in the Schwinger-Dyson approach, we choose a quartic trunca-

tion for the effective potential,

$$u(\rho) = \begin{cases} m_\phi^2 \rho + \frac{1}{2}\lambda_\phi \rho^2 + ... & \text{SYM} \\ \frac{\lambda_\phi}{2}(\rho - \rho_0)^2 + ... & \text{SSB} \end{cases} \tag{7.21}$$

where SYM and SSB denote the symmetric and superfluid (spontaneously symmetry-broken) phases. Both ansätze are continuously connected at the critical line $\rho_0 = 0, m_\phi^2 = 0$.

7.2.2 Choice of the Cutoff Functions: Flowing with the Chemical Potential

In order to choose cutoff functions for the crossover problem, we study the off-diagonal entries of the dimensionless renormalized fermion and boson propagators (C.7,C.11). Those parts of the propagators contain the frequency and momentum dependence in our truncation and need to be regularized by the scale-dependent cutoff functions R_F, R_ϕ. It is sufficient to restrict to the symmetric phase,

$$\begin{aligned} P_F(\tilde{Q})^{-1} &= \big(\mathrm{i}\,(2n+1)\pi\tilde{T} + A_\psi \tilde{q}^2 - \tilde{\sigma} + R_F\big), \\ P_\phi(\tilde{Q})^{-1} &= \big(\mathrm{i}2n\pi\tilde{T} + A_\phi \tilde{q}^2 + m_\phi^2 + R_\phi\big)^{-1}. \end{aligned} \tag{7.22}$$

We first discuss the infrared regularization of the propagators. Due to the odd Matsubara frequencies, the fermion propagator is not plagued by infrared divergencies except for $\tilde{T} = 0$. The boson propagator, on the other hand, has a zero mode $n = 0$ which potentially causes infrared problems. As usual, the propagation is suppressed for large mass terms $\tilde{\sigma}$, m_ϕ^2. We can mimic this effect by choosing the cutoff functions

$$R_F = -\tilde{\sigma}_c, \qquad R_\phi = -2\tilde{\sigma}_c. \tag{7.23}$$

The chemical potential can play the role of an infrared regulator. This choice of the regulator is a very physical one – the effective average action at a scale $\tilde{\sigma}_c$ describes a physical system at the chemical potential

$$\tilde{\sigma}_{tot} = \tilde{\sigma} + \tilde{\sigma}_c. \tag{7.24}$$

However, the physical situations of interest to us require one additional condition as discussed below. It can always be formulated as a condition for the "physical part" $\tilde{\sigma}$ of the total chemical potential $\tilde{\sigma}_{tot}$. This allows us to stop the flow for $\tilde{\sigma}_c \to 0$.

The cutoff functions have mass dimension 2 ($\tilde{\sigma} \hat{=} k^2$) and can be viewed as analytically continued frequencies. The regularization affects, however, both frequency and momentum modes in the infrared – there is no need to choose galilean invariant cutoff functions regularizing explicitly both frequency and momentum modes from

the infrared point of view. Since they do not modify the structure of the Matsubara frequencies, they allow for an analytical treatment of the Matsubara sums.

Our cutoff functions (7.23) feature coefficient 1 in the *renormalized* (Z_ψ, Z_ϕ - rescaled) propagators – this corresponds to the use of $\bar{R}_F = -Z_\psi\tilde{\sigma}, \bar{R}_\phi = 2Z_\phi\tilde{\sigma}$ in the "bare" dimensionless propagators. This ensures the use of renormalization group invariant cutoff functions and will generate anomalous dimension terms in the scale derivatives of the propagators.

The cutoff functions (7.23) are momentum independent and therefore do not fulfill the usual requirement (7.19) $\partial_k R_k \to 0$ for $q \gg k$ (or $\tilde{\sigma}$ here). Instead, they are simple mass terms with

$$\partial_{\tilde{\sigma}_c} R_F = -1, \qquad \partial_{\tilde{\sigma}_c} R_\phi = -2. \tag{7.25}$$

Cutoff functions of this type are called Callan-Szymanzik regulators and can cause problems in the ultraviolet, necessitating explicit ultraviolet regularization. We note, however, that the frequency (Matsubara sum) and momentum space integrals for our particular problem are *finite* for any of the running couplings we are going to consider. The flow of the effective action itself can be made finite by the same argument as we have used to render the particle densities finite – this will become apparent below. Hence there is no particular need to choose cutoff functions that regularize the ultraviolet momentum and frequency modes. As argued above, our choice has the conceptual advantage that the flow equations can be given a physical interpretation at any scale – the flow directly explores the thermodynamic space of different particle densities. Further, by choosing the chemical potential as a cutoff, fermion and boson propagators are regularized in a completely symmetric way. On the other hand, by choosing a Callan-Szymanzik regulator, we loose the technical advantage of locality in momentum space as argued above. In the future, cutoff functions ensuring the latter property should also be investigated.

7.2.3 Flow Equations

The most important flow equations for the crossover problem can be obtained from derivatives of the field dependent effective potential which is discussed in app. D.4. We consider the flow of the field dependent one-loop effective potential

$$\partial_{\tilde{\sigma}_c}\tilde{u}_1 = \partial_{\tilde{\sigma}_c}\tilde{u}_1^{(F)} + \partial_{\tilde{\sigma}_c}\tilde{u}_1^{(B)} \tag{7.26}$$

where we separate the fermionic and the bosonic contribution. The fermionic part reads

$$\begin{aligned} \partial_{\tilde{\sigma}_c}\tilde{u}_1^{(F)}(\tilde{\sigma},\hat{\rho}) &= -2\tilde{T}\int \frac{d^3\tilde{q}}{(2\pi)^3}\big(\partial_{\tilde{\sigma}_c}\gamma_\phi \tanh\gamma_\phi - 1\big) \\ &= (1-\eta_\psi)\int \frac{d^3\tilde{q}}{(2\pi)^3}\Big(\frac{\gamma}{\gamma_\phi}\tanh\gamma_\phi - 1\Big) \end{aligned} \tag{7.27}$$

where we have used eq. (D.32) and the ultraviolet renormalization procedure for the two-point function motivated in sect. 4.2.3, rendering the momentum space integral for the flow of the fermionic part of the effective potential finite. Clearly this property will also hold for all couplings obtained by derivatives of the effective potential. The second line holds for our particular choice of truncation and cutoff function. The dimensionless field dependent functions γ_ϕ, γ and their scale derivatives read in our truncation

$$\begin{aligned} \gamma_\phi &= \frac{((A_\psi \tilde{q}^2 - \tilde{\sigma} - \tilde{\sigma}_c)^2 + h_\phi^2 \rho)^{1/2}}{2\tilde{T}}, \quad \partial_{\tilde{\sigma}_c} \gamma_\phi = -(1-\eta_\psi) \frac{\gamma}{2\tilde{T}\gamma_\phi}, \\ \gamma &= \frac{A_\psi \tilde{q}^2 - \tilde{\sigma} - \tilde{\sigma}_c}{2\tilde{T}}, \quad \partial_{\tilde{\sigma}_c} \gamma = -(1-\eta_\psi) \frac{1}{2\tilde{T}}. \end{aligned} \tag{7.28}$$

The fermion anomalous dimension is defined as

$$\eta_\psi = -\tilde{\sigma}_c \partial_{\tilde{\sigma}_c} \log Z_\psi = -\partial_t \log Z_\psi \tag{7.29}$$

with the dimensionless scale derivative [3]

$$\partial_t = \tilde{\sigma}_c \partial_{\tilde{\sigma}_c}, \quad t = \log(-\tilde{\sigma}_c). \tag{7.30}$$

Using t as the flow variable represents the flow on a logarithmic scale, thereby allowing for a compact plot of solutions of the flow equations over many orders of magnitude and a high resolution of the infrared flow where the interesting physics is expected to happen.

The bosonic contribution to the flow of the effective potential reads

$$\begin{aligned} \partial_{\tilde{\sigma}_c} \tilde{u}_1^{(B)} &= \tilde{T} \int \frac{d^3\tilde{q}}{(2\pi)^3} \big(\partial_{\tilde{\sigma}_c} \alpha_\phi \coth \alpha_\phi - 1 \big) \\ &= -(1-\eta_\phi) \int \frac{d^3\tilde{q}}{(2\pi)^3} \Big(\frac{\alpha + \kappa}{\alpha_\phi} \coth \alpha_\phi - 1 \Big). \end{aligned} \tag{7.31}$$

[3] "Dimensionless" here alludes to the fact that the canonical dimension of ∂_t is 0, while that of $\partial_{\tilde{\sigma}_c}$ is -2 since the canonical dimension of $\tilde{\sigma}_c$ is 2. We usually use the term "dimensionless" in another sense throughout this work, e.g. $\tilde{\sigma}_c$ is dimensionless in the sense that it is measured in units of the Fermi energy $k_F^2/2M$.

Here we use the dimensionless functions $\alpha_\phi, \alpha, \kappa$ and their scale derivatives

$$\begin{aligned}
\alpha_\phi &= \frac{1}{2\tilde{T}}\big[(A_\phi\tilde{q}^2 + m_\phi^2 - 2\tilde{\sigma}_c)^2 \\
&\qquad +2\lambda_\phi(2\rho-\rho_0)(A_\phi\tilde{q}^2 + m_\phi - 2\tilde{\sigma}_c) + \lambda_\phi^2(3\rho^2 - 4\rho_0\rho + \rho_0^2)\big]^{1/2}, \\
\partial_{\tilde{\sigma}_c}\alpha_\phi &= -(1-\eta_\phi)\frac{\alpha+\kappa}{\tilde{T}\alpha_\phi}, \\
\alpha &= \frac{A_\phi\tilde{q}^2 + m_\phi^2 - 2\tilde{\sigma}_c}{2\tilde{T}}, \quad \partial_{\tilde{\sigma}_c}\alpha = -(1-\eta_\phi)\frac{1}{\tilde{T}}, \\
\kappa &= \frac{\lambda_\phi(2\rho-\rho_0)}{2\tilde{T}}, \quad \partial_{\tilde{\sigma}_c}\kappa = 0.
\end{aligned} \tag{7.32}$$

with the boson anomalous dimension

$$\eta_\phi = -\partial_t \log Z_\phi. \tag{7.33}$$

The flow of the couplings we are interested in are obtained by projection with appropriate derivatives, and setting the fields to their values at the minimum of the potential.

Flow equations from the effective potential

With these preparations, we can specify the flow equations for the mass term and the four-boson coupling. In SYM, they read ($\int_{\tilde{q}} = (2\pi)^{-3}\int d^3\tilde{q} = 1/(2\pi^2)\int d\tilde{q}\tilde{q}^2$)

$$\begin{aligned}
\partial_t m_\phi^2 &= -e^t\big\{(1-\eta_\psi)\frac{h_\phi^2}{8\tilde{T}^2}\int_{\tilde{q}}\gamma^{-2}\big(\gamma\cosh^{-2}\gamma - \tanh\gamma\big) + (1-\eta_\phi)\frac{\lambda_\phi}{\tilde{T}}\int_{\tilde{q}}\sinh^{-2}\alpha\big\} \\
&\quad +\eta_\phi m_\phi^2, \qquad (7.34) \\
\partial_t\lambda_\phi &= -e^t\big\{(1-\eta_\psi)\frac{h_\phi^4}{64\tilde{T}^4}\int_{\tilde{q}}\gamma^{-4}\big(3\tanh\gamma - \gamma\cosh^{-2}\gamma(3+2\gamma\tanh\gamma)\big) \qquad (7.35) \\
&\quad -(1-\eta_\phi)\frac{\lambda_\phi^2}{4\tilde{T}^2}\int_{\tilde{q}}\alpha^{-2}\big[\coth\alpha + \alpha\sinh^{-2}\alpha + 8\coth\alpha\sinh^{-2}\alpha\big]\big\} + 2\eta_\phi\lambda_\phi.
\end{aligned}$$

The factors of $-e^t = \tilde{\sigma}_c$ (eq. (7.30)) account for the use of the dimensionless scale derivatives. This shows that the flow is suppressed for very small cutoff or $t \to -\infty$. In SSB with $\rho_0 \neq 0$, we can infer the flow of the minimum of the potential ρ_0 from the scale dependent field equation for the effective potential ($\tilde{u}' = \partial\tilde{u}/\partial\rho$ and analogous for $\tilde{u}''$),

$$\begin{aligned}
\frac{\partial\tilde{u}}{\partial\phi^*}\Big|_{\rho=\rho_0} &= \frac{\partial\tilde{u}}{\partial\rho}\Big|_{\rho=\rho_0}\cdot\phi_0 \stackrel{!}{=} 0 \quad \stackrel{SSB}{\Leftrightarrow} \quad \tilde{u}' = 0 \qquad (7.36) \\
\Rightarrow \frac{d}{dt}\tilde{u}' &= \partial_t\tilde{u}' + (\partial_t\rho_0)\,\tilde{u}'' = 0,
\end{aligned}$$

where in our truncation

$$\tilde{u}'' = \lambda_\phi. \tag{7.37}$$

The relevant flows read

$$\begin{aligned}\partial_t \rho_0 &= \frac{e^t}{\lambda_\phi}\Big\{(1-\eta_\psi)\frac{h_\phi^2}{8\tilde{T}^2}\int_{\tilde{q}} \gamma\gamma_\phi^{-3}\big(\gamma_\phi \cosh^{-2}\gamma_\phi - \tanh\gamma_\phi\big) + \\ &\qquad (1-\eta_\phi)\frac{\lambda_\phi}{2\tilde{T}}\int_{\tilde{q}} \alpha_\phi^{-3}\big[\alpha_\phi(2\alpha^2+3\alpha\kappa+\kappa^2)\sinh^{-2}\alpha_\phi + \kappa(\kappa-\alpha)\coth\alpha_\phi\big]\Big\} - \eta_\phi\rho,\end{aligned} \tag{7.38}$$

where λ_ϕ is determined by

$$\begin{aligned}\partial_t \lambda_\phi &= -e^t\Big\{(1-\eta_\psi)\frac{h_\phi^4}{64\tilde{T}^4}\int_{\tilde{q}} \gamma\gamma_\phi^{-5}\big[3\tanh\gamma_\phi - \gamma_\phi\cosh^{-2}(3+2\gamma_\phi\tanh\gamma_\phi)\big] \\ &\quad -(1-\eta_\phi)\frac{\lambda_\phi^2}{4\tilde{T}^2}\int_{\tilde{q}} \alpha_\phi^{-5}\big[\alpha_\phi(\alpha^3-5\alpha^2\kappa+\alpha\kappa^2+3\kappa^3)\sinh^{-2}\alpha_\phi \\ &\qquad + \coth\alpha_\phi(\alpha^3-5\alpha^2\kappa+\alpha\kappa^2+3\kappa^3+2\alpha_\phi^2(\alpha+\kappa)(2\alpha+\kappa)^2\sinh^{-2}\alpha_\phi)\big]\Big\} \\ &\quad +2\eta_\phi\lambda_\phi.\end{aligned} \tag{7.39}$$

Technically important, both the scale derivative and all field derivatives can be expressed in terms of six dimensionless functions $\gamma, \gamma_\phi, \beta$ and $\alpha, \alpha_\phi, \kappa$. We will call them basis functions. They allow for a compact notation. For a more general choice of $\gamma, \gamma_\phi, \beta$ and $\alpha, \alpha_\phi, \kappa$, the truncation can easily be extended beyond the quartic approximation, still keeping the functional form of eqs. (7.27,7.31). Further, different cutoff functions can easily be implemented, if the regularization affects the spacelike momenta only.

At this point we note that the bosonic one-loop diagrams included in the flow equations are precisely the ones which we have taken into account in the Schwinger-Dyson equations for the boson mass and coupling. The fermionic diagrams are the "mean field" contributions already present from integrating out the fermions. In the frame of partially bosonized functional RG equations, a systematic inclusion of boson diagrams in the flow of further couplings is straightforward, which would be hard in the Schwinger-Dyson approach.

Anomalous dimensions

The choice of renormalized fields and couplings (rescaled with the WFRs) leads to a set of flow equations which does not explicitly involve Z_ϕ, Z_ψ as running couplings – the corresponding information enters the flow via the anomalous dimensions. This has the technical advantage to reduce the set of flow equations by two, since the

anomalous dimensions are loop integral expressions depending on the running couplings.

According to our truncation, the anomalous dimension is extracted from the flow of the frequency dependent one-loop correction to off-diagonal entries of the propagators ($\propto \psi^\dagger\psi, \phi^*\phi$)

$$\eta_{\psi,\phi} = -\partial_t \log Z_{\psi,\phi} = -\partial_t \frac{\partial \mathrm{Im}\Delta P_{F,\phi}(\tilde{\omega}, \vec{\tilde{q}} = 0)}{\partial \tilde{\omega}}\Big|_{\tilde{\omega}=0} \tag{7.40}$$

where $\Delta P_{F,\phi}(\tilde{\omega}, \vec{\tilde{q}})$ is specified in app. C, eqs. (C.22, C.23). Here we need to consider the imaginary part of the loop correction in order to accommodate the fact that the operators $\psi^\dagger \mathrm{i}\omega\psi$, $\phi^* \mathrm{i}\omega\phi$ are purely imaginary [4]

The scale derivatives produce factors $(1 - \eta_\psi)$ and $(1 - \eta_\phi)$ when acting on the fermionic or bosonic basis functions, respectively. Hence eq. (7.40) gives only an implicit definition of the anomalous dimensions, still depending on η_ψ, η_ϕ. On the other hand, the coupled system of linear equations is easily solved for η_ψ, η_ϕ, giving the desired explicit results. In the case $\eta_\psi = 0$, which is relevant in the BEC regime, (7.40) is an explicit definition for η_ϕ.

We do not display the results of performing the cutoff derivatives explicitly – this produces very lengthy results. Using the cutoff derivatives (7.28,7.32), the computation of the anomalous dimensions is, however, implemented straightforwardly from the loop expressions eqs. (D.4,D.5) for η_ψ and (D.6,D.7) for η_ϕ.

Similarly, for the flow equations of the gradient coefficients, we refer to eqs. (D.21 - D.23), for the Yukawa coupling h_ϕ to (D.24), and for the four-fermion coupling λ_ψ to (D.26).

7.3 Two-body Limit and the Choice of Initial Conditions

7.3.1 Flow Equations

The measured two-body observables can be viewed as quantities which are modified by "vacuum fluctuations" compared to their "bare" counterparts. Clearly we want to formulate our results in terms of the measured quantities. In (5.49) we have specified how to project on the two-body limit in the effective action formalism. The flow

[4] Here we do not distinguish between a wave function renormalization for the radial and the Goldstone mode. The same is true for the gradient coefficient. This should be included in a future treatment.

equations in this limit, supplemented with the constraints (5.50), provide us with the means to continuously connect the bare (ultraviolet) with the physical (infrared) quantities. Therefore, we choose our initial conditions such that the flow matches these values in the infrared. The infrared limit, i.e. the point where we have to stop the flow, is defined by the constraints (5.50) being fulfilled. This constitutes an UV renormalization procedure. It is fully nonperturbative and allows to UV-renormalize all couplings simultaneously. It can be seen as the FRG analog to the Schwinger-Dyson procedure provided in sect. 5.6.1. On top of an efficient UV renormalization, it also allows us to substantially improve the approximation for the four-boson coupling (or the bosonic scattering length a_M) in vacuum.

This UV renormalization procedure also forms the basis for the description of the many-body system. Here the task is to compute observables as a function of the microscopic observables $(\bar{h}_\phi, a, a_{bg})$, and additionally the thermodynamic scales $\tilde{T}, k_F = (3\pi^2 n)^{1/3}$. In this case we use the mapping between bare and observed quantities in order to eliminate the bare quantities from our computation. The procedure is described in more detail in the next section.

Adding to these practically motivated issues, it is well known that the two body problem involving only two-body interactions as described by a four-fermion coupling (single-channel model) can be solved analytically (cf. e.g. [41]). We can confirm this result in our two-channel model in the frame of the renormalization group equations, and generalize it to the case that pointlike four-fermion interactions are included.

In the two-body limit, the system of renormalization group equations greatly simplifies since a number of diagrams vanish identically. This can be seen by the aid of the residue theorem, and we can put it in the form of the following theorem:

All diagrams whose inner lines point in the same direction (thereby forming a closed tour) do not contribute to the flow in vacuum.

To prove this theorem, we first note that for $T = 0$ the Matsubara sums turn into continuous integrations,

$$\mathrm{i}\tilde{\omega}_{F/\phi} \to \mathrm{i}\tilde{q}_0, \quad \sum_n \tilde{T} \to \int \frac{d\tilde{q}_0}{2\pi}. \tag{7.41}$$

Further there is no spontaneous breaking of the $U(1)$ symmetry in the physical vacuum such that $\rho_0 = 0$. Hence both fermionic and bosonic regularized propagators are fully characterized by the functions

$$\begin{aligned} P_F(\tilde{Q}) &= \mathrm{i}\tilde{q}_0 + A_\psi \tilde{q}^2 - \tilde{\sigma} - \tilde{\sigma}_c, \\ P_\phi(\tilde{Q}) &= \mathrm{i}\tilde{q}_0 + A_\phi \tilde{q}^2 + m_\phi^2 - 2\tilde{\sigma}_c. \end{aligned} \tag{7.42}$$

Lines pointing in the same direction represent integrals over products of P_F^{-1}, P_ϕ^{-1} with the *same* sign of the frequency and momentum variable $\tilde{Q}$; without loss of generality, we can choose it positive.

In the presence of a nonzero cutoff, the spacelike part of the propagators including the mass terms are always positive. Hence, the poles all lie in the upper half of the complex plane. One then closes the integration contour below, such that no residues are picked up, showing that these integrals vanish. The cutoff derivative increments the number of inner lines P_F^{-1}, P_ϕ^{-1} by one (it changes the multiplicity of the poles), but does not affect the sign of the momentum variable, such that our argument is valid for both the regularized loops and their cutoff derivative entering the flow equation.

The consideration is strictly valid in the presence of a nonzero cutoff. For $\tilde{\sigma}_c \to 0$ we have the constraints $\tilde{\sigma} = 0, m_\phi^2 > 0$ on the BCS side and $\tilde{\sigma} > 0, m_\phi^2 = 0$ on the BEC side of the resonance. Our argument strictly applies to diagrams with less than two inner lines with a zero mass entry ($\tilde{\sigma} < 0$ constitutes a mass term for the fermions); for two and more, there are IR divergences at $\vec{\tilde{q}} = 0$. On resonance, where simultaneously $\tilde{\sigma} = m_\phi^2 = 0$, IR divergences are even enhanced. However, since the flow vanishes identically for all $\tilde{\sigma}_c > 0$, it seems physically sensible to discard these diagrams from our system of flow equations in vacuum.

Let us now discuss different types of diagrams explicitly which do not contribute to the vacuum flow.

- The mixed diagram with two inner lines, driving the renormalization of the fermion propagator, does not contribute. This implies

$$Z_\psi = 1, \quad \eta_\psi = 0, \quad A_\psi = 1, \quad \Delta m_\psi^2 = 0. \tag{7.43}$$

- The box diagram with two inner boson and fermion lines, in principle generating a four-fermion interaction even for vanishing background coupling, does not appear. For $\lambda_{\psi,0} = 0$ we thus have

$$\lambda_\psi = 0 \tag{7.44}$$

  at all scales. In a vague sense, this means that partial bosonization is very efficient in this limit – fluctuations are completely absorbed into the bosonic sector, and there is no "backreaction" on the fermion propagator.

- The diagrams involving solely *one* inner fermion or boson line [5] are zero. This is directly related to the fact that the particle density vanishes by construction

[5] Strictly speaking, the residue theorem can only be applied for the cutoff derivative of the diagram, since a single inner line does not have sufficient convergence properties for its applicability.

– diagrammatically, the trace over the full propagator is represented as a closed loop coupled to an external current, the chemical potential (tadpole graph). This is relevant for the bosonic contribution to the boson mass which thus vanishes – the renormalization of the boson mass in the physical vacuum is purely driven by the fermion loop.

- The "bubble diagrams" (involving two inner boson or two inner fermion lines forming a closed tour) vanish.

The "ladder diagrams" instead, which have lines pointing in the same direction, contribute. Due to the opposite signs of the momentum variables in the propagators, the poles of these diagrams are located in both the upper and the lower half plane. It is worth noting that the four-boson coupling receives such a bosonic ladder contribution. This is the only bosonic diagram in our truncation which survives the vacuum limit. The formal IR divergence of the diagram for $m_\phi = 0$ is regulated by the cutoff function to give a finite result for the four-boson coupling in the physical limit $\tilde{\sigma}_c \to 0$ (cf. fig. 7.1).

Adding to the massive structural simplifications, the remaining loop integrals can be performed analytically. We find for the remaining system of renormalization group equations

$$\begin{aligned}
\partial_t m_\phi^2 &= -\frac{h_\phi^2}{16\pi}\frac{\tilde{\sigma}_c}{(-\tilde{\sigma}_c-\tilde{\sigma}_A)^{1/2}} + \eta_\phi m_\phi^2, \qquad (7.45)\\
\partial_t h_\phi^2 &= -\frac{\lambda_\psi h_\phi^2}{8\pi}\frac{\tilde{\sigma}_c}{(-\tilde{\sigma}_c-\tilde{\sigma}_A)^{1/2}} + \eta_\phi h_\phi^2,\\
\partial_t \lambda_\psi &= -\frac{\lambda_\psi^2}{16\pi}\frac{\tilde{\sigma}_c}{(-\tilde{\sigma}_c-\tilde{\sigma}_A)^{1/2}},\\
\partial_t \lambda_\phi &= \frac{3h_\phi^4}{256\pi}\frac{\tilde{\sigma}_c}{(-\tilde{\sigma}_c-\tilde{\sigma}_A)^{5/2}} - (1-\eta_\phi)\frac{\lambda_\phi^2}{8\pi}\frac{\tilde{\sigma}_c}{A_\phi^{3/2}(m_\phi^2-2\tilde{\sigma}_c)^{1/2}} + 2\eta_\phi\lambda_\phi,\\
\partial_t A_\phi &= \frac{h_\phi^2}{128\pi}\frac{\tilde{\sigma}_c}{(-\tilde{\sigma}_c-\tilde{\sigma}_A)^{3/2}} + \eta_\phi A_\phi
\end{aligned}$$

with the anomalous dimension

$$\eta_\phi = -\frac{h_\phi^2}{64\pi}\frac{\tilde{\sigma}_c}{(-\tilde{\sigma}_c-\tilde{\sigma}_A)^{3/2}}. \qquad (7.46)$$

We denote the "chemical potential" in vacuum (half the binding energy of a molecule) with $\tilde{\sigma}_A$ as in sect. 5.5. Here we have already inserted the simplifications resulting from the non-renormalization of the fermion propagator. The "core" of flow equations for the mass m_ϕ^2, Yukawa coupling h_ϕ^2 and four-fermion coupling λ_ψ constitute a closed set of equations in our truncation. The RG equations for λ_ϕ, A_ϕ decouple from this core.

7.3.2 Solution of the Core System and Initial Conditions

The core system can be solved analytically by consecutive integration. To see this, we rewrite these equations in the "bare" form (without Z_ϕ-rescaling, $\tilde{s} = -(\tilde{\sigma}_c + \tilde{\sigma}_A)$),

$$\begin{aligned} \partial_{\tilde{\sigma}_c} \tilde{m}_\phi^2 &= -\frac{\tilde{h}_\phi^2}{16\pi} \frac{1}{\tilde{s}^{1/2}}, \\ \partial_{\tilde{\sigma}_c} \tilde{h}_\phi^2 &= -\frac{\tilde{\lambda}_\psi \tilde{h}_\phi^2}{8\pi} \frac{1}{\tilde{s}^{1/2}}, \\ \partial_{\tilde{\sigma}_c} \tilde{\lambda}_\psi &= -\frac{\tilde{\lambda}_\psi^2}{16\pi} \frac{1}{\tilde{s}^{1/2}}. \end{aligned} \tag{7.47}$$

The solution of the last equation matches the corresponding result from solving the Schwinger-Dyson equations presented in sect. 5.6.1, eq. (5.102),

$$\tilde{\lambda}_\psi^{-1} = \tilde{\lambda}_{\psi,\Lambda}^{-1} + \frac{1}{8\pi}\left(\sqrt{\tilde{s}_\Lambda} - \sqrt{\tilde{s}}\right) = \tilde{\lambda}_{\psi,0}^{-1} - \frac{\sqrt{-\tilde{s}}}{8\pi} \tag{7.48}$$

($\tilde{s}_\Lambda = -(\tilde{\sigma}_\Lambda + \tilde{\sigma}_A)$). This structure renders $\tilde{\lambda}_\psi$ almost independent of $\tilde{s}$ if $\sqrt{\tilde{s}} \ll \sqrt{\tilde{s}_\Lambda} + 8\pi/\tilde{\lambda}_{\psi,\Lambda}$. Here we assume implicitly that $\tilde{\lambda}_{\psi,\Lambda}$ is not too much negative such that $\tilde{\lambda}_\psi$ remains finite in the whole $\tilde{s}$ - range of interest. For positive $\tilde{\lambda}_\psi$ the self-consistency of the flow requires an upper bound $\tilde{\lambda}_{\psi,0}/(8\pi) < 1/\sqrt{\tilde{s}_\Lambda}$. In contrast, the solution for the renormalized $h_\phi^2 = \tilde{h}_\phi^2/Z_\phi$ for $\tilde{\lambda}_\psi = 0$

$$h_\phi^{-2} = h_{\phi,\Lambda}^{-2} + \frac{1}{32\pi}\left(\tilde{s}^{-1/2} - \tilde{s}_\Lambda^{-1/2}\right) \tag{7.49}$$

is dominated by small $\tilde{s}$.

For $\tilde{\lambda}_\psi \neq 0$ the flow of h_ϕ is modified, without changing, the characteristic behavior for $\tilde{\sigma}_c \to 0$. Indeed, in the limit $\tilde{s} \to 0$ (close to the resonance) the term $\sim \tilde{\lambda}_\psi$ becomes subdominant for the evolution of h_ϕ^2. The flow for the ratio $h_\phi^2/\sqrt{\tilde{s}}$ reaches a fixed point 32π. With $x = \sqrt{-\tilde{s}}$ one obtains

$$\begin{aligned} \tilde{h}_\phi^2 &= \tilde{h}_{\phi,\Lambda}^2 \exp\Big\{-\frac{1}{4\pi}\int_{\sqrt{\tilde{s}}}^{\sqrt{\tilde{s}_\Lambda}} dx \tilde{\lambda}_\psi(x)\Big\} = \tilde{h}_{\phi,\Lambda}^2 \left(1 - c_{bg}\sqrt{\tilde{s}_\Lambda}\right)^2 \left(1 - c_{bg}\sqrt{\tilde{s}}\right)^{-2} \\ &= \tilde{h}_{\phi,0}^2 \big(1 - c_{bg}\sqrt{\tilde{s}}\big)^{-2}. \end{aligned} \tag{7.50}$$

Again comparing to sect. 5.6.1, this fits with eq. (5.101) (for removed cutoff $\tilde{\sigma}_c = 0$). For the wave function renormalization one gets

$$\begin{aligned} Z_\phi &= Z_{\phi,\Lambda} + \frac{1}{32\pi}\int_{\tilde{s}_\Lambda^{-1/2}}^{\tilde{s}^{-1/2}} d(x^{-1}) \tilde{h}_\phi^2(x^{-1}) \\ &= Z_{\phi,\Lambda} + \frac{\tilde{h}_{\phi,0}^2}{32\pi}\Big\{\frac{1}{\sqrt{\tilde{s}}}\big(1 - \frac{c_{bg}}{1/\sqrt{\tilde{s}} - c_{bg}}\big) + 2c_{bg}\ln\frac{1/\sqrt{\tilde{s}} - c_{bg}}{c_{bg}} - (\tilde{s} \to \tilde{s}_\Lambda)\Big\}, \end{aligned} \tag{7.51}$$

with $1/\sqrt{\tilde{s}} > c_{bg} = \tilde{\lambda}_{\psi,0}/(8\pi)$. Obviously, for $\tilde{s} \to 0$ the ratio $\tilde{h}_\phi^2/\tilde{h}_{\phi,\Lambda}^2$ reaches a constant depending on $\lambda_{\psi,\Lambda}, \tilde{s}_\Lambda$ whereas Z_ϕ diverges $\approx \tilde{h}_{\phi,0}^2/(32\pi\sqrt{\tilde{s}})$, consistent with the fixed point behavior $h_\phi^2 \approx 32\pi\sqrt{\tilde{s}}$. The values $\tilde{h}_{\phi,0}^2 = \tilde{h}_\phi^2(\tilde{s} = \tilde{\sigma}_A = 0)$ and $\tilde{\lambda}_{\psi,0} = \tilde{\lambda}_\psi(\tilde{s} = \tilde{\sigma}_A = 0)$ can be extracted from atom scattering in vacuum or the dependence of the molecular binding energy on the magnetic field (cf. sect. 5.5.3).

We finally investigate the flow equation for $\tilde{m}_\phi^2$ (7.47). The solution reads [6]

$$\tilde{m}_\phi^2 = \frac{2M\bar{\mu}}{\hat{k}^2}(B - B_0) - 2\tilde{\sigma}_c + \delta\tilde{\nu} - \frac{1}{8\pi}\int_{\sqrt{\tilde{s}}}^{\sqrt{\tilde{s}_\Lambda}} dx \tilde{h}_\phi^2(x). \tag{7.52}$$

$\frac{2M\bar{\mu}}{\hat{k}^2}(B - B_0) - 2\tilde{\sigma}_c = \tilde{m}_{\phi,\Lambda}^2$ is the initial condition for the mass. The mass shift $\delta\tilde{\nu}$ is an integration constant which we can fix by the requirement that the boson mass vanish at the resonance, $\tilde{m}_\phi^2(\tilde{\sigma}_c = \tilde{\sigma}_A = 0, B = B_0) = 0$ – this is analogous to the procedure presented in sect. 5.6.1. It implies

$$\delta\tilde{\nu} = \frac{1}{8\pi}\int_0^{\sqrt{\tilde{s}_\Lambda}} dx \quad \tilde{h}_\phi^2(x) \tag{7.53}$$

such that

$$\tilde{m}_\phi^2 = \frac{2M\bar{\mu}}{\hat{k}^2}(B - B_0) - 2\tilde{\sigma}_c + \frac{\tilde{h}_{\phi,0}^2}{8\pi}\frac{\sqrt{\tilde{s}}}{1 - c_{bg}\sqrt{\tilde{s}}}. \tag{7.54}$$

This is in accordance with eq. (5.100) in the Schwinger-Dyson framework (for $\tilde{\sigma}_c = 0$). Due to the equivalence of the Schwinger-Dyson results eqs. (5.102,5.101,5.100) and eqs. (7.48,7.50,7.54) (the order is such that the equations correspond to each other), we can follow the same route in order to reconstruct the fermionic scattering length from the result of the FRG computation.

In our practical computations, we initialize the system with vanishing or negative background coupling with $\tilde{s}_\Lambda = 10^6$. If the background coupling is positive, we have to ensure $1/\sqrt{\tilde{s}_\Lambda} > c_{bg}$.

In fig. 7.2 we compare the sensitivity of various couplings w.r.t to the value of the Yukawa coupling $\tilde{h}_{\phi,0}$ in the two-body limit. As expected from our earlier results, $\tilde{h}_{\phi,0}$ sets the scale for the absolute value of the wave function renormalization Z_ϕ (cf. fig. 7.2 (a)). An appropriate rescaling with Z_ϕ, as carried out for the renormalized quantities, produces a pronounced insensitivity of these couplings w.r.t. a variation of $\tilde{h}_{\phi,0}$ (cf. fig. 7.2 (c),(d)). This reflects the validity of our universality hypothesis for broad Feshbach resonances in the FRG framework.

[6] We write the fiducial momentum unit $\hat{k}$ instead of k_F in order to prevent confusion with the physical Fermi momentum associated to the particle density.

7.3.3 Bosonic Scattering Length on the BEC Side

We consider the bosonic scattering length in vacuum on the BEC side. For simplicity we work in the broad resonance limit and at zero background coupling ($a = a_R$). As we have seen in sect. 6.4, renormalization with fermionic diagrams then yields the result

$$\frac{a_M}{a} = 2. \tag{7.55}$$

However, the solution of the Schrödinger equation for the four-body problem under the assumption that the particles are grouped into two pairs with small interparticle spacing indicates [75]

$$\frac{a_M}{a} \approx 0.6. \tag{7.56}$$

The above assumptions obviously describe the deep BEC regime with strongly bound molecules. This result has subsequently been confirmed in the frame of Quantum Monte Carlo simulations [84] and in a very sophisticated diagrammatic approach [85]. The Camerino group finds $a_M/a \approx 0.75(4)$ from a resummation of the effective boson-boson interaction ladder [21]. All these approaches necessitate a very high numerical effort.

In this section we will analyze the problem in the frame of FRG equations in the BEC limit. Our implementation amounts to a resummation similar to the one performed in [21] and indeed we find $a_M/a \approx 0.81$, while the numerical effort is negligible and only involves the numerical solution of a single nonlinear differential equation. Additionally, relying on the simplified diagrammatic structure in vacuum, we can give an estimate for the effective boson-boson interaction not only deep in the BEC regime, but also close to and on the resonance. On the BCS side of the resonance, we also find a certain scaling behavior as will be discussed below. In the future, it remains to be seen if the value $a_M/a \approx 0.6$ can be obtained in an extended truncation involving a fermion-boson vertex $\sim \psi^\dagger\psi\phi^*\phi$ and a generalized Yukawa term $\sim \phi^*\psi^T\epsilon\psi\phi^*\phi$ in addition to the fermion-fermion (described as a tree level exchange of a molecule) and boson-boson vertex. Indeed there are one-loop graphs contributing to these vertices which survive the vacuum limit.

The bosonic scattering length can be obtained from the four-boson scattering amplitude at zero external momenta as described in app. A, eq. (A.12). In contrast to the fermions, the bosonic composite objects are *indistinguishable* particles such that the second relation in (A.12) has to be used,

$$a_M = \frac{M_M}{8\pi}\Big|\frac{\delta^4\Gamma}{\delta\phi_R^*(p_1)\delta\phi_R(p_2)\delta\phi_R^*(p_3)\delta\phi_R(p_4)}\Big|_{p_1=\ldots=p_4=0} = \frac{M_M\bar{\lambda}_\phi}{4\pi Z_\phi^2}. \tag{7.57}$$

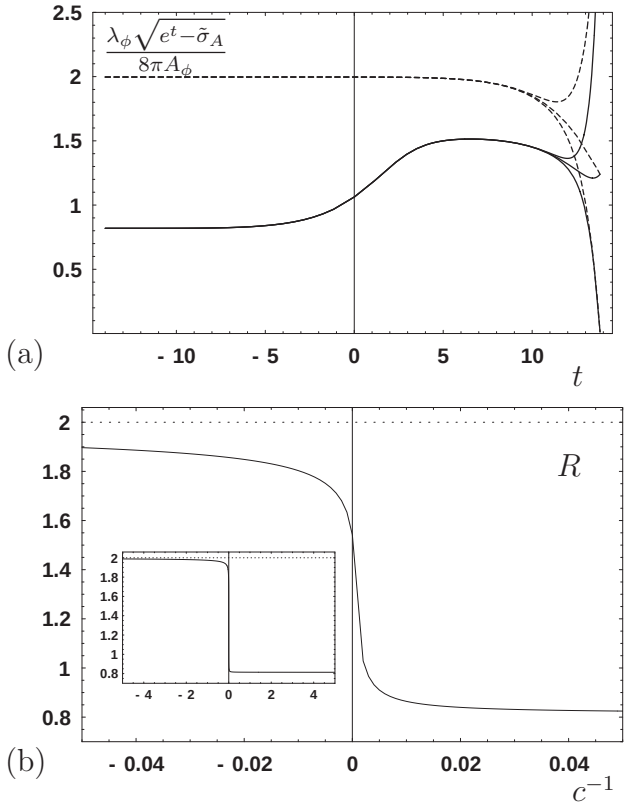

Figure 7.1: (a) Flow of the reduced bosonic scattering length on the BEC side, $a_M(t)/a(t) = \lambda_\phi(t)\sqrt{e^t - \tilde{\sigma}_A}/(8\pi A_\phi(t))$. There is a pronounced insensitivity with respect to the initial condition. The dashed lines omit the bosonic contribution to the flow of λ_ϕ, leading to an infrared fixed point at $a_M/a = 2$. Including this contribution shifts the fixed point to $a_M/a = 0.814$. (b) The scaling function R across the resonance (cf. eq. (7.62) for a definition). It reduces to the ratio a_M/a on the BEC side of the resonance – the boson coupling vanishes $\propto a$. In the BEC regime, the system settles to a fixed point whose value is given above. Evolving to the resonance, the ratio a_M/a moves away from the BEC fixed point and we find $a_M/a = 1.542$ at resonance – the boson coupling diverges $\propto a$. Beyond the resonance on the BCS side, the interpretation of R as the ratio of scattering lengths does not hold.

The field variations are performed w.r.t. dimensionful renormalized fields ϕ_R, such that the effective bosons have a standard time evolution. This amounts to calculating the dimensionful renormalized four-boson vertex $2\bar{\lambda}_\phi/Z_\phi^2$ – the factor of 2 comes from our choice of truncation $U \ni \lambda_\phi/2(\phi^*\phi)^2, \lambda_\phi = \partial^2 U/\partial\rho\partial\rho$. The effective mass M_M of the molecules can be extracted from the gradient term in the bosonic propagator

[7],

$$\frac{\bar{P}_\phi}{Z_\phi} \ni \frac{\bar{A}_\phi}{Z_\phi} q^2 = A_\phi \frac{q^2}{2M} =: \frac{q^2}{2M_M}. \tag{7.58}$$

In sum we find for the molecular scattering length

$$a_M = \frac{M\bar{\lambda}_\phi}{4\pi Z_\phi^2 A_\phi}, \tag{7.59}$$

or, in dimensionless variables,

$$a_M \hat{k} = \frac{\lambda_\phi}{8\pi A_\phi}. \tag{7.60}$$

In order to calculate A_ϕ and λ_ϕ we consider the last two equations in (7.45). The flow for A_ϕ can be written as

$$\partial_{\tilde{\sigma}_c} A_\phi \;=\; \frac{h_\phi^2}{64\pi} \frac{1}{\tilde{s}^{3/2}} \, (1/2 - A_\phi) \tag{7.61}$$

and exhibits a fixed point at $A_\phi = 1/2$ – there is no deviation from the result obtained in our previous approach taking into account fermion diagrams only. Indeed there is no bosonic contribution to A_ϕ from boson fluctuations in vacuum. The numerical solution in the broad resonance limit shows that the fixed point is approached very quickly, cf. fig. 7.2 (c).

The equation for λ_ϕ is more involved. In this work we present the (trivial) numerical solution of the corresponding differential equation. We note, however, that finding the ratio a_M/a may alternatively be formulated as a fixed point problem in the RG framework. Finding the solution of a differential equation is then replaced by solving an algebraic equation. We will present this calculation elsewhere.

To analyze the flow of the four-boson coupling we define the function

$$R = \lim_{t \to -\infty} \frac{\lambda_\phi(t) \sqrt{e^t - \tilde{\sigma}_A}}{4\pi}. \tag{7.62}$$

On the BEC side of the resonance, $-\tilde{\sigma}_A = 1/c^2 > 0$ and for $t \to \infty$ we find with eq. (7.60) and the fixed point $A_\phi = 1/2$

$$R = \frac{\lambda_\phi}{4\pi c} = \frac{a_M}{a}. \tag{7.63}$$

[7] Alternatively, it can be obtained from the bosonic dispersion relation $\omega = q^2/(4M)$ (cf. eq. (5.67) and related comments). This procedure does not rely on an expansion in the external momentum q, but gives the same result.

The scaling behavior $a_M/a = 0.814$ in the BEC regime is clearly seen in fig. 7.1 (b), in particular in the inset where we focus on a more extended range of $c^{-1} = (a\hat{k})^{-1}$. Very close to the resonance, one observes deviations from this number. The interpretation of R as the ratio of scattering lengths can be extrapolated up to the resonance $c^{-1} = \sqrt{-\tilde{\sigma}_A} = 0_+$. One still observes a scaling behavior at resonance, indicated by the finite value of the ratio a_M/a, but instead of vanishing $\propto a$, a_M now *diverges* $\propto a^{-1}$ when approaching the strongly interacting region, terminating in $a_M/a = 1.542$ at $c^{-1} = 0$. On the BCS side, one has $\tilde{\sigma}_A = 0$ and R does no longer describe a ratio of scattering lengths. Instead, one observes an IR divergence of λ_ϕ for $t \to -\infty$ which is compensated by the exponential term in (7.62). For large $|c^{-1}|$, the bosonic contribution to the flow of λ_ϕ is suppressed since $m_\phi^2 > 0$ on the BCS side. The divergence of the four-boson coupling is now driven by the fermion loop, which is reflected by the fact that $R \to 2$ for $c^{-1} \to -\infty$, cf. eq. (7.55). Approaching the resonance, $R(t \to -\infty)$ remains continuous. In any case, a scaling behavior is expected since the fermionic scattering length is the only scale for the vacuum problem.

7.4 Many-body System in the BEC Regime

In the two-body limit we exclusively had to consider observables like the scattering length for fermions and molecules which are *local* in momentum space. This situation is different in the many-body context. Here we generically have to deal with a *nonlocal* observable, the particle density. More precisely, the connected two-point functions entering this quantity (cf. eq. (4.62)) involve traces of the full fermionic and bosonic propagators over frequency and momentum space. If the couplings entering these full propagators depend on the momentum scale in a substantial way, then the use of local couplings – taken e.g. in the infrared limit – might lead to quantitatively inaccurate results. As we have argued qualitatively in the context of Schwinger-Dyson equations in sect. 5.3, such a situation is met for the boson propagator. It is therefore desirable to resolve the momentum dependence of the couplings entering the full propagators. In the following we will demonstrate that this is feasible in the frame of functional renormalization group equations. Roughly speaking, the momentum dependence is translated to the scale dependence of the couplings in the flow equations. As an important conceptual result, in this way it is possible to reconcile the generic infrared freedom of bosonic $O(N)$ models in the symmetry broken regime [60] with the fact that remnants of interactions at higher momentum scales indeed manifest themselves e.g. through a condensate depletion at zero temperature – if the theory were completely free, no depletion could be observed ($\lambda_\phi = 0$ at all momentum scales). In this setting, we find a Bogoliubov-type theory at low temperature agreeing quantitatively with QMC simulations, while the phase transition at higher temperature is of second order.

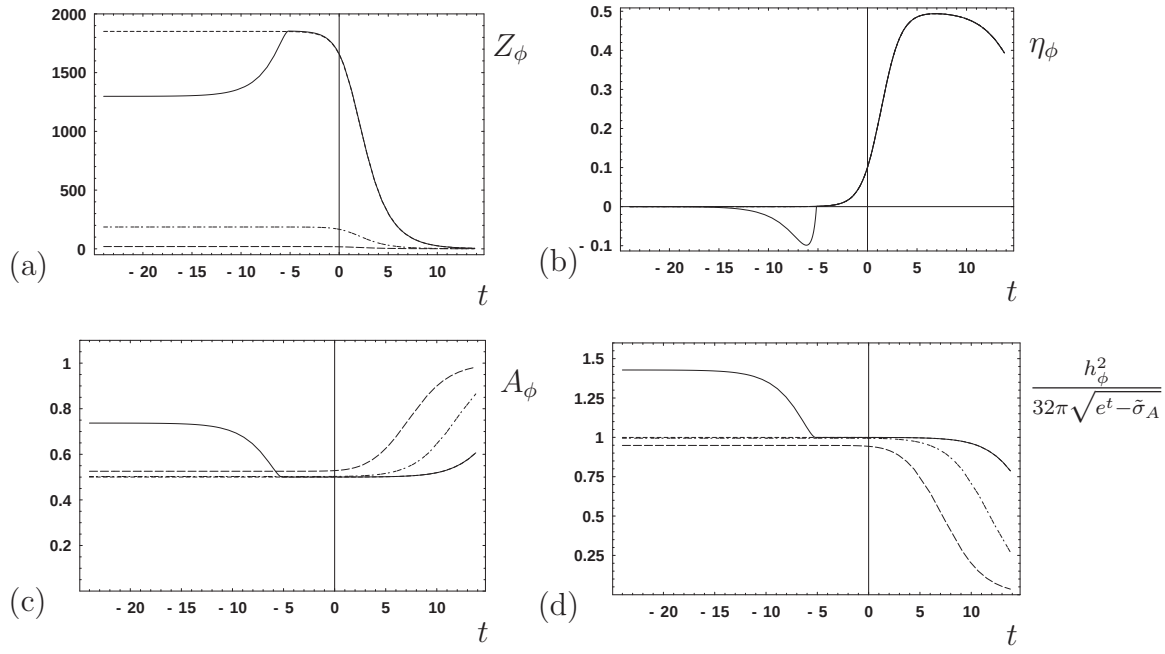

Figure 7.2: Upper Row: (a) Flow of the wave function renormalization Z_ϕ for different two-body values of $\tilde{h}_{\phi,0}$ ($\tilde{h}^2_{\phi,0} = 3.72 \cdot 10^5$ (dashed), $\tilde{h}^2_{\phi,0} = 3.72 \cdot 10^4$ (dashed-dotted) and $\tilde{h}^2_{\phi,0} = 3.72 \cdot 10^3$ (long dashed)). Z_ϕ involves $\tilde{h}_{\phi,0}$ directly, such that its final infrared value strongly depends on this scale. (b) Flow of the anomalous dimension $\eta_\phi = -\partial_t \log Z_\phi$. By its definition, η_ϕ is highly insensitive to $\tilde{h}_{\phi,0}$ and the plots for different values of $\tilde{h}_{\phi,0}$ coincide. The solid line again shows many-body effects in the SSB phase, respectively. Deviations from the two-body result which are driven by the bosonic loops $\propto \rho$ are observed. Lower row: The renormalization with Z_ϕ produces quantities which are insensitive to a variation of $\tilde{h}_{\phi,0}$, in accordance with our earlier findings (cf. chapt 6). This is manifest in the flow of the bosonic gradient coefficient A_ϕ (a) and the reduced Yukawa coupling (b). Only for the smallest value of $\tilde{h}_{\phi,0}$ a deviation from the broad resonance limit is visible for the renormalized gradient coefficient and reduced Yukawa coupling. The solid line represents again the flow in the many-body system (for $\tilde{h}^2_{\phi,0} = 3.72 \cdot 10^5$).

For this purpose we consider the BEC regime $-\tilde{\sigma}/\tilde{T} \gg 1$ in the broad resonance limit $\tilde{h}_\phi \to \infty$ and for $\lambda_\psi = 0$. As we have argued in chapt. 6 our approximation scheme is well under control in this regime and we can concentrate on the above aspects. In particular, the effects from mixed bubble diagrams renormalizing the fermion propagator as well as box diagrams which would require rebosonization [50] are exponentially suppressed for $-\tilde{\sigma}/\tilde{T} \gg 1$ – the large negative chemical potential in the fermion propagator acts to strongly suppress these diagrams. We can thus ignore

the flow of Z_ψ, A_ψ and possible modifications on the chemical potential appearing in the fermion propagator. Similarly, for a physical value $\lambda_\psi = 0$ in the two-body limit, the flow of λ_ψ is generated by mixed bubble diagrams only, which are exponentially small as well. This greatly simplifies the system of flow equations and we have a well-controlled truncation. The concrete truncation can be read off from (7.20, 7.21) with $Z_\psi = A_\psi = 1, \lambda_\psi = 0$ at all scales.

7.4.1 Regimes in the Renormalization Group Flow

In the last section we have solved the two-body problem with renormalization group equations. This allows us to fix the "microscopic" couplings for the many-body problem by an appropriate choice of the initial conditions for the flow equations. Two- and many-body problem are treated on completely equal footing in our framework. In the situation specified above, the only microscopic interaction scale is set by the scattering length a for the fermions. However, we can easily incorporate more microscopic information as discussed in the preceding section

We can identify three major regimes for the renormalization group flow.

Ultraviolet regime: Fixing initial conditions

The UV regime is characterized by the cutoff being much larger than all thermodynamic scales, $\sigma_c \gg \tilde{T}\hat{k}^2/(2M), \hat{k}^2/(2M)$ (we will discuss below how the fiducial $\hat{k}$ is related to the physical $k_F = (3\pi^2 n)^{1/3}$ in the many-body context; for the simple scale arguments presented here we can think of $\hat{k} \sim k_F$). Physically speaking, the fluctuations included by evolving the flow equations act on much smaller wave lengths than the size T^{-1} of the Matsubara torus or the typical interparticle spacing k_F^{-1}. It is therefore obvious that the thermodynamic scales "decouple" and the flow of the many-body system coincides with the one of the two-body system in this regime, which can be clearly seen in figs. 7.3, 7.2, 7.7. These plots nicely visualize our strategy to fix the two-body observables: In a first run we tune the initial conditions at the UV scale Λ to match the desired two-body low energy observables for the thermodynamic scales T, k_F switched off. We then reverse the flow and switch on the thermodynamic scales at the initial scale. In the next step we run the system down to the infrared again; for a long "renormalization group time" t the new trajectory coincides with the two-body trajectory, and only for a low cutoff the thermodynamics manifests itself by deviations of the couplings from the two-body results.

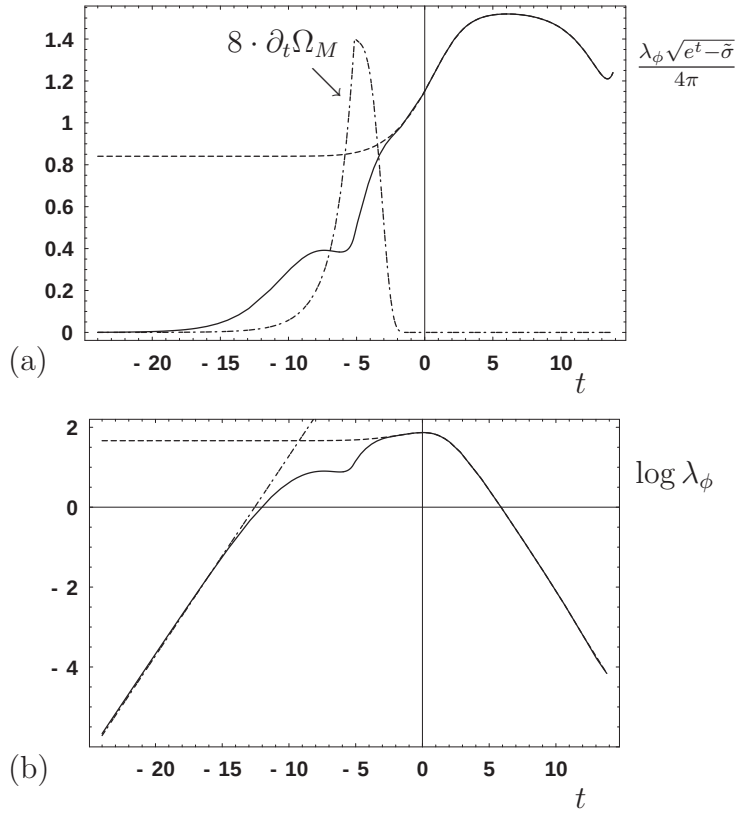

Figure 7.3: (a) Reduced four-boson coupling in the two-body limit and for the many-body situation. In the UV regime, both plots coincide. Deviations become visible in the thermodynamic regime starting at $t \sim -2$. The scale for spontaneous symmetry breaking is $t = -5.15$ – the value of the reduced bosonic scattering length is substantially below the two-body result. We also plot the flow of the connected bosonic density fraction (dashed-dotted), receiving its dominant contribution in the thermodynamic regime. This shows that a phenomenological Bogoliubov theory which uses the two-body result for λ_ϕ is quantitatively inaccurate away from zero temperature ($\tilde{T} = 0.15$ here), cf. also fig. 7.9. (b) Resolving the universal deep IR regime. Independently of the many-body scales the flow of the logarithm of the four-boson coupling converges to the dashed-dotted line parameterized by $t/2 + 2\pi$ in the symmetry-broken phase. The further parameters for this plot are $\tilde{\sigma} = -7.65, c^{-1} = 2.77, \Omega_C = 0.42, \Omega_M = 0.58, \Omega_F = 1.8 \cdot 10^{-4}$.

Thermodynamic regime: Many-body effects and spontaneous symmetry breaking

The thermodynamic regime is entered when the cutoff becomes comparable to the thermodynamic scales, $\sigma_c \approx \tilde{T}\hat{k}^2/(2M), \hat{k}^2/(2M)$. For some quantities, this leads to

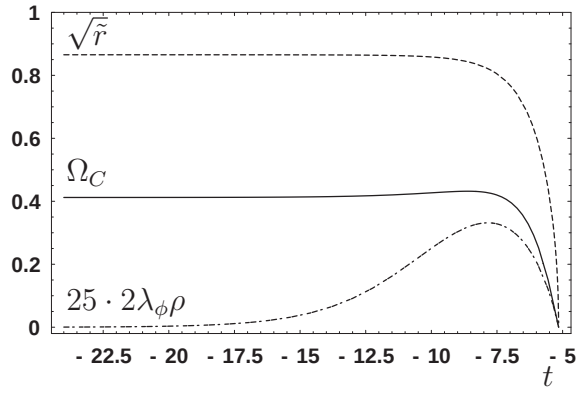

Figure 7.4: Solution of the flow for the three RG invariants involving the bosonic field expectation value ρ: Condensate fraction $\Omega_C(t)$ (solid; the condensate fraction can be read off in the IR, $\Omega_C = \Omega_C(-\infty) = 0.41$), fermionic mass gap $\tilde{r} = h_\phi^2 \rho$ and $2\lambda_\phi \rho$, giving rise to a radial mass for the bosons in the SSB phase. While the condensate and the fermion gap approach nonvanishing saturation values as expected in three spacelike dimensions, the bosonic radial mass term vanishes due to the IR freedom of the $O(2)$ theory.

substantial deviations from the two-body results even in the BEC regime, especially in the symmetry-broken phase. Approaching the resonance, many-body effects are expected to be even more pronounced. Subdividing this regime again, we observe that the flow is first generated by the fermionic diagrams. These saturate quickly to their final infrared values. In the following, the flow is dominated by bosonic diagrams – they are "initialized" by the fermion fluctuations. This nicely illustrates the generation of an effective bosonic theory from the renormalization group point of view.

In this regime we also deal with the phenomenon of spontaneous symmetry breaking, which is the most prominent many-body effect for our system and takes place at low enough temperature. Its onset is marked by the physical boson mass hitting zero at some finite cutoff scale, as will be made more precise below. A condensate forms, which is a local contribution to the equation of state. It quickly saturates to its final infrared value. This is quite different in two dimensions, where the Mermin-Wagner theorem [86] forbids long-range order associated to a broken continuous symmetry [8], such that spontaneous symmetry breaking can only be a finite size effect [87].

[8]The Kosterlitz-Thouless transition circumvents the Mermin-Wagner theorem in two dimensions.

Deep infrared sector: Universal behavior

Most of the couplings saturate to stable infrared values in the thermodynamic regime. There are, however, quantities which "never stop running" even for the cutoff scale $\sigma_c \ll T, \hat{k}^2/(2M)$. Prominent examples for such a situation are anomalous dimensions: Close to a second order phase transition, the massless mode causes the wave function renormalization to diverge in such a way that $\eta = -\lim_{t\to-\infty} \partial_t \log Z$ acquires a nonzero value [9]. We encounter a very similar effect for the "many-body four-boson coupling" λ_ϕ in the symmetry broken phase as visible in fig. 7.3 (b) where we show λ_ϕ in a double logarithmic plot. We can directly read off the scaling

$$\lim_{t\to-\infty} \partial_t \log \lambda_\phi = \frac{1}{2}. \tag{7.64}$$

It expresses the IR behavior $\lambda_\phi \propto 1/\sqrt{-\tilde{\sigma}_c}$ independent of temperature, density and coupling strength as we have verified numerically for several points in the $\tilde{T} - c^{-1}-$ plane in the BEC regime.

The sign of this quantity is opposite to the anomalous dimension – λ_ϕ is contracted to zero. This is the *infrared freedom* in the symmetry broken phase previously observed in relativistic bosonic $O(N)$ models [60; 61] and determined by the structure of the flow equation in this regime,

$$\partial_t \lambda_\phi = -\lambda_\phi^2 I(t, \lambda_\phi) \tag{7.65}$$

with a positive integral I which exhibits an IR divergence for $t \to -\infty, m_\phi^2 = 0$. However, the wave lengths of the fluctuations included by the renormalization group flow in this regime are much larger than the lengths set by thermodynamic scales as stated above. Similar to the UV regime, this leads to a decoupling from these scales, such that we approach indeed a universal domain in the sense of statistical mechanics, which has no memory of the precise thermodynamic scales and the two-body interaction strength.

We note that in presence of a trap, this deep infrared regime is never approached: The length scale set by the trap is comparable to those of temperature and particle density in a typical experimental setup, cf. tab. 2.1. Unlike temperature and particle density, it acts as quite a sharp infrared cutoff, since it eliminates the possibility of fluctuations on length scales larger than the trap size. It is hence questionable if critical behavior will be observable in trapped quantum gases in the future.

[9] We have not yet investigated this effect in detail for our model; in the $O(2)$ model in three dimensions, the anomalous dimension is known to be very small anyways ($\eta = 0.038$), cf. [60] and references therein.

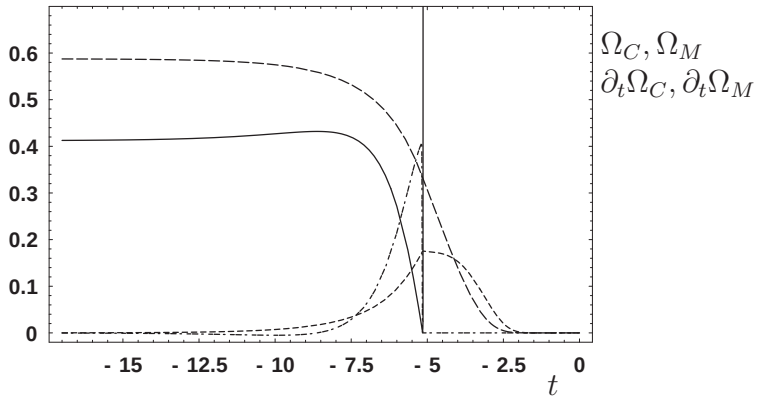

Figure 7.5: Flow and solution of the flow for the density fractions Ω_M, Ω_C ($\Omega_F = \mathcal{O}(10^{-4})$ in this regime). The scale for SSB at $t = 5.15$ is indicated by a vertical line. The legend is Ω_C – solid, Ω_M – long dashed, $\partial_t\Omega_C$ – dashed-dotted, $\partial_t\Omega_M$ – dashed. The contribution of Ω_F is negligible in the BEC regime ($\mathcal{O}(10^{-4})$) – Ω_M and Ω_C add up to one.

7.4.2 Reconstructing the Particle Density

The most severe complication in the many-body regime compared to the two-body limit is the intrinsic need to accurately determine the particle density $n = k_F^3/(3\pi^2)$ – eventually we want to provide dimensionless results which are all written in units of k_F or ϵ_F. The particle density is composed of the connected fermionic and bosonic two-point functions plus a disconnected bosonic part in the superfluid regime. Exact expressions for the two-point functions are given by the trace over the *full* propagators [10],

$$n_{F/\phi} = \mathrm{Tr}\ \mathcal{P}^{-1}_{F/\phi}(g_i(Q); Q) \tag{7.66}$$

where the trace runs over the discrete matrix entries and over momentum space. Consequently, in order to reconstruct these nonlocal observables, there is a need to resolve the momentum dependence of the couplings entering the propagators, here collectively denoted by $g_i(Q)$. As we have discussed in the context of Schwinger-Dyson equations in sect. 5.3, especially the effective, i.e. fluctuation induced bosonic couplings might exhibit a substantial momentum dependence. For example, it is obvious that the deep infrared value $\lambda_\phi = 0$ is not the right one to insert into the bosonic propagator. This is most clearly visible in fig. 7.3 where $\lambda_\phi(t)(\exp t - \tilde{\sigma})^{1/2}/(4\pi)$ ($\approx \lambda_\phi/(4\pi a)$ for $t \ll 0$ and in the BEC regime) and the flow of the connected bosonic density fraction $\partial_t\Omega_M(t)$ are plotted. Instead, the coupling at intermediate scales where $\partial_t\Omega_M(t)$ is peaked should be relevant. This picture strengthens the *ad*

[10] A zero point shift has to be subtracted, cf. sect. 4.2.3.

hoc procedure used in the Schwinger-Dyson framework in chapt. 5 where we employed the intermediate fermion-induced coupling $\lambda_\phi^{(F)}$, though the solution of the system of SDEs yielded the infrared value $\lambda_\phi = 0$. However, $\lambda_\phi^{(F)}$ includes only renormalization with fermion diagrams, while fig. 7.1 shows that there is a substantial effect from boson fluctuations in the BEC regime – $\lambda_\phi^{(F)}$ strongly overestimates the true four-boson coupling.

Both of the shortcomings of our earlier approach can be cured by a successive reconstruction of the connected particle density contributions from the flow equation. We obtain the connected part of the particle density (including the connected fermion and boson two-point function) from the full one-loop effective potential,

$$\Omega_{conn} = -\frac{\partial \tilde{u}_1}{\partial \tilde{\sigma}} = -\frac{\partial \tilde{u}_1^{(F)}}{\partial \tilde{\sigma}} - \frac{\partial \tilde{u}_1^{(B)}}{\partial \tilde{\sigma}} \tag{7.67}$$

where the partial derivative is taken w.r.t. to the *physical* chemical potential (and not the cutoff). Since in our truncation the fermion propagator is not modified by fluctuations, the derivative is carried out straightforwardly. For the bosonic contribution, we use a prescription analogous to eq. (4.82), generating the trace over the *dressed* boson propagator, i.e. the dressed connected boson density. Since we know the flow equation for the effective potential (7.18), the flow equation for the connected part of the particle density is directly available – our procedure is analogous to the strategy embarked on for obtaining the boson mass and the four-boson coupling, where we projected on the couplings using ρ-derivatives. The desired flow equation reads

$$\begin{aligned} \partial_t \Omega_{conn} &= -e^t \Big\{ \frac{1}{2\tilde{T}} \int_{\tilde{q}} \gamma_\phi^{-3} \big[\gamma_\phi \gamma^2 \cosh^{-2} \gamma_\phi + \beta^2 \tanh \gamma_\phi \big] \\ &\quad + \frac{1}{\tilde{T}} \int_{\tilde{q}} \alpha_\phi^{-3} \big[\alpha_\phi (\alpha + \kappa)^2 \sinh^{-2} \alpha_\phi + \kappa \coth \alpha_\phi \big] \Big\}, \end{aligned} \tag{7.68}$$

reducing in the symmetric phase to

$$\partial_t \Omega_{conn} = -e^t \Big\{ \frac{1}{2\tilde{T}} \int_{\tilde{q}} \cosh^{-2} \gamma + \frac{1}{\tilde{T}} \int_{\tilde{q}} \sinh^{-2} \alpha \Big\}. \tag{7.69}$$

These equations decouple from the remaining FRG equations – while they depend on the remaining set of flow equations, they do not feed back. In practice, one can even consider separate flow equations for n_F and n_M, since these contributions do not couple to each other. In this way, it is possible to differentiate between the fermion and the boson density contribution similar to the Schwinger-Dyson analysis, cf. fig. 4.1. Importantly, our prescription includes the effects of a scale dependence of the couplings via their implicit t-dependence. Associating the cutoff scale with momentum scales, we can interpret this procedure as resolving the momentum dependence

of the couplings – in each renormalization group step, the appropriate coupling is feeded into the respective density contributions. The importance of such an effect is clearly visible for the four-boson coupling entering the bosonic density fraction (cf. fig. 7.3 (a)): Naively inserting the deep infrared value $\lambda_\phi = 0$ would produce a quantitatively inaccurate result, since λ_ϕ differs substantially from zero in the thermodynamic regime where the bosonic two-point function picks up its dominant contribution. Finally, we note that the accuracy of such a procedure could be enhanced in the future by the use of a momentum dependent cutoff which additionally acts as a regulator for high momentum modes, since this achieves stronger locality of the flow in momentum space.

The flow of the disconnected (or "classical") part contributing to the particle density as a condensate in the superfluid phase does not appear in the one-loop flow equation for the effective average action (7.18). It would be present if we worked with the flow equation for $\hat{\Gamma}$, eq. (7.16). We obtain the total particle number by simply adding up the disconnected and connected contributions (the proper normalization is discussed below). This procedure is inspired by the fact that each of the contributions (also n_F and n_M separately) forms an RG invariant (invariant under the rescaling with the wave function renormalization factors; for the fermions, we have $Z_\psi = 1$ in the BEC regime). It differs from the derivation in chapt. 4 where we obtained the equation of state via a systematic expansion of the functional integral. In this scheme, the equation of state was composed of a mixture of bare and renormalized quantities (cf. eq. (4.66)). It could then be written in terms of RG invariants after appropriate manipulations (eqs. (4.74,4.75)), still leaving a certain degree of arbitrariness in the definition of the wave function renormalization. In the renormalization group framework, one works with renormalized quantities from the outset. However, our definition of the total particle number in the context of FRG equations has not yet been proven with the same rigor as its counterpart in sect. 4.2.2. A strong hint for the correctness of our procedure is provided by the observation that the dressed condensate acquires a substantial value in the BEC regime (cf. fig. 7.5) and has the correct characteristic temperature dependence of a Bose-Einstein condensate in the BEC regime (cf. fig. 7.9), while the dressed fermion density contribution is negligible (cf. fig. 7.5). This is very different from the approximation scheme advocated in sect. 4.2.2, where the dressed condensate was "hidden" in the fermionic mean field two-point function, cf. eq. (4.78). There, adding the dressed condensate to the equation of state would clearly result in a double counting. This would imply an incorrect result for the condensate fraction as a function of temperature. The result presented in fig. 7.9 thus strengthens the faith in our prescription.

There is presently still a weak point in our scheme which we do not want to hide. If we work with a scale dependent mass in eqs. (7.68,7.69), then the critical temperature for Bose-Einstein condensation is notoriously too low. This is even true in the limit $c^{-1} \to \infty$ where the critical temperature for the tightly bound mole-

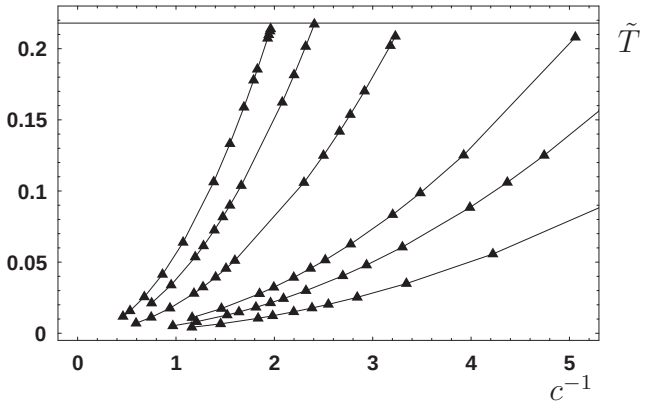

Figure 7.6: Scan of the parameter space performed so far. The critical temperature for Bose-Einstein condensation is plotted, $\tilde{T}_c^{BEC} = 0.218$. Our most accurate fine tuning (seven decimal digits; second trajectory from the left) allows to narrow the critical interval down to $\tilde{T}_c \in (0.217, 0.219)$.

cules should indeed take the value $\tilde{T}_c^{BEC} = 0.218$ characteristic for a free Bose gas. Technically, our problem is easily understood by noting that the connected bosonic contribution to the particle density is very sensitive to the value of the boson mass, $\sim \mathrm{Li}_{3/2}(e^{-m_\phi^2/\tilde{T}})$ (Li the polylogarithmic function). The mass is a relevant parameter according to naive power counting, exhibits a strong running in the infrared, cf. fig. 7.7, and is always positive during the flow for $T > T_c$. At T_c, it reaches zero only for $t \to -\infty$, i.e. it has positive values in the thermodynamic regime of the flow. Due to the high sensitivity of the boson density w.r.t the mass, we substantially underestimate $\tilde{T}_c$ in the naive procedure. Our *ad hoc* remedy to this problem is to put in front of the bosonic contribution in (7.68,7.69) a factor of

$$1 - \partial_{\tilde{\sigma}_c} m_\phi^2/2. \tag{7.70}$$

This effectively eliminates the memory of the mass term on higher cutoff scales in the bosonic contribution (similar to the removal of the cutoff itself for $\tilde{\sigma} \to 0$), such that only the infrared value of the mass term is relevant for the connected boson density. By this token, the theory is indeed effectively massless at all scales at the phase transition. In particular, this ensures the correct critical temperature in the deep BEC limit $c^{-1} \to \infty$. We stress that such a procedure can be omitted if one is not interested in the absolute value of k_F (or the particle density). For example, k_F-independent ratios (as displayed e.g. in fig. 7.8) can be computed without knowledge of k_F. Further, the system can be tuned to criticality without this information. On the other hand, in order to determine the correct dimensionless critical temperature, or the position of a certain observable in the phase diagram (cf. fig. 7.6) the value of k_F is needed.

Our procedure to reconstruct the particle density differs from the approach presented in [81] which advocates to keep the particle density fixed during the flow, adjusting the chemical potential accordingly. In our approach, the particle density, which comprises two-point correlations, builds up continuously during the flow. This seems to be more natural – at high cutoff scales the effective action reduces to the classical action containing no correlation effects. The two-point functions in question are exponentially suppressed for large values of the cutoff. Furthermore, the UV renormalization is done independently of the FRG analysis in [81] and restricted to a single parameter (the scattering length), very different from our approach.

7.4.3 Thermodynamic Observables in the BEC Regime

In this section we present the many-body results obtained so far in the frame of FRG equations. In particular, we focus on the condensate fraction as a benchmark for the quality of our approach.

Scanning the parameter space

Our practical procedure to compute thermodynamic observables in the crossover problem relies on the scaling form introduced in chapt. 3. Having fixed the microscopic physics in the way described above, we choose $c^{-1} = (a\hat{k})^{-1}$ and $\tilde{T} = 2MT/\hat{k}^2$ where $\hat{k}$ is an *a priori* arbitrary unit as in the two-body limit. A third quantity which has to be chosen to initialize the system of flow equations is the physical chemical potential $\tilde{\sigma} = 2M\sigma/\hat{k}^2$ appearing explicitly in the fermion propagator, which we have to distinguish from the flow variable $\tilde{\sigma}_c$. The fermion and boson propagator now feature scale dependent mass terms

$$P_F \ni -\tilde{\sigma} - \tilde{\sigma}_c, \quad P_\phi \ni m_\phi^2(\tilde{\sigma}, \tilde{\sigma}_c) - 2\tilde{\sigma}_c \tag{7.71}$$

where the mass terms couple to the renormalized fields [11].

Eventually we want to fix the particle number for the crossover problem. So far all quantities are measured in units of an arbitrary $\hat{k}$. It can be given a physical meaning by *requiring* a relation analogous to (4.74), defining the physical impact of $k_F = (3\pi^2 n)^{1/3}$ in the many-body context:

$$\Omega_{conn} + \Omega_C = \Omega_F + \Omega_M + \Omega_C \stackrel{!}{=} k_F^3 \tag{7.72}$$

where the density contributions are extracted from the $t \to -\infty$ limit of flow as described above. According to their canonical scaling behavior (cf. eq. (B.1)), we

[11] Due to $Z_\psi = 1$ in the BEC regime, the multiplicative renormalization of the fermion field is trivial.

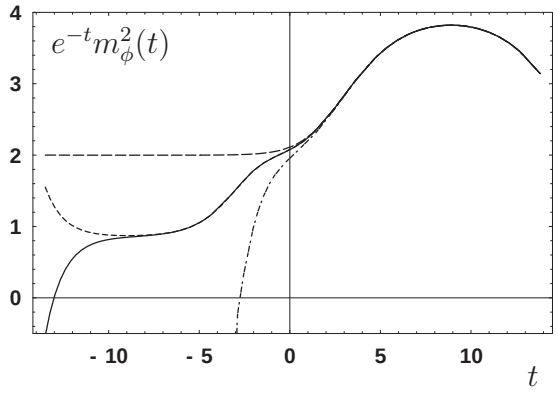

Figure 7.7: Fine tuning for the scaling form of the boson mass. In the UV regime, the flow of the mass is indistinguishable for all sets of initial values considered here. The highly nonlinear nature of the dependence on the initial conditions is only revealed in the IR. We compare two-body limit (long dashed) and many-body regime. The two-body limit is driven by the fermion loop only, and has the scaling $-m_\phi^2(\tilde{\sigma}_c)/\tilde{\sigma}_c = 2$ as expected (in order to produce the scaling behavior, a fine tuning in the 8th decimal digit is necessary). The many-body regime involves a bosonic contribution to the running of the mass. The two trajectories differ in the 7th digit and describe the system close criticality. The dashed line corresponds to the symmetric phase. The solid line ends in the symmetry-broken phase at small cutoff. Expressed in physical units we have $c^{-1} = 2.41, \tilde{T} = 0.217, \Omega_C = 6.8{\cdot}10^{-3}$ (solid) and $c^{-1} = 2.42, \tilde{T} = 0.219$ (dashed). The dashed-dotted line corresponds to a situation deeper in the SSB phase ($c^{-1} = 1.66, \tilde{T} = 0.10$).

can then rescale all observables with the absolute number obtained for k_F in order to arrive at the desired normalization in units of $k_F = (3\pi^2 n)^{1/3}$ and $\epsilon_F = k_F^2/(2M)$.

This procedure has an important technical advantage: we do not need any matching for the particle density in the infrared, which would necessitate to run the system several times in order to arrive at the intended density. Contact to the desired normalization of all quantities in units of k_F can be made by a simple rescaling of our input parameters.

Fig. 7.6 shows the scan of the phase diagram performed so far. Practically, we choose a certain combination $\tilde{T}, c^{-1}$ and vary the chemical potential $\tilde{\sigma}$. In the BEC regime a good initial guess for the chemical potential is $\tilde{\sigma} \approx -c^2$ which is exact in the two-body limit. We then write $\tilde{\sigma} = -c^2 + \delta\tilde{\sigma}$ and vary $\delta\tilde{\sigma} > 0$ to produce the trajectories in fig. 7.6.

In the BEC regime, we find that for a small positive $\delta\tilde{\sigma}_{crit}$ we can tune the system

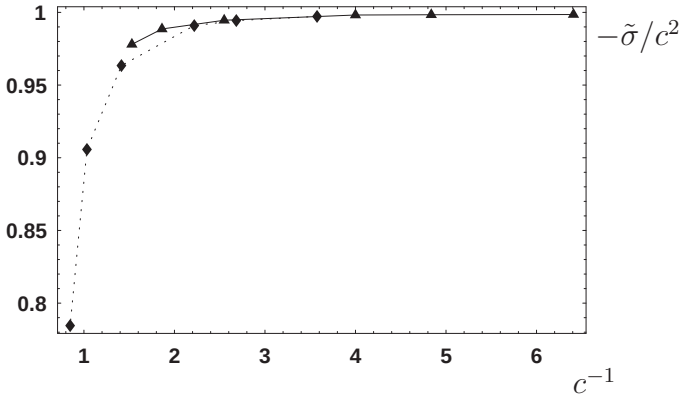

Figure 7.8: The reduced chemical potential $-\tilde{\sigma}/c^2 = -\sigma/a^2$ in the BEC regime for two different temperatures (solid: $\tilde{T} = 0.13$, dashed: $\tilde{T} = 0.04$). Deep in the BEC regime the two-body result $-\sigma/a^2 = 1$ is approached. For low temperatures and closer to the resonance, substantial deviations from this scaling behavior are observed.

to criticality, i.e.

$$\lim_{t\to-\infty} m_\phi^2(t) = 0_+. \tag{7.73}$$

Here we encounter the typical fine-tuning problems associated to a second order phase transition, which is reflected in fig. 7.7 where we choose two values of $\delta\tilde{\sigma}$ which differ in the seventh digit only. For values $\delta\tilde{\sigma} < \delta\tilde{\sigma}_{crit}$ the mass terms remains positive during the flow and we end up in the symmetric phase. For $\delta\tilde{\sigma} > \delta\tilde{\sigma}_{crit}$ the mass term m_ϕ^2 vanishes at a finite negative t_{SSB} and we use this as a criterion to enter the symmetry broken regime. Note that the full scale dependent mass term $m_\phi^2 + 2e^t$ is always positive, protecting the system from potential IR divergences. Below t_{SSB} we switch to a set of flow equations adapted to this phase, defined in eq. (7.36) *et sqq*, which is initialized by the values of the couplings at t_{SSB}. In particular, eq. (7.36) guarantees $m_\phi^2 = 0$ for $t < t_{SSB}$.

The values slightly above $\delta\tilde{\sigma}_{crit}$ correspond to the points close to the critical temperature for Bose-Einstein condensation, $\tilde{T}_c^{BEC} = 0.218$, and we can reproduce this result (using the prescription to deal with the mass term described above): The endpoints of the trajectories in fig. 7.6 thus map out the phase diagram. Our most precise fine-tuning up to seven decimal digits (second trajectory from the left) delimits the temperature interval including the critical temperature to $\tilde{T}_c \in (0.217, 0.219)$. This corresponds to the behavior of the mass in fig. 7.7. The small condensate fraction $\Omega_C = 6.8 \cdot 10^{-3}$ for the temperature slightly below T_c strongly suggests a second order phase transition. So far we do not find a shift in T_c away from the "critical" temperature of Bose-Einstein condensation in the noninteracting gas

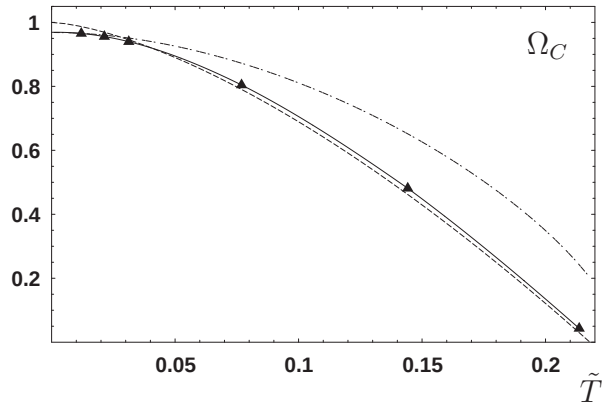

Figure 7.9: Condensate fraction as a function of temperature for $c^{-1} = 1.96$. We compare a free Bose gas (dashed), a Bogoliubov theory with phenomenologically inserted molecular scattering length $a_M = 0.6$, and the result of our RG calculation. For low temperature, we find excellent agreement with the Bogoliubov theory. Our results strongly suggest a second order phase transition (cf. the text also), while Bogoliubov theory becomes grossly inadequate in the vicinity of T_c. Our result for the condensate fraction is close to the free gas in this regime.

[12]. Such a shift ($\Delta T_c/T_c^{BEC} = \kappa a n^{1/3} = \kappa/(3\pi^2)^{1/3} c$, strictly valid for $0 < c \ll 1$) was found by Blaizot *et al.* [88]. Later they computed the coefficient $\kappa \approx 1.3$ with FRG methods, focusing on the resolution of the momentum dependence of the interaction [89–91]. Establishing this shift constitutes an interesting problem for future, more thorough investigations of the region close to T_c, but premises a better understanding of the correct treatment of the mass term.

The main results of this section are given in figs. 7.8, 7.9. They correspond to cuts in the phase diagram scanned in fig. 7.6. For fig. 7.8, we fix the temperature and study the behavior of the ratio $-\tilde{\sigma}/c^2 = -\sigma/a^2$. Deep in the BEC regime we observe the expected scaling of the chemical potential with the squared scattering length, expressed in the saturation of this ratio at 1. $\tilde{\sigma}$ is uniquely determined by the scattering length and its canonical scaling $\propto k_F^2$, with no implicit dependence on the thermodynamic scales k_F and $\tilde{T}$. To a very good approximation, σ behaves like the binding energy in vacuum in this regime. This is in line with our discussion of the BEC regime in sect. 6. In future work we shall investigate if tiny scaling deviations from $-\sigma/a^2 = 1$ due to the thermodynamic scales can be established. In contrast, coming closer to the resonance, the deviations from $-\sigma/a^2 = 1$ become more pronounced, in particular at low temperature.

In fig. 7.9 we fix the coupling strength at a moderate BEC value ($c^{-1} = 1.96$)

[12]Of course, there is no true phase transition in a free gas. In particular, all critical exponents are trivial.

and plot the condensate fraction as a function of temperature. At temperatures close to $\tilde{T}_c$, we find a second order phase transition as expected for an effective bosonic theory, while an effective Bogoliubov theory which artificially uses the correct two-body value for the bosonic scattering length $a_M = 0.6a$ yields a grossly inadequate result. The FRG formalism might cure our problems with a (presumably fake) first order phase transition which we encountered in the vicinity of the Feshbach resonance. The condensate fraction is close to the result for a free Bose gas, which is quite satisfactory at moderate interaction strength. For low temperatures we find excellent agreement with the effective Bogoliubov theory – this is the regime where the latter scheme is expected to be good. This demonstrates that our formalism indeed correctly resolves the scale or momentum dependence of the four-boson coupling as anticipated above (cf. also fig. 7.3). Though the infrared value of λ_ϕ is zero, the nonzero value of λ_ϕ on the relevant thermodynamic scales leads to a condensate depletion at low temperatures. This reconciles the generic infrared freedom of the effective bosonic theory in the superfluid phase for the BEC regime with the fact that remnants of interactions on higher momentum scales are still visible at low temperature as a condensate depletion.

Chapter 8

Conclusions and Outlook

The basic mechanism for the crossover from BCS-type to BEC-type physics can be understood by considering the frequency and momentum dependence of the effective four-fermion interaction – this gives a complementary view to the position space picture provided in the introduction. For small attractive interactions or $c^{-1} = (ak_F)^{-1} \to -\infty$ the BCS mechanism is operative: We deal with effective momentum independent or pointlike interactions, where the confinement of momenta to a narrow region in momentum space is due to the presence of a sharp Fermi surface at low temperature. The strong localization in momentum space translates to a highly delocalized situation in position space – this gives rise to the picture of Cooper pairs. Increasing the coupling or sending $c^{-1} \to 0$, fermionic fluctuations induce a shrinking of the Fermi surface. The frequency and momentum dependence of the effective interaction in the "Cooper channel" $\sim \psi\psi$ becomes less restricted. In our formalism, this is mirrored by the onset of an effective bosonic density adding to the fermionic two-point correlations – the effective bosonic two-point function counts frequency and momentum modes in the $\psi\psi$ channel. Indeed, in the crossover regime one deals with a mixture of the characteristics of fermionic and bosonic systems, reflected by the fact that both fermionic and effective bosonic correlations are of the same order of magnitude. Evolving further to the BEC regime $c^{-1} \to \infty$, the chemical potential becomes negative. The absence of a Fermi surface strongly suppresses fermionic correlations at low temperature, and there is no longer a restriction of the momentum dependence in this limit. Instead, controlled by the large negative value of the chemical potential, the effective interaction acquires a momentum structure which can be directly related to the emergence of an effective molecular propagator in our formalism. On the level of renormalization with fermion diagrams only, this effective propagator precisely exhibits the properties expected from simple symmetry considerations, as e.g. the double fermion mass and double scattering length. The delocalization in momentum space, in turn, translates to the existence of strongly localized bosonic molecules in position space. Indeed, the chemical potential can be

interpreted as the binding energy of a molecule in this regime.

Our functional integral approach for the effective action allows you to establish this picture in a direct way. It exhibits a high degree of analyticity and treats fermionic and bosonic fluctuations on equal footing. This is most obvious in the Bogoliubov approximation presented in chapt. 4, where the functional integral for both fermionic and bosonic fluctuations is solved in a two-step procedure at the one-loop level. This construction combines BCS theory for the fermions with a Bogoliubov-type approximation for the bosons, and forms the basis for the picture described above.

Besides the practical advantages, the effective action formalism allows you to fully exploit the presence of the global $U(1)$ symmetry. The equation of state for the particle number is obtained as the conserved Noether charge of the full nonrelativistic theory. The construction hinges on a systematic derivative expansion of the functional integral. The concept of dressed bosonic fields emerges naturally from this derivation. A reasonable approximation to this nonlocal object – it involves momentum space traces over the fermionic and effective bosonic propagators – is crucial for a description of crossover physics.

The thermodynamic phases can be classified by a symmetry consideration as well. While the thermodynamic equilibrium state exhibits the full symmetry of the effective action in the normal gas phase above T_c, it has a spontaneously broken $U(1)$ symmetry for $T < T_c$. The associated massless bosonic mode gives rise to superfluidity. An order parameter is provided by the dressed bosonic condensate which comprises both fermion-fermion correlations and the expectation value of classical bosons present in our two-channel model. This makes close contact to the description of Bose-Einstein condensates. Alternatively, one can use the concept of a fermionic mass gap for the whole range of interaction strengths, in analogy to BCS theory. Both quantities are proper renormalization group invariant observables. In our Yukawa formalism, both objects are intimately connected by the renormalized Feshbach coupling. This, together with the classification of the thermodynamic phases via a symmetry analysis, reveals the universality of the condensation phenomenon in a clear way, and underlines the fact that the transition from BCS to BEC is indeed a crossover and not a sharp phase transition.

Our functional approach to the crossover problem is highly scalable and opens the toolbox of many sophisticated techniques from quantum field theory and statistical mechanics. We go beyond the exactly solvable Bogoliubov approximation using suitable Schwinger-Dyson equations. This allows for a systematic inclusion of effective bosonic fluctuations beyond mean field and solves certain self-consistency problems. As a result, we find good agreement with Quantum Monte Carlo simulations for the gap parameter and the chemical potential at resonance and zero temperature. We compare our findings to recent experiments focusing on bare and dressed mole-

cule fields. Excellent quantitative agreement is found for the bare molecules, while dressed molecules show only qualitative consistency. Limitations of the Schwinger-Dyson approach mainly emerge in the superfluid phase close to the critical line. They can be traced back to an insufficient treatment of the momentum dependence of the effective interactions, together with the requirement to reconstruct a nonlocal observable, the particle density.

The physics extracted from the Yukawa model (3.1) exhibits several aspects of universality. The scaling form of the effective action is a first example, allowing for density independent calculations in the crossover. Further aspects are associated to the irrelevance of model parameters in different limiting cases. In detail, we establish an exact solution of the many-body problem in the limit of narrow resonances, physically equivalent to interactions with a large effective range. In the broad resonance limit, we demonstrate the equivalence of our model to a purely fermionic setting with pointlike interaction and no physical bosonic degrees of freedom on the microscopic level. We also discuss the BCS and BEC limits where the Feshbach coupling becomes irrelevant. From the point of view of field theory, both limits correspond to a "loss of memory" of field degrees of freedom – either the boson (BCS regime) or the fermion (BEC regime) degrees of freedom are irrelevant in the respective regions. Even in a situation where no microscopic degrees of freedom are present in the model, we obtain an effective Bogoliubov theory for composite bosons of double fermion mass in the BEC limit, as expected from a simple symmetry consideration. Besides this, we use the opportunity to discuss the validity of our approximations, and show how ordering principles emerge in our functional integral formalism in the various limits. As it is expected, the pointlike limit in the vicinity of a Feshbach resonance does not exhibit an obvious ordering principle.

In the view of a realistic description of concrete atomic systems as ^{6}Li or ^{40}K, the effective action approach proves to be useful. In one and the same framework, we can make contact to experimental observables by a prescription which projects the effective action on the physical vacuum, where the 1PI vertices encoded in this object can directly be interpreted as the amputated scattering functions. Physically, the procedure implies diluting the system by sending the mean interparticle spacing to infinity. As a byproduct, this projection provides an elegant UV renormalization procedure, trading the "bare" model parameters for the physical low energy vacuum observables. We further find that the crossover terminates in a sharp second order "phase transition" in the vacuum limit. In the view of realistic modelling of Feshbach resonances, so far we have considered a classical energy dependence of the interaction, an effective range and a pointlike background scattering, but in the future even more microphysical information can be systematically included if necessary.

Finally we provide the framework for an analysis of the crossover problem with functional renormalization group equations. In a first step we investigate the two-body limit where we can massively reduce the system of renormalization group

equations by a simple diagrammatic argument. We find a substantial improvement of the ratio of molecular vs. fermionic scattering length $a_M/a = 0.81$ in the BEC regime, and we find that this scaling coefficient is shifted to $a_M/a = 1.54$ in the unitary limit.

For the many-body problem we concentrate on the BEC regime where our truncation is quantitatively reliable. We achieve control over the whole regime of temperatures, including the low temperature phase where a condensate forms. Though still preliminary, our results are very promising. In particular, we can make progress in view of the proper determination of the particle density as a nonlocal observable by a successive reconstruction from the flow. Important from a technical point of view, this allows to reconcile the generic infrared freedom of bosonic $O(N)$ theories in the symmetry broken or superfluid phase with the fact that remnants of interactions are manifest e.g. through a condensate depletion at low temperature. As to the physical results, our approach shows the features characteristic of a Bogoliubov-type approximation at low temperatures, while yielding a second order phase transition at higher temperature.

The crossover problem still holds some challenges for future work. In particular, the strongly coupled regime close to unitarity lacks an obvious ordering principle for broad resonances. Close to the phase transition, the problem combines the difficulties of criticality with the need for an appropriate treatment of a microscopically massless bosonic theory strongly coupled to the fermions. This is mirrored by the discrepancy of our result for the critical temperature at unitarity and recent QMC calculations [68]. We might speculate that the relevant physics in this region could be captured by taking into account an effect analogous to Gorkov's famous improvement of BCS theory. A proper rebosonization program [50] could pave the way to achieve this task. In the BEC regime, an even more precise determination of the ratio a_M/a seems possible by the inclusion of additional boson-fermion and generalized Yukawa terms. Indeed there is a class of diagrams surviving the vacuum limit which we did not consider so far. Additional scaling relations could possibly be identified in the many-body context in the BEC regime. It will also be interesting to see to what extent the inclusion of further microphysical scales induces scaling violations which are visible in the macrophysics of atomic systems, in particular against the background of our universality hypothesis. It remains to be seen if future experiments will be able to resolve critical behavior in trapped quantum gases – the first steps for quantifying correlations have already been taken [92]. In this case a proper renormalization group treatment should allow for theoretical investigations.

Another aspect which has not yet been considered in much detail is the possibility to explore the macrophysics of condensates in cold atom gases beyond the Thomas-Fermi approximation with our formalism. If fluctuations are operative on much smaller length scales than the characteristic length scale of a trap – which should be true except very close to the phase transition – a scale separation argument

applies, allowing to solve the fluctuation problem in a homogeneous setup. The effect of a trap can then be incorporated in a straightforward manner by promoting the homogeneous (condensate) fields ϕ to dynamical fields $\phi(t, \vec{x})$. In a second step, one can solve the field equations obtained from the effective action in presence of a trap, which plays the role of a source term. In particular, nontrivial topological configurations such as vortices [93] could then be studied on a firm theoretical basis. This, in turn, underlines again the flexibility of the concept of the effective action, ranging from the description of two-body scattering processes to the solution of effective field equations analogous to Maxwell's theory of electromagnetism.

The theoretical framework developed in this thesis provides us with the means to attack different setups in cold atom physics as well. One example involves optical lattices: a cold gas is loaded in a trap where standing light waves induced by counter-propagating laser beams provide a lattice-like position space structure for the atoms [94–96]. This allows to implement a number of models proposed in the context of condensed matter physics, as e.g. the Hubbard model [97; 98] for both bosons and fermions, in cold atom systems [99; 100]. In this sense, cold atom physics can provide a testground for theoretical methods applied in condensed matter physics. The controlled microphysics makes the cold gases much cleaner than their condensed matter counterparts, where the microscopic physics is usually only poorly known. On the other hand, there are also obvious differences, such as the fact that a generic experimental setup for trapped gases works at a fixed particle number instead of a fixed chemical potential as usual in a condensed matter context. Here, the formalism developed in this work should prove useful.

Another upcoming area of both experimental and theoretical research are imbalanced fermion systems, i.e. mixtures of fermions with an unequal number of spin-up and spin-down constituents. This implies different chemical potentials for the two species, and a wealth of new interesting phenomena, as e.g. phase separation of the superfluid and normal gas component [101] or exotic forms of superfluidity [102–104]. Recent experimental progress for such systems [101; 105; 106] has already triggered a number of theoretical investigations [107–109; 109–111], but the picture is still inconclusive. Due to the different chemical potentials, Quantum Monte Carlo simulations are plagued with a severe sign problem, clearly necessitating the use of nonperturbative techniques beyond mean field theory in the strongly interacting regime.

Cold atom gases thus provide us with a remarkable wealth of possibilities for creating and manipulating intriguing physical situations. Due to the central role of Feshbach resonances, a quantitatively accurate theoretical understanding of the crossover problem seems to be at the heart of future progress in ultracold fermion physics. This, together with the fact that the microphysics of these systems is well-known, makes such systems prime candidates for both the test and further development of modern nonperturbative field theory techniques.

Appendix A

Basic Definitions for Scattering

In this section, we review some basic definitions of elastic scattering in the frame of quantum mechanics, and relate them to the objects that appear in quantum field theory. More complete compilations of definitions for scattering in quantum mechanics can be found in [41; 112]

We consider atoms of mass M interacting through a short-range potential in the center of mass frame (opposite momenta (or wave numbers) $\pm\vec{k}$ and total kinetic energy (or frequency) $\omega = \vec{k}^2/M$). The wave function for this system is stationary and depends on the interatomic distance vector $\vec{r}$. For $r \to \infty$, the wave function acquires the asymptotic form

$$\chi(\vec{r}) = e^{\mathrm{i}kz} + f_k(\theta)\frac{e^{\mathrm{i}kr}}{r}. \tag{A.1}$$

This defines the quantum mechanical (qm) *scattering amplitude* $f_k(\theta)$, which depends on the scattering angle θ and the wave number $k := \sqrt{2M\omega}$. We note that this word is often used in field theory for another object, related to the quantum mechanical scattering amplitude by a dimensionful factor, see below. For clarity we therefore add "qm" here. The *differential cross section* can be expressed in terms of the qm scattering amplitude as

$$\frac{d\sigma}{d\Omega} = |f_k(\theta) \pm f_k(\pi - \theta)|^2. \tag{A.2}$$

In order to compute the differential cross section for given qm scattering amplitude, one has to distinguish four cases: For distinguishable particles (irrespective if fermions or bosons), the second term has to be omitted. For spinless bosons (spin 1/2 fermions) the plus (minus) sign holds (irrespective if distinguishable or identical / polarized particles). These prescriptions arise from the fact that the statistics of the particles have to be introduced in quantum mechanics "by hand", via the (anti-)

symmetrization of the wave function. In quantum field theory, this is built in from the outset. The elastic cross section $\sigma(\omega)$ is obtained by

$$\sigma_{\rm dist}(\omega) = \int d\Omega \frac{d\sigma}{d\Omega}, \quad \sigma_{\rm id}(\omega) = \frac{1}{2}\int d\Omega \frac{d\sigma}{d\Omega}. \tag{A.3}$$

Here the convention is to integrate over half the solid angle for identical (irrespective if fermions or bosons), and over the full solid angle for distinguishable particles (irrespective if fermions or bosons). This is to avoid double counting of identical particles, whose scattering in the solid angle element around the scattering angle θ cannot be distinguished from a process in $\pi - \theta$. This is purely conventional and has to be considered when reconstructing the cross section from field theory.

The *scattering length* is defined as the zero energy (or momentum) limit of the qm scattering amplitude,

$$f_{k\to 0}(\theta) \to -a. \tag{A.4}$$

Scattering becomes isotropic in this limit. From this definition, it is obvious that the concept of the scattering length is directly meaningful in quantum mechanics only – it is extracted from $1/r$ decay of the wave function (A.1). Hence the relation to quantities accessible in field theory can merely be made by a sensible definition, see below. According to (A.3), one has

$$\sigma_{\rm dist}(\omega \to 0) = 4\pi a^2, \quad \sigma_{\rm id}(\omega \to 0) = 8\pi a^2. \tag{A.5}$$

Let us pause for a moment with our task of relating the scattering length to field theoretical quantities and briefly discuss how an energy dependence of scattering processes can be included in the quantum mechanical treatment. To organize the qm scattering amplitude, one expands e.g. in the complete set of eigenfunctions of definite angular momenta l (partial wave expansion), such that it takes the form

$$f_k(\theta) = \sum_{l=0}^{\infty} \frac{2l+1}{k\cot\delta_l(k) - {\rm i}k} P_l(\cos\theta), \tag{A.6}$$

where $\delta_l(k)$ are the *phase shifts* for the lth partial wave and P_l are the Legendre polynomials. For elastic scattering, the phase shifts are real valued. The cross section obtained in this way is

$$\sigma(\omega)_{\rm dist} = \frac{4\pi}{k^2}\sum_{\{l\}}(2l+1)\sin^2\delta_l(k), \quad \sigma(\omega)_{\rm id} = \frac{8\pi}{k^2}\sum_{\{l\}}(2l+1)\sin^2\delta_l(k). \tag{A.7}$$

For identical bosons (fermions), only even (odd) eigenvalues $l = 0, 2, 4, ...(1, 3, 5, ...)$ contribute to the cross section which is indicated by $\{l\}$. Specializing to short-range

interactions, one can compute the phase shifts in the low energy limit and finds $\delta_l(k \to 0) \propto k^{2l+1}$. This allows for a systematic expansion of the cross section in powers of k. As an important consequence, s – wave scattering ($l = 0$) dominates the low energy scattering, except for identical fermions where the p – wave ($l = 1$) dominates (starting at $\mathcal{O}(k^4)$ in the cross section). At low energies, the relevant expression involving the s – wave phase shift has an expansion

$$k \cot \delta_0(k) = -\frac{1}{a} + \frac{1}{2} r_s k^2 + ... \tag{A.8}$$

This is called the *effective range expansion*, with the *effective range* r_s. This number characterizes the lowest order momentum dependence of the scattering processes.

In the case of interactions with a long range part $\propto 1/r^n$ (e.g. van der Waals interactions, $n = 6$), the phase shifts do not scale like k^{2l+1}. The effective range expansion to the order written down in (A.8) is, however, still valid.

In the frame of quantum field theory, the basic object to describe scattering processes are the amputated Green's or 1PI vertex functions (cf. chapt. 4). A two-body scattering process is uniquely characterized by the off-shell four-point vertex. Putting all momenta on-shell and working in the cm frame, this object reduces to what is often called scattering amplitude $\mathcal{A}(\omega)$ in field theory. There is, however, a mismatch in definition with the qm scattering amplitude $f_k(\theta)$. $\mathcal{A}$ can be directly computed by appropriate derivatives of the effective action Γ w.r.t. the fields,

$$\mathcal{A}(\omega) = \Gamma^{(4)}\big|_{\text{on-shell,cm}}. \tag{A.9}$$

This object takes care of the statistics of the scattering particles, and of the their (in-) distinguishability (via the quantum numbers other than position carried by the field). Specializing to nonrelativistic field theory, the differential cross section reads in terms of $\mathcal{A}$ [113]

$$\frac{d\sigma}{d\Omega}(\omega) = \frac{M^2 |\mathcal{A}(\omega)|^2}{16\pi^2}. \tag{A.10}$$

In order to compute the total cross section, we apply the above conventions (A.3), such that

$$\begin{aligned} \sigma_{\text{dist}}(\omega) &= \int d\Omega \frac{d\sigma}{d\Omega}(\omega) \overset{\omega \to 0}{\longrightarrow} \frac{M^2 |\mathcal{A}(0)|^2}{4\pi}, \\ \sigma_{\text{id}}(\omega) &= \frac{1}{2} \int d\Omega \frac{d\sigma}{d\Omega}(\omega) \overset{\omega \to 0}{\longrightarrow} \frac{M^2 |\mathcal{A}(0)|^2}{8\pi}. \end{aligned} \tag{A.11}$$

As explained above, the relation to the scattering length can only be made by an appropriate definition. Using the quantum mechanical results for the cross section

(A.5), we can figure out the relation up to the sign. Further defining the sign of a by the sign of $\mathcal{A}$, we get

$$\begin{aligned} a &= \frac{M\mathcal{A}(0)}{8\pi} \quad \text{for identical particles,} \\ a &= \frac{M\mathcal{A}(0)}{4\pi} \quad \text{for distinguishable particles.} \end{aligned} \tag{A.12}$$

For this work, the first result is relevant for the scattering length of the composite spin 0 particles which emerge dynamically in the BEC regime, while the second one is relevant for the scattering length of the spin 1/2 fermions - they can be distinguished by their spin quantum number.

Appendix B

Dimensionful, Dimensionless and Renormalized Couplings

As argued in sects. 2.1,3.3, the Fermi momentum sets a natural scale for momenta in a thermodynamic situation. Hence it is favorable to measure momenta in units of the Fermi momentum $k_F = (3\pi^2 n)^{1/3}$ and energies in units of the Fermi energy $\epsilon_F = k_F^2/2M$. This fixes the canonical scaling behavior of all couplings and fields. We display the relations between dimensionless (with a tilde) and dimensionful (with a bar for the couplings, without modification for momenta and energies) units ($\epsilon_q = q^2/(2M), \epsilon_F = k_F^2/(2M)$),

$$\begin{aligned} \tilde{q}^2 &= q^2/k_F^2 = \epsilon_q/\epsilon_F, \quad \tilde{T} = T/\epsilon_F, \quad \tilde{\rho} = \bar{\rho}/k_F^3, \\ \tilde{A}_\psi &= 2M\bar{A}_\psi, \quad \tilde{\sigma} = \sigma/\epsilon_F, \quad \tilde{h}_\phi = 2M\bar{h}_\phi/k_F^{1/2}, \quad \tilde{\lambda}_\psi = 2Mk_F\bar{\lambda}_\psi, \\ \tilde{A}_\phi &= 2M\bar{A}_\phi, \quad \tilde{m}_\phi^2 = \bar{m}_\phi^2/\epsilon_F, \quad \tilde{\lambda}_\phi = 2Mk_F\bar{\lambda}_\phi. \end{aligned} \tag{B.1}$$

The quantities h_σ and Z_ψ, Z_ϕ are left unchanged, they scale $\propto k_F^0$.

Further we display the relation between "renormalized" (i.e., rescaled with the appropriate power of the wave function renormalization) and "bare" dimensionless quantities. The wave function renormalizations (WFRs) Z_ψ, Z_ϕ are defined as the coefficients of the time derivative operator in the effective action,

$$\Gamma \ni \int_Q \bar{\psi}^\dagger(Q) Z_\psi \mathrm{i}\omega_F \bar{\psi}(Q), \qquad \int_Q \bar{\phi}^*(Q) Z_\phi \mathrm{i}\omega_\phi \bar{\phi}(Q). \tag{B.2}$$

We compute the WFRs in a derivative expansion in momentum space from

$$\begin{aligned} Z_\psi \cdot \mathbf{1}_{2\times 2} &= \mathrm{Im} \frac{\partial}{\partial\omega} \frac{\overrightarrow{\delta}}{\delta\bar{\psi}^\dagger(Q)} \Gamma \frac{\overleftarrow{\delta}}{\delta\bar{\psi}(Q)}\Big|_{\omega=\vec{q}=0}, \\ Z_\phi &= \mathrm{Im} \frac{\partial}{\partial\omega} \frac{\overrightarrow{\delta}}{\delta\bar{\phi}^*(Q)} \Gamma \frac{\overleftarrow{\delta}}{\delta\bar{\phi}(Q)}\Big|_{\omega=\vec{q}=0}. \end{aligned} \tag{B.3}$$

The fermionic WFR is diagonal in spinor space. We can absorb the wave function renormalizations by rescaling the fields according to

$$\bar{\psi} \to \psi = \sqrt{Z_\psi}\bar{\psi}, \qquad \bar{\phi} \to \phi = \sqrt{Z_\phi}\bar{\phi}. \tag{B.4}$$

We call the fields before the rescaling (with a bar) "bare" and the rescaled fields "renormalized". If we rotate back to Minkowski space, our rescaling induces a standard time evolution for the renormalized fields.

The effective action must be invariant under such a rescaling and we conclude the following transformation laws for the various couplings, defining the "renormalized couplings". First we note that obviously under a rescaling with the WFRs

$$Z_\psi \to 1, \quad , Z_\phi \to 1. \tag{B.5}$$

The other couplings transform as

$$\begin{aligned} A_\psi &= \tilde{A}_\psi/Z_\psi, \quad h_\phi^2\rho = \tilde{h}_\phi^2\tilde{\rho}/Z_\psi, \quad \lambda_\psi = \tilde{\lambda}_\psi/Z_\psi^2 \\ A_\phi &= \tilde{A}_\phi/Z_\phi, \quad m_\phi^2 = \tilde{m}_\phi^2/Z_\phi, \quad \lambda_\phi\rho = \tilde{\lambda}_\phi\tilde{\rho}/Z_\phi. \end{aligned} \tag{B.6}$$

The current $\tilde{\sigma}$ is left untouched under the Z_ϕ, Z_ψ rescaling. From the last formula we can read off

$$h_\phi = \tilde{h}_\phi/(Z_\phi Z_\psi^2)^{1/2}, \quad \lambda_\phi = \tilde{\lambda}_\phi/Z_\psi^2, \quad \rho = Z_\phi\tilde{\rho}. \tag{B.7}$$

Two particularly important invariants under the rescaling transformation $\mathcal{Z}$ (cf. chapt. 4.2.2) are the absolute square of the renormalized boson field (condensate) and the fermion gap,

$$\rho = Z_\phi\tilde{\rho}, \quad , \tilde{r} = \tilde{h}_\phi^2\tilde{\rho}. \tag{B.8}$$

Appendix C

Computation of the 1 PI Vertex Functions

In this section present a way to systematically compute the loop corrections for the coefficients of the effective action. This is particularly important for the coefficients which cannot be deduced from the effective potential. These are all couplings in the effective action involving frequency or momentum dependencies, or external fermion fields. We work with renormalized, dimensionless fields and couplings. For the momentum variables, we omit the tilde's in this section in order not to overcharge the notation.

We introduce a generalized field and its transposed by

$$\hat{\chi}(X) = \begin{pmatrix} \hat{\phi} \\ \hat{\phi}^* \\ \hat{\psi} \\ \hat{\psi}^* \end{pmatrix}(X), \qquad \hat{\chi}^T(X) = \big(\hat{\phi}, \hat{\phi}^*, \hat{\psi}^T, \hat{\psi}^\dagger\big)(X). \tag{C.1}$$

Here $\hat{\phi}, \hat{\phi}^*$ and $\hat{\psi}, \hat{\psi}^*$ are considered as independent field variables. Hence $\hat{\chi}, \hat{\chi}^T$ carry the same information. Sticking to the convention for the Fourier transform (3.4), $\hat{\chi}(X) = \int_Q \exp(\mathrm{i}QX)\hat{\chi}(Q)$ we now find for the components

$$\hat{\chi}(Q) = \begin{pmatrix} \hat{\phi}(Q) \\ \hat{\phi}^*(-Q) \\ \hat{\psi}(Q) \\ \hat{\psi}^*(-Q) \end{pmatrix}, \qquad \hat{\chi}^T(-Q) = \big(\hat{\phi}(-Q), \hat{\phi}^*(Q), \psi^T(-Q), \psi^\dagger(Q)\big). \tag{C.2}$$

The minus sign in $\hat{\chi}^T(-Q)$ is introduced by hand to get the correct momentum structure of the bilinears. These conventions have been introduced in [50], where the case of real fields is also treated.

The fluctuation matrix is defined as

$$\Gamma^{(2)}(Q_1,Q_2)=\frac{\overrightarrow{\delta}}{\delta\chi^T(-Q_1)}\Gamma\frac{\overleftarrow{\delta}}{\delta\chi(Q_2)}. \tag{C.3}$$

We write the fluctuation matrix as

$$\Gamma^{(2)}=\mathcal{P}+\mathcal{F} \tag{C.4}$$

with $\mathcal{F}$ the part that depends on the fluctuating fields, while $\mathcal{P}$ contains the inverse propagators including background fields. The decomposition is implemented by inserting the ansatz

$$\hat{\chi}(Q)=\chi\delta(Q)+\delta\hat{\chi}(Q) \tag{C.5}$$

with a homogenous background value χ ($\psi=0$ for fermions) and a fluctuating part $\delta\chi(Q)$ that still contains an arbitrary momentum dependence. $\mathcal{P}(Q_1,Q_2)=P(Q_1)\delta(Q_1-Q_2)$ is then diagonal in momentum space, block diagonal in its discrete index structure and hence easily invertible. This yields

$$\mathcal{P}(Q_1,Q_2) = \begin{pmatrix} \mathcal{P}_\phi(Q_1) & 0 \\ 0 & \mathcal{P}_{F,\alpha\beta}(Q_1) \end{pmatrix}\delta(Q_1-Q_2). \tag{C.6}$$

It is inverted by inverting the submatrices. These submatrices and their inverses read

$$\begin{aligned} \mathcal{P}_{F,\alpha\beta}(Q_1) &= \begin{pmatrix} -\epsilon_{\alpha\beta}h_\phi\phi^* & -\delta_{\alpha\beta}P_F(-Q_1) \\ \delta_{\alpha\beta}P_F(Q_1) & \epsilon_{\alpha\beta}h_\phi\phi \end{pmatrix}, \\ \mathcal{P}^{-1}_{F,\alpha\beta}(Q_1) &= \frac{1}{P_F^{|2|}(Q_1)}\begin{pmatrix} \epsilon_{\alpha\beta}h_\phi\phi & \delta_{\alpha\beta}P_F(-Q_1) \\ -\delta_{\alpha\beta}P_F(Q_1) & -\epsilon_{\alpha\beta}h_\phi\phi^* \end{pmatrix}, \end{aligned} \tag{C.7}$$

with

$$\begin{aligned} P_F(Q) &= \mathrm{i}\,\omega_F+A_\psi q^2-\sigma=\mathrm{i}\,\omega_F+f_1, \\ P_F^{|2|}(Q) &= P_F(-Q)P_F(Q)+h_\phi^2\rho=\omega_F^2+F_1^2,\quad F_1^2=f_1^2+h_\phi^2\rho. \end{aligned} \tag{C.8}$$

(The fermionic Matsubara frequencies are given by $\omega_F=(2n+1)\pi T$ and we abbreviate $\rho=\phi^*\phi$.) These functions have the obvious properties

$$\begin{aligned} P_F(-\omega,\vec{q}) &= P_F^*(\omega,\vec{q}),\quad P_F(\omega,-\vec{q})=P_F(\omega,\vec{q}), \\ P_F^{|2|}(-Q) &= P_F^{|2|}(Q). \end{aligned} \tag{C.9}$$

The relation between bare dimensionful and renormalized dimensionless fermion propagator reads

$$\mathcal{P}_F=(Z_\psi\epsilon_F)^{-1}\bar{\mathcal{P}}_F. \tag{C.10}$$

In the symmetric phase (SYM, $\phi = \phi^* = 0$) the matrix is purely off-diagonal.

Similarly, the inverse boson propagator can be written as

$$\begin{aligned} \mathcal{P}_\phi(Q_1) &= \begin{pmatrix} \lambda_\phi \phi^* \phi^* & P_\phi(-Q_1) \\ P_\phi(Q_1) & \lambda_\phi \phi\phi \end{pmatrix}, \\ \mathcal{P}_\phi^{-1}(Q_1) &= \frac{1}{P_\phi^{|2|}(Q_1)} \begin{pmatrix} -\lambda_\phi \phi\phi & P_\phi(-Q_1) \\ P_\phi(Q_1) & -\lambda_\phi \phi^* \phi^* \end{pmatrix} \end{aligned} \tag{C.11}$$

with

$$\begin{aligned} P_\phi(Q) &= \mathrm{i}\omega_\phi + A_\phi q^2 + m_\phi^2 + \lambda_\phi \rho = \mathrm{i}\,\omega_\phi + f_2, \\ P_\phi^{|2|}(Q) &= P_\phi(-Q) P_\phi(Q) - (\lambda\rho)^2 = \omega_\phi^2 + F_2^2, \quad F_2^2 = f_2^2 - (\lambda\rho)^2 \geq 0. \end{aligned} \tag{C.12}$$

(The bosonic Matsubara frequencies are given by $\omega_\phi = 2n\pi T$.) These functions have the obvious properties

$$\begin{aligned} P_\phi(-\omega, \vec{q}) &= P_\phi^*(\omega, \vec{q}), \quad P_\phi(\omega, -\vec{q}) = P_\phi(\omega, \vec{q}), \\ P_\phi^{|2|}(-Q) &= P_\phi^{|2|}(Q). \end{aligned} \tag{C.13}$$

The relation between bare dimensionful and renormalized dimensionless boson propagator reads

$$\mathcal{P}_\phi = (Z_\phi \epsilon_F)^{-1} \bar{\mathcal{P}}_\phi. \tag{C.14}$$

The mass matrix for the bosons is degenerate and purely off-diagonal in SYM. In SSB, we have $\rho \neq 0$ and Goldstone's theorem dictates $m_\phi^2 = 0$. "Off-diagonalization" [1] yields the eigenvalues $(2\lambda\rho, 0)$ – the zero eigenvalue signals the Goldstone mode characteristic for superfluidity. (This of course also holds in an extended truncation with higher order ϕ – terms.) We refer to sect. D.4.2 for a detailed discussion of the boson propagator. For practical purposes it is useful to implement the transition from SSB to SYM by $F_i \to f_i, \phi = \phi^* = 0$.

We further decompose the fluctuation part according to the field contents [2]:

$$\begin{aligned} \mathcal{F}(Q_1, Q_2) &= \bar{F}^\phi(Q_1, Q_2) + \bar{F}^{\phi^*}(Q_1, Q_2) \\ &\quad + \bar{F}^\psi(Q_1, Q_2) + \bar{F}^{\psi^\dagger}(Q_1, Q_2) \\ &\quad + \bar{G}^{\phi^*\phi}(Q_1, Q_2) + \bar{G}^{\phi^*\phi^*}(Q_1, Q_2) + \bar{G}^{\phi\phi}(Q_1, Q_2) \\ &\quad + \bar{G}^{\psi^\dagger\psi}(Q_1, Q_2) + \bar{G}^{\psi^\dagger\psi^\dagger}(Q_1, Q_2) + \bar{G}^{\psi\psi}(Q_1, Q_2) \\ &= F^\phi \delta\phi(Q_1 - Q_2) + F^{\phi^*} \delta\phi^*(-(Q_1 - Q_2)) \end{aligned}$$

[1] Conventions could also be chosen such that a diagonalization procedure has to be implemented.

[2] The bars here have nothing to do with the notation for the bare fields and couplings.

$$
\begin{aligned}
&+F^{\psi}_{\alpha}\delta\psi_{\alpha}(Q_1-Q_2)+F^{\psi^\dagger}_{\alpha}\delta\psi^\dagger_{\alpha}(-(Q_1-Q_2))\\
&+G^{\phi^*\phi}\int\limits_{Q}\delta\phi^*(Q)\delta\phi(Q+(Q_1-Q_2))\\
&+G^{\phi^*\phi^*}\int\limits_{Q}\delta\phi^*(Q)\delta\phi^*(-Q-(Q_1-Q_2))\\
&+G^{\phi\phi}\int\limits_{Q}\delta\phi(Q)\delta\phi(-Q+(Q_1-Q_2))\\
&+G^{\psi^\dagger\psi}_{\alpha\beta}\int\limits_{Q}\delta\psi^\dagger_{\alpha}(Q)\delta\psi_{\beta}(Q+(Q_1-Q_2))\\
&+G^{\psi^\dagger\psi^\dagger}_{\alpha\beta}\int\limits_{Q}\delta\psi^\dagger_{\alpha}(Q)\delta\psi^\dagger_{\beta}(-Q-(Q_1-Q_2))\\
&+G^{\psi\psi}_{\alpha\beta}\int\limits_{Q}\delta\psi_{\alpha}(Q)\delta\psi_{\beta}(-Q+(Q_1-Q_2))
\end{aligned}
\tag{C.15}
$$

In the second line, the momentum dependence is separated from the discrete index structure. We find explicitly:

$$
\begin{aligned}
F^{\phi} &= \begin{pmatrix} 0 & 2\lambda_\phi\phi^* & 0 & 0\\ 2\lambda_\phi\phi^* & 2\lambda_\phi\phi & 0 & 0\\ 0 & 0 & 0 & 0\\ 0 & 0 & 0 & h_\phi\epsilon_{\kappa\rho}\end{pmatrix},\\
F^{\phi^*} &= \begin{pmatrix} 2\lambda_\phi\phi^* & 2\lambda_\phi\phi & 0 & 0\\ 2\lambda_\phi\phi & 0 & 0 & 0\\ 0 & 0 & -h_\phi\epsilon_{\kappa\rho} & 0\\ 0 & 0 & 0 & 0\end{pmatrix},\\
F^{\psi}_{\alpha} &= \begin{pmatrix} 0 & 0 & 0 & 0\\ 0 & 0 & -h_\phi\epsilon_{\alpha\kappa} & 0\\ 0 & h_\phi\epsilon_{\alpha\rho} & 0 & 0\\ 0 & 0 & 0 & 0\end{pmatrix},\\
F^{\psi^*}_{\alpha} &= \begin{pmatrix} 0 & 0 & 0 & h_\phi\epsilon_{\alpha\kappa}\\ 0 & 0 & 0 & 0\\ 0 & 0 & 0 & 0\\ -h_\phi\epsilon_{\alpha\rho} & 0 & 0 & 0\end{pmatrix}.
\end{aligned}
\tag{C.16}
$$

The bosonic G matrices have nonzero entries only in the 2×2 ϕ – sector. We only display these blocks:

$$
G^{\phi^*\phi}\ni\begin{pmatrix} 0 & 2\lambda_\phi\\ 2\lambda_\phi & 0\end{pmatrix},\quad G^{\phi^*\phi^*}\ni\begin{pmatrix} \lambda_\phi & 0\\ 0 & 0\end{pmatrix},\quad G^{\phi\phi}\ni\begin{pmatrix} 0 & 0\\ 0 & \lambda_\phi\end{pmatrix}.
\tag{C.17}
$$

The fermionic G matrices have nonzero entries only in the 4×4 ψ – sector. We only display these blocks (mind the position of the indices in the first matrix!):

$$\begin{aligned} G^{\psi^\dagger\psi}_{\alpha\beta} &\ni \begin{pmatrix} 0 & \lambda_\psi(\delta_{\gamma\alpha}\delta_{\delta\beta} - \delta_{\gamma\delta}\delta_{\alpha\beta}) \\ -\lambda_\psi(\delta_{\alpha\delta}\delta_{\gamma\beta} - \delta_{\gamma\delta}\delta_{\alpha\beta}) & 0 \end{pmatrix}, \qquad \text{(C.18)} \\ G^{\psi^\dagger\psi^\dagger}_{\alpha\beta} &\ni \begin{pmatrix} -\lambda_\psi\delta_{\gamma\alpha}\delta_{\delta\beta} & 0 \\ 0 & 0 \end{pmatrix}, \quad G^{\psi\psi}_{\alpha\beta} \ni \begin{pmatrix} 0 & 0 \\ 0 & -\lambda_\psi\delta_{\gamma\alpha}\delta_{\delta\beta} \end{pmatrix}. \end{aligned}$$

We further define the matrices

$$\begin{aligned} \bar{N}^\chi(Q_1, Q_2) &= \mathcal{P}^{-1}(Q_1)\bar{F}^\chi(Q_1, Q_2), \qquad \text{(C.19)} \\ N^\chi(Q_1) &= \mathcal{P}^{-1}(Q_1)F^\chi, \\ \bar{M}^{\phi^{(*)}\phi^{(*)}}(Q_1, Q_2) &= \mathcal{P}^{-1}(Q_1)\bar{G}^{\phi^{(*)}\phi^{(*)}}(Q_1, Q_2), \qquad \text{(C.20)} \\ M^{\phi^{(*)}\phi^{(*)}}(Q_1) &= \mathcal{P}^{-1}(Q_1)G^{\phi^{(*)}\phi^{(*)}}. \end{aligned}$$

and analogous for $\bar{M}^{\psi^{(\dagger)}\psi^{(\dagger)}}_{\alpha\beta}$. The matrices with bars are supermatrices while those without are not. The supermatrices are constructed in order to properly account for the Grassmann nature of the fermion fields. Most importantly, an appropriately defined "supertrace" (STr) accounts for the relative minus sign for the traces over the purely fermionic (FF) and the purely bosonic (BB) blocks in the supermatrices,

$$\mathrm{STr}A = \mathrm{Tr}A_{BB} - \mathrm{Tr}A_{FF}. \qquad \text{(C.21)}$$

Supertrace and "superdeterminant" (Sdet) obey the usual rules for trace and determinant manipulation (cyclicity under the supertrace, product rule for the superdeterminant etc.). For the detailed manipulation rules of supermatrices, see the appendix of [49].

With these preparations we can compute the necessary supertraces running over products of the supermatrices. The following expressions always include the prefactors from the log expansion, and we use a sum convention for repeated discrete indices. The matrix multiplication for the ordinary matrices N^χ is understood; note that they cannot be manipulated according to the rules for STr; str just runs over the discrete indices, accounting for the appropriate overall sign for the fermion sector and is not a supertrace in the above sense. In the following, we first display the general formulae in terms of the supermatrices. Then, we rearrange the indices in such a way that we get an explicit representation in terms of traces over the fields.

Fermion Propagator

We consider the one-loop corrections to the off-diagonal components of the fermion propagator (cf. eq. (C.7)). This part involves the momentum dependence from which

we can extract the kinetic coefficients Z_ψ, A_ψ.

$$
\begin{aligned}
&\int_K \delta\psi^\dagger(K)\Delta P_F(K)\delta\psi(K) \qquad\qquad (C.22)\\
&= -\frac{1}{2}\mathrm{STr}\big[\bar{N}^{\psi^\dagger}\bar{N}^{\psi} - \bar{M}^{\psi^\dagger\psi}\big]\\
&= -\frac{1}{2}\int_K \delta\psi^\dagger_\alpha(K)\big\{\mathrm{str}\int_Q N^{\psi^\dagger}_\alpha(Q)N^{\psi}_\beta(Q+K) - M^{\psi^\dagger\psi}_{\alpha\beta}(Q)\big\}\delta\psi_\beta(K)\\
&= \int_K \delta\psi^\dagger_\alpha(K)\delta\psi_\beta(K)\big\{\int_Q \Big[\frac{h_\phi^2}{2}\Big(\frac{P_\phi(-Q-K)P_F(-Q)}{P_\phi^{|2|}(Q+K)P_F^{|2|}(Q)} + \frac{P_\phi(Q)P_F(Q+K)}{P_\phi^{|2|}(Q)P_F^{|2|}(Q+K)}\Big)\\
&\quad -\frac{\lambda_\psi}{2}\frac{P_F(Q)+P_F(-Q)}{P_F^{|2|}(Q)}\Big]\delta_{\alpha\beta}\big\}.
\end{aligned}
$$

The term $\propto \lambda_\psi$ is momentum independent, representing a tadpole graph. We stress that for diagrams involving both internal fermion and boson lines, on must be very careful when applying transformations on the momentum arguments such as reflections $Q \to -Q$, or shifts $Q \to Q + K$. Matsubara sums over both frequencies $\sim 2n$ and $\sim 2n+1$ do not respect the usual invariance properties of continuous integrations.

Boson propagator

Again the momentum dependence we are interested in arises in the off-diagonal components of the boson propagator (cf. eq. (C.11)). Hence we consider

$$
\begin{aligned}
&\int_K \phi^*(K)\Delta P_\phi(K)\phi(K) \qquad\qquad (C.23)\\
&= -\frac{1}{2}\mathrm{STr}[\bar{N}^{\phi^*}\bar{N}^{\phi} - \bar{M}^{\phi^*\phi}]\\
&= -\frac{1}{2}\int_K \delta\phi^*(K)\big\{\mathrm{str}\int_Q N^{\phi^*}(Q)N^{\phi}(Q+K) - M^{\phi^*\phi}(Q)\big\}\delta\phi(K)\\
&= \int_K \delta\phi^*(K)\delta\phi(K)\Big\{\int_Q -h_\phi^2\frac{P_F(Q)P_F(-Q-K)}{P_F^{|2|}(Q)P_F^{|2|}(Q+K)}\\
&\quad +\lambda_\phi\Big[\frac{P_\phi(Q)+P_\phi(-Q)}{P_\phi^{|2|}(Q)} - 2\lambda_\phi\rho\Big(2\frac{P_\phi(Q)P_\phi(Q+K)}{P_\phi^{|2|}(Q)P_\phi^{|2|}(Q+K)} + \frac{P_\phi(-Q)P_\phi(Q+K)}{P_\phi^{|2|}(Q)P_\phi^{|2|}(Q+K)}\Big)\\
&\quad +4(\lambda_\phi\rho)^2\frac{P_\phi(Q+K)+P_\phi(-Q)}{P_\phi^{|2|}(Q)P_\phi^{|2|}(Q+K)} - 4(\lambda_\phi\rho)^3\frac{1}{P_\phi^{|2|}(Q)P_\phi^{|2|}(Q+K)}\Big]\Big\}.
\end{aligned}
$$

The ϕ propagator receives a frequency and momentum dependent correction from the fermion fluctuations. In SYM, the bosonic fluctuations yield a momentum independent part only. Momentum dependent bosonic parts are compatible with the symmetries in SSB. The graphs $\propto (\lambda_\phi \rho)^2, (\lambda_\phi \rho)^3$ in SSB involve 4 and 6 inner boson lines, thus corresponding to more and more irrelevant coupling. We omit these contributions in practical computations. The graphs $\propto \lambda_\phi \rho$ play a subleading role as we have verified numerically. The higher order graphs might play an important role for the computation of critical exponents.

Yukawa coupling

The symmetries of our theory are not compatible with a diagram involving two inner fermion and an inner ϕ – boson line in SYM. Indeed we find

$$\frac{1}{2}\mathrm{STr}\bar{N}^{\phi}\bar{N}^{\psi^\dagger}\bar{N}^{\psi^\dagger} = 0. \tag{C.24}$$

In SSB this result remains true if we ignore contributions starting at $\lambda_\phi \rho^2$. Interestingly, terms $\propto \phi^2 \rho$ and $\propto \phi^{*2}\rho$ arise from $\phi\psi^\dagger\psi^\dagger$ and $\phi^*\psi\psi$ – $U(1)$ invariance is only ensured if both terms are considered. In the following, we restrict to the correction to $\phi\psi^\dagger\psi^\dagger$. A direct contribution to the renormalization of the Yukawa coupling is, generated in the presence of a pointlike four-fermion coupling and reads

$$\begin{aligned}
& -\frac{1}{2}\mathrm{STr}\bar{N}^{\phi}\bar{M}^{\psi^\dagger\psi^\dagger} \qquad (C.25)\\
= \; & -\frac{1}{2}\int\limits_{K_1,K_2,K_3} \delta\phi(K_1)\delta\psi^\dagger_\alpha(K_2)\delta\psi^\dagger_\beta(K_3)\delta(K_1-(K_2+K_3)) \\
& \big\{\mathrm{str}\int\limits_Q N^{\phi}(Q+K_1)M^{\psi^\dagger\psi^\dagger}_{\alpha\beta}(Q)\big\} \\
= \; & \int\limits_{K_1,K_2,K_3} \delta\phi(K_1)\delta\psi^\dagger_\alpha(K_2)\delta\psi^\dagger_\beta(K_3)\delta(K_1-(K_2+K_3)) \\
& \big\{-\frac{\lambda_\psi h_\phi}{2}\int\limits_Q \frac{P_F(Q)P_F(-Q+K_1)}{P_F^{|2|}(Q)P_F^{|2|}(Q+K_1)}\epsilon_{\alpha\beta}\big\}.
\end{aligned}$$

In the absence of a pointlike background coupling, direct renormalization effects on h_ϕ are expected to be weak – in this case, λ_ψ can only be generated by "rebosonization" graphs. A strong renormalization effect comes, however, from the anomalous dimension terms.

Four-fermion coupling

$$
\begin{aligned}
&-\frac{1}{4}\mathrm{STr}\big\{\bar{N}^{\psi^\dagger}\bar{N}^{\psi}\big[\bar{N}^{\psi^\dagger}\bar{N}^{\psi}+2\bar{N}^{\psi}\bar{N}^{\psi^\dagger}\big]+\bar{M}^{\psi^\dagger\psi}\bar{M}^{\psi^\dagger\psi}+2\bar{M}^{\psi^\dagger\psi^\dagger}\bar{M}^{\psi\psi}\big\} \qquad \text{(C.26)}\\
&+\frac{1}{2}\mathrm{STr}\big[\big(\bar{N}^{\psi}\bar{N}^{\psi^\dagger}+\bar{N}^{\psi^\dagger}\bar{N}^{\psi}\big)\bar{M}^{\psi^\dagger\psi}+\bar{N}^{\psi}\bar{N}^{\psi}\bar{M}^{\psi^\dagger\psi^\dagger}+\bar{N}^{\psi^\dagger}\bar{N}^{\psi^\dagger}\bar{M}^{\psi\psi}\big]\\
=\;&\int\limits_{K_1\ldots K_4}\delta\psi^\dagger_\alpha(K_1)\delta\psi_\beta(K_2)\delta\psi^\dagger_\gamma(K_3)\delta\psi_\delta(K_4)\delta(K_1+K_3-(K_2+K_4))\\
&\Big\{\mathrm{str}\int\limits_Q-\frac{1}{4}\big\{N^{\psi^\dagger}_\alpha(Q)N^{\psi}_\beta(Q+K_1)\big[N^{\psi^\dagger}_\gamma(Q+K_1-K_2)N^{\psi}_\delta(Q+K_1+K_3-K_2)\\
&\quad-2N^{\psi}_\delta(Q+K_1-K_2)N^{\psi^\dagger}_\gamma(Q+K_1-(K_2+K_4))\big]\\
&\quad+M^{\psi^\dagger\psi}_{\alpha\beta}(Q)M^{\psi^\dagger\psi}_{\gamma\delta}(Q+K_1-K_2)-M^{\psi^\dagger\psi^\dagger}_{\alpha\gamma}(Q)M^{\psi\psi}_{\beta\delta}(Q+K_1+K_3)\big\}\\
&\quad+\frac{1}{2}\big\{\big[N^{\psi^\dagger}_\alpha(Q)N^{\psi}_\beta(Q+K_1)-N^{\psi}_\beta(Q)N^{\psi^\dagger}_\alpha(Q-K_2)\big]M^{\psi^\dagger\psi}_{\gamma\delta}(Q+K_1-K_2)\\
&\quad-N^{\psi}_\beta(Q)N^{\psi}_\delta(Q-K_2)M^{\psi^\dagger\psi^\dagger}_{\alpha\gamma}(Q-(K_2+K_4))\\
&\quad-N^{\psi^\dagger}_\alpha(Q)N^{\psi^\dagger}_\gamma(Q+K_1)M^{\psi\psi}_{\beta\delta}(Q+K_1+K_3)\big\}\Big\}\\
\overset{SYM}{=}\;&\int\limits_{K_1\ldots K_4}\delta\psi^\dagger_\alpha(K_1)\delta\psi_\beta(K_2)\delta\psi^\dagger_\gamma(K_3)\delta\psi_\delta(K_4)\delta(K_1+K_3-(K_2+K_4))\\
&\Big\{-\frac{1}{2}\int\limits_Q\big\{\frac{1}{2}\big[\frac{h_\phi^4}{P_\phi(-Q)P_F(-Q-K_1)P_\phi(-Q-K_1+K_2)P_F(-Q-K_1+K_2-K_3)}\\
&+\frac{h_\phi^4}{P_F(Q)P_\phi(Q+K_1)P_F(Q+K_1-K_2)P_\phi(Q+K_1-K_2+K_3)}\big]\\
&+\big[\frac{\lambda_\psi^2}{P_F(Q)P_F(-Q-K_1)}+\frac{\lambda_\psi^2}{P_F(Q)P_F(Q+K_1)}\big]\\
&+\big[\frac{\lambda_\psi h_\phi^2}{P_F(-Q)P_\phi(-Q+K_2)P_F(-Q-K_1+K_2)}\\
&+\frac{\lambda_\psi h_\phi^2}{P_F(Q)P_\phi(Q+K_1)P_F(Q+K_1-K_2)}\big]\big\}\delta_{\alpha\beta}\delta_{\gamma\delta}\\
&+\frac{1}{2}\int\limits_Q\big\{\frac{\lambda_\psi h_\phi^2}{P_F(-Q)P_\phi(-Q+K_2)P_F(-Q-K_1+K_2)}\\
&+\frac{\lambda_\psi h_\phi^2}{P_F(Q)P_\phi(Q+K_1)P_F(Q+K_1-K_2)}\big\}\epsilon_{\alpha\gamma}\epsilon_{\beta\delta}\Big\}.
\end{aligned}
$$

We display the result of the summation over the discrete indices only in the symmetric phase – the full expression in the broken phase extends over several pages already at this level of tracing out the indices, if the full momentum dependence is kept! Note that we do not apply shift and reflection operations on the momenta for mixed diagrams as argued above.

We display the loop result for zero external momenta in SSB,

$$\begin{aligned}
&\mathrm{Re}\int\limits_Q \Big\{ -\frac{h_\phi^4}{2}\frac{P_\phi(Q)^2 P_F(Q)^2 + (\lambda_\phi\rho)^2 P_F(Q)P_F(-Q)}{(P_\phi^{|2|}(Q)P_F^{|2|}(Q))^2} \\
&-\frac{\lambda_\psi^2}{2}\frac{P_F(Q)P_F(-Q)+P_F(Q)^2}{P_F^{|2|}(Q)^2} \\
&-\lambda_\psi h_\phi^2 \frac{P_\phi(Q)P_F(Q)^2 - h_\phi^2\rho(P_\phi(Q)+P_\phi(-Q)) + h_\phi^2\lambda_\phi\rho^2}{P_\phi^{|2|}(Q)P_F^{|2|}(Q)^2}\Big\}\delta_{\alpha\beta}\delta_{\gamma\delta} \\
&+\Big\{ -\frac{h_\phi^4}{2}\frac{h_\phi^2\rho P_\phi(Q)P_\phi(-Q)}{(P_\phi^{|2|}(Q)P_F^{|2|}(Q))^2} - \frac{\lambda_\psi^2}{2}\frac{h_\phi^2\rho}{P_F^{|2|}(Q)^2} + \lambda_\psi h_\phi^2\frac{P_\phi(Q)P_F(Q)^2}{P_\phi^{|2|}(Q)P_F^{|2|}(Q)^2}\Big\}\epsilon_{\alpha\gamma}\epsilon_{\beta\delta}.
\end{aligned} \tag{C.27}$$

Taking the real part only compensates for imaginary parts generated from only considering particular sign arrangements in P_F, P_ϕ.

Appendix D

Explicit Loop Results

D.1 Wave Function Renormalization Factors

According to the definition (B.3), the one-loop corrections to the wave function renormalization (WFR) factors Z_ψ, Z_ϕ can be computed from the imaginary part of the *bare* loop corrections to the propagators,

$$\Delta Z_i = \lim_{\omega_e \to 0} \mathrm{Im} \frac{\Delta \bar{P}_i(\omega_e, \vec{k}^2 = 0) - \Delta \bar{P}_i(\omega_e = 0, \vec{k}^2 = 0)}{\omega_e}. \tag{D.1}$$

The index i in (D.1) stands for either F (fermionic WFR) or ϕ (bosonic WFR). The fact that the operators $\psi^\dagger \mathrm{i}\omega\psi$, $\phi^* \mathrm{i}\omega\phi$ are imaginary implies that we only have to consider the imaginary part of the loop correction.

In app. B we have defined the "renormalized" quantities by a rescaling with the wave function renormalizations Z_ψ, Z_ϕ. In these units one finds $\Delta Z_i \propto Z_i$ such that we can conveniently write

$$\Delta \log Z_i = \frac{\Delta Z_i}{Z_i} = \frac{\partial \mathrm{Im} \Delta P_i(\omega_e, \vec{q} = 0)}{\partial \omega_e}\Big|_{\omega_e = 0}. \tag{D.2}$$

Taking the *negative* cutoff derivative then produces the anomalous dimensions for fermions and bosons,

$$\eta_i = -\partial_t \log Z_i = -\partial_t \Delta \log Z_i. \tag{D.3}$$

The desired loop correction for the fermions reads

$$\begin{aligned}\Delta\log Z_\psi &= \frac{h_\phi^2}{16\tilde{T}^2}\int\frac{d^3\tilde{q}}{(2\pi)^3}[(\pi/2)^4+2(\pi/2)^2(\alpha_\phi^2+\gamma_\phi^2)+(\alpha_\phi^2-\gamma_\phi^2)^2]^{-2} \\ &\times\big\{2\gamma_\phi^{-1}\big[(\pi/2)^6\gamma-(\alpha_\phi^2-\gamma_\phi^2)^2(\alpha_\phi^2\gamma+(2\alpha+\gamma)\gamma_\phi^2) \\ &\quad+(\pi/2)^4(\alpha_\phi^2\gamma+(6\alpha+\gamma)\gamma_\phi^2)-(\pi/2)^2(\alpha_\phi^4\gamma-2\alpha_\phi^2(2\alpha+5\gamma)\gamma_\phi^2 \\ &\quad+(\gamma-4\alpha)\gamma_\phi^4\big]\tanh\gamma_\phi-\big[\alpha\leftrightarrow\gamma,\alpha_\phi\leftrightarrow\gamma_\phi,\tanh\alpha_\phi\leftrightarrow\coth\alpha_\phi\big] \\ &\quad+[(\pi/2)^2(\alpha-\gamma)+(\alpha+\gamma)(\alpha_\phi^2-\gamma_\phi^2)] \\ &\quad\times[(\pi/2)^4+2(\pi/2)^2(\alpha_\phi^2+\gamma_\phi^2)+(\alpha_\phi^2-\gamma_\phi^2)^2][\sinh^{-2}\alpha_\phi-\cosh^{-2}\gamma_\phi]\big\}\end{aligned} \tag{D.4}$$

reducing in SYM to

$$\begin{aligned}\Delta\log Z_\psi &= \frac{h_\phi^2}{16\tilde{T}^2}\int\frac{d^3\tilde{q}}{(2\pi)^3}((\pi/2)^2+(\alpha-\gamma)^2)^{-2} \\ &\quad\times\big[2[(\pi/2)^2-(\alpha-\gamma)^2][\tanh\gamma-\coth\alpha] \\ &\quad+(\alpha-\gamma)[(\pi/2)^2+(\alpha-\gamma)^2][\sinh^{-2}\alpha-\cosh^{-2}\gamma]\big].\end{aligned} \tag{D.5}$$

The bosonic expression is given by

$$\begin{aligned}\Delta\log Z_\phi &= \frac{h_\phi^2}{16\tilde{T}^2}\int\frac{d^3\tilde{q}}{(2\pi)^3}\gamma\gamma_\phi^{-3}\big[\tanh\gamma_\phi-\gamma_\phi\cosh^{-2}\gamma_\phi\big] \\ &\quad-\lambda_\phi\rho\frac{\lambda_\phi}{8\tilde{T}^2}\int\frac{d^3\tilde{q}}{(2\pi)^3}\alpha\alpha_\phi^{-3}\big[\coth\alpha_\phi+\alpha_\phi\sinh^{-2}\alpha_\phi+4\alpha_\phi^2\coth\alpha_\phi\sinh^{-2}\alpha_\phi\big]\end{aligned} \tag{D.6}$$

where we omit terms $\mathcal{O}((\lambda_\phi\rho)^2)$. In SYM this reduces to

$$\Delta\log Z_\phi = \frac{h_\phi^2}{16\tilde{T}^2}\int\frac{d^3\tilde{q}}{(2\pi)^3}\gamma^{-2}\big[\tanh\gamma-\gamma\cosh^{-2}\gamma\big]. \tag{D.7}$$

D.2 Gradient Coefficients

The one-loop correction to the gradient coefficients can be obtained as

$$\Delta A_i=\lim_{\vec{k}^2\to0}\mathrm{Re}\frac{\Delta P_i(\omega_e=0,\vec{k}^2)-\Delta P_i(\omega_e=0,0)}{\vec{k}^2}. \tag{D.8}$$

We note that there is no first order contribution due to the identity

$$\int d^dq\,(\vec{q}\cdot\vec{k})\,f(\vec{q}^2)=0. \tag{D.9}$$

The index i in (D.8) stands for either F (fermionic gradient coefficient) or ϕ (bosonic gradient coefficient). Reality of the operators $\psi^\dagger q^2 \psi$, $\phi^* q^2 \phi$ implies that we only have to consider the real part of the loop correction. Using the properties (C.9,C.13) and restricting to the real part, the general form of $\Delta P_i(0, \vec{k}^2)$ can be written as (cf. eqs. (C.22,C.23))

$$\Delta P_i(0, \vec{k}^2) \;=\; c_i \sum_{n=-\infty}^{\infty} T \int \frac{d^3q}{(2\pi)^3} \frac{P_j(\omega, \vec{q})}{P_j^{|2|}(\omega, \vec{q})} \frac{P_l(\pm\omega, \vec{q}+\vec{k})}{P_l^{|2|}(\omega, \vec{q}+\vec{k})}. \tag{D.10}$$

Note the appearance of either $+$ or $-$ sign in the second factor – they correspond to "bubble" or "ladder" type contributions. c_i stands for the prefactor of the integral. For the fermionic gradient coefficient A_ψ, we have

$$i = F, \quad c_i = h_\phi^2, \quad P_j = P_F, \quad P_l(\omega, \vec{q}+\vec{k}) = P_\phi(\omega, \vec{q}+\vec{k}) \tag{D.11}$$

with the positive sign in front of the Matsubara frequency in P_ϕ, while for the bosonic expression A_ϕ one finds

$$i = \phi, \quad c_i = -h_\phi^2, \quad P_j = P_F, \quad P_l(-\omega, \vec{q}+\vec{k}) = P_F(-\omega, \vec{q}+\vec{k}) \tag{D.12}$$

with the negative sign in front of the Matsubara frequency in P_F.

In SSB, there are both ladder and bubble type contributions to $A_\phi \propto \rho$ stemming from boson fluctuations. They can be computed from the above formula with

$$i = \phi, \quad c_i = -2\lambda_\phi^2 \rho, \quad P_j = P_\phi, \quad P_l(-\omega, \vec{q}+\vec{k}) = P_\phi(-\omega, \vec{q}+\vec{k}) \tag{D.13}$$

(ladder piece) and

$$i = \phi, \quad c_i = -4\lambda_\phi^2 \rho, \quad P_j = P_\phi, \quad P_l(\omega, \vec{q}+\vec{k}) = P_\phi(\omega, \vec{q}+\vec{k}) \tag{D.14}$$

(bubble piece).

The following considerations only refer to the integration over the spacelike momenta. They can be performed for any fixed Matsubara mode. We slightly generalize the discussion to d spacelike dimensions.

We have to perform an expansion of $\Delta P_i(0, \vec{k})$ at $\mathcal{O}(\vec{k}^2)$. Since $(\vec{q}+\vec{k})^2 = \vec{q}^2 + 2\vec{q}\vec{k} + \vec{k}^2$ there will be contributions from $(\vec{q}\vec{k})^2$ and $\vec{k}^2$. It is, however, possible to express (D.8) in terms of first order derivatives only [1]. To see this, we first write

$$G_m(\vec{k}) \equiv \frac{P_j(\pm\omega, \vec{q}+\vec{k})}{P_j^{|2|}(\omega, \vec{q}+\vec{k})} = G_m^{(0)} + G_m^{(1)}(\vec{q}\cdot\vec{k}) + G_m^{(2)}\vec{k}^2. \tag{D.15}$$

[1] Thanks to Holger Gies for pointing this out to me!

(The sign of ω must be taken care for in the concrete calculation.) Now consider, for an arbitrary Matsubara mode,

$$\int \frac{d^dq}{(2\pi)^3} G_j(0)G_l(\vec{k}) = \int \frac{d^dq}{(2\pi)^3} G_j(-\vec{k})G_l(0) = \int \frac{d^dq}{(2\pi)^3} G_j(-\vec{k}/2)G_l(\vec{k}/2) \quad \text{(D.16)}$$

which at the order k^2 implies

$$\begin{aligned} &\int \frac{d^dq}{(2\pi)^3} G_j^{(2)}G_l^{(0)}\vec{k}^2 = \int \frac{d^dq}{(2\pi)^3} G_j^{(0)}G_l^{(2)}\vec{k}^2 \qquad \text{(D.17)} \\ = \; &-\frac{1}{4}\int \frac{d^dq}{(2\pi)^3} G_j^{(1)}G_l^{(1)}(\vec{q}\cdot\vec{k})^2 + \frac{1}{4}\int \frac{d^dq}{(2\pi)^3}\big(G_j^{(2)}G_l^{(0)} + G_j^{(0)}G_l^{(2)}\big)\vec{k}^2. \end{aligned}$$

Each of these expressions can be taken to compute the gradient coefficient (D.8). On the other hand, the last equations can be used to eliminate the second order terms from the practical computation of A_i. Using the identity

$$\int d^dq(\vec{q}\cdot\vec{k})^2 f(\vec{q}^2) = \frac{\vec{k}^2}{d}\int d^dq\vec{q}^2 f(\vec{q}^2) \quad \text{(D.18)}$$

we can write down the formula for the computation of ΔA_i,

$$\Delta A_i = -\frac{c_i}{2d}\mathrm{Re}\sum_{n=-\infty}^{\infty} T\int \frac{d^3q}{(2\pi)^3}\ \vec{q}^2\ G_j^{(1)}G_l^{(1)}. \quad \text{(D.19)}$$

For practical reasons, it is preferable to perform the Matsubara sum before expanding G_j to first order. With $G_j^{(1)} = 2A_j\partial G_j(y)/\partial y|_{\vec{k}=0}$, $y = (\vec{q}+\vec{k})^2$, we can write the last equation as

$$\Delta A_i = -\frac{2A_jA_lc_i}{d}\mathrm{Re}\int \frac{d^3q}{(2\pi)^3}\frac{\partial}{\partial y}\frac{\partial}{\partial x}\sum_{n=-\infty}^{\infty} T\vec{q}^2\ G_j(y)G_l(x). \quad \text{(D.20)}$$

The resulting loop expressions are quite lengthy. E.g. A_ψ extends over some pages in SSB. For this coupling we only display the result in SYM,

$$\begin{aligned} \Delta A_\psi \;=\; &\frac{A_\phi A_\psi h_\phi^2}{24\tilde{T}^3}\int \frac{d^3\tilde{q}}{(2\pi)^3}\ \tilde{q}^2((\pi/2)^2 + (\alpha-\gamma)^2)^{-3} \qquad \text{(D.21)} \\ &\times\big[2[(\alpha-\gamma)^2 - 3(\pi/2)^2)(\alpha-\gamma)][\tanh\gamma - \coth\alpha] \\ &+[(\alpha-\gamma)^4 - (\pi/2)^4][\cosh^{-2}\gamma - \sinh^{-2}\alpha]\big]. \end{aligned}$$

The bosonic gradient coefficient reads

$$\begin{aligned}\Delta A_\phi &= \frac{h_\phi^2 A_\psi^2}{288\tilde{T}^3}\int\frac{d^3\tilde{q}}{(2\pi)^3}\;\tilde{q}^2\gamma_\phi^{-7}\big[3(5\gamma^4-5\gamma^2\gamma_\phi^2+2\gamma_\phi^4)[\tanh\gamma_\phi-\gamma_\phi\cosh^{-2}\gamma_\phi]\\ &\qquad +2\gamma^2\gamma_\phi(\gamma^2-\gamma_\phi^2)[\gamma_\phi\cosh^{-4}\gamma_\phi-6\tanh\gamma_\phi-2\gamma_\phi\tanh^2\gamma_\phi]\big]\\ &\quad +\lambda_\phi\rho\,\frac{\lambda_\phi A_\phi^2}{144\tilde{T}^3}\int\frac{d^3\tilde{q}}{(2\pi)^3}\;\tilde{q}^2\alpha_\phi^{-7}\big[3\coth\alpha_\phi\big\{\alpha^2(-19\alpha_\phi^2+15\kappa^2)\\ &\qquad +15\alpha^4+6\alpha_\phi^4+30\alpha^3\kappa-20\alpha\alpha_\phi^2\kappa-\alpha_\phi^2\kappa^2\big\}\\ &\qquad +\alpha_\phi\sinh^{-2}\alpha_\phi\big\{18\alpha_\phi^4+3\alpha^4(15+4\alpha_\phi^2)+4\alpha\alpha_\phi^2(-15+2\alpha_\phi^2)\kappa\\ &\qquad +6\alpha^3(15+4\alpha_\phi^2)\kappa+\alpha_\phi^2(-3+4\alpha_\phi^2)\kappa^2\\ &\qquad +\alpha^2(45\kappa^2+\alpha_\phi^2(-57+4\alpha_\phi^2+12\kappa^2))\\ &\qquad +36\alpha\alpha_\phi(\alpha+\kappa)(-\alpha_\phi^2+\alpha(\alpha+\kappa))\coth\alpha_\phi\big\}\\ &\qquad +6\alpha_\phi^3(3\alpha^2+\alpha_\phi^2)(\alpha+\kappa)^2\sinh^{-4}\alpha_\phi\big],\end{aligned}\tag{D.22}$$

where we omit terms $\mathcal{O}((\lambda_\phi\rho)^2)$. In SYM this reduces to

$$\Delta A_\phi = \frac{h_\phi^2 A_\psi^2}{48\tilde{T}^3}\int\frac{d^3\tilde{q}}{(2\pi)^3}\;\tilde{q}^2\gamma^{-3}\big[\tanh\gamma-\gamma\cosh^{-2}\gamma\big].\tag{D.23}$$

D.3 Yukawa and Four-Fermion Coupling

The loop corrections for the Yukawa and the four-fermion coupling are evaluated at zero external frequency and momentum.

From eq. (C.25), we find for the loop correction to the Yukawa coupling, after performing the Matsubara sum,

$$\Delta\frac{h_\phi}{2} = -\frac{h_\phi\lambda_\psi}{16\tilde{T}}\int\frac{d^3\tilde{q}}{(2\pi)^3}\gamma_\phi^{-3}\big[\gamma_\phi(\gamma_\phi^2-\gamma^2)\cosh^{-2}\gamma_\phi-(\gamma_\phi^2+\gamma^2)\tanh\gamma_\phi\big]\tag{D.24}$$

Our truncation features a term (cf., e.g., (3.5) or (7.20))

$$\Gamma\ni\int\limits_{K_1,K_2,K_3}\phi(K_1)\psi_\alpha^\dagger(K_2)\psi_\beta^\dagger(K_3)\delta(K_1-(K_2+K_3))\Big\{\frac{h_\phi}{2}\epsilon_{\alpha\beta}\Big\}.\tag{D.25}$$

Comparison of the coefficients reveals that the loop integral in eq. (C.25) corresponds to $\Delta h_\phi/2$. Since we are further mainly interested in $\Delta h_\phi^2 = 2h_\phi\Delta h_\phi$, the above loop correction has to be premultiplied with $4h_\phi$ in order to get the desired expression.

From eq. C.27, we find for the loop correction to the four-fermion coupling, after performing the Matsubara sum and in SYM,

$$\begin{aligned}\Delta\frac{\lambda_\psi}{2} &= -\frac{\lambda_\psi^2}{8\tilde{T}}\int\frac{d^3\tilde{q}}{(2\pi)^3}\gamma^{-1}\big[\tanh\gamma-\gamma\cosh^{-2}\gamma\big] \\ &\quad+\frac{3\lambda_\psi h_\phi^2}{8\tilde{T}^2}\int\frac{d^3\tilde{q}}{(2\pi)^3}\big((\pi/2)^2+(\alpha-\gamma)^2\big)^{-2} \\ &\qquad\times\big[\big((\pi/2)^2-(\alpha-\gamma)^2\big)\big(\coth\alpha-\tanh\gamma\big) \\ &\qquad\quad+\big((\pi/2)^2+(\alpha-\gamma)^2\big)(\alpha-\gamma)\cosh^{-2}\gamma\big] \\ &\quad-\frac{h_\phi^4}{32\tilde{T}^3}\int\frac{d^3\tilde{q}}{(2\pi)^3}\big((\pi/2)^2+(\alpha-\gamma)^2\big)^{-3} \\ &\qquad\times\big[2\big(-3(\pi/2)^2+(\alpha-\gamma)^2\big)(\alpha-\gamma)\big(\coth\alpha-\tanh\gamma\big) \\ &\qquad\quad+\big((\alpha-\gamma)^4-(\pi/2)^4\big)\big(\sinh^{-2}\alpha-\cosh^{-2}\gamma\big)\big].\end{aligned} \tag{D.26}$$

For the term $\propto \lambda_\psi h_\phi^2$ we have grouped the term with ϵ^2-structure together with the term featuring δ^2-structure (cf. eq. C.27) by an appropriate Fierz rearrangement. Similar to the discussion for the Yukawa term, the loop integral has to be premultiplied with a factor 2 since our truncation involves $\lambda_\psi/2$.

D.4 Effective Potential

The effective potential is formally obtained by setting $\delta\hat{\psi}=0$ from the outset. In this case, the fluctuation matrix $\Gamma^{(2)}|_{\delta\hat{\psi}=0}(Q_1,Q_2)$ is block diagonal in the discrete indices. If we assume homogeneous fields [2] and momentum independent couplings, the matrix is further diagonal in momentum space, $\Gamma^{(2)}|_{\delta\hat{\psi}=0}(Q_1)\delta(Q_1-Q_2)$. Hence the corresponding determinants can be performed explicitly for fluctuating boson fields and the effective potential can be computed straightforwardly. A large number of diagrams relevant for our problem can then be computed by field variation of the effective potential. Due to the block diagonal structure of the fluctuation matrix, we can split up the one-loop contribution to the effective potential into a fermionic and a bosonic contribution,

$$\bar{U}_1=\bar{U}_1^{(F)}+\bar{U}_1^{(B)}. \tag{D.27}$$

The dimensionful and dimensionless version of the effective potential $\bar{U}=\Gamma/V$ are related by

$$\tilde{u}=(k_F^3\epsilon_F)^{-1}\bar{U}=(k_F^5/(2M))^{-1}\bar{U}, \tag{D.28}$$

[2] Homogeneous fluctuating fields do not make sense from the physics point of view, but this is used here as a computational trick.

in accordance with the different scaling of energies and momenta in our nonrelativistic problem. As the effective action, the effective potential is invariant under rescaling transformation $\mathcal{Z}$, cf. chapt. 4.2.2.

D.4.1 Fermionic Contribution

Omitting the δ-function, we find for the fermionic sector of the fluctuation matrix

$$\Gamma_F^{(2)}(\tilde{\sigma}, \hat{\phi}^*, \hat{\phi}) = \begin{pmatrix} -\epsilon_{\alpha\beta} h_\phi \hat{\phi}^* & -\delta_{\alpha\beta} P_F(-\tilde{Q}) \\ \delta_{\alpha\beta} P_F(\tilde{Q}) & \epsilon_{\alpha\beta} h_\phi \hat{\phi} \end{pmatrix}. \tag{D.29}$$

The determinant w.r.t. the discrete indices of this matrix depends only on the invariant $\hat{\rho} = \hat{\phi}^* \hat{\phi}$ and reads

$$\begin{aligned} \det_{4\times 4}(\Gamma_F^{(2)}) &= \left(P_F(\tilde{Q}) P_F(-\tilde{Q}) + h_\phi^2 \rho\right)^2 = (P_F^{|2|}(\tilde{Q}))^2 && \text{(D.30)} \\ &= \left(\tilde{\omega}_F^2 + (A_\psi \tilde{q}^2 - \tilde{\sigma})^2 + h_\phi^2 \hat{\rho}\right)^2. && \text{(D.31)} \end{aligned}$$

The one-loop potential reads

$$\begin{aligned} \tilde{u}_1^{(F)}(\tilde{\sigma}, \hat{\rho}) &= -\frac{1}{2} \log\det(\Gamma_F^{(2)}) = -\int_{\tilde{Q}} \log P_F^{|2|}(\tilde{Q}) && \text{(D.32)} \\ &= -2\tilde{T} \int \frac{d^3\tilde{q}}{(2\pi)^3} \log\cosh \gamma_\phi \\ &= -2\tilde{T} \int \frac{d^3\tilde{q}}{(2\pi)^3} \log\left(e^{\gamma_\phi - \gamma} + e^{-\gamma_\phi - \gamma}\right) + \text{const.} \end{aligned}$$

$\gamma_\phi(\tilde{\sigma}, \hat{\rho}), \gamma(\tilde{\sigma})$ are dimensionless, field dependent functions which are additionally invariant under the rescaling with the WFRs. They read

$$\begin{aligned} \gamma_\phi(\tilde{\sigma}, \hat{\rho}) &= \frac{((A_\psi \tilde{q}^2 - \tilde{\sigma})^2 + h_\phi^2 \hat{\rho})^{1/2}}{2\tilde{T}}, && \text{(D.33)} \\ \gamma(\tilde{\sigma}) &= \frac{A_\psi \tilde{q}^2 - \tilde{\sigma}}{2\tilde{T}}. \end{aligned}$$

Their "equilibrium values", obtained by setting $\hat{\rho} \to \rho_0$, are discussed in the subsequent appendix. In the last step we have omitted an infinite quantity which depends only on $\tilde{\sigma}$ (through $\gamma(\tilde{\sigma})$). Its omission is justified in sect. 4 by a comparison of the operator vs. the path integral formalism.

In the second line we have performed the Matsubara sum using

$$2\ln\cosh(x) = \sum_{n=-\infty}^{\infty} \ln\left(1 + \frac{x^2}{(n+1/2)^2\pi^2}\right) \tag{D.34}$$

and omitting another infinite constant, which is irrelevant for the thermodynamics.

The potential minimum is reached by setting $\hat{\rho} = \rho_0$. Further, the SYM phase is obtained by considering the symmetric vacuum state $\rho_0 = 0$, and the effective potential reduces to the standard form from statistical mechanics,

$$\tilde{u}_1^{(F)} = -2\tilde{T} \int \frac{d^3\tilde{q}}{(2\pi)^3} \log\left(1 + e^{-2\gamma}\right). \tag{D.35}$$

The coefficients entering the function γ can, however, be modified by fluctuations.

D.4.2 Bosonic Contribution

The bosonic sector of the fluctuation matrix is given by

$$\Gamma_\phi^{(2)}(\tilde{\sigma}, \rho_0, \hat{\phi}^*, \hat{\phi}) = \begin{pmatrix} -\lambda_\phi \hat{\phi}\hat{\phi} & P_\phi(-Q) + \lambda_\phi(2\hat{\rho} - \rho_0) \\ P_\phi(Q) + \lambda_\phi(2\hat{\rho} - \rho_0) & -\lambda_\phi \hat{\phi}^*\hat{\phi}^* \end{pmatrix}. \tag{D.36}$$

Both fluctuating fields (with hat) and background values appear in this formula. Again the determinant of this matrix depends only on the invariants $\hat{\rho} = \hat{\phi}^*\hat{\phi}, \rho$ and reads

$$\begin{aligned} \det(\Gamma_\phi^{(2)}) &= \tilde{\omega}_B^2 + (A_\phi \tilde{q}^2 + m_\phi^2(\tilde{\sigma}))^2 + 2\lambda_\phi (A_\phi \tilde{q}^2 + m_\phi(\tilde{\sigma})^2)(2\hat{\rho} - \rho_0) \\ &\quad + \lambda_\phi^2 (3\hat{\rho}^2 - 4\hat{\rho}\rho_0 + \rho_0^2). \end{aligned} \tag{D.37}$$

Here we work with a $\tilde{\sigma}$-dependence for m_ϕ^2. This is motivated by the discussion of the effective chemical potential in sect. 4.2.2. A $\tilde{\sigma}$-derivative acts on the mass term as

$$\frac{\partial m_\phi^2}{\partial \tilde{\sigma}} = -2, \tag{D.38}$$

while it does not act on the other couplings (A_ϕ, λ_ϕ). Our prescription produces the dressed connected molecule density, if applied to the bosonic effective potential.

This one-loop effective potential reads

$$\begin{aligned} \tilde{u}_1^{(B)}(\tilde{\sigma}, \hat{\rho}) &= \frac{1}{2} \log\det(\Gamma_\phi^{(2)}) \\ &= \tilde{T} \int \frac{d^3\tilde{q}}{(2\pi)^3} \log\sinh \alpha_\phi \\ &= \tilde{T} \int \frac{d^3\tilde{q}}{(2\pi)^3} \log\left(e^{\alpha_\phi - \alpha} - e^{-\alpha_\phi - \alpha}\right) + \text{const.} \end{aligned} \tag{D.39}$$

Similar to the fermionic case, $\alpha_\phi(\tilde{\sigma},\hat{\rho}), \alpha(\tilde{\sigma})$ are dimensionless, field dependent functions which are additionally invariant under the rescaling with the WFRs. They read

$$\begin{aligned} \alpha_\phi(\tilde{\sigma},\hat{\rho}) &= \frac{1}{2\tilde{T}}\big[(A_\phi\tilde{q}^2+m_\phi^2(\tilde{\sigma}))^2 \\ &\quad +2\lambda_\phi(2\hat{\rho}-\rho_0)(A_\phi\tilde{q}^2+m_\phi^2(\tilde{\sigma}))+\lambda_\phi^2(3\hat{\rho}^2-4\rho\hat{\rho}_0+\rho_0^2)\big]^{1/2}, \\ \alpha(\tilde{\sigma},\hat{\rho}) &= \frac{A_\phi\tilde{q}^2+m_\phi^2(\tilde{\sigma})}{2\tilde{T}}. \end{aligned} \tag{D.40}$$

In the calculation we use the same arguments as above in order to deal with the infinite constants. In the second line we have performed the Matsubara sum using

$$2\ln\sinh(x)=\sum_{n=-\infty}^{\infty}\ln\left(1+\frac{x^2}{n^2\pi^2}\right). \tag{D.41}$$

As stated above, $m_\phi^2(\tilde{\sigma})$ contains a dependence on the current $\tilde{\sigma}$. As for the fermionic contribution, the potential minimum is reached by setting $\hat{\rho}=\rho$. Further, the SYM phase is obtained by setting $\rho=0$, in SSB we can make use of Goldstone's theorem implying $m_\phi^2=0$.

We can now generate all momentum independent couplings which do not involve derivatives w.r.t. the fermion fields from these formulae,

$$\tilde{u}^{(n)}=\frac{\partial^n\tilde{u}}{\partial\hat{\rho}^n}\Big|_{\hat{\rho}=\rho_0}. \tag{D.42}$$

Since we work in a quartic truncation, we are especially interested in

$$m_\phi^2=\tilde{u}^{(1)},\quad \lambda_\phi=\tilde{u}^{(2)}. \tag{D.43}$$

With our conventions for the effective chemical potential, we can also obtain the particle number by a derivative,

$$k_F^{-3}n=-\frac{\tilde{u}}{\partial\tilde{\sigma}} \tag{D.44}$$

where we have to consider eqs. (4.82,D.38) for a practical implementation.

D.4.3 The functions γ_ϕ,γ,β and $\alpha_\phi,\alpha,\kappa$

In order to characterize the loop integrals at the minimum of the effective potential ($\hat{\rho}=\rho_0$), we need six functions, γ_ϕ,γ,β for the fermionic sector and α_ϕ,α, and κ for the bosonic sector (after having performed the Matsubara summation). Note that

the effective potential (D.30,D.39) cannot be written in terms of these functions – it still involves the fluctuating fields. The use of these functions makes only sense after having performed the derivatives with respect to the fluctuating fields and having set the fields to their background values.

The functions have two important properties: First, they are dimensionless (invariant under k_F rescaling), such that all entries can be written both in dimensionful or dimensionless units. Second, they are invariant under a rescaling with the wave function renormalizations Z_ψ, Z_ϕ. We display these functions expressed in dimensionless renormalized units,

$$\begin{aligned}
\gamma_\phi(\tilde{\sigma},\rho_0) &= \frac{\left[(A_\psi\tilde{q}^2-\tilde{\sigma})^2+h_\phi^2\rho_0\right]^{1/2}}{2\tilde{T}} \\
\gamma(\tilde{\sigma}) &= \frac{A_\psi\tilde{q}^2-\tilde{\sigma}}{2\tilde{T}}, \quad \beta(\rho_0)=\frac{h_\phi^2\rho_0}{2\tilde{T}}, \qquad \text{(D.45)} \\
\alpha_\phi(\tilde{\sigma},\rho_0) &= \frac{\left[(A_\phi\tilde{q}^2+m_\phi^2(\tilde{\sigma}))^2+2\lambda_\phi\rho_0(A_\phi\tilde{q}^2+m_\phi^2(\tilde{\sigma}))\right]^{1/2}}{2\tilde{T}} \\
\alpha(\tilde{\sigma}) &= \frac{A_\phi\tilde{q}^2+m_\phi^2(\tilde{\sigma})}{2\tilde{T}}, \quad \kappa(\rho_0)=\frac{\lambda_\phi\rho_0}{2\tilde{T}} \qquad \text{(D.46)}
\end{aligned}$$

We have the following relations between these functions,

$$\begin{aligned}
\gamma_\phi^2 &= \gamma^2+\beta^2, \qquad \text{(D.47)} \\
\alpha_\phi^2 &= \alpha^2+2\kappa\alpha.
\end{aligned}$$

The two phases are characterized by

- SYM

$$\begin{aligned}
\beta=0, \quad \gamma_\phi &= \gamma, \qquad \text{(D.48)} \\
\kappa=0, \quad \alpha_\phi &= \alpha.
\end{aligned}$$

  This leads to great simplifications especially for the bosonic contributions involving a lot of free κ's.

- SSB

$$m_\phi^2=0, \quad \alpha=\frac{A_\phi\tilde{q}^2}{2\tilde{T}}. \qquad \text{(D.49)}$$

In the presence of a cutoff, the functions α and γ are modified by additional mass terms, while all algebraic properties are preserved.

Bibliography

[1] A. Einstein. *Sitz.ber. Kgl. Preuss. Akad. Wiss.*, 1924:261, 1924.

[2] A. Einstein. *Sitz.ber. Kgl. Preuss. Akad. Wiss.*, 1925:3, 1925.

[3] M. H. Anderson, J. R. Ensher, M. R. Matthews, C. E. Wieman, and E. A. Cornell. *Science*, 269:198, July 1995.

[4] C. C. Bradley, C. A. Sackett, J. J. Tollett, and R. G. Hulet. *Phys. Rev. Lett.*, 75:1687, August 1995.

[5] K. B. Davis, M.-O. Mewes, M. R. Andrews, N. J. van Druten, D. S. Durfee, D. M. Kurn, and W. Ketterle. *Phys. Rev. Lett.*, 75:3969, November 1995.

[6] L. Cooper. *Phys. Rev.*, 104:1189, 1956.

[7] J. Bardeen, L. Cooper, and J. Schrieffer. *Phys. Rev.*, 108:1175, 1957.

[8] D.M. Eagles. *Phys. Rev.*, 186:456, 1969.

[9] A. J. Leggett. *in: Modern Trends in the Theory of Condensed Matter*. Springer Verlag, Berlin, A. Pekalski and R Przystawa edition, 1980.

[10] P. Nozières and S. Schmitt-Rink. *J. Low Temp. Phys.*, 59:195, 1985.

[11] C. A. R. Sa de Melo, M. Randeria, and J. R. Engelbrecht. *Phys. Rev. Lett.*, 71:3202, 1993.

[12] H. T. C. Stoof, M. Houbiers, C. A. Sackett, and R. G. Hulet. *Phys. Rev. Lett.*, 76:10, 1996.

[13] R. Combescot. *Phys. Rev. Lett.*, 83:3766–3769, 1999.

[14] H. Heiselberg, C. J. Pethick, H. Smith, and L. Viverit. *Phys. Rev. Lett.*, 85:2418–2421, 2000.

[15] C. A. Regal, M. Greiner, and D. S. Jin. *Phys. Rev. Lett.*, 92:040403, 2004.

[16] M.W. Zwierlein, A. Stan, C. H. Schunck, S. M. F. Raupach, A. J. Kerman, and W. Ketterle. *Phys. Rev. Lett.*, 92:120403, 2004.

[17] C. Chin, M. Bartenstein, A. Altmeyer, S. Riedl, S. Jochim, J. Hecker Denschlag, and R. Grimm. *Science*, 305:1128, 2004.

[18] J. Kinast, S. L. Hemmer, M. E. Gehm, A. Turlapow, and J. E. Thomas. *Phys. Rev. Lett.*, 92:150402, 2004.

[19] T. Bourdel, K. Khaykovich, J. Cubizolles, J. Zhang, F. Chevy, L. Teichmann, M. Tarruell, S. J. Kokkelmans, and C. Salomon. *Phys. Rev. Lett.*, 93:050401, 2004.

[20] K. E. Strecker, G. B. Partridge, and R. G. Hulet. *Phys. Rev. Lett.*, 91:080406, 2003.

[21] P. Pieri and G. C. Strinati. *Phys. Rev. B*, 62:15370, 2000.

[22] P. Pieri and G. C. Strinati. *Phys. Rev. Lett.*, 91:030401, 2003.

[23] A. Perali, P. Pieri, and G. C. Strinati. *Phys. Rev. A.*, 68:031601, 2003.

[24] F. Pistolesi and G. C. Strinati. *Phys. Rev. B*, 53:15168, 1996.

[25] A. Perali, P. Pieri, L. Pisani, and G. C. Strinati. *Phys. Rev. Lett*, 92:220404, 2004.

[26] H. Hu, X. Liu, and P. Drummond. 2005, `cond-mat/0506046`.

[27] S. J. Kokkelmans, M. L. Chiofalo, R. Walser, and M. J. Holland. *Phys. Rev. Lett*, 87:120406, 2001.

[28] M. L. Chiofalo, S. J. Kokkelmans, J. N. Milstein, and M. J. Holland. *Phys. Rev. A*, 66:043604, 2002.

[29] M. L. Chiofalo, S. J. Kokkelmans, J. N. Milstein, and M. J. Holland. *Phys. Rev. Lett.*, 88:090402, 2002.

[30] A. Griffin and Y. Ohashi. *Phys. Rev. Lett.*, 89:130402, 2002.

[31] A. Griffin and Y. Ohashi. *Phys. Rev. A*, 67:033603, 2003.

[32] E. Timmermans, K. Furuya, P. W. Milonni, and A. Kerman. *Phys. Lett. A*, 285:228, 2001.

[33] Q. Chen, K. Levin, J. Stajic, and S. Tan. *Phys. Rev. A*, 69:063610, 2004.

[34] Q. Chen, M. L. Chiofalo, M. Holland, K. Levin, J. N. Milstein, and J. Stajic. *Physics Reports*, 412:1, 2005.

[35] R. A. Duine and H. T. C. Stoof. *J. Opt. B: Quantum Semiclass. Opt.*, 5:S212, 2003.

[36] R. A. Duine and H. T. C. Stoof. *Phys. Rep.*, 396:115, 2004.

[37] G. M. Falco and H. T. C. Stoof. *Phys. Rev. Lett.*, 92:140402, 2004.

[38] G. M. Falco and H. T. C. Stoof. *Phys. Rev. A*, 71:063614, 2005.

[39] S. Diehl and C. Wetterich. *Phys. Rev. A*, 73:033615, 2006, `cond-mat/0502534`.

[40] S. Diehl and C. Wetterich. 2005, `cond-mat/0510407`.

[41] E. Braaten and H. W. Hammer. *Phys. Rept.*, 428:259–390, 2006, `cond-mat/0410417`.

[42] M. Houbiers, H. T. C. Stoof, W. I. McAlexander, and R. G. Hulet. *Phys. Rev. A*, 57:R1497, 1998.

[43] J. Chwedenczuk, K. Goral, T. Köhler, and P.S. Julienne. *Phys. Rev. Lett.*, 93:260403, 2004.

[44] S. Jochim, M. Bartenstein, J. Hecker Denschlag, G. Hendl, A. Mosk, M Weidemüller, and R. Grimm. *Phys. Rev. Lett.*, 89:273202, 2002.

[45] S. Gupta, Z. Hadzibabic, M.W. Zwierlein, C.A. Stan, K. Dieckmann, C. H. Schunck, E. G. M. van Kempen, B. J. Verhaar, and W. Ketterle. *Science*, 300:1723, 2003.

[46] M. Bartenstein, A. Altmeyer, S. Riedl, R. Geursen, S. Jochim, C. Chin, J. Hecker Denschlag, R. Grimm, A. Simoni, E. Tiesinga, C. J. Williams, and P.S. Julienne. *Phys. Rev. Lett.*, 94:103201, 2005.

[47] C. J. Pethick and H. Smith. *Bose-Einstein Condensation in Dilute Gases. Cambridge University Press, Cambridge UK*, 2002.

[48] T. Köhler, K. Goral, and P. S. Julienne. 2006, `cond-mat/0601420`.

[49] T. Baier. A Renormalization Group Approach to the Hubbard Model. *Ph.D. thesis, Heidelberg*, 2002.

[50] H. Gies and C. Wetterich. *Phys. Rev. D*, 65:065001, 2001.

[51] D. Amit and V. Martin-Major. *Field Theory, Renormalization Group, and Critical Phenomena. World Scientific Publishing, Singapore (3rd edition)*, 2005.

[52] M. W. J. Romans and H. T. C. Stoof. 2005, `cond-mat/0506282`.

[53] F. J. Dyson. *Phys. Rev.*, 75:1736, 1949.

[54] J. S. Schwinger. *Proc. Nat. Acad. Sci.*, 37:452–455, 1951.

[55] Jan M. Pawlowski. 2005, `hep-th/0512261`.

[56] C. Wetterich. 2002, `cond-mat/0208361`.

[57] C. Wetterich. *Z. Phys.*, C 57:451, 1993.

[58] J. Berges, N. Tetradis, and C. Wetterich. *Phys. Rept.*, 363:223, 2000.

[59] N. Tetradis and C. Wetterich. *Nucl. Phys. B*, 398:659, 1993.

[60] N. Tetradis and C. Wetterich. *Nucl. Phys. B*, 422:541, 1994.

[61] J. Berges, N. Tetradis, and C. Wetterich. *Phys. Rev. Lett.*, 77:873, 1996.

[62] J. Carlson, S.-Y. Chang, V.R. Pandharipande, and K.E. Schmidt. *Phys. Rev. Lett.*, 91:050401, 2003.

[63] G. B. Partridge, K. E. Strecker, R. I. Kamar, M. W. Jack, and R. G. Hulet. *Phys. Rev. Lett.*, 95:020404, 2005.

[64] T. L. Ho. *Phys. Rev. Lett.*, 92:090402, 2004.

[65] Q. Chen and K. Levin. 2005, `cond-mat/0505689`.

[66] Q. Chen, J. Stajic, and K. Levin. *Phys. Rev. Lett.*, 95:260405, 2005.

[67] J. Kinast, A. Turlapow, J. E. Thomas, Q. Chen, J. Stajic, and K. Levin. *Science*, 307:1296, 2005.

[68] E. Burovski, N. Prokofev, B. Svistunov, and M. Troyer. *Phys. Rev. Lett.*, 96:160402, 2006.

[69] A. Schwenk and C. J. Pethick. *Phys. Rev. Lett.*, 95:160401, 2005.

[70] L. Jensen. 2004, `cond-mat/0412431`.

[71] M. H. Szymanska, K. Goral, T. Köhler, and K. Burnett. *Phys. Rev. A*, 72:013610, 2005.

[72] L. P. Gorkov and T. K. Melik-Barkhudarov. *Zh. Eksp. Teor. Fiz.*, 40:1452, 1961, [Sov. Phys. - JETP 13, 1018 (1961)].

[73] R. Shankar. *Rev. Mod. Phys.*, 66:129, 1994.

[74] R. Haussmann. *Z. Phys. B*, 91:291, 1993.

[75] D.S. Petrov, C. Salomon, and G.V. Shlyapnikov. *Phys. Rev. Lett*, 93:090404, 2004.

[76] A. Bulgac and P. F. Bedaque. 2002, cond-mat/0210217.

[77] G.E. Astrakharchik, J. Boronat, J. Casulleras, and S. Giorgini. 2005, cond-mat/0507483.

[78] L. P. Kadanoff. *Physics*, 2:263, 1966.

[79] K. G. Wilson. *Phys. Rev. B*, 4:3174, 1971.

[80] F. J. Wegner. *Phys. Rev. A*, 8:401, 1973.

[81] M. C. Birse, B. Krippa, J. A. McGovern, and N. R. Walet. *Phys. Lett. B*, 605:287, 2005.

[82] B. Krippa. *J. Phys.*, A39:8075, 2006.

[83] B. Krippa. 2006, nucl-th/0605071.

[84] G.E. Astrakharchik, J. Boronat, J. Casulleras, and S. Giorgini. *Phys. Rev. Lett*, 93:200404, 2004.

[85] I.V. Brodsky, A.V. Klaptsov, Yu. M. Kagan, R. Combescot, and X. Leyronas. 2005, cond-mat/0507240.

[86] N. D. Wagner and H. Mermin. *Phys. Rev. Lett.*, 17:1133, 1966.

[87] T. Baier, E. Bick, and C. Wetterich. *Phys. Lett. B*, 605:144, 2005.

[88] G. Baym, M. Holzmann, J.-P. Blaizot, F. Laloë, and D. Vautherin. *Phys. Rev. Lett.*, 83:1703, 1999.

[89] J.-P. Blaizot, R. Mendez-Galain, and N. Wschebor. 2004, cond-mat/0412481.

[90] J.-P. Blaizot, R. Mendez-Galain, and N. Wschebor. 2005, hep-th/0512317.

[91] J.-P. Blaizot, R. Mendez-Galain, and N. Wschebor. 2006, hep-th/0603163.

[92] S. Fölling, F. Gerbier, A. Widera, O. Mandel, T. Gericke, and I. Bloch. *Nature*, 434:481, 2005.

[93] M.W. Zwierlein, J.R. Abo-Shaeer, C. H. Schunck, A. Schirotzek, and W. Ketterle. *Nature*, 435:1047, 2005.

[94] M. Köhl, H. Moritz, T. Stöferle, K. Günter, and T. Esslinger. *Phys. Rev. Lett.*, 94:080403, 2005.

[95] M. Köhl, H. Moritz, T. Stöferle, K. Günter, and T. Esslinger. *Phys. Rev. Lett.*, 946:030401, 2006.

[96] G. Thalhammer, K. Winkler, F. Lang, S. Schmid, R. Grimm, and J. Hecker Denschlag. *Phys. Rev. Lett.*, 96:050402, 2006.

[97] M. C. Gutzwiller. *Phys. Rev. Lett.*, 10:159, 1963.

[98] J. Hubbard. *Proc. Roy. Soc. (London)*, A 276:238, 1963.

[99] D. Jaksch, C. Bruder, J.I. Cirac, C. W. Gardiner, and P. Zoller. *Phys. Rev. Lett.*, 81:3108, 1998.

[100] W. Hofstetter, J.I. Cirac, P. Zoller, E. Demler, and M. D. Lukin. *Phys. Rev. Lett.*, 89:220407, 2002.

[101] Y. Shi, M.W. Zwierlein, A. Schirotzek, C. H. Schunck, and W. Ketterle. 2006, `cond-mat/0606432`.

[102] G. Sarma. *J. Phys. Chem. Solids*, 24:1029, 1963.

[103] F. Wilczek and W. V. Liu. *Phys. Rev. Lett.*, 90:047002, 2003.

[104] M. McNeil Forbes, E. Gubankova, W. V. Liu, and F. Wilczek. *Phys. Rev. Lett.*, 94:017001, 2005.

[105] G. B. Partridge, W. Li, R. I. Kamar, Y. Liao, and R. G. Hulet. *Science*, 311:503, 2006.

[106] M.W. Zwierlein, A. Schirotzek, C. H. Schunck, and W. Ketterle. *Science*, 311:492, 2006.

[107] L. Kinnunen, L. M. Jensen, and P. Törmä. *Phys. Rev. Lett.*, 96:110403, 2006.

[108] P. Pieri and G. C. Strinati. *Phys. Rev. Lett.*, 96:150404, 2006.

[109] M. Iskin and C. A. R. Sa de Melo. 2006, `cond-mat/0603601`.

[110] M. Haque and H. T. C. Stoof. 2006, `cond-mat/0601321`.

[111] K. B. Gubbels, M. W. J. Romans, and H. T. C. Stoof. 2006, `cond-mat/0606330`.

[112] J. Dalibard. In *The Theory of Superconductivity in the High-T_c Cuprates*, ed. M. Inguscio, S. Stringari, C. E. Wieman, pp. 321 - 349. *IOS Press, Amsterdam*, 1999.

[113] C. Wetterich. Quantum Field Theory I. *Lecture Notes*, 2006.

Dank

Für die kompetente, motivierende und freundliche Betreuung dieser Promotion möchte ich mich herzlich bei Prof. Dr. Christof Wetterich bedanken. Für die gute zielgerichtete Zusammenarbeit, die dennoch genügend Raum für eigene Ideen ließ.

PD Dr. Jan Martin Pawlowski danke ich für die Übernahme des Zweitgutachtens.

Für die vorliegende Arbeit habe ich viel von interessanten und zum Teil leidenschaftlich geführten Diskussionen profitiert. Insbesondere PD Dr. Jan Martin Pawlowski, PD Dr. Holger Gies, Hans Christian Krahl, Philipp Strack, PD Dr. Thomas Gasenzer und Prof. Dr. Jörg Schmiedmayer bin ich hierfür sehr dankbar.

Esther möchte ich herzlich und tief empfunden für die schöne gemeinsam verbrachte Zeit in Freiburg, Frankfurt und schließlich Heidelberg danken, sowie für ihre konstante Unterstützung meiner Arbeit.

Meinen Freunden danke ich für die Freundschaft.

Ich danke herzlich meinen Eltern, die mich in meinen Vorhaben immer unterstüzt und bestärkt haben.

Der Studienstiftung des deutschen Volkes bin ich für die finanzielle und ideelle Förderung dieser Promotion zu großem Dank verpflichtet.